

UNITED STATES AIR FORCE  
SUMMER RESEARCH PROGRAM -- 1996  
HIGH SCHOOL APPRENTICESHIP PROGRAM FINAL REPORTS

VOLUME 15B

WRIGHT LABORATORY

RESEARCH & DEVELOPMENT LABORATORIES  
5800 Uplander Way  
Culver City, CA 90230-6608

Program Director, RDL  
Gary Moore

Program Manager, AFOSR  
Major Linda Steel-Goodwin

Program Manager, RDL  
Scott Licoscos

Program Administrator, RDL  
Johnetta Thompson

Program Administrator, RDL  
Rebecca Kelly

Submitted to:

20010307 171

AIR FORCE OFFICE OF SCIENTIFIC RESEARCH  
Bolling Air Force Base

Washington, D.C.  
December 1996

**DISTRIBUTION STATEMENT A**  
Approved for Public Release  
Distribution Unlimited

AQU01-01 0030

# REPORT DOCUMENTATION PAGE

Public reporting burden for this collection of information is estimated to average 1 hour per response, including the time for reviewing instructions, the collection of information. Send comments regarding this burden estimate or any other aspect of this collection of information, including Operations and Reports, 1215 Jefferson Davis Highway, Suite 1204, Arlington, VA 22202-4302, and to the Office of Management and Budget.

g and reviewing  
for Information

AFRL-SR-BL-TR-00-

0748

			5. FUNDING NUMBERS F49620-93-C-0063
1. AGENCY USE ONLY (Leave blank)	2. REPORT DATE December, 1996	3. R	
4. TITLE AND SUBTITLE 1996 Summer Research Program (SRP), High School Apprenticeship Program (HSAP), Final Reports, Volume 15B, Wright Laboratory			8. PERFORMING ORGANIZATION REPORT NUMBER
6. AUTHOR(S) Gary Moore			
7. PERFORMING ORGANIZATION NAME(S) AND ADDRESS(ES) Research & Development Laboratories (RDL) 5800 Uplander Way Culver City, CA 90230-6608			
9. SPONSORING/MONITORING AGENCY NAME(S) AND ADDRESS(ES) Air Force Office of Scientific Research (AFOSR) 801 N. Randolph St. Arlington, VA 22203-1977			10. SPONSORING/MONITORING AGENCY REPORT NUMBER
11. SUPPLEMENTARY NOTES			
12a. DISTRIBUTION AVAILABILITY STATEMENT Approved for Public Release			12b. DISTRIBUTION CODE
13. ABSTRACT (Maximum 200 words) The United States Air Force Summer Research Program (USAF-SRP) is designed to introduce university, college, and technical institute faculty members, graduate students, and high school students to Air Force research. This is accomplished by the faculty members (Summer Faculty Research Program, (SFRP)), graduate students (Graduate Student Research Program (GSRP)), and high school students (High School Apprenticeship Program (HSAP)) being selected on a nationally advertised competitive basis during the summer intersession period to perform research at Air Force Research Laboratory (AFRL) Technical Directorates, Air Force Air Logistics Centers (ALC), and other AF Laboratories. This volume consists of a program overview, program management statistics, and the final technical reports from the HSAP participants at the Wright Laboratory.			
14. SUBJECT TERMS Air Force Research, Air Force, Engineering, Laboratories, Reports, Summer, Universities, Faculty, Graduate Student, High School Student			15. NUMBER OF PAGES
			16. PRICE CODE
17. SECURITY CLASSIFICATION OF REPORT Unclassified	18. SECURITY CLASSIFICATION OF THIS PAGE Unclassified	19. SECURITY CLASSIFICATION OF ABSTRACT Unclassified	20. LIMITATION OF ABSTRACT UL

## PREFACE

Reports in this volume are numbered consecutively beginning with number 1. Each report is paginated with the report number followed by consecutive page numbers, e.g., 1-1, 1-2, 1-3; 2-1, 2-2, 2-3.

Due to its length, Volume 15 is bound in three parts 15A, and 15B. Volume 15A contains #1-27. Volume 15B contains reports #28-58. The Table of Contents for Volume 15 is included in all parts.

This document is one of a set of 16 volumes describing the 1996 AFOSR Summer Research Program. The following volumes comprise the set:

<u>VOLUME</u>	<u>TITLE</u>
1	Program Management Report <i>Summer Faculty Research Program (SFRP) Reports</i>
2A & 2B	Armstrong Laboratory
3A & 3B	Phillips Laboratory
4	Rome Laboratory
5A , 5B & 5C	Wright Laboratory
6	Arnold Engineering Development Center, Wilford Hall Medical Center and Air Logistics Centers <i>Graduate Student Research Program (GSRP) Reports</i>
7A & 7B	Armstrong Laboratory
8	Phillips Laboratory
9	Rome Laboratory
10A & 10B	Wright Laboratory
11	Arnold Engineering Development Center, United States Air Force Academy, Wilford Hall Medical Center, and Wright Patterson Medical Center <i>High School Apprenticeship Program (HSAP) Reports</i>
12A & 12B	Armstrong Laboratory
13	Phillips Laboratory
14	Rome Laboratory
15A&15B	Wright Laboratory
16	Arnold Engineering Development Center

**HSAP FINAL REPORT TABLE OF CONTENTS****i-xiv**

<b>1. INTRODUCTION</b>	<b>1</b>
<b>2. PARTICIPATION IN THE SUMMER RESEARCH PROGRAM</b>	<b>2</b>
<b>3. RECRUITING AND SELECTION</b>	<b>3</b>
<b>4. SITE VISITS</b>	<b>4</b>
<b>5. HBCU/MI PARTICIPATION</b>	<b>4</b>
<b>6. SRP FUNDING SOURCES</b>	<b>5</b>
<b>7. COMPENSATION FOR PARTICIPATIONS</b>	<b>5</b>
<b>8. CONTENTS OF THE 1996 REPORT</b>	<b>6</b>

**APPENDICIES:**

<b>A. PROGRAM STATISTICAL SUMMARY</b>	<b>A-1</b>
<b>B. SRP EVALUATION RESPONSES</b>	<b>B-1</b>

**HSAP FINAL REPORTS**

**SRP Final Report Table of Contents**

<b>Author</b>	<b>University/Institution Report Title</b>	<b>Armstrong Laboratory Directorate</b>	<b>Vol-Page</b>
Julio E Ayala	South San Antonio High School , San Antonio , TX Chemical Preparations of Drinking Water for Radioanalysis	AL/OEMH	12 - 1
Mark Beebe	Beavercreek High School , Dayton , OH Application of World Wide Web Technologies to Enhance Information Visualization	AL/HRGO	12 - 2
Andrew J Binovi	St. Anthony Catholic High , San Antonio , TX Creating a Longitude & Latitude Plot Using SAS/Graph Software	AL/AOEP	12 - 3
Jennifer S Burnett	Bay County High School , Panama City , FL The Effect of Prolonged Growth on a Non-Selective Medium on the Ability of <i>Pseudomonas</i> <i>Pseudoalcalig</i>	AL/EQC	12 - 4
Nicholas G Butel	James Madison High School , San Antonio , TX Recent Developments in Dosimetry Research Within AL/OER	AL/OER	12 - 5
Lenis P Chen	Centerville High School , Centerville , OH A Study of the Influence of Relative Loads & G-Forces on Electromyographic Activity	AL/CFBV	12 - 6
Carolyn K Chen	MacArthur High School , San Antonio , TX Correlations of Body Composition and VO <sub>2</sub> Max	AL/AOCY	12 - 7
Christopher C Garcia	Edgewood ISD , San Antonio , TX Consultation Resources	AL/OEBQ	12 - 8
Lori M Gilliam	Saint Mary's Hall , San Antonio , TX The Neuropharmacological Characterization of G-Induced Loss of Consciousness	AL/CFTF	12 - 9
Aaron R Hamid	Robert G. Cole Sr. High School , San Antonio , TX Easy Reference"" Psychological Reference Page Creator	AL/HRMC	12 - 10
Gregory T Hannibal	Northside Health Careers High School , San Antonio , TX In-Vitro Simulation of Physiologic Aortic Pressure & Flow Profiles	AL/AOCY	12 - 11

**SRP Final Report Table of Contents**

<b>Author</b>	<b>University/Institution Report Title</b>	<b>Armstrong Laboratory Directorate</b>	<b>Vol-Page</b>
Daniel L Hardmeyer	James Madison High School, San Antonio, TX Neuropsychological Testing of Pilots	AL/AOCN	12 - 12
Eric W Inge	Rutherford High School , PANAMA CITY , FL The Study & Application of C++Programming	AL/EQP	12 - 13
Nafisa Islam	Centerville High School , Centerville , OH Determination of Skin:Air Partition Coefficients for Human Stratum Corneum	AL/OET	12 - 14
Kelly M Keish	Vandalia-Butler High School , Vandalia , OH Psychophysiological Data: Eyeblinks Heart Rate and Respiration	AL/CFHP	12 - 15
Adriana Y Lopez	East Central High School , San Antonio , TX An Anaysis of Oil/Grease in Water and Soil	AL/OE	12 - 16
Darby M Mahan	Tippecanoe High School , Tipp City , OH Evaluation of Alternative Control Technologies	AL/CFHP	12 - 17
Christina R Maimone	Chaminade-Julienne High School , Dayton , OH Application of World Wide Web Technologies to Enhance Information Visualization	AL/HRCO	12 - 18
Alison B Martin	A. Crawford Mosely High School , Lynn Haven , FL Electrochemiluminescence (ECL) Sensors REsearch & Development	AL/EQC	12 - 19
Lisa A Mattingley	A. Crawford Mosely High School , Lynn Haven , FL The Biodegradation of Ammmonium Perchlorate in a Fixed Bed Reactor	AL/EQ	12 - 20
Priscilla M Medina	PSJ High School , Port Saint Joe , FL	AL/EQP	12 - 21
Lila C Medrano	L.W.Fox Academic & Tech High School , San Antonio , TX The Study of Gamma Radiation Present in the Environment	AL/OEM	12 - 22

**SRP Final Report Table of Contents**

<b>Author</b>	<b>University/Institution Report Title</b>	<b>Armstrong Laboratory Directorate</b>	<b>Vol-Page</b>
David J Miller		AL/HRTD	12 - 23
	<b>Samuel Clemens High School, Schertz, TX</b> <b>Raid: Redundant Array of Independent/Inexpensive Disks</b>		
Jennifer M Patterson		AL/HRTI	12 - 24
	<b>John Marshall High School , San Antonio , TX</b> <b>Instruction in Scientific Inquiry Skills (ISIS)</b>		
Amanda G Perrie		AL/EQC	12 - 25
	<b>A. Crawford Mosely High School , Lynn Haven , FL</b> <b>Fuel Identification Based on Naphthalene and Benzene Derivatives</b>		
Ester I Resendiz		AL/CFTF	12 - 26
	<b>William Howard Taft High School , San Antonio , TX</b> <b>A Study of the VErtical Shifts in Scene Perception Memory</b>		
William B Richardson		AL/EQP	12 - 27
	<b>A. Crawford Mosely High School , Lynn Haven , FL</b>		
Alejandro F Ruiz		AL/OEBW	12 - 28
	<b>South San Antonio High School , San Antonio , TX</b> <b>A Study of the Deicing of Aircraft</b>		
Marc A Salazar		AL/OEBW	12 - 29
	<b>Judson High School , Converse , TX</b> <b>A Study of De-Icing Fluids, Methods, &amp; Effects As Used on Military Aircraft</b>		
Jonathan Samm		AL/OES	12 - 30
	<b>Theodore Roosevelt High School , San Antonio , TX</b> <b>Electromagnetic Fields in a Single Slab For Oblique Incidence</b>		
Keith A Shaw		AL/CFTS	12 - 31
	<b>MacArthur High School , San Antonio , TX</b> <b>Analysis of Poly-Alpha Olephin by Gas Chromatography</b>		
Michelle C Wadsworth		AL/HRM	12 - 32
	<b>Tom C. Clark High School , San Antonio , TX</b> <b>Comprehensive Testing for the Selection of Air Force Crew Members</b>		
Elizabeth A Walker		AL/AOHR	12 - 33
	<b>Theodore Roosevelt High School , San Antonio , TX</b> <b>The Effect of Hyperbaric Oxygenation on Du-145 Cells</b>		

**SRP Final Report Table of Contents**

<u>Author</u>	<u>University/Institution Report Title</u>	<u>Armstrong Laboratory Directorate</u>	<u>Vol-Page</u>
Mollie L Webb	Fairmount High School, Kettering, OH Swipe Method Development for the Trace Analysis of Unicharge (M231 & M232) Components in Cottin Gau	AL/OET	12 - 34
Eric Yu	Fairborn High School, Fairborn, OH Cerebral Oxygen Levels as a Psychophysiological Measure of Pilot Workload	AL/CFBS	12 - 35
Stephanie L Zigmund	East Central High School, San Antonio, TX Analysis of Human Muscle Movement Under Increased Acceleration	AL/CA	12 - 36

**SRP Final Report Table of Contents**

<u>Author</u>	<u>University/Institution Report Title</u>	<u>Phillips Laboratory Directorate</u>	<u>Vol-Page</u>
Michael L Berry	Highland High School, Palmdale, CA Synthesis of A High-Energy Binder	PL/RKS	13 - 1
Emily R Blundell	Rosamond High School, Rosamond, CA Using a Scanner & Computer to Update a Technical Instruction Manual	PL/RKO	13 - 2
Lillian A Capell	Quartz Hill High School, Quartz Hill, CA The Synthesis of 3-Oxaquadricyclane	PL/RKS	13 - 3
Rebecca P Cohen	Sandia Prep School, Albuquerque, NM The Production of Carbon Composite Grid Structures Utilizing an Automated Process	PL/VTSC	13 - 4
Bryan S Ericson	Tehachapi High School, Tehachapi, CA	PL/RKEE	13 - 5
Jeffery A Fisher	Paraclete High School, Quartz Hill, CA	PL/RKS	13 - 6
Greg A Fisher	Quartz Hill High School, Quartz Hill, CA	PL/RKE	13 - 7
Erica S Gerken	Manzano High School, Albuquerque, NM Electrical & Optical Characterization of Strategic Infrared Detectors in Benign & Radiation Environments	PL/VTRP	13 - 8
James C Ha	Tehachapi High School, Tehachapi, CA	PL/RKO	13 - 9
Douglas G Havlik	Albuquerque Academy, Albuquerque, NM Neodymium Fiber Laser	PL/LIDN	13 - 10
Karl J Iliev	Antelope Valley High School, Lancaster, CA Solar Thermal Propulsion From Concept to Reality	PL/RKE	13 - 11
Caroline H Lee	Lexington Sr. High School, Lexington, MA Combined Effects of Gravity and Geomagnetic Field on Crystal Growth	PL/GPI	13 - 12
Maureen D Long	Chelmsford High School, North Chelmsford, MA An Investigation of Cataloging Procedures for Point Sources in the Galactic Plane	PL/GPO	13 - 13
Ruben E Marin	Littlerock High School, Littlerock, CA Instrumentation and Data Acquisition	PL/RKEE	13 - 14

**SRP Final Report Table of Contents**

<b>Author</b>	<b>University/Institution Report Title</b>	<b>Phillips Laboratory Directorate</b>	<b>Vol-Page</b>
Fawn R Miller	Manzano High School, Albuquerque, NM Ferroelectric Liquid Crystals for Satellite Communications Phase II	PL/VTRA	13 - 15
Lewis P Orchard	Sandia Prep School, Albuquerque, NM Writing Diagnostic Software for Photoluminescence Studies	PL/LIDA	13 - 16
Seth B Schuyler	Sandia High School, Albuquerque, NM The Use of Reverberation Chambers for Susceptibility Testing on Airplane Electronics	PL/WS	13 - 17
William D Shuster	Albuquerque Academy, Albuquerque, NM A Study of the Characterization in Semiconductor Lasers	PL/LIDA	13 - 18
Raj C Singaraju	Albuquerque Academy, Albuquerque, NM Fabrication of a Wide Spectrum Impulse Radiating Antenna	PL/WS	13 - 19
Gaurav Tuli	Waltham High School, Waltham, MA A Cell Structured Plane System for Monte Carlo Photon Transport	PL/GPO	13 - 20

**SRP Final Report Table of Contents**

<u>Author</u>	<u>University/Institution Report Title</u>	<u>Rome Laboratory Directorate</u>	<u>Vol-Page</u>
Robert C Altshuler	Newton North High School, Newtonville, MA	RL/ERH	14 - 1
Michael A Bartley	Waltham High School , Waltham , MA	RL/ERH	14 - 2
Daniel T Brown	Sauquoit Valley Senior High , Sauquoit , NY Preparation o& Placement of Matl's on the World-Wide Web	RL/IRE	14 - 3
Daniel E Grabski	Holland Patent High School , Holland Patent , NY Information on the Internet & PEM Test Circuit Design	RL/ERDA	14 - 4
Nicholas Hrycan	Thomas R. Proctor High School , Utica , NY Memories of the Future A Study of Bit-Oriented Optical Memory	RL/IRAE	14 - 5
Sandra L Jablonka	Oneida Senior High School , Oneida , NY Magnitude Measurement of Electromagnetic Field INTensities Using an Infrared Measurement Technique	RL/ERST	14 - 6
Matthew A Lam	Thomas R. Proctor High School , Utica , NY Spell Checking w/a Directory-Trie in Prolog	RL/C3CA	14 - 7
Joanna D Lisker	Newton North High School , Newtonville , MA	RL/ERH	14 - 8
Pamela L McNeil	Austin Prep School , Reading , MA	RL/ERH	14 - 9
Anthony J Perritano	Sauquoit Valley Senior High , Sauquoit , NY Using Spreadsheets and Programming in a Unix Environment	RL/IRDS	14 - 10
Michael A Scarpulla	Andover High School , Andover , MA	RL/ERH	14 - 11

**SRP Final Report Table of Contents**

<b>Author</b>	<b>University/Institution Report Title</b>	<b>Rome Laboratory Directorate</b>	<b>Vol-Page</b>
Patricia M Swanson	Holland Patent High School, Holland Patent, NY Hypertext Markup Language: Caught in the WEB	RL/C3CA	14 - 12
Brain B Tuch	New Hartford Senior High School, New hartford, NY A Study of the Computer Networking Environment	RL/C3CB	14 - 13
Cheryl G Zaglaniczny	Whitesboro High School, Whitesboro, NY Determining the Static Voltage Distribution on Circuit Structures	RL/ERST	14 - 14

**SRP Final Report Table of Contents**

<b>Author</b>	<b>University/Institution Report Title</b>	<b>Wright Laboratory Directorate</b>	<b>Vol-Page</b>
Jesse J Anderson	Chaminade-Julienne High School, Dayton, OH The Creation of a Shell Prog to Interface to Confor	WL/MLIM	15 - 1
Mark A Bartsch	Carroll High School, Dayton, OH A Study of the Generalization & Classification Abilities of a Backpropagation Neural Network	WL/AACA	15 - 2
Amy E Beam	Beavercreek High School, Dayton, OH Compressor Testing	WL/POTF	15 - 3
Crystal W Bhagat	Dayton Christian High School, Dayton, OH A Study of the Effects of Varying Chain Length Surfactants on Polymer Dispersed Liquid Crystal	WL/MLPJ	15 - 4
Daniel A Binkis	Beavercreek High School, Dayton, OH A Trial of Microencapsulated Phase Change Material of Use in Modern Aircraft	WL/FI	15 - 5
Matthew L Blanton	Wayne High School, Huber Heights, OH Prediction of Paratroop/Wake Vortex Encounters During Formation Airdrop	WL/FI	15 - 6
Brian E Brumfield	Tippecanoe High School, Tipp City, OH The Study of a Basic LDV System	WL/POPT	15 - 7
Jason M Burris	Dayton Christian High School, Dayton, OH A Study of the Bending and Torsional Energies of Biphenyl	WL/MLBP	15 - 8
Kim Cabral	Choctawhatchee High School, Ft Walton Beach, FL Laser Radar (LADAR) Imagery Analysis Task	WL/MNGA	15 - 9
Sarah C Calvert	Yellow Springs High School, Yellow Springs, OH A Study Measuring the Acceleration of Vibrating Structures Using a Microphone	WL/FI	15 - 10
Shannon M Campbell	Carroll High School, Dayton, OH An Investigation into Red Dye Contamination of Aviation Fuel	WL/POTF	15 - 11
Christopher R Clark	Niceville Senior High School, Niceville, FL Neural Networks & Digital Image Processing	WL/MNGA	15 - 12

**SRP Final Report Table of Contents**

<b>Author</b>	<b>University/Institution Report Title</b>	<b>Wright Laboratory Directorate</b>	<b>Vol-Page</b>
Allyn J Crowe	Bellbrook High School, Bellbrook, OH Maximal Length Sequences & Circuit Development	WL/AAM	15 - 13
Aaron Davis	Niceville Senior High School, Niceville, FL Polymerization Mechanisms for Electrodeposited Polypyrrole	WL/MNMF	15 - 14
Brad L Day	Greeneview High School, Xenia, OH	WL/POSF	15 - 15
Julie L Deibler	Choctawhatchee High School, Ft Walton Beach, FL Investigations of the IR Band in .1 Micron Increments using Synthetic Imagery	WL/MNGA	15 - 16
Cindi L Dennis	Beavercreek High School, Dayton, OH Multiple quantum Wells in the Semiconductor Mat'l GaAs/A <sub>1-x</sub> Ga <sub>1-x</sub> -As & Computational Chemistry	WL/MLPO	15 - 17
Mark T Fecke	Chaminade-Julienne High School, Dayton, OH Exhaust Fan Measurements with A Wedge Probe	WL/POTF	15 - 18
Landon W Frymire	Laurel Hill High School, Laurell Hill, FL Data Analysis for Redesign of the 105mm Blast Diffuser	WL/MNAV	15 - 19
Jenny R Garringer	Miami Trace High School, Washington, OH The Creation of Oving and Stationary Acquistion and Recognition and Infrared Visual Data WEB Pages	WL/AACI	15 - 20
Douglas S Ginger	Centerville High School, Centerville, OH A Study of the Lubricating Properties of Commercial Lubricants with Respect to Relative Humidity	WL/MLBT	15 - 21
Julie A Glaser	Carroll High School, Datyon, OH	WL/MLPO	15 - 22
Robert J Glaser	Carroll High School, Dayton, OH Pitot Probe Measurements of Air Flow Through a Duct and Diffuser	WL/POSF	15 - 23
Stephen M Govenar	Beavercreek High School, Dayton, OH Developing an Automatic Neural Network Training Algorithm and Using Neural Networks as Circuit Simulator Models	WL/AADM	15 - 24

**SRP Final Report Table of Contents**

<b>Author</b>	<b>University/Institution Report Title</b>	<b>Wright Laboratory Directorate</b>	<b>Vol-Page</b>
Neil P Griffy	WL/FI		15 - 25
	Brookville High School, Brookville, OH Analysis of the Flame-Out Parameter on an Experimental Combuster WEB Page Design Using HTML Program		
Shaun R Guillermin	WL/POOS		15 - 26
	Chaminade-Julienne High School, Dayton, OH Observation of de Gausing Through Repeated Thermocycling of Samarium Cobalt Magnets		
Angela C Helm	WL/AA		15 - 27
	Carroll High School, Dayton, OH The Study of the Neotam* Computational Model		
David B Hernandez	WL/MNSE		15 - 28
	Freeport High School, Freeport, FL Laser Firing Control System		
Anna S Hill	WL/POSF		15 - 29
	Carroll High School, Dayton, OH An Investigation into Red Dye Contamination of Aviation Fuel		
Daniel J Holmes	WL/MNM		15 - 30
	Niceville Senior High School, Niceville, FL The EPIC Penetration Event Generator (EPEG)		
Andrew J Jutte	WL/PO		15 - 31
	Northmont High School, Clayton, OH A Study of Acoustic Wave Propagation in Non-Equilibrium Plasmas		
Nicholas A Klosterman	WL/AACI		15 - 32
	Chaminade-Julienne High School, Dayton, OH Hyper Text Markup Language		
Kelly A Lakatos	WL/MLPO		15 - 33
Jonathan S Mah	WL/AASI-I		15 - 34
	Centerville High School, Centerville, OH Enhancement of CAD Packages for Electronic & Computational Applications		
David Mandel	WL/MNM		15 - 35
	Niceville Senior High School, Niceville, FL The Optimization of an Impedance Matching Transformer for an Explosive Flux Generator & Static Load		
Michele V Manuel	WL/MNSE		15 - 36
	Crestview High School, Crestview, FL The Removal of Hazardous Compounds Using a Non-Thermal Discharge Device		

**SRP Final Report Table of Contents**

<u>Author</u>	<u>University/Institution Report Title</u>	<u>Wright Laboratory Directorate</u>	<u>Vol-Page</u>
Bud A Miyahara	Carroll High School , Dayton , OH Computer Applications for Speed & Efficiency	WL/AADM _____	15 - 37
Disha J Patel	Fairmont High School , Kettering , OH The Study of The Neotam Computational Model	WL/AACT _____	15 - 38
Neill W Perry	Crestview High School , Crestview , FL A Study on Detection & Measurement of Atmospheric Backscatter Using Direct Detection Backscatter	WL/MNGS _____	15 - 39
Michael D Powell	Beavercreek High School , Dayton , OH Digital Signal Processing of Maximal Length Sequences	WL/AAOP _____	15 - 40
Shaun G Power	Heritage Christian School , Xenia , OH Development of Webpages	WL/AACI _____	15 - 41
Matthew R Rabe	Carroll High School , Dayton , OH	WL/POPT _____	15 - 42
Angela C Rabe	Carroll High School , Dayton , OH Dimensional Changes Affecting HS50 and HA50HS Iron-Cobalt Alloys due to Annealing	WL/POOS _____	15 - 43
Rajeev Raghavan	Centerville High School , Centerville , OH A Study on the Impact of Voltage & Frequency Levels on the Conductivities & Effects of Polymer	WL/MLPJ _____	15 - 44
Kristan M Raymond	Walton High School , DeFuniak SPRINGS , FL Tungsten Alloys: Corrosion Potential & Desirability for Use in Munitions	WL/MNSE _____	15 - 45
Adam Z Reed	Tippecanoe High School , Tipp City , OH Improvement of Automatic Data Processing Equipment (ADPE) Accountability System	WL/FI _____	15 - 46
Franklin K Reyher III	Niceville Senior High School , Niceville , FL Development & Testing of an Optical Scan Characterizer	WL/MNGS _____	15 - 47

**SRP Final Report Table of Contents**

<b>Author</b>	<b>University/Institution Report Title</b>	<b>Wright Laboratory Directorate</b>	<b>Vol - Page</b>
Brian R Riestenberg	Centerville High School , Centerville , OH A Study of Wear Using A Cameron-Plint Tribometer	WL/MLBT	15 - 48
Douglas M Ritchie	Niceville Senior High School , Niceville , FL Neural Networks & Digital Image Processing	WL/MNGA	15 - 49
Trisha A Silkauskas	Centerville High School , Centerville , OH A Study of Improving The Computed Air Release Point Using Neural Networks	WL/FI	15 - 50
Michael J Steiger	Oakwood High School , Dayton , OH Summer Science Projects	WL/MLBP	15 - 51
Kari D Sutherland	Dayton Christian High School , Dayton , OH A Study of the Effects of Octanoic Acid on Polymer Dispersed Liquid Crystal Holographic Gratings	WL/MLPJ	15 - 52
Matt V Temple	Chaminade-Julienne High School , Dayton , OH FIGP-2 WEB SITE	WL/FI	15 - 53
Jeroen W Thompson	Beavercreek High School , Dayton , OH Bandgap Properties of (100)-Grown InAs/In <sub>x</sub> Ga <sub>1-x</sub> Sb As a Function of Growth-Induced Disorder	WL/MLPO	15 - 54
Jonathan D Tidwell	Rocky Bayou Christian School , Niceville , FL Interim Qualification Testing of TUNG 5 Mod 6	WL/MNM	15 - 55
Joshua A Weaver	Niceville Senior High School , Niceville , FL Hydrocode Support Development	WL/MNM	15 - 56
Aaron B Wilson	Miamisburg High School , Miamisburg , OH	WL/FI	15 - 57
Tuan P Yang	Choctawhatchee High School , Ft Walton BEACH , FL Pre & Post Microstructure Damage Analysis of TUNG 5 Mod 6	WL/MNM	15 - 58

**SRP Final Report Table of Contents**

<b>Author</b>	<b>University/Institution Report Title</b>	<b>Laboratory Directorate</b>	<b>Vol-Page</b>
Sara E Allen	Coffee County Central High School, Manchester, TN Operating Map Preparation Using ARC Heater Correlations	AEDC	16 - 1
Erica D Brandon	Coffee County Central High School, Manchester, TN Environmental Aspects in an Industrial Setting	AEDC	16 - 2
Philip a Chockley III	Shelbyville Central High School, Shelbyville, TN A Program to Determine Static Force and Moment Force Balance Calculations	AEDC	16 - 3
Jennifer L Counts	Franklin County Senior High School, Winchester, TN Stagnation Pressure Loss in Rocket Combustion Chambers	AEDC	16 - 4
Wesley A Dixon	Shelbyville Central High School, Shelbyville, TN	AEDC	16 - 5
Jason E Hill	Shelbyville Central High School, Shelbyville, TN Constructing an Internet Home Page Using Hypertext Markup Language	AEDC	16 - 6
Michael R Munn	Coffee County Central High, Manchester, TN Modernization of the AEDC Turbine Engine Test an Analysis Standard Computer Software	AEDC	16 - 7
Daniel B Sipe	Coffee County Central High School, Manchester, TN Turbine Engine Model Library	AEDC	16 - 8
Daniel M Thompson	Shelbyville Central High School, Shelbyville, TN A Methodology for Assessing the Performance of the J-4 Rocket Test Facility	AEDC	16 - 9
Matthew M Wiedemer	Tullahoma High School, Tullahoma, TN Assessment of Hydrazine Monopropellant Plume Conductivity	AEDC	16 - 10

## **INTRODUCTION**

The Summer Research Program (SRP), sponsored by the Air Force Office of Scientific Research (AFOSR), offers paid opportunities for university faculty, graduate students, and high school students to conduct research in U.S. Air Force research laboratories nationwide during the summer.

Introduced by AFOSR in 1978, this innovative program is based on the concept of teaming academic researchers with Air Force scientists in the same disciplines using laboratory facilities and equipment not often available at associates' institutions.

The Summer Faculty Research Program (SFRP) is open annually to approximately 150 faculty members with at least two years of teaching and/or research experience in accredited U.S. colleges, universities, or technical institutions. SFRP associates must be either U.S. citizens or permanent residents.

The Graduate Student Research Program (GSRP) is open annually to approximately 100 graduate students holding a bachelor's or a master's degree; GSRP associates must be U.S. citizens enrolled full time at an accredited institution.

The High School Apprentice Program (HSAP) annually selects about 125 high school students located within a twenty mile commuting distance of participating Air Force laboratories.

AFOSR also offers its research associates an opportunity, under the Summer Research Extension Program (SREP), to continue their AFOSR-sponsored research at their home institutions through the award of research grants. In 1994 the maximum amount of each grant was increased from \$20,000 to \$25,000, and the number of AFOSR-sponsored grants decreased from 75 to 60. A separate annual report is compiled on the SREP.

The numbers of projected summer research participants in each of the three categories and SREP "grants" are usually increased through direct sponsorship by participating laboratories.

AFOSR's SRP has well served its objectives of building critical links between Air Force research laboratories and the academic community, opening avenues of communications and forging new research relationships between Air Force and academic technical experts in areas of national interest, and strengthening the nation's efforts to sustain careers in science and engineering. The success of the SRP can be gauged from its growth from inception (see Table 1) and from the favorable responses the 1996 participants expressed in end-of-tour SRP evaluations (Appendix B).

AFOSR contracts for administration of the SRP by civilian contractors. The contract was first awarded to Research & Development Laboratories (RDL) in September 1990. After

completion of the 1990 contract, RDL (in 1993) won the recompetition for the basic year and four 1-year options.

## 2. PARTICIPATION IN THE SUMMER RESEARCH PROGRAM

The SRP began with faculty associates in 1979; graduate students were added in 1982 and high school students in 1986. The following table shows the number of associates in the program each year.

YEAR	SRP Participation, by Year			TOTAL
	SFRP	GSRP	HSAP	
1979	70			70
1980	87			87
1981	87			87
1982	91	17		108
1983	101	53		154
1984	152	84		236
1985	154	92		246
1986	158	100	42	300
1987	159	101	73	333
1988	153	107	101	361
1989	168	102	103	373
1990	165	121	132	418
1991	170	142	132	444
1992	185	121	159	464
1993	187	117	136	440
1994	192	117	133	442
1995	190	115	137	442
1996	188	109	138	435

Beginning in 1993, due to budget cuts, some of the laboratories weren't able to afford to fund as many associates as in previous years. Since then, the number of funded positions has remained fairly constant at a slightly lower level.

### 3. RECRUITING AND SELECTION

The SRP is conducted on a nationally advertised and competitive-selection basis. The advertising for faculty and graduate students consisted primarily of the mailing of 8,000 52-page SRP brochures to chairpersons of departments relevant to AFOSR research and to administrators of grants in accredited universities, colleges, and technical institutions. Historically Black Colleges and Universities (HBCUs) and Minority Institutions (MIs) were included. Brochures also went to all participating USAF laboratories, the previous year's participants, and numerous individual requesters (over 1000 annually).

RDL placed advertisements in the following publications: *Black Issues in Higher Education*, *Winds of Change*, and *IEEE Spectrum*. Because no participants list either *Physics Today* or *Chemical & Engineering News* as being their source of learning about the program for the past several years, advertisements in these magazines were dropped, and the funds were used to cover increases in brochure printing costs.

High school applicants can participate only in laboratories located no more than 20 miles from their residence. Tailored brochures on the HSAP were sent to the head counselors of 180 high schools in the vicinity of participating laboratories, with instructions for publicizing the program in their schools. High school students selected to serve at Wright Laboratory's Armament Directorate (Eglin Air Force Base, Florida) serve eleven weeks as opposed to the eight weeks normally worked by high school students at all other participating laboratories.

Each SFRP or GSRP applicant is given a first, second, and third choice of laboratory. High school students who have more than one laboratory or directorate near their homes are also given first, second, and third choices.

Laboratories make their selections and prioritize their nominees. AFOSR then determines the number to be funded at each laboratory and approves laboratories' selections.

Subsequently, laboratories use their own funds to sponsor additional candidates. Some selectees do not accept the appointment, so alternate candidates are chosen. This multi-step selection procedure results in some candidates being notified of their acceptance after scheduled deadlines. The total applicants and participants for 1996 are shown in this table.

1996 Applicants and Participants			
PARTICIPANT CATEGORY	TOTAL APPLICANTS	SELECTEES	DECLINING SELECTEES
SFRP	572	188	39
(HBCU/MI)	(119)	(27)	(5)
GSRP	235	109	7
(HBCU/MI)	(18)	(7)	(1)
HSAP	474	138	8
<b>TOTAL</b>	<b>1281</b>	<b>435</b>	<b>54</b>

#### 4. SITE VISITS

During June and July of 1996, representatives of both AFOSR/NI and RDL visited each participating laboratory to provide briefings, answer questions, and resolve problems for both laboratory personnel and participants. The objective was to ensure that the SRP would be as constructive as possible for all participants. Both SRP participants and RDL representatives found these visits beneficial. At many of the laboratories, this was the only opportunity for all participants to meet at one time to share their experiences and exchange ideas.

#### 5. HISTORICALLY BLACK COLLEGES AND UNIVERSITIES AND MINORITY INSTITUTIONS (HBCU/MIs)

Before 1993, an RDL program representative visited from seven to ten different HBCU/Mis annually to promote interest in the SRP among the faculty and graduate students. These efforts were marginally effective, yielding a doubling of HBCI/MI applicants. In an effort to achieve AFOSR's goal of 10% of all applicants and selectees being HBCU/MI qualified, the RDL team decided to try other avenues of approach to increase the number of qualified applicants. Through the combined efforts of the AFOSR Program Office at Bolling AFB and RDL, two very active minority groups were found, HACU (Hispanic American Colleges and Universities) and AISES (American Indian Science and Engineering Society). RDL is in communication with representatives of each of these organizations on a monthly basis to keep up with their activities and special events. Both organizations have widely-distributed magazines/quarterlies in which RDL placed ads.

Since 1994 the number of both SFRP and GSRP HBCU/MI applicants and participants has increased ten-fold, from about two dozen SFRP applicants and a half dozen selectees to over 100 applicants and two dozen selectees, and a half-dozen GSRP applicants and two or three selectees to 18 applicants and 7 or 8 selectees. Since 1993, the SFRP had a two-fold applicant

increase and a two-fold selectee increase. Since 1993, the GSRP had a three-fold applicant increase and a three to four-fold increase in selectees.

In addition to RDL's special recruiting efforts, AFOSR attempts each year to obtain additional funding or use leftover funding from cancellations the past year to fund HBCU/MI associates. This year, 5 HBCU/MI SFRPs declined after they were selected (and there was no one qualified to replace them with). The following table records HBCU/MI participation in this program.

YEAR	SRP HBCU/MI Participation, By Year			
	SFRP		GSRP	
	Applicants	Participants	Applicants	Participants
1985	76	23	15	11
1986	70	18	20	10
1987	82	32	32	10
1988	53	17	23	14
1989	39	15	13	4
1990	43	14	17	3
1991	42	13	8	5
1992	70	13	9	5
1993	60	13	6	2
1994	90	16	11	6
1995	90	21	20	8
1996	119	27	18	7

## 6. SRP FUNDING SOURCES

Funding sources for the 1996 SRP were the AFOSR-provided slots for the basic contract and laboratory funds. Funding sources by category for the 1996 SRP selected participants are shown here.

1996 SRP FUNDING CATEGORY	SFRP	GSRP	HSAP
AFOSR Basic Allocation Funds	141	85	123
USAF Laboratory Funds	37	19	15
HBCU/MI By AFOSR (Using Procured Addn'l Funds)	10	5	0
<b>TOTAL</b>	<b>188</b>	<b>109</b>	<b>138</b>

SFRP - 150 were selected, but nine canceled too late to be replaced.

GSRP - 90 were selected, but five canceled too late to be replaced (10 allocations for the ALCs were withheld by AFOSR.)

HSAP - 125 were selected, but two canceled too late to be replaced.

## 7. COMPENSATION FOR PARTICIPANTS

Compensation for SRP participants, per five-day work week, is shown in this table.

1996 SRP Associate Compensation

PARTICIPANT CATEGORY	1991	1992	1993	1994	1995	1996
Faculty Members	\$690	\$718	\$740	\$740	\$740	\$770
Graduate Student (Master's Degree)	\$425	\$442	\$455	\$455	\$455	\$470
Graduate Student (Bachelor's Degree)	\$365	\$380	\$391	\$391	\$391	\$400
High School Student (First Year)	\$200	\$200	\$200	\$200	\$200	\$200
High School Student (Subsequent Years)	\$240	\$240	\$240	\$240	\$240	\$240

The program also offered associates whose homes were more than 50 miles from the laboratory an expense allowance (seven days per week) of \$50/day for faculty and \$40/day for graduate students. Transportation to the laboratory at the beginning of their tour and back to their home destinations at the end was also reimbursed for these participants. Of the combined SFRP and

GSRP associates, 65 % (194 out of 297) claimed travel reimbursements at an average round-trip cost of \$780.

Faculty members were encouraged to visit their laboratories before their summer tour began. All costs of these orientation visits were reimbursed. Forty-five percent (85 out of 188) of faculty associates took orientation trips at an average cost of \$444. By contrast, in 1993, 58 % of SFRP associates took orientation visits at an average cost of \$685; that was the highest percentage of associates opting to take an orientation trip since RDL has administered the SRP, and the highest average cost of an orientation trip. These 1993 numbers are included to show the fluctuation which can occur in these numbers for planning purposes.

Program participants submitted biweekly vouchers countersigned by their laboratory research focal point, and RDL issued paychecks so as to arrive in associates' hands two weeks later.

In 1996, RDL implemented direct deposit as a payment option for SFRP and GSRP associates. There were some growing pains. Of the 128 associates who opted for direct deposit, 17 did not check to ensure that their financial institutions could support direct deposit (and they couldn't), and eight associates never did provide RDL with their banks' ABA number (direct deposit bank routing number), so only 103 associates actually participated in the direct deposit program. The remaining associates received their stipend and expense payments via checks sent in the US mail.

HSAP program participants were considered actual RDL employees, and their respective state and federal income tax and Social Security were withheld from their paychecks. By the nature of their independent research, SFRP and GSRP program participants were considered to be consultants or independent contractors. As such, SFRP and GSRP associates were responsible for their own income taxes, Social Security, and insurance.

## 8. CONTENTS OF THE 1996 REPORT

The complete set of reports for the 1996 SRP includes this program management report (Volume 1) augmented by fifteen volumes of final research reports by the 1996 associates, as indicated below:

1996 SRP Final Report Volume Assignments

LABORATORY	SFRP	GSRP	HSAP
Armstrong	2	7	12
Phillips	3	8	13
Rome	4	9	14
Wright	5A, 5B	10	15
AEDC, ALCs, WHMC	6	11	16

## **APPENDIX A -- PROGRAM STATISTICAL SUMMARY**

### **A. Colleges/Universities Represented**

Selected SFRP associates represented 169 different colleges, universities, and institutions, GSRP associates represented 95 different colleges, universities, and institutions.

### **B. States Represented**

SFRP -Applicants came from 47 states plus Washington D.C. and Puerto Rico. Selectees represent 44 states plus Puerto Rico.

GSRP - Applicants came from 44 states and Puerto Rico. Selectees represent 32 states.

HSAP - Applicants came from thirteen states. Selectees represent nine states.

Total Number of Participants	
SFRP	188
GSRP	109
HSAP	138
<b>TOTAL</b>	<b>435</b>

Degrees Represented			
	SFRP	GSRP	TOTAL
Doctoral	184	1	185
Master's	4	48	52
Bachelor's	0	60	60
<b>TOTAL</b>	<b>188</b>	<b>109</b>	<b>297</b>

SFRP Academic Titles	
Assistant Professor	79
Associate Professor	59
Professor	42
Instructor	3
Chairman	0
Visiting Professor	1
Visiting Assoc. Prof.	0
Research Associate	4
<b>TOTAL</b>	<b>188</b>

Source of Learning About the SRP		
Category	Applicants	Selectees
Applied/participated in prior years	28%	34%
Colleague familiar with SRP	19%	16%
Brochure mailed to institution	23%	17%
Contact with Air Force laboratory	17%	23%
<i>IEEE Spectrum</i>	2%	1%
<i>BIIHE</i>	1%	1%
Other source	10%	8%
<b>TOTAL</b>	<b>100%</b>	<b>100%</b>

## **APPENDIX B – SRP EVALUATION RESPONSES**

### **1. OVERVIEW**

Evaluations were completed and returned to RDL by four groups at the completion of the SRP. The number of respondents in each group is shown below.

Table B-1. Total SRP Evaluations Received

Evaluation Group	Responses
SFRP & GSRPs	275
HSAPs	113
USAF Laboratory Focal Points	84
USAF Laboratory HSAP Mentors	6

All groups indicate unanimous enthusiasm for the SRP experience.

The summarized recommendations for program improvement from both associates and laboratory personnel are listed below:

- A. Better preparation on the labs' part prior to associates' arrival (i.e., office space, computer assets, clearly defined scope of work).
- B. Faculty Associates suggest higher stipends for SFRP associates.
- C. Both HSAP Air Force laboratory mentors and associates would like the summer tour extended from the current 8 weeks to either 10 or 11 weeks; the groups state it takes 4-6 weeks just to get high school students up-to-speed on what's going on at laboratory. (Note: this same argument was used to raise the faculty and graduate student participation time a few years ago.)

## 2. 1996 USAF LABORATORY FOCAL POINT (LFP) EVALUATION RESPONSES

The summarized results listed below are from the 84 LFP evaluations received.

### 1. LFP evaluations received and associate preferences:

Table B-2. Air Force LFP Evaluation Responses (By Type)

Lab	Evals Recv'd	How Many Associates Would You Prefer To Get ?				(% Response)			
		SFRP				GSRP (w/Univ Professor)			
		0	1	2	3+	0	1	2	3+
AEDC	0	-	-	-	-	-	-	-	-
WHMC	0	-	-	-	-	-	-	-	-
AL	7	28	28	28	14	54	14	28	0
FJSRL	1	0	100	0	0	100	0	0	0
PL	25	40	40	16	4	88	12	0	0
RL	5	60	40	0	0	80	10	0	0
WL	46	30	43	20	6	78	17	4	0
Total	84	32%	50%	13%	5%	80%	11%	6%	0%
						73%	23%	4%	0%

**LFP Evaluation Summary.** The summarized responses, by laboratory, are listed on the following page. LFPs were asked to rate the following questions on a scale from 1 (below average) to 5 (above average).

### 2. LFPs involved in SRP associate application evaluation process:

- a. Time available for evaluation of applications:
- b. Adequacy of applications for selection process:
- 3. Value of orientation trips:
- 4. Length of research tour:
- 5. a. Benefits of associate's work to laboratory:  
b. Benefits of associate's work to Air Force:
- 6. a. Enhancement of research qualifications for LFP and staff:  
b. Enhancement of research qualifications for SFRP associate:  
c. Enhancement of research qualifications for GSRP associate:
- 7. a. Enhancement of knowledge for LFP and staff:  
b. Enhancement of knowledge for SFRP associate:  
c. Enhancement of knowledge for GSRP associate:
- 8. Value of Air Force and university links:
- 9. Potential for future collaboration:
- 10. a. Your working relationship with SFRP:  
b. Your working relationship with GSRP:
- 11. Expenditure of your time worthwhile:

(Continued on next page)

12. Quality of program literature for associate:  
 13. a. Quality of RDL's communications with you:  
     b. Quality of RDL's communications with associates:  
 14. Overall assessment of SRP:

Table B-3. Laboratory Focal Point Responses to above questions

	<i>AEDC</i>	<i>AL</i>	<i>FJSRL</i>	<i>PL</i>	<i>RL</i>	<i>WHMC</i>	<i>WL</i>
<i># Evals Recv'd</i>	0	7	1	14	5	0	46
<i>Question #</i>							
2	-	86 %	0 %	88 %	80 %	-	85 %
2a	-	4.3	n/a	3.8	4.0	-	3.6
2b	-	4.0	n/a	3.9	4.5	-	4.1
3	-	4.5	n/a	4.3	4.3	-	3.7
4	-	4.1	4.0	4.1	4.2	-	3.9
5a	-	4.3	5.0	4.3	4.6	-	4.4
5b	-	4.5	n/a	4.2	4.6	-	4.3
6a	-	4.5	5.0	4.0	4.4	-	4.3
6b	-	4.3	n/a	4.1	5.0	-	4.4
6c	-	3.7	5.0	3.5	5.0	-	4.3
7a	-	4.7	5.0	4.0	4.4	-	4.3
7b	-	4.3	n/a	4.2	5.0	-	4.4
7c	-	4.0	5.0	3.9	5.0	-	4.3
8	-	4.6	4.0	4.5	4.6	-	4.3
9	-	4.9	5.0	4.4	4.8	-	4.2
10a	-	5.0	n/a	4.6	4.6	-	4.6
10b	-	4.7	5.0	3.9	5.0	-	4.4
11	-	4.6	5.0	4.4	4.8	-	4.4
12	-	4.0	4.0	4.0	4.2	-	3.8
13a	-	3.2	4.0	3.5	3.8	-	3.4
13b	-	3.4	4.0	3.6	4.5	-	3.6
14	-	4.4	5.0	4.4	4.8	-	4.4

### **3. 1996 SFRP & GSRP EVALUATION RESPONSES**

The summarized results listed below are from the 257 SFRP/GSRP evaluations received.

Associates were asked to rate the following questions on a scale from 1 (below average) to 5 (above average) - by Air Force base results and over-all results of the 1996 evaluations are listed after the questions.

1. The match between the laboratories research and your field:
2. Your working relationship with your LFP:
3. Enhancement of your academic qualifications:
4. Enhancement of your research qualifications:
5. Lab readiness for you: LFP, task, plan:
6. Lab readiness for you: equipment, supplies, facilities:
7. Lab resources:
8. Lab research and administrative support:
9. Adequacy of brochure and associate handbook:
10. RDL communications with you:
11. Overall payment procedures:
12. Overall assessment of the SRP:
13.
  - a. Would you apply again?
  - b. Will you continue this or related research?
14. Was length of your tour satisfactory?
15. Percentage of associates who experienced difficulties in finding housing:
16. Where did you stay during your SRP tour?
  - a. At Home:
  - b. With Friend:
  - c. On Local Economy:
  - d. Base Quarters:
17. Value of orientation visit:
  - a. Essential:
  - b. Convenient:
  - c. Not Worth Cost:
  - d. Not Used:

SFRP and GSRP associate's responses are listed in tabular format on the following page.

Table B-4. 1996 SFRP & GSRP Associate Responses to SRP Evaluation

# res	Arnold	Brooks	Edwards	Eglin	Griffis	Hanscom	Kelly	Kirtland	Lackland	Robins	Tyndall	WPAFB	average
1	4.8	4.4	4.6	4.7	4.4	4.9	4.6	4.6	5.0	5.0	4.0	4.7	4.6
2	5.0	4.6	4.1	4.9	4.7	4.7	5.0	4.7	5.0	5.0	4.6	4.8	4.7
3	4.5	4.4	4.0	4.6	4.3	4.2	4.3	4.4	5.0	5.0	4.5	4.3	4.4
4	4.3	4.5	3.8	4.6	4.4	4.4	4.3	4.6	5.0	4.0	4.4	4.5	4.5
5	4.5	4.3	3.3	4.8	4.4	4.5	4.3	4.2	5.0	5.0	3.9	4.4	4.4
6	4.3	4.3	3.7	4.7	4.4	4.5	4.0	3.8	5.0	5.0	3.8	4.2	4.2
7	4.5	4.4	4.2	4.8	4.5	4.3	4.3	4.1	5.0	5.0	4.3	4.3	4.4
8	4.5	4.6	3.0	4.9	4.4	4.3	4.3	4.5	5.0	5.0	4.7	4.5	4.5
9	4.7	4.5	4.7	4.5	4.3	4.5	4.7	4.3	5.0	5.0	4.1	4.5	4.5
10	4.2	4.4	4.7	4.4	4.1	4.1	4.0	4.2	5.0	4.5	3.6	4.4	4.3
11	3.8	4.1	4.5	4.0	3.9	4.1	4.0	4.0	3.0	4.0	3.7	4.0	4.0
12	5.7	4.7	4.3	4.9	4.5	4.9	4.7	4.6	5.0	4.5	4.6	4.5	4.6
Numbers below are percentages													
13a	83	90	83	93	87	75	100	81	100	100	100	86	87
13b	100	89	83	100	94	98	100	94	100	100	100	94	93
14	83	96	100	90	87	80	100	92	100	100	70	84	88
15	17	6	0	33	20	76	33	25	0	100	20	8	39
16a	-	26	17	9	38	23	33	4	-	-	-	30	
16b	100	33	-	40	-	8	-	-	-	-	36	2	
16c	-	41	83	40	62	69	67	96	100	100	64	68	
16d	-	-	-	-	-	-	-	-	-	-	-	0	
17a	-	33	100	17	50	14	67	39	-	50	40	31	35
17b	-	21	-	17	10	14	-	24	-	50	20	16	16
17c	-	-	-	-	10	7	-	-	-	-	-	2	3
17d	100	46	-	66	30	69	33	37	100	-	40	51	46

#### **4. 1996 USAF LABORATORY HSAP MENTOR EVALUATION RESPONSES**

Not enough evaluations received (5 total) from Mentors to do useful summary.

## 5. 1996 HSAP EVALUATION RESPONSES

The summarized results listed below are from the 113 HSAP evaluations received.

HSAP apprentices were asked to rate the following questions on a scale from 1 (below average) to 5 (above average)

1. Your influence on selection of topic/type of work.
2. Working relationship with mentor, other lab scientists.
3. Enhancement of your academic qualifications.
4. Technically challenging work.
5. Lab readiness for you: mentor, task, work plan, equipment.
6. Influence on your career.
7. Increased interest in math/science.
8. Lab research & administrative support.
9. Adequacy of RDL's Apprentice Handbook and administrative materials.
10. Responsiveness of RDL communications.
11. Overall payment procedures.
12. Overall assessment of SRP value to you.
13. Would you apply again next year? Yes (92 %)
14. Will you pursue future studies related to this research? Yes (68 %)
15. Was Tour length satisfactory? Yes (82 %)

	Arnold	Brooks	Edwards	Egin	Griffiss	Hanscom	Kirtland	Tyndall	WPAFB	Totals
# resp	5	19	7	15	13	2	7	5	40	113
1	2.8	3.3	3.4	3.5	3.4	4.0	3.2	3.6	3.6	3.4
2	4.4	4.6	4.5	4.8	4.6	4.0	4.4	4.0	4.6	4.6
3	4.0	4.2	4.1	4.3	4.5	5.0	4.3	4.6	4.4	4.4
4	3.6	3.9	4.0	4.5	4.2	5.0	4.6	3.8	4.3	4.2
5	4.4	4.1	3.7	4.5	4.1	3.0	3.9	3.6	3.9	4.0
6	3.2	3.6	3.6	4.1	3.8	5.0	3.3	3.8	3.6	3.7
7	2.8	4.1	4.0	3.9	3.9	5.0	3.6	4.0	4.0	3.9
8	3.8	4.1	4.0	4.3	4.0	4.0	4.3	3.8	4.3	4.2
9	4.4	3.6	4.1	4.1	3.5	4.0	3.9	4.0	3.7	3.8
10	4.0	3.8	4.1	3.7	4.1	4.0	3.9	2.4	3.8	3.8
11	4.2	4.2	3.7	3.9	3.8	3.0	3.7	2.6	3.7	3.8
12	4.0	4.5	4.9	4.6	4.6	5.0	4.6	4.2	4.3	4.5
Numbers below are percentages										
13	60%	95%	100%	100%	85%	100%	100%	100%	90%	92%
14	20%	80%	71%	80%	54%	100%	71%	80%	65%	68%
15	100%	70%	71%	100%	100%	50%	86%	60%	80%	82%

Laser Firing Control System

David B. Hernandez

Freeport High School  
Kylea Laird Dr.  
Freeport, FL 32439

Final Report for:  
High School Apprenticeship Program  
Wright Laboratory

Sponsored by:  
Air Force Office of Scientific Research  
Bolling Air Force Base, DC

and

Wright Laboratory

August 1996

## Laser Firing Control System

David B. Hernandez  
Freeport High School

### Abstract

The Instrumentation Technology Branch (MNSI) of the Wright Laboratory Armament Directorate is involved in developing and evaluating new and better ways to accurately depict warhead/target interaction. One of these ways is by developing and making holograms of the warhead as it interacts with a target. Current methods are inadequate in providing reliable data on such things as the fragment mass, shape, orientation, and velocity. A new method that has been developed is a holographic technique to capture 3-dimensional images of the warhead/target interaction and the ensuing results of that interaction. The end product is a cylindrical 3-dimensional image that can be tilted, rotated, and digitally photographed to obtain the best possible image for analysis.

The aim of this project is to develop a computer program that automatically initializes, runs and controls all of the equipment, primarily the ruby pulse laser (see Figure 2 in back), used to capture and record the image of warhead/target interaction onto holographic film. This project is required to provide a good, understandable interface for a user to control the equipment used in the image capturing process. Without this interface, valuable man hours are spent using an old, outdated, and inadequate computer program to control the laser firing control system. The program currently in use is not as effective nor as efficient as a program written in a newer programming language would be in capturing and recording the necessary data of warhead/target interaction. The goal of this project is to update and rewrite the existing interface currently in use as the laser firing control system.

## Laser Firing Control System

David B. Hernandez  
Freeport High School

### Introduction

This project dealt with computer software programming to control a ruby pulse laser and systems for capturing the image of warhead/target interaction onto holographic film. Once the image is recorded onto film, the film is developed and reconstructed with a HeNe laser creating a 3-D image of the event. An electronic camera is then used to digitize a series of 2-D images (see Figure 3 and Figure 4 in back) into a Sun Computer Workstation. These 2-D images are taken from the reconstructed hologram using the electronic camera. After a series of these 2-D images are taken of a single hologram they are then compiled in the Sun Computer Workstation to form a 3-D computed model of the hologram, which depicts a projectile as it penetrates an armor plate. The holograms that are taken clearly show the debris and exactly how the projectile interacts with the armor plate. The objective of this project was to write a program in Visual Basic 4.0 that automatically initializes and controls the ruby pulse laser, and all of the equipment used to capture and record the image onto holographic film. Once this objective is accomplished the setup is to be used to analyze a projectile's effectiveness in flight.

### Discussion of Problem

The problem was that there was no main computer program that provided an efficient means to initialize and control the ruby pulse laser and the laser firing control system. The program that was being used was in severe need to be updated to modern standards. What needed to be done is the current program had to be totally rewritten, modified, and redesigned in order to provide an easy to use interface for the user. This would provide a more effective, and accurate means for controlling the laser firing control system.

Currently the way the program already in use works is it would only charge the laser and then fire the laser when indicated by the user. The program needed to be made more versatile and dynamic. Options such as firing the laser several times to record multiple images onto a single piece of film needed to be included into the main program. There was also a need to give more control over the delay between each pulse shot of the laser. All of these options and several others need to be included into the program in order to more accurately capture and record fragmentation data.

### Methodology

The first objective of my research project this summer was to learn Visual Basic 4.0. Visual Basic is a graphic user interface (GUI) programming language used primarily in a windows based environment. Toward this endeavor I was given a hands-on tutorial book on Visual Basic 4.0. It was filled with examples of code and many source utilities designed to teach someone completely ignorant of Visual Basic how to program well with Visual Basic. For the next couple of weeks I worked my way through the tutorial book in order to learn how to program with Visual Basic. Once I completed the tutorial book I was proficient enough at programming with Visual Basic to begin rewriting the laser firing control program that was being used.

The goal at this time was to completely rewrite the current program using Visual Basic instead of the original programs QBasic. This program was to be written so that it automatically initialized the ruby pulse laser and went through the steps to set-up the laser firing control system in order to record images onto holographic film which would later be reconstructed at the holographic research facility (Bay 10).

The holograms at Bay 10 (see Figure 1 in back) were made using the ruby pulse laser that has a wavelength of 694 nm. The film that is used to capture the image is first cut and placed in a cylinder 180 degrees around the cylinder. The cylinder is then placed in front of the projectile launcher so that when the projectile is fired it's flight path would take it straight through the center of the cylinder. A single pulse from the ruby pulse laser is then shot to record the image of the projectile as it penetrates the target, normally an armor plate. Each time the ruby pulse laser sends a pulse of laser light into the chamber it captures an image onto the film. Sometimes two or more pulses of laser light are fired creating an overlap effect that shows the projectile a number of times equal to the number of pulses fired (i.e. two pulses shows the projectile twice on one piece of film; Figure 4 was made with two pulses of laser light). Multiple pulses are used to help calculate the projectile's velocity and position when the laser was fired.

As the laser light floods the area within the cylinder, the laser light reflects off of the projectile, the armor plate and all the debris generated from that interaction. The light reflected from the projectile and the debris is called the object beam and as it reflects back it interferes with the incoming laser light, called the reference beam. This interference is captured on the film and is what creates the hologram. A hologram is simply a 3-D representation of an object using light waves to reconstruct the image by the interference of an object beam and a reference beam. Once the hologram is developed and viewed the debris from the warhead/target interaction can be clearly seen and analyzed.

The following is a list of equipment that was used for this project. The ruby pulse laser, with a wavelength of 694 nm, is used to capture and record an image onto holographic film in order to later view the reconstructed hologram. The electric camera is used to take 2-D black and white pictures of the reconstructed hologram so the debris from the armor plate can be seen. The rotary turn table is used to rotate the hologram, and the XY stepper motion control is used to move the camera along the XY axis. The Visual Basic 4.0 program was written on a 486 DX2/33 PC, and the Sun Computer Workstation is used to compile all of the 2-D pictures taken of the hologram into a 3-D computed model to view the placement of debris from the armor plate and collect other essential data.

### Results

The results of this project are that the programming language Visual Basic 4.0 was learned, preliminary testing of the program to see if it would work as an effective interface for controlling the ruby pulse laser has been completed, and the actual use of the program can now be initiated. The final computer program that was written in Visual Basic 4.0 is able to control the ruby pulse laser, and the equipment used to charge the laser. The setup that was designed should work quite well. This setup will be used to capture the image of a projectile as it interacts with a target armor plate. It can now be used more effectively to analyze and compile the data gathered from images recorded onto film.

### Conclusion

The conclusion of this project is that the program I wrote provides a good, solid interface for controlling the ruby pulse laser. The program can be used as the control for the ruby pulse laser and all of the equipment used to set-up the laser, charge the laser, and then proceed through the firing sequence. However, due to the fact that I was unable to test this program more thoroughly with the ruby pulse laser because I was not cleared to actually fire or work with the laser the program is, as yet, not as effective as it could be in running the laser firing control system. I have documented what add-ins I feel would prevent any problems with the program and my ideas and suggestions to make this program run smoother in case there are any difficulties with the set-up. Complete testing of this program and set-up system are pending with the clearance of my mentor, David Watts, and his colleague, Joseph Gordon to work and operate the ruby pulse laser.

# HOLOGRAPHIC RESEARCH AREA (BAY 10)

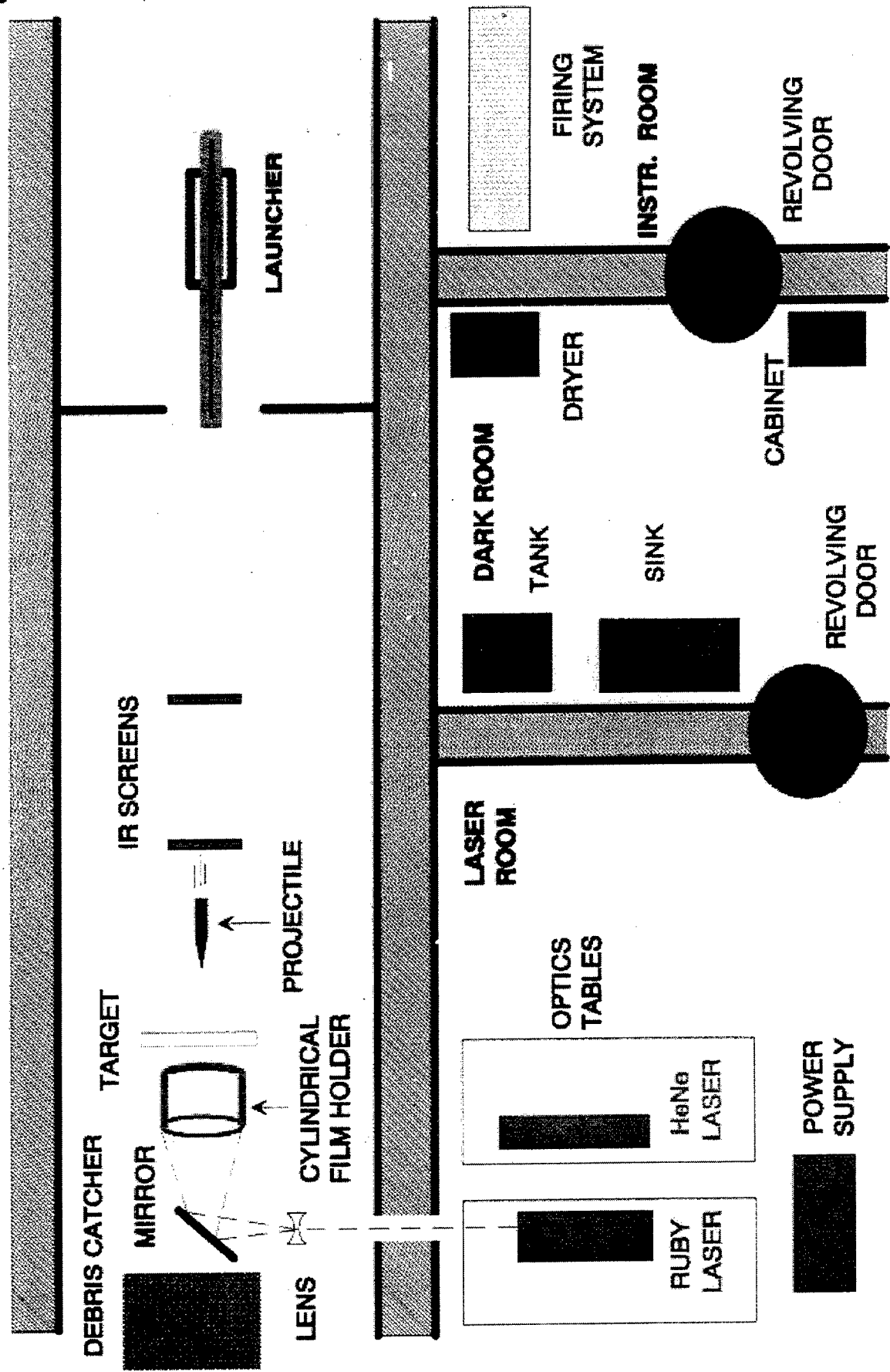
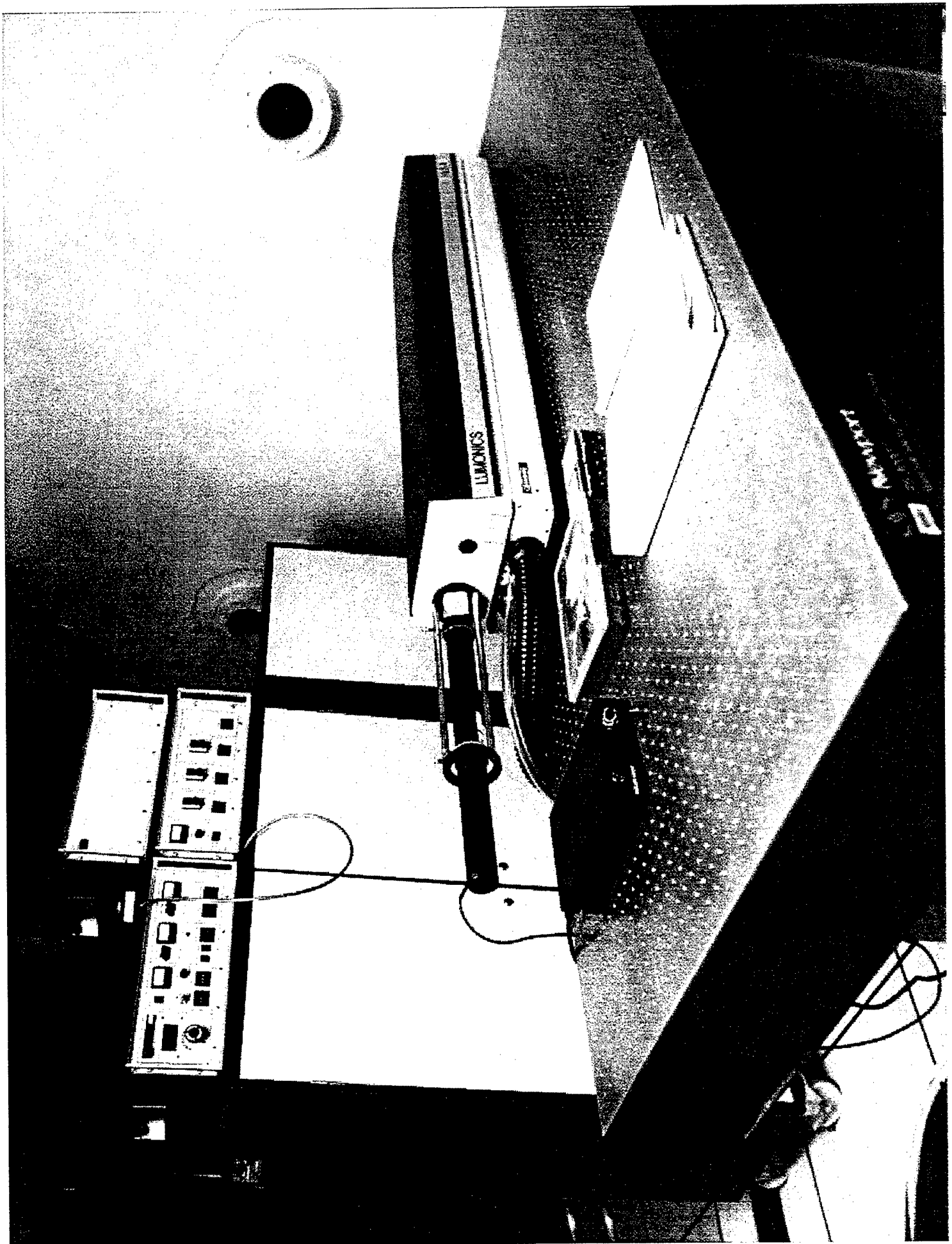


Figure 1. Holographic Research Area



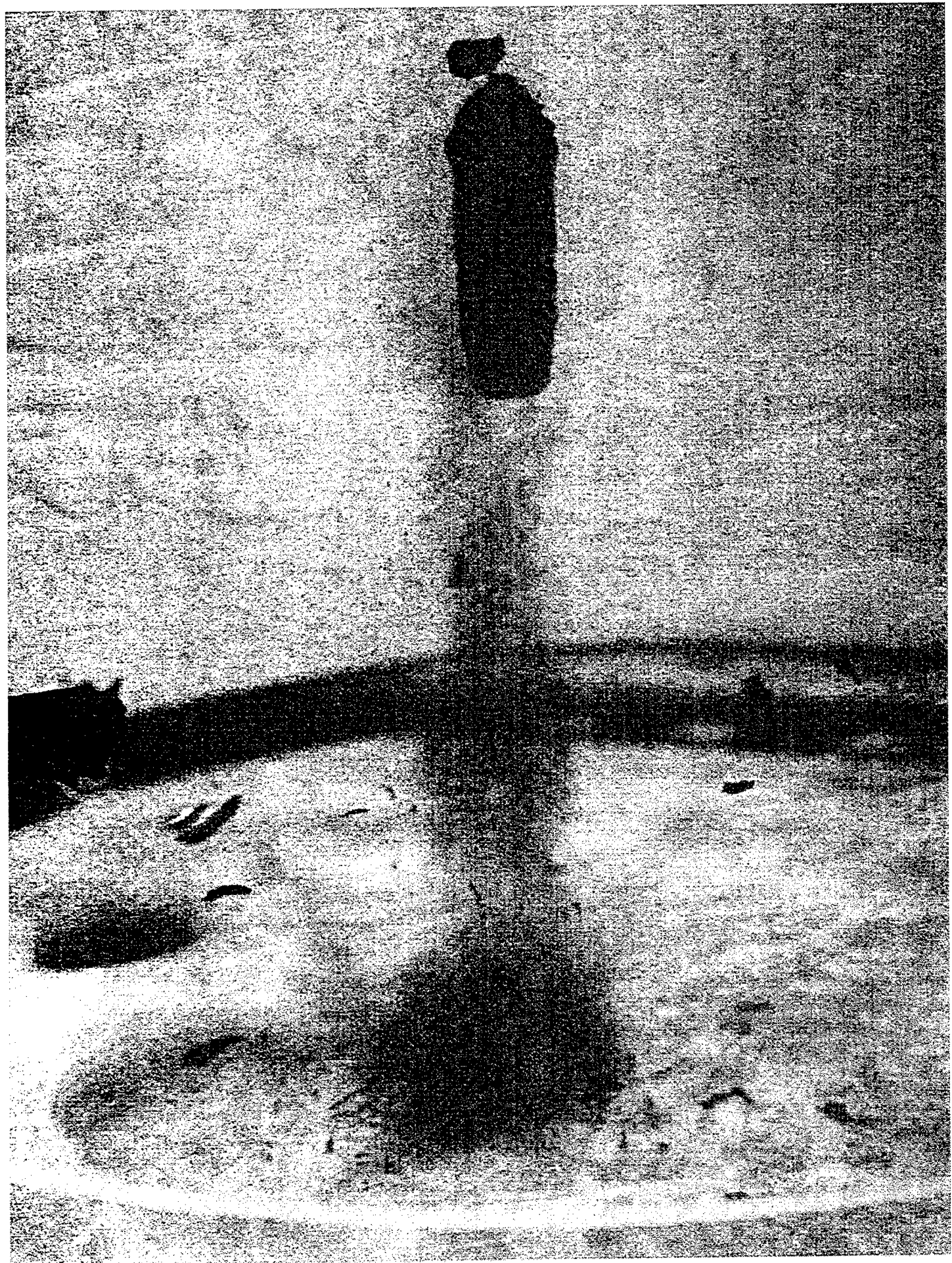
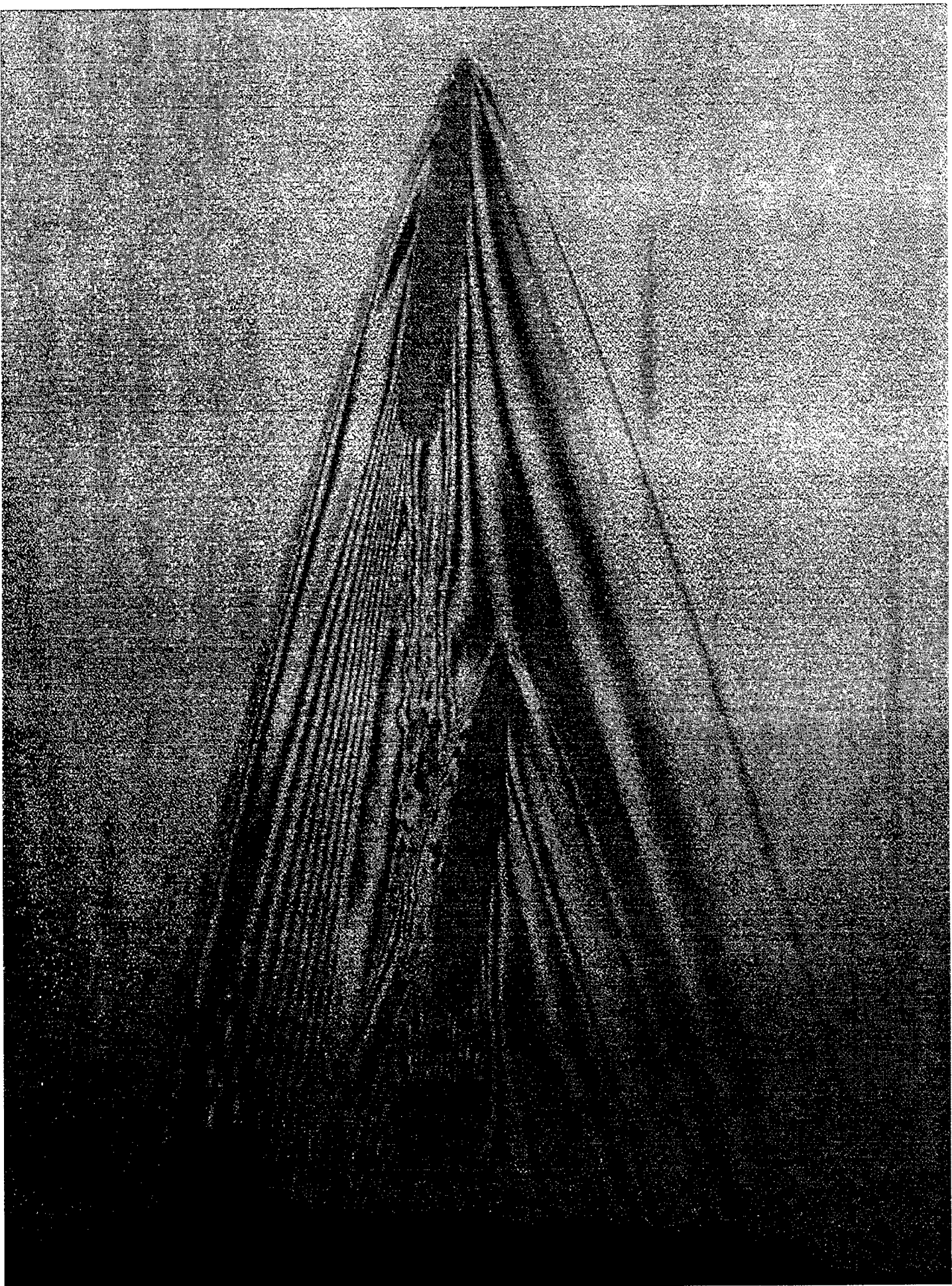


Figure 3. Cylindrical Hologram of 50 Cal. Projectile Perforating Armor

Figure 4. Cylindrical Hologram of 50 Cal. Projectile made with Two Pulses



### Acknowledgments

I would like to thank the following people for their help and support this summer: David Watts, my mentor, who kept me focused; Joseph Gordon, who was always there to lend advice and who taught me all about lasers; Kristan Raymond; for helping me with my presentation in Power Point; Josh Weaver, Daniel Holmes, Doug Ritchie, and Christopher Clark, for helping me with my program; Don Harrison and Mike Deiler, for coordinating the HSAP Program and giving high school student's the opportunity to be involved in such a rewarding experience; and everyone in my branch, MNSI, for their support.

AN INVESTIGATION INTO RED DYE CONTAMINATION  
OF AVIATION FUEL

Anna Solveig Hill

Carroll High School  
4524 Linden Ave.  
Dayton, OH 45432

Final Report For:  
High School Apprentice Program  
Wright Laboratory

Sponsored by:  
Air Force Office of Scientific Research  
Wright-Patterson Air Force Base, OH

and

Wright Laboratory

August 1996

AN INVESTIGATION INTO RED DYE CONTAMINATION  
OF AVIATION FUEL

Anna Solveig Hill  
Carroll High School

ABSTRACT

Research was conducted to investigate how red dye contamination in aviation fuel affects the thermal stability of the fuel. A thermal oxidized test was performed on aviation fuel with and without the dye contamination by researchers in the fuel industry. The data was collected by an international coordination council. Several samples were run with different concentrations of dye and each sample's breakpoint temperature, test pressure, and color was recorded. An analysis of the data showed that the dye may not be the sole factor in the degradation of the thermal stability. High sulfur levels acquired from diesel fuel traces, or carbon and/or dye deposits left on the filter may be responsible for the lower breakpoints of the fuel.

## TABLE OF CONTENTS

Title Page	29-1
Abstract	29-2
Table of Contents	29-3
Introduction/ Discussion of Problem	29-5
Methodology	29-4
Results	29-6
JFTOT Breakpoint Results (Texaco)	29-7
JFTOT Breakpoint Results (Amoco)	29-8
JFTOT Breakpoint Results For Undyed Fuel (Amoco)	29-9
JFTOT Breakpoint Results For 2.5% Dyed Fuel (Amoco)	29-10
JFTOT Breakpoint Results For 0.5% Dyed Fuel (Amoco)	29-11
JFTOT Breakpoint Results For 0.5%* Dyed Fuel (Amoco)	29-12
Conclusion	29-13
References	29-15

# AN INVESTIGATION INTO RED DYE CONTAMINATION OF AVIATION FUEL

ANNA SOLVEIG HILL

## INTRODUCTION/ DISCUSSION OF PROBLEM

Due to recent pollution concerns, the EPA requires low sulfur diesel fuel in some states and encourages its use in others. In order to visually determine the difference between the high and low sulfur diesel fuel a red dye was added. This action was supported by the IRS who taxed the high sulfur diesel fuel use. The dye used is DPM 5160-1 Red Dye, which is similar to the Active Solvent Red 164 Dye that the Air Force used to detect leaks on the grounded aircraft, but the dye was never approved for flight.

The problem developing right now is the red dye, being used in the high-sulfur diesel fuel, is showing up in aviation fuel. Since the pipe line companies use the same pipes for all fuel types, some of the DPM 5160-1 Red Dye is either sticking to the pipe walls and getting picked up in the aviation fuel or the pipeline companies are not thoroughly cleaning out the pipes and traces of dyed diesel fuel are contaminating the aviation fuel.

Airlines were concerned whether or not they could fly with dyed fuel. The engine companies had reached a general consensus as of April 1996. They agreed to have either a zero tolerance for the contaminated fuel or to allow only emergency use of the tainted fuel if it was retested to ASTM D1655, the aviation fuel specification, met all specification requirements, and contained less than of 2.5% dye. However, the companies are performing different types of tests to determine if the dyed fuel is safe for flying. The military will not allow the use of red dyed aviation fuel for flying.

## METHODOLOGY\*

"Standard Test Method For Thermal Oxidation Stability of Aviation Turbine Fuels (JFTOT Procedure)," was used for rating the tendencies of fuel to deposit oxidative decomposition products within the fuel system. The test method was developed to simulate conditions present in real aircraft systems. To summarize the test procedure, approximately 600 mL of jet fuel is filtered, aerated, and then sealed in the JFTOT reservoir. After pressurizing the JFTOT system with nitrogen, the fuel is pumped at a constant flow rate over a resistively heated aluminum heater tube and through a precision stainless steel filter for a given period of time. At the end of the test, the aluminum heater tube and pressure change across the filter are evaluated for decomposition products. Test conditions for the various fuels have been established in both commercial and military specifications. For commercial Jet A fuel, ASTM D 1655, states the evaluation of the aluminum heater tube may be performed by a tube deposit rater (TDR) or visual comparison to ASTM color standard. A TDR rating measures the maximum difference in reflected light from the aluminum heater tube before and after the test. The JFTOT test conditions for commercial Jet A Fuel are a heater tube temperature of 260° C, a system pressure of 3.45 MPa (500 psi), a fuel flow rate of 3.0 mL/min., and a test duration of 150 min.

\*This methodology was developed by Patricia D. Liberio, Chemical Engineer at Wright-Patterson AFB, Dayton, OH.

## RESULTS

ALL DATA COURTESY OF TEXACO, DEC. 1995  
AND AMOCO, FEB. TO APRIL 1996

ALL JET A FUEL NOT THE SAME; EACH COMPANY SUPPLIED  
IT'S OWN AVIATION FUEL

DIESEL FUELS PREPARED BY HOWELL HYDROCARBONS

# JFTOT BREAKPOINT RESULTS

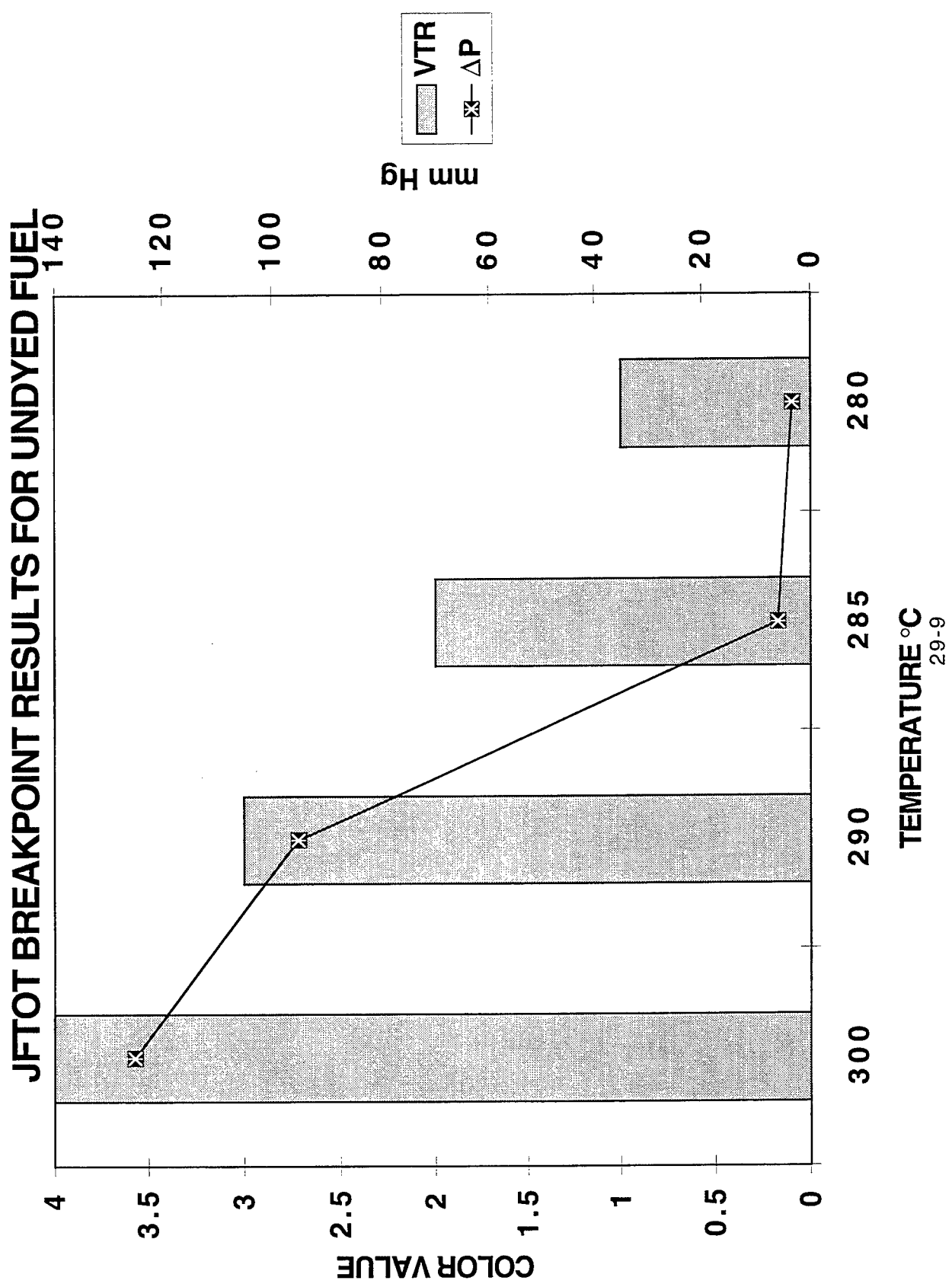
FUEL	T°C	VTR	ΔP, PSI
1. Avjet A	285	<1	0.1
	290	<4P	0.1
2. Avjet A + 0.40mg/L red dye (0.14 PTB)	280	<1	0
	285	<3P	0.1
3. Fuel 2+2.5 (v)% undyed, high sulfur No. 2 diesel fuel	290	<4P	0
	235	<1	2.8
	240	<1	12.5
(test shut down)			Breakpoint

The concentration of dye (0.40mg/L =0.14 PTB) in sample No. 2 was not great enough to cause a degradation in the thermal stability of avjet A. However, in sample No. 3 the JFTOT breakpoint was decreased 50° C due to the dilution of the dyed fuel.

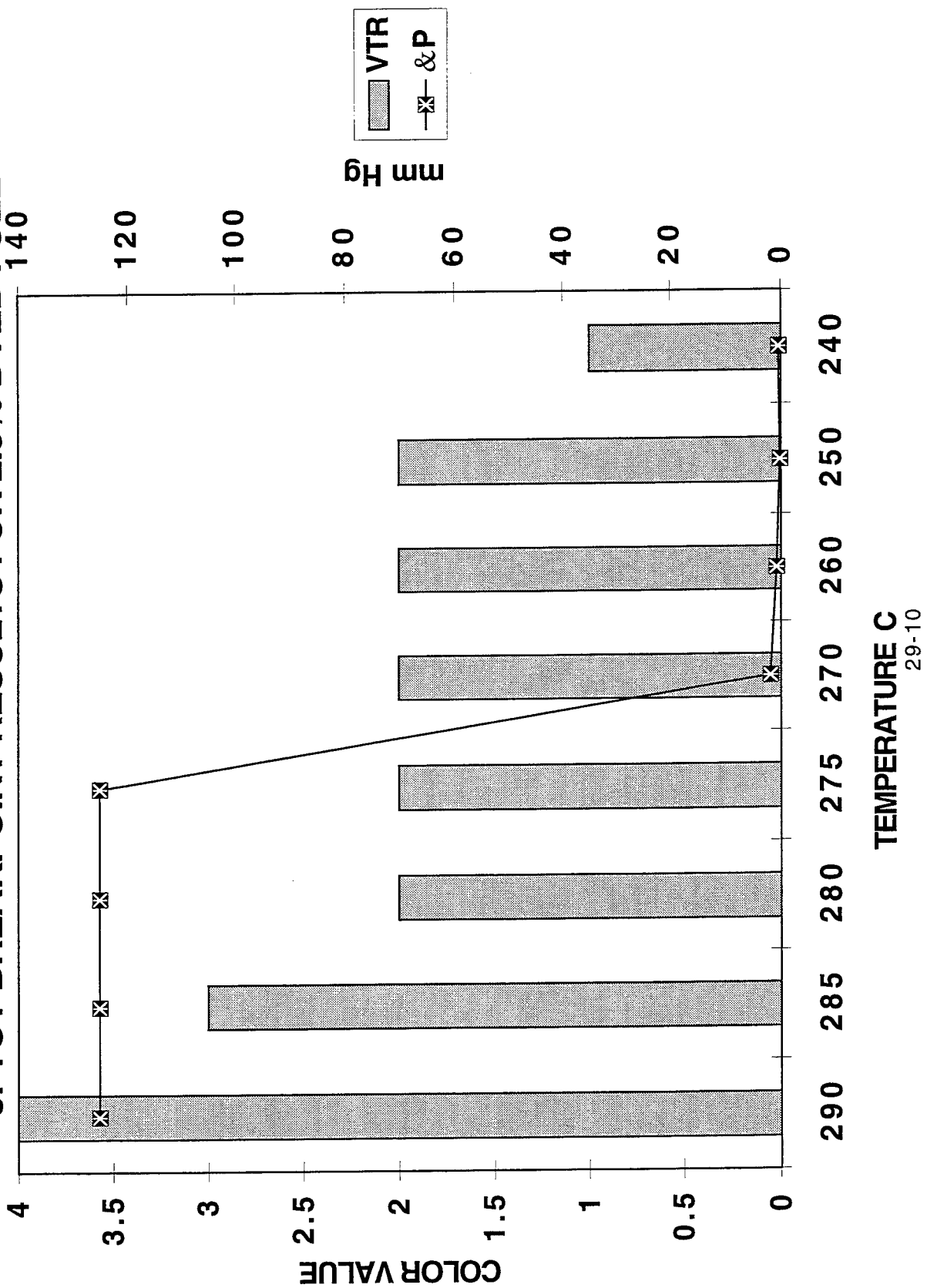
Avjet A = Jet A

# JFTOT BREAKPOINT RESULTS

FUEL	% DYE	T ° C	VTR	ΔP, mm Hg
Jet A	0	300	4	>125
Jet A	0	290	<3	95.1
Jet A	0	285	<2	5.9
Jet A	0	280	<1	3.2
Jet A	2.5	290	4	>125
Jet A	2.5	285	<3	>125
Jet A	2.5	280	2	>125
Jet A	2.5	275	<2	>125
Jet A	2.5	270	<2	1.8
Jet A	2.5	260	<2	0.7
Jet A	2.5	250	<2	0.1
Jet A	2.5	240	1	0.4
Jet A	0.5	290	4	>125
Jet A	0.5	280	<3	>125
Jet A	0.5	270	<2	>125
Jet A	0.5	260	<2	>125
Jet A	0.5	255	1	0.4
Jet A	0.5	250	1	0.1
Jet A	0.5*	275	<2	9.4
Jet A	0.5*	270	<2	2.8
Jet A	0.5*	260	<2	0.2
*Condition repeated with new dye solution blend, same base fuel				

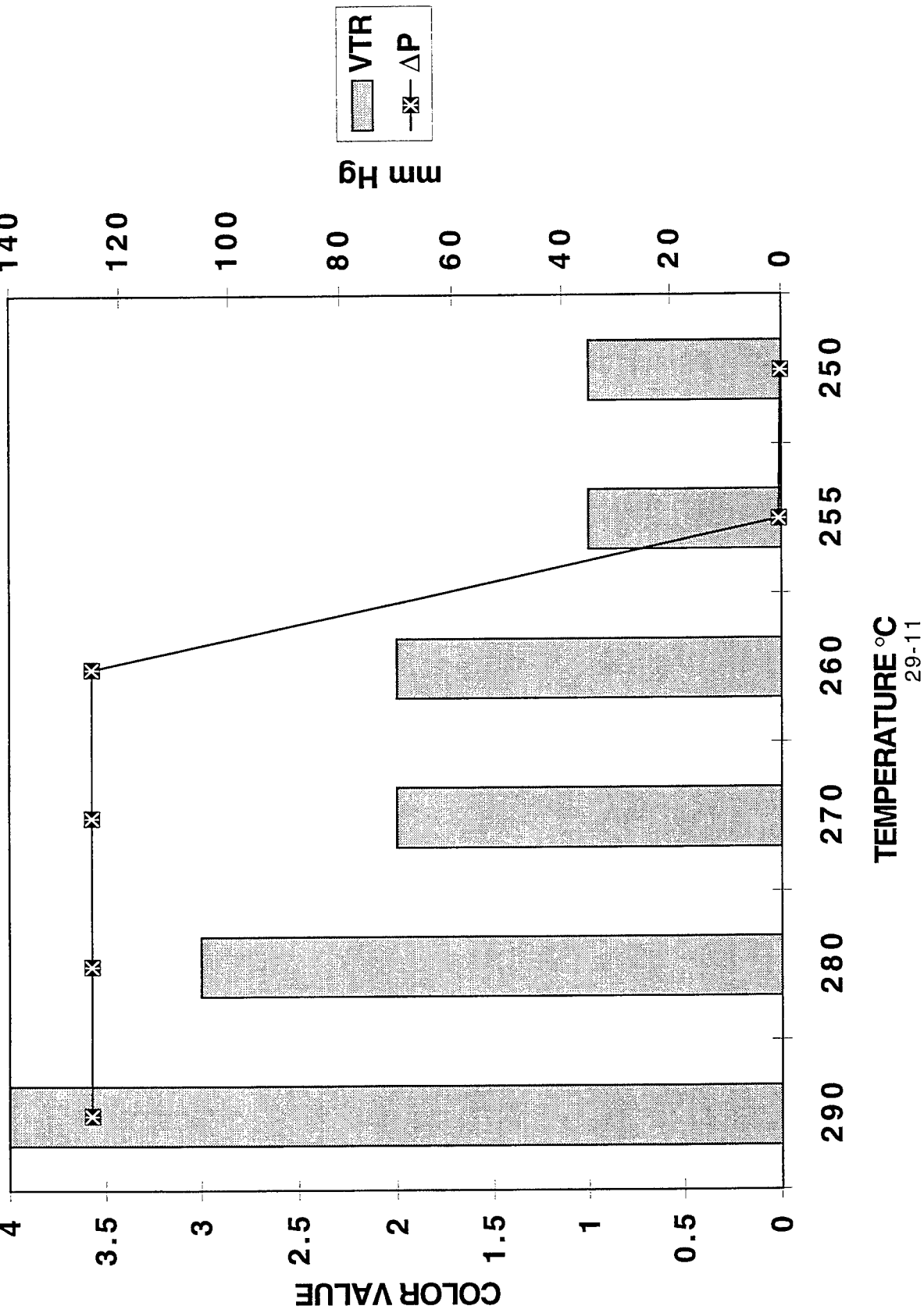


# JFTOT BREAKPOINT RESULTS FOR 2.5% DYED FUEL<sub>140</sub>



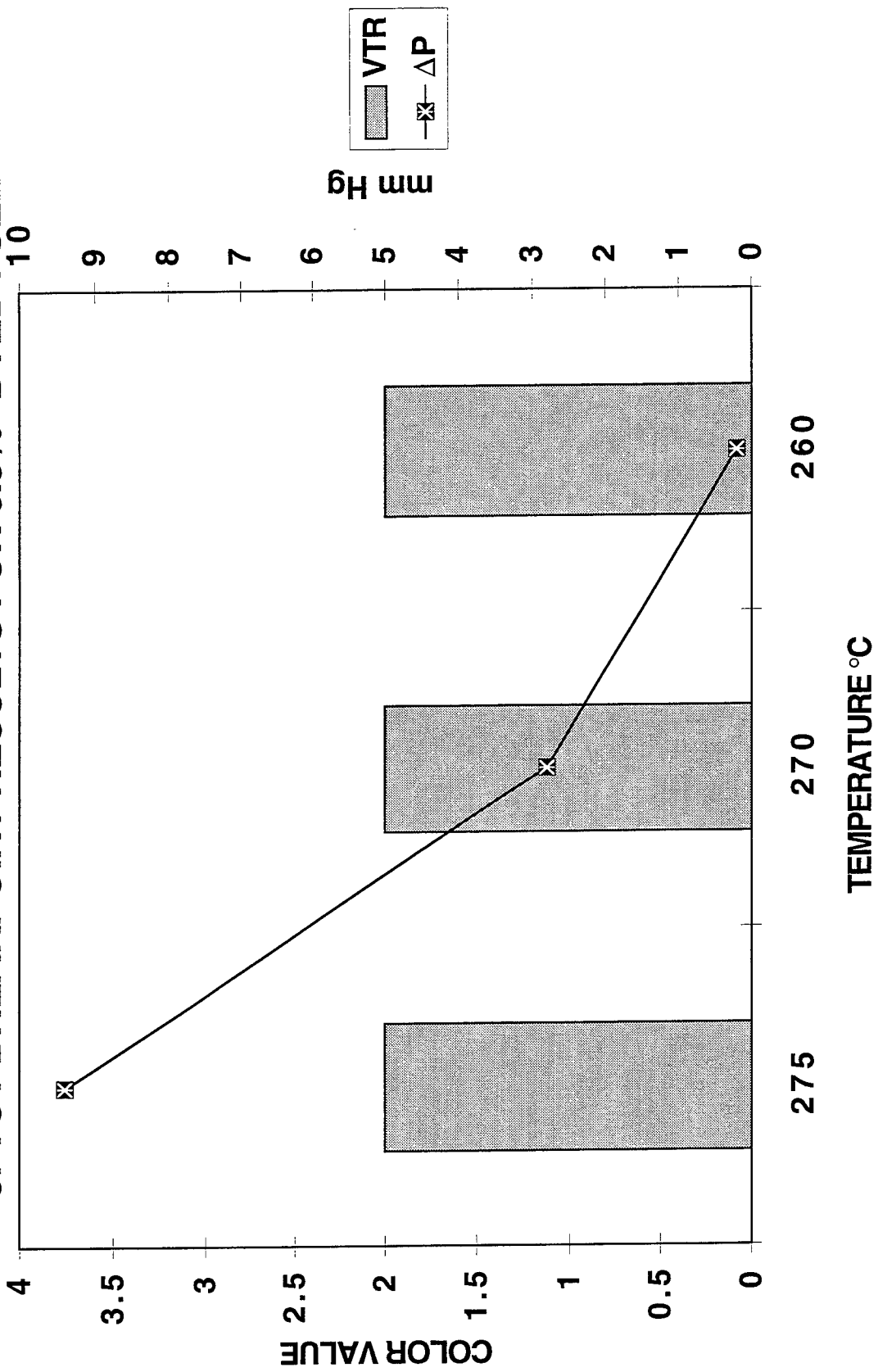
TEMPERATURE C  
29-10

# JFTOT BREAKPOINT RESULTS FOR 0.5% DYED FUEL



29-11

# JFTOT BREAKPOINT RESULTS FOR 0.5%\* DYED FUEL



\*Condition repeated with new dye solution blend, same base fuel

29-12

## CONCLUSIONS AND RECOMMENDATIONS

The combined efforts of the Coordinating Research Council along with Texaco Inc. and Amoco Research and Development gave supportive evidence to the following conclusions: The results from Chart #1 (Texaco) indicated that the avjet A's thermal stability was not degraded because of the dye, but rather was degraded as the result of the addition of high sulfur diesel fuel. Sample number 2 produced a slightly lower breakpoint temperature than the pure avjet A (sample number 1). However, when diesel fuel was added to the pure aviation fuel, the breakpoint temperature decreased dramatically by 50°C. This suggested that the sulfur level was the primary reason for the deterioration of the thermal stability in the jet fuel.

Even though the diesel fuel contamination affected the breakpoint of the aviation fuel during the JFTOT testing, it may not be the only factor reducing thermal stability. From data gathered by Amoco, the solubility of the dye in the fuel was questionable. Some samples of the Amoco data failed due to an unexpected increase in pressure. Possible reasons for this are particles of either dye or carbon have dropped out of the fuel and deposited onto the filter, thus causing an increase in the pressure or the dye is affecting fuel chemistry. From the Amoco data the dyed fuel failed  $\Delta P$  at a lower temperature than failure a visual rating. Most fuels fail visual at lower temperature than  $\Delta P$  failure. Further study of why  $\Delta P$  fails before the visual rating fails needs to be conducted. Recommendations for this would be to test the filter deposits for traces of dye or carbon in order to determine whether the pressure increase was caused by dye, carbon, or some other compound from the fuel.

Analyzing the data from both Amoco and Texaco upheld the hypothesis that dyed fuel would have an adverse effect on the thermal stability but not to the extent as anticipated. What has now come to light is that high sulfur diesel fuel is possibly the main contaminant in the aviation fuel. The source of contamination could be dyed diesel fuel or dye is adhering to the pipe walls. Once the source is established the companies should try to eliminate or decrease the amount of contamination. Further research should be conducted in order to distinguish between the problems

caused by the dye as opposed to the sulfur contamination. Research is currently being done in the form of an engine component test in order to determine long term effects of dye on the fuel system materials.

REFERENCES

CRC Group on Dye in Diesel Fuel, Minutes, Atlanta, GA, Dec. 6,1994

Dye In Aviation Turbine Fuel Group, Unconfirmed Minutes, Indianapolis, IN, June 20, 1995

Dye In Aviation Turbine Fuel Group, Unconfirmed Minutes, Chicago, IL, Oct. 11,1995

Dye In Aviation Turbine Fuel Group, Unconfirmed Minutes, Houston, TX, Dec. 5,1995

Group on Dye In Aviation Turbine Fuels, Unconfirmed Minutes, Chicago, IL, Oct. 26, 1994

Group on Dye In Aviation Turbine Fuels, Unconfirmed Minutes, Alexandria, VA, April 26,1995

Personal Communications, from Booth, Dr. David L., April 29, 1994

Personal Communications, from Harrison, William E. III, Oct .25, 1994

Personal Communications, from Makris, Nick, March 7, 1996

Personal Communications, from Makris, Nick, Feb. 9, 1996

Personal Communications, from Oppenheim, Lee Feb. 9, 1996

Personal Communications, from Zengel, Alan E., May 25, 1995

Zengel, Alan E., IASH, Newsletter No. 17, "Dyed Fuel Group", pg. 6, Feb. 1996

## **The EPIC Penetration Event Generator (EPEG)**

Dann Holmes

Mentor: Michael E Nixon

Niceville High School

800 E. John Sims Pkwy.

Niceville, FL 32578

Final Report for:

High School Apprentice Program

Wright Laboratory

Sponsored by:

Air Force Office of Scientific Research

Bolling Air Force Base, DC

and

Wright Laboratory

August 1996

## The EPIC Penetration Event Generator (EPEG)

Dann Holmes

### **Abstract**

My project this summer was to write a graphical user interface (GUI) for the EPIC hydrocode. To do this, I had to write a program for Windows in Visual Basic 4.0. The program that I wrote makes it easy to set up a typical penetrator/target scenario. By having only the most important and useful options that an EPIC user needs, the program expedites the input creation process. The program that I wrote successfully creates an input deck that any user could use to model a scenario. Hopefully in the future, I can expand upon this program and make it more robust, with more options and scenarios.

## Introduction

This summer, my project was to develop a graphical user interface (GUI) for the EPIC hydrocode. EPIC is a penetration and explosion modeling program developed for Wright Laboratory. Such a GUI is useful for EPIC because information the user wants to pass to EPIC has to be in a structured and archaic form, as illustrated in Figure 1.

```
$ RESEARCH EPIC EXAMPLE 3 - PROJECTILE NORMAL IMPACT AND TARGET PERFORATION
$ 
$TYPE CASE....DESCRIPTION.OF.PROBLEM.....  
2 3 EXAMPLE 3 - 2D NORMAL IMPACT AND PERFORATION  
$GEOM PRNT SAVE NSLD NMAS NRST NRIG NCHK NOCK SCATpcRTZ SPLT DP3 UNIT//// PER  
6 0 1 2 0 0 0 1 0 03 0 0 0 0  
$MATL 0 DAM FAIL DFRC EFAL solids from library  
1 0 1 1 1.0 999. $  
23 0 1 1 1.0 999. $  
$ BLANK FOR END OF MATERIALS  
$ PROJECTILE NODES  
$ X/RSCALE YSCALE ZSCALE X/RSHIFT ZSHIFT ROTATE SLANT X/R0 Z0  
1.0 0.0 1.0  
$ ROD NODES  
$ 2 NOR NIR NPLN RAD AX CROS JOIN N1 NTOP ZTOP ZBOT EXPAND  
2 5 0 17 1 0 1 0 1 0 2.5 0.5 1.0  
$ ROTOP RITOP ROBOT RIBOT  
0.5 0.0 0.5 0.0  
$ NOSE NODES  
$ 3 TYPE NOR NIR RAD AX CROS//// N1//// ZTOP ZMIN  
3 2 5 0 1 0 1 183 0.5 0.0001  
$ ROTOP RITOP  
0.5 0.0  
$ BLANK FOR END OF PROJECTILE NODES
```

Figure 1

Due to this format, it can be difficult and time consuming for a beginning or intermediate EPIC user to construct an input deck. My program, the EPIC Penetration Event Generator (EPEG), expedites this process by having a pre-set format that is used to calculate and export the data into an EPIC-readable form. This format is a basic penetrator/target scenario, with several options available. Although the output generated by EPEG can be used for quite plausible scenarios, by using this program, a person can save time by setting up a basic problem with the program, and then fine-tuning it to his or her needs.

After this introduction screen, Figure 2, the user sees the general information menu. (Figure 3) At this screen, the user makes a few choices about how he wants the program to run, its name, and gives it a specific case number. From this screen, the user chooses whether he wants a penetrator with or without a payload, or a solid penetrator. After a penetrator type has been chosen, the program goes to the appropriate form, and waits for input. At this screen the dimensions of the penetrator are set using corners as guides, as seen in Figure 4 and 5. These screens are the penetrator with payload and solid-bodied penetrator screens, respectively. Also on these screens are the materials for the penetrator and the option of crossed or uncrossed elements. After the dimensions of the penetrator have been set up, the program goes to the target form (Figure 6), where the target dimensions are set in a similar manner. Then after all the data has been entered, the user can click on the export button and choose a file name. The data is then calculated and exported to a file as a working EPIC input deck. An example of an EPEG input deck is contained in Appendix A

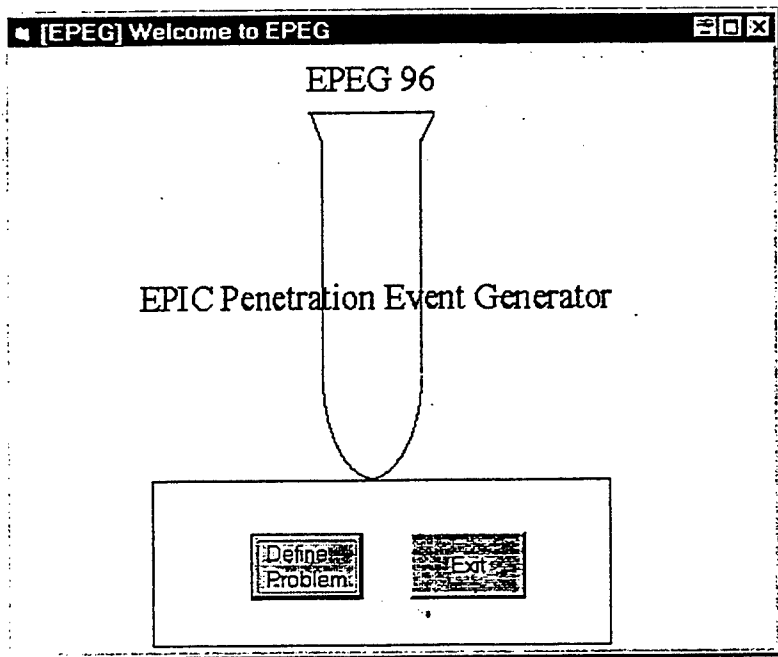


Figure 2

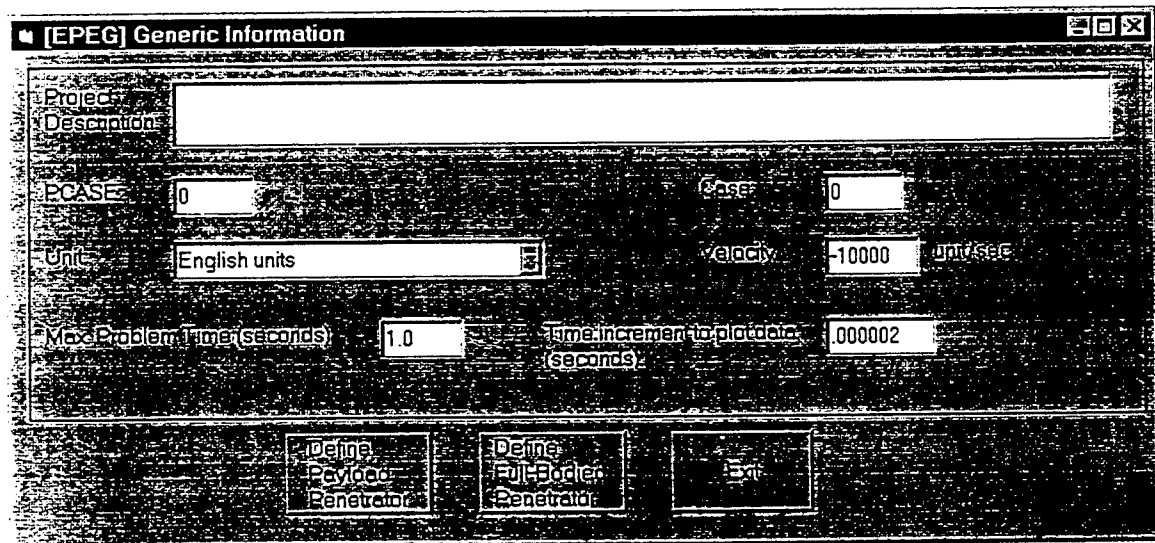
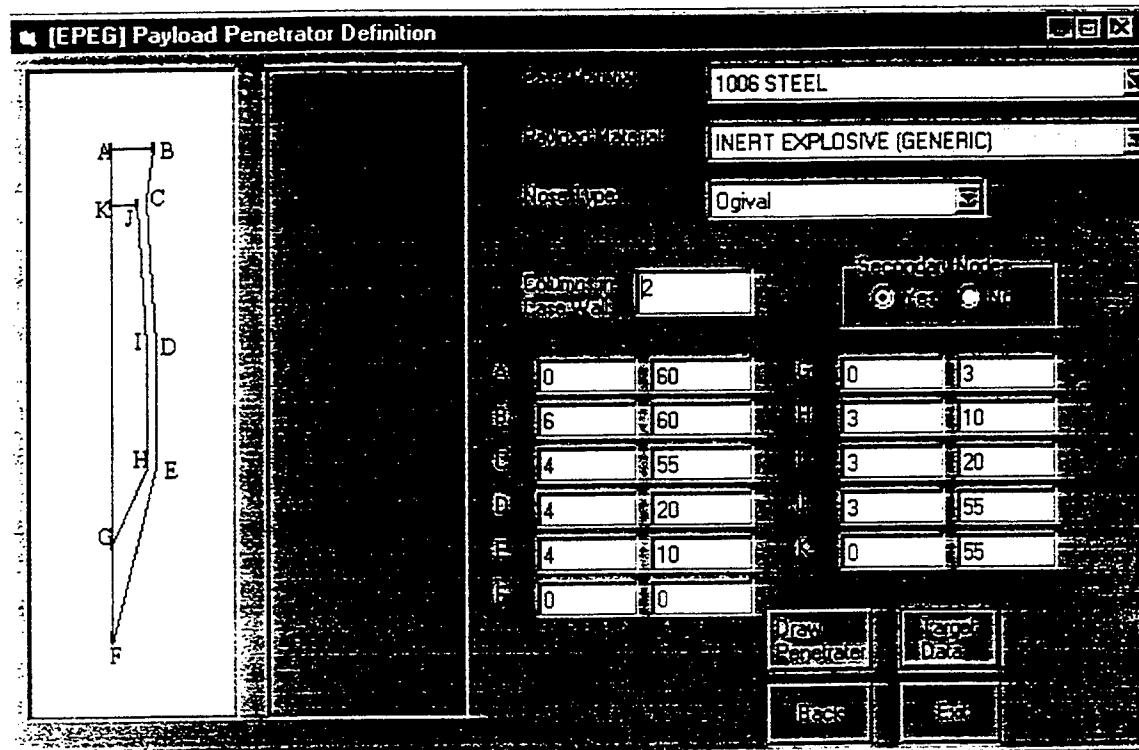
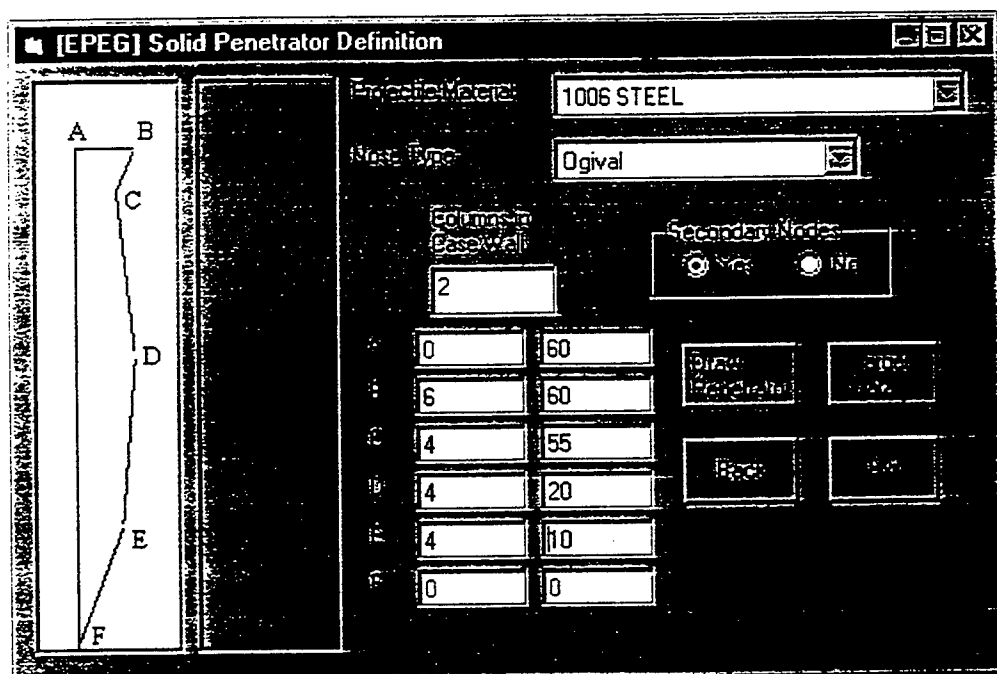


Figure 3



**Figure 4**



**Figure 5**

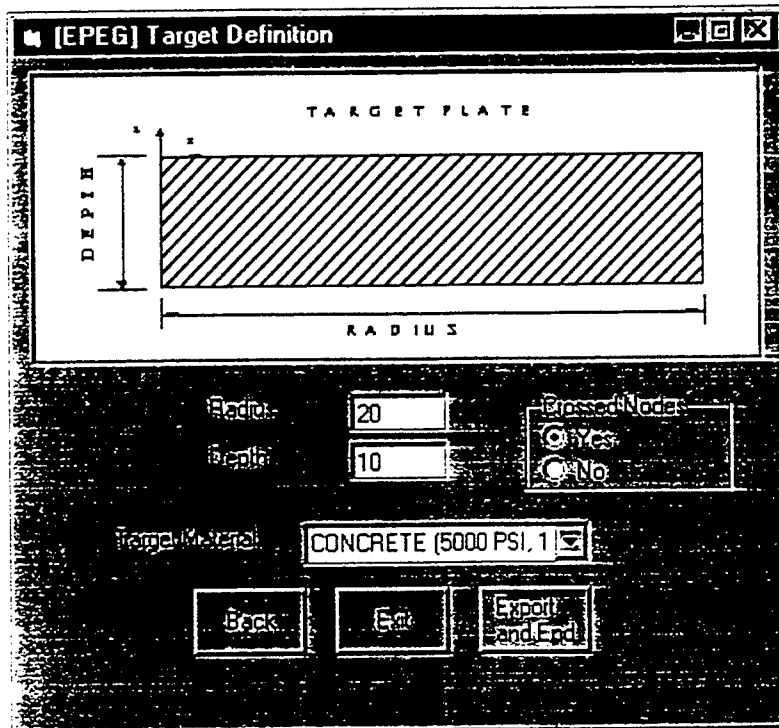


Figure 6

### Equipment used

Gateway 486DX/66 IBM compatible computer with Windows 95

Unisys 386DX/20 IBM compatible computer with DOS 6.22 and Windows for Workgroups 3.11

SGI Indy 150 MHz RISC-based workstation with IRIX 5.3

SGI Indigo 33 MHz RISC-based workstation with IRIX 5.3

Research EPIC for SGIs

Visual Basic 4.0 programming language

lots and lots of soda

### Methodology

Before creating this program, I had to first understand the way that a user would pass data to EPIC, as well as understanding the way that EPIC determined node numbers. Figure 1 shows a portion of a typical EPIC input deck. It is easy to see that such a file would be hard to create for an inexperienced EPIC user. Also, this input format is very dynamic, and any GUI written for EPIC must be able to handle many different possibilities. As more options are added to a GUI, the program becomes more and more complex. If too many options are implemented, the program becomes so difficult to use that setting up the EPIC input file would be an easier task to complete. A medium had to be reached so that a user could easily set up an input deck that was close to or exactly what he or she wanted. Figure 3, 4 and 5 show the general information screen and the two different penetrator screens, respectively. These screens allow the user to define the simple projectile information. Overall, this format seemed to be the easiest to user, as well as being concise, while still offering a few of the EPIC options, including nose types, different materials, and crossed and uncrossed element formats. This form also asks the user to input the number of columns of elements in the case wall. The number of columns of elements in the case wall is important in that it defines the relative size of the problem.

The target form is laid out in a similar manner, as seen in Figure 6. This form includes options for radius, depth, and materials.

## **Results**

This was programmed in Visual Basic, an easy-to-learn GUI builder for Windows 3.1 and Windows 95. The program was re-written many times, as it became apparent that certain ways of doing things would be easier to understand and use than others. The two most difficult parts of programming this were in the areas of formatting the output and calculating the node numbers. The formatting of the output was greatly facilitated by the Fwrite routine, which was written by Josh Weaver. This routine allows a person to input a string classifying how the variables are to be written out and, when passed the variables, will output them in a format that follows with EPIC's input structure. The other challenge in programming this GUI was calculating the number of nodes. Many different formulas were tried while calculating this, but, by modifying them a bit, the ones in the EPIC user manual turned out to be the easiest to implement. After much trial-and-error, a working formula was obtained. After getting the node numbers correct, the other options were relatively simple to add.

Although the program does not have as many options as it possibly could, it is now a working GUI for EPIC. Possible future options could include: a menu to define your own material, options to define nodes and elements to be checked at runtime, as well as going into more detail in defining the projectile and target. Currently it is quite possible to go into EPEG with a sketch of a penetrator's geometry and knowing the materials, and within 5 minutes have a working EPIC input deck.

**Thanks to:**

Michael E Nixon

Don Harrison and Mike Deiler

all of WL/MNNMW

Josh Weaver

all the other HSAPs

## Appendix A

```
$TYPE CASE....DESCRIPTION.OF.PROBLEM.....  
2 1Sample Problem 1  
$GEOM PRNT SAVE NSLD NMAS NRST NRIG NCHK NOCK SCATpcRTZ SPLT DP3 UNTT//// PER  
6 0 1 4 0 0 0 0 0 7000 0 0 1 0  
$MATL 0 DAM FAIL DFRC EFAL solids from library  
10 0 1 1 1.0999.0  
44 0 1 1 1.0999.0  
16 0 1 1 1.0999.0  
$Blank for end of materials  
$Begin of Projectile data  
$ X/SCALE YSCALE ZSCALE X/RSHIFT ZSHIFT ROTATE SLANT X/R0 Z0  
1.0 1.0 1.0 0.0 0.0 0.0 0.0 0.0 0.0  
$ ROD NODES  
$ 2 NOR NIR NPLN RAD AX CROS JOIN N1 NTOP ZTOP ZBOT EXPAND  
2 12 0 3 1 0 1 0 1 0 56.0 55.0 1.0  
$ ROTOP RITOP ROBOT RIBOT  
6.0 0.0 4.0 0.0  
$ ROD NODES  
$ 2 NOR NIR NPLN RAD AX CROS JOIN N1 NTOP ZTOP ZBOT EXPAND  
2 12 9 114 1 0 1 0 67 054.6666666 17.0 1.0  
$ ROTOP RITOP ROBOT RIBOT  
4.0 3.0 4.0 4.0  
$ ROD NODES  
$ 2 NOR NIR NPLN RAD AX CROS JOIN N1 NTOP ZTOP ZBOT EXPAND  
2 12 9 30 1 0 1 1 858 0 17.0 7.0 1.0  
$ ROTOP RITOP ROBOT RIBOT  
4.0 4.0 4.0 3.0  
$NOSE NODES  
$ 3 TYPE NOR NIR RAD AX CROS//// N1//// ZTOP ZMIN  
3 3 12 9 1 2 1 1065 7.0 0.0  
$ ROTOP RITOP  
4.0 3.0  
$Minimum Z values  
2.25 1.5 0.75 0.0  
$LINE OF NODES NODE DATA  
$ 1 #NDE XYZ N1 INC EXPAND  
1 3 000 64 1 1.0  
$ X/R1 Y1 Z1 X/RN TN ZN  
3.16666666 0.054.8333333.8333333 0.054.8333333  
$ ROD NODES  
$ 2 NOR NIR NPLN RAD AX CROS JOIN N1 NTOP ZTOP ZBOT EXPAND  
2 9 0 114 1 0 1 0 4064 0 55.0 17.0 1.0  
$ ROTOP RITOP ROBOT RIBOT  
3.0 0.0 4.0 0.0  
$ ROD NODES  
$ 2 NOR NIR NPLN RAD AX CROS JOIN N1 NTOP ZTOP ZBOT EXPAND  
2 9 0 30 1 0 1 1 6211 0 17.0 7.0 1.0  
$ ROTOP RITOP ROBOT RIBOT  
4.0 0.0 3.0 0.0  
$NOSE NODES  
$ 3 TYPE NOR NIR RAD AX CROS//// N1//// ZTOP ZMIN  
3 3 9 0 1 0 1 6772 7.0 2.25  
$ ROTOP RITOP  
3.0 0.0  
$Blank for end of Projectile  
$Begin of Target data
```

```

$ X/RSCALE YSCALE ZSCALE X/RSHIFT ZSHIFT ROTATE SLANT X/R0 Z0
  1.0  1.0  1.0  0.0  0.0  0.0  0.0  0.0  0.0
$ 4 TYPE NX/R NY NZ FIX CROS JOIN N1 INC X/REXP YEXP ZEXP
  4 1 23 0 12 0 1 0 9772 0 1.0 0.0 1.0
$NRND NZND RPRT ZPRT RMAX RMIN ZMAX ZMIN
  0 0 0.0 0.0 9.0 0.0 0.0 -10.0
$Blank for end of Target DATA
$BEGIN PROJECTILE ELEMENT DATA
 999 1 0
$Rod Elements
$ 2 MATL N1 DIAG NOER NIER NLAY FULL SHEL PLAC RZN 1234 THICK RELAX
  2 10 1 5 12 1 2 0 0 0 0 0000 0.0 0.0
$Rod Elements
$ 2 MATL N1 DIAG NOER NIER NLAY FULL SHEL PLAC RZN 1234 THICK RELAX
  2 10 67 5 12 10 113 0 0 0 0 0000 0.0 0.0
$Rod Elements
$ 2 MATL N1 DIAG NOER NIER NLAY FULL SHEL PLAC RZN 1234 THICK RELAX
  2 10 858 5 12 10 29 0 0 0 0 0000 0.0 0.0
$Nose Elements
$ 3 MATL N1 DIAG NOER NIER FULL SHEL THICK
  3 10 1065 5 12 10 0 0 0.0
$Line of nodes Element data
$ 1 MATL #CMP N1 N2 N3 N4 N5 N6 N7 N8 INC SHEL BRCK T/A
  1 10 3 60 67 68 61 64 0 0 0 1 0 0 0.0
  999 1 1
$Rod Elements
$ 2 MATL N1 DIAG NOER NIER NLAY FULL SHEL PLAC RZN 1234 THICK RELAX
  2 44 4064 5 9 1 113 0 0 0 0 0000 0.0 0.0
$Rod Elements
$ 2 MATL N1 DIAG NOER NIER NLAY FULL SHEL PLAC RZN 1234 THICK RELAX
  2 44 6211 5 9 1 29 0 0 0 0 0000 0.0 0.0
$Nose Elements
$ 3 MATL N1 DIAG NOER NIER FULL SHEL THICK
  3 44 6772 5 9 1 0 0 0.0
  999 0 1
$Blank for end of Projectile Element Data
$BEGIN TARGET ELEMENT DATA
 999 1 0
$ 4 MATL N1 DIAG TYPE LX/R NLY NLZ SHEL PLAC RZN 1234 THICK RELAX
  4 16 9772 5 1 22 0 11 0 0 0 0000 0.0 0.0
  999 0 1
$Blank for end of Target Element Data
$here are the slide lines
$NMG NMN NSG NSN NSR TYPE MBOT ISR IT1 IT2 REF VEL ERODE FRICTION
  1 0 1 0 0 -2 0 0 1 0 0.0 0.0 0.0
$ 9 RSYM MAX NODE MIN NODE MIN ELE MIN ELE MATL 9
  9 0 0 0 0 0 0 10 9
$S1G SNG INC CHNK SURF
  0 0 0 2 1
$NMG NMN NSG NSN NSR TYPE MBOT ISR IT1 IT2 REF VEL ERODE FRICTION
  1 0 1 0 0 -2 0 0 1 0 0.0 0.0 0.0
$ 9 RSYM MAX NODE MIN NODE MIN ELE MIN ELE MATL 9
  9 0 0 0 0 0 0 44 9
$S1G SNG INC CHNK SURF
  0 0 0 1 1
$NMG NMN NSG NSN NSR TYPE MBOT ISR IT1 IT2 REF VEL ERODE FRICTION
  1 0 1 0 0 -2 0 0 1 0 0.0 0.0 0.0
$ 9 RSYM MAX NODE MIN NODE MIN ELE MIN ELE MATL 9
  9 0 0 0 0 0 0 10 9
$S1G SNG INC CHNK SURF
  0 0 0 3 1
$NMG NMN NSG NSN NSR TYPE MBOT ISR IT1 IT2 REF VEL ERODE FRICTION
  1 0 0 0 1 -2 0 0 1 0 0.0 0.0 0.0
$ 9 RSYM MAX NODE MIN NODE MIN ELE MIN ELE MATL 9
  9 0 0 0 0 0 0 16 9
$S1G SNG INC CHNK SURF
  9 0 10 0 0
$End of Slide Lines, Beginning of Detonation .

```

```
$ X/RDET YDET ZDET
  0.0   0.0   0.0
$ PX/RDOT PY/TDOT PZDOT
  0.0   0.0 -10000.0
$End of Detonation, Beginning of Main Section
$CYCL/// TIME DTMAX DTMIN SSF TMAX CPMAX EMAX
  0     0.0   1.0   0.0   0.9   0.05  0.0    0.0
$TPLT DROP/// PRES PUSH HRG VFRACT
  1 0   0 0 0
$SYS NPLT LPLT DPLT DTSYS TSYS DTNODE TNODE DTDYN TDYN
  1 0 0 1 0.000002 0.0 0.000002 0.0 0.000002 0.0
$End of Main Section, Beginning of Time Output
$ TIME ECHECK NCHECK RDAMP SAVE BURN YPRT NDAT SLPY PROJ PAT RZON
  0.0 1000.0 1000.0 0.0 0 0 0 0 0 0 0 1 0
  1.050002 1000.0 1000.0 0.0 0 0 0 0 0 0 0 1 4
$End for now
```

A Study of Acoustic Wave  
Propagation in Non-Equilibrium Plasmas

Andrew J. Jutte

Northmont High School  
4500 National Road  
Clayton, OH. 45415

Final Report for:  
High School Apprentice Program  
Wright Laboratory

Sponsored by:

Air Force Office of Scientific Research  
Bolling Air Force Base, DC

and

Wright Laboratory,  
Wright Patterson Air Force Base  
Dayton, Ohio

August 1996

A Study of Acoustic Wave  
Propagation in Non-Equilibrium Plasmas

Andrew J. Jutte  
Northmont High School

Abstract

The properties of acoustic shock waves produced in non-equilibrium plasma were studied. Gas discharges were created using currents of 50 and 100 milliamperes in a vacuum tube under varied pressures. Acoustic shock waves were produced by a spark gap at one end of the tube. The effects of the plasmas on the shock waves were measured using a laser and a photo-acoustic deflection measurement device. Experimental results show shock wave amplitude dissipated in weakly ionized non-equilibrium plasmas. Shock wave dissipation seems dependent on fractional ionization.

A Study of Acoustic Wave  
Propagation in Non-Equilibrium Plasmas

Andrew J. Jutte

Introduction

The study of gas discharges began in the 1920's by Langmuir and Tonks. The need for vacuum tubes that could carry large currents lead to work with weakly ionized gas discharges and plasmas (2). The transition of a gas to an ionized gas, or plasma, occurs gradually with increasing temperature. During this process, a molecular gas dissociates first into an atomic gas which, with increasing temperature, is ionized as the collisions between atoms are able to free the outermost orbital electrons. Resulting plasma consists of a mixture of neutral particles, positive ions, and negative electrons. In weakly ionized plasma the charge-neutral interactions are still important, while in strongly ionized plasma the multiple Coulomb interactions are dominant. (4) Weakly ionized gasses operate at low temperatures (60-80 degrees F). Plasma physics has grown to a major area of study since the early experiments done with vacuum tubes. Many discontinuities that arise in plasma such as shock waves, are of major interest. While plasma shock waves have been study greatly in past years, acoustic shock wave and their interaction with plasma has only become a topic of interest in recent years. Acoustic shock waves here are of supersonic speed. The waves create a barrier of pressure and the interaction between these waves and plasmas are of interest. Shocks waves create regions where plasma goes through dramatic changes in density, temperature, magnetic field strength, and/or field flow. By gaining a better understanding of these properties and in this case acoustic shock waves, and their unique behavior in plasma, scientists can gain a better understanding of plasma as a whole and continue to develop new uses for it in the future.

## Methodology

By sending a shock wave through plasma and measuring the wave amplitude, the effects of the plasma on the wave are able to be determined. A shock wave is produced at a set pressure with no current and is used as a constant (a discharge only occurs if there is current flowing between the anode and cathode). The current will then be turned on (creating a discharge). To determine the effects of the discharge on the shock wave, the discharge will be turned off using a solid state switch, after the shock wave is triggered. The discharge will turn back on after a set number of milliseconds. A pulsar is used to control the triggering of the shock wave and the delay of the switch (on and off) controlling the discharge (see page 31-6) A non-equilibrium plasma dc discharge is produced using a Pyrex discharge tube with a 21 mm internal diameter and an anode and cathode placed 24 cm apart. A spark gap consisting of two tungsten electrodes 1 cm. apart is attached to one end of the tube. Gas flow and pressure in the tube are maintained through inlets in the side of the tube (see page 31-7). A pressure range of 10 - 30 Torr and discharge currents of 50 and 100 mA is used.

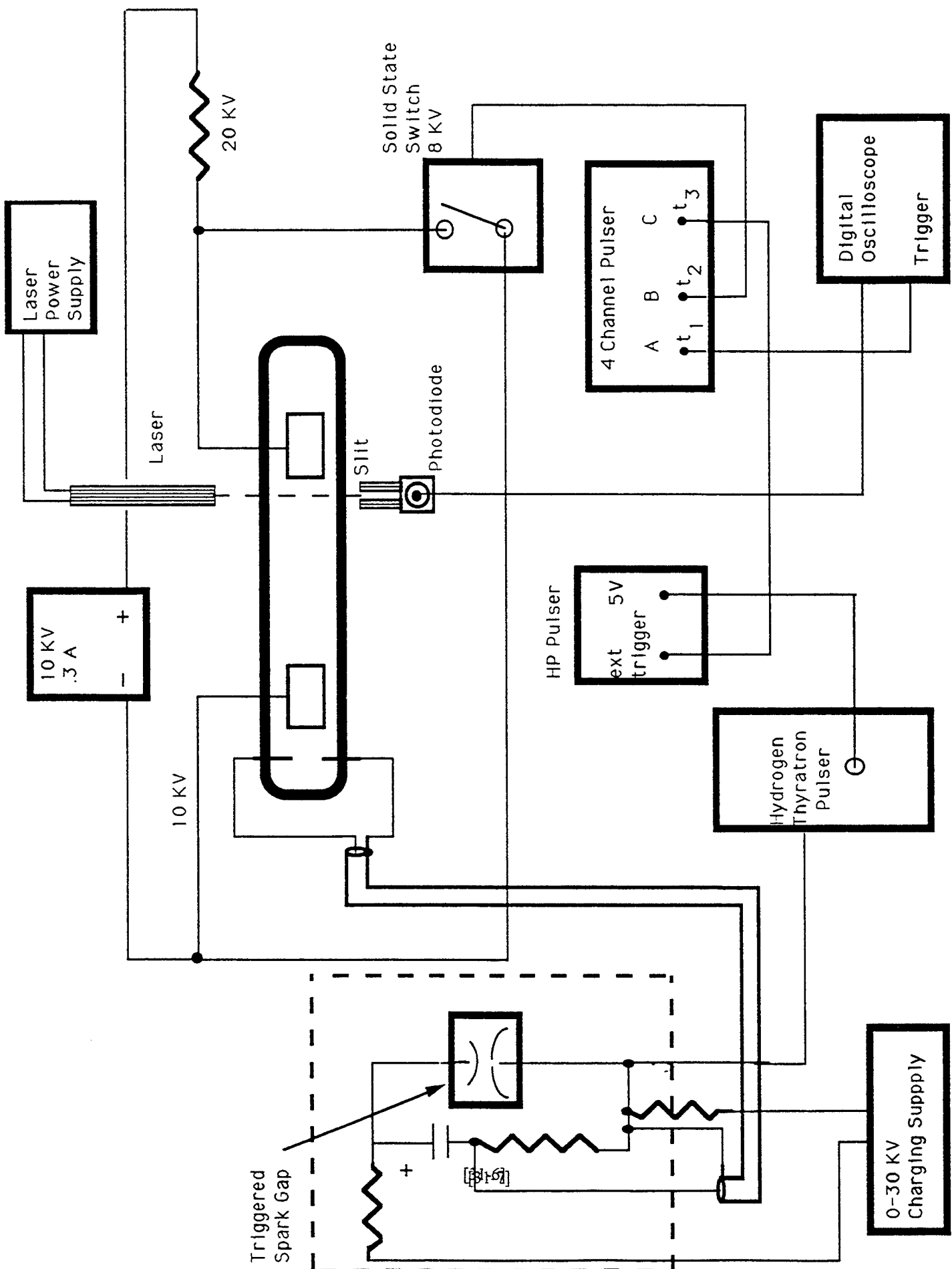
## Results

Trials were performed with molecular nitrogen at pressures 3.15, 10, 30 and 50 torr each at 50 and 100 milliamperes.

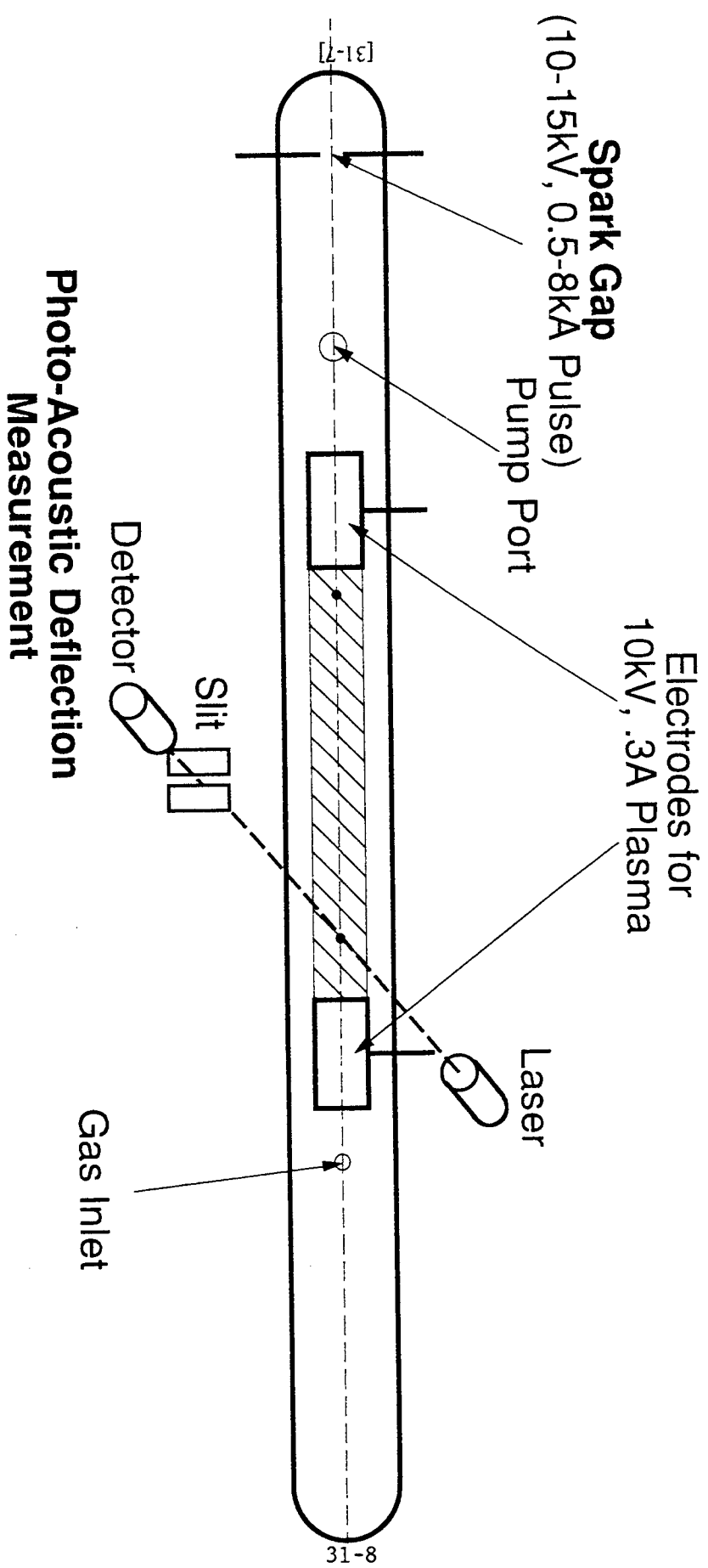
Results show as pressure increased, the time for a wave in a discharge to recover fully and regain the amplitude of a shock wave produced lacking a discharge decreased. Wave recovery was also more dramatic after 100 milliseconds of delay. This indicates the plasmas contributed to wave dampening and amplitude dissipation. Also, time required for a shock wave to reach the point of measurement (velocity) increased as the time of the delay decreased. An increase in velocity of the shock wave, occurred when the shock wave was traveling through the plasma medium. This may be explained by the fact that like a normal gas, collisions occur between neutral molecules and the wave energy is transferred, but unlike a normal gas, gas discharges also can transfer wave energy via the collisionless interactions of the ions and electrons. By there being more collisions the rate at which the wave energy is transferred is increased.

### Conclusion

Results show that waves produce in non-equilibrium discharge differ from those produce in a nonionized gas as expected. The data shows supersonic shock wave amplitude dissipation occurs in weakly ionized non-equilibrium plasmas. By plotting switch delay vs. the time required for the wave to reach the point of measurement an exponential curve can be calculated. This curve showed the shock wave in plasma will never fully recover to the amplitude of a wave in a non ionized gas. Shock wave amplitude and dispersion and damping is dependent on fractional ionization or current. Continued experimentation with varied gasses, and new diagnostics will be needed to gain a better understanding of shock induced electric field, modulation, and energy coupling.



# Measurement of Shock Wave Propagation in Non-equilibrium Plasmas



## References

- [1] Burgess, D., "Collisionless Shocks", in Introduction to Space Physics, eds. M.G. Kivelson and C.T. Russell, Cambridge University Press, 1993
- [2] Chen, Francis F., Introduction to Plasma Physics, Plenum Press, New York, 1984
- [3] Giancoli, Douglas C., Physics: principles with applications Prentice Hall, New York, 1980
- [4] Von Engel, A., Ionized Gases, Oxford University Press, London, 1965

## HYPER TEXT MARKUP LANGUAGE

Nicholas A. Klosterman

Chaminade Julienne Catholic High School  
505 South Ludlow Street  
Dayton, Ohio 45402

Final Report for:  
High School Apprentice Program  
Wright Laboratory  
WL/AACI

Sponsored By:  
Air Force Office of Scientific Research  
Bolling Air Force Base, DC

and

Wright Laboratory

August 1996

## HYPER TEXT MARKUP LANGUAGE

Nick Klosterman  
Chaminade-Julienne Catholic High School

### ABSTRACT

Hyper Text Markup Language (HTML), a computer language used to communicate data on the Internet, was learned so that creation of HTML pages for the Model Based Vision Laboratory (MBVLab) could be made. After learning HTML, we developed two sites on the Internet for the MBVLab. These sites used a type of interactive display for presenting the data and letting the user access it.

## HYPER TEXT MARKUP LANGUAGE

Nicholas Klosterman  
Chaminade-Julienne Catholic High School

### INTRODUCTION

Before work could begin on making the HTML pages for the MBVLab, HTML needed to be learned. The Hyper Text Markup Language was learned by examining other individual's source code of HTML from their Internet page. After examining their source code, we manipulated the code to see the different effects these alterations had and thereby learn how to write web pages in HTML. We also learned how to write HTML pages by consulting with our partners and sharing our knowledge. Where one didn't know how to do something another seemed to. If we became stuck we would look up and find how to do it in a book or we would look throughout the Internet for the answer to the question. Through searching the Internet we found out how to navigate through it and use it to its fullest extent as a research resource. We used our gained knowledge as we progressed by constructing our own Internet web pages incorporating what we had learned into these pages. We honed our skills as we progressed on these web pages as we attempted to outdo each other. We learned from online tutorials as well as stealing the source code of a page that used something new to us.

### METHODOLOGY

To present the requested data we needed a way to let the user access it through menus. We searched our resources and decided to use "frames" a HTML command that lets one split the

screen into separate areas. This splitting of the screen allowed us to present menus for the user to choose from. The different menus allowed the user to change from viewing vehicles and the different viewing angles. The pages being similar both used this format to present access to the data.

## RESULTS

### *MSTAR TARGET DATA*

There were 14 targets each with varying views of the vehicle. We were set out to produce a clickable interface of bringing up each picture. Splitting the page into three distinct sections called frames allowed us to produce this clickable interface. The first section held a menu of thumbnail pictures that allowed you to choose the vehicle whose data set you wanted to access. This then triggered an adjacent frame to display that vehicles available data. This second menu held a chart menu that displayed the available data according to the azimuth and depression angle specifics of the data. From this menu the user then chose which image they wanted displayed. The image then came up in the third frame. When the site is accessed a default setting pops up as an example for the user to follow.

### *IR IMAGE DATA*

The IR data page was set up much the same way. The screen was split into four distinct sections. The first held a menu of which months data set was needed. This then accessed a list of target objects and vehicles that had IR pictures taken of them in that month. A selection from this menu then triggered a chart that held the time and date of the various images. A selection from here would then produce the desired picture in the viewing frame. For easier use we included a

button in the frame with the picture that allows the user to either go forward or back so as to see the changes in the imaging over the different hours of the day. This page also had a default example for the user to follow.

#### *LOCATION*

The resulting pages were then ready to post. The first page may be found at <http://www.mbvlab.wpafb.af.mil/MBVDATA/TARGETS/index.htm>. This page needs a password and therefore isn't reachable by the public.

The page for the IR data is yet to be posted and therefore the data resides only on a hard drive.

#### CONCLUSION

It was discovered that HTML is a very versatile language however it lacks certain aspects that could make it a more dynamic medium. This is accomplished by using various Internet specific programming languages. The current languages include Java and Common Gateway Interface (CGI) languages such as Perl. This allows for more dynamic interfaces, applications, and easier navigation.

The knowledge of one of these languages could easily be used to enhance the page. This is not feasible or newcomers to the Internet and to programming. A base knowledge of computer programming is needed to comprehend these languages and use them to their fullest to develop web sites. Knowledge was also gained, although not applied, of Virtual Reality Modeling Language. This new Internet language allows the creation of virtual worlds and objects in 3 dimensions. This can be quite nice in presentation of targeting

data as the vehicles can be presented as complex 3D models that allow the user to manoeuvre around them. VRML has all of the advantages at its disposal, allowing dynamic display of information in a "live" 3D format.

HTML being such a simple straight forward language was easy to use and learn. There was no need for an authoring tool to produce the results we wanted. However to produce nice graphics to display one might think of investing in some type of graphics package or in a company to provide you with graphics. The HTML language was easy to learn but there are various elements of style that help produce outstanding pages that are not only visually stunning but also quick and easy to use.

Kelly A. Lakatos report was not available at the time of publication.

Enhancement of CAD Packages  
for Electronic and  
Computational Applications

Jonathan Mah

Centerville High School  
500 East Franklin St.  
Centerville, OH 45459

Final Report for:  
High School Apprentice Program  
Wright Labs

Sponsored by:  
Air Force Office of Scientific Research  
Bolling Air Force Base, DC

and

Wright Labs

August 1996

### **Abstract**

In the field of circuit design, engineers need many tools to facilitate the synthesis and analysis of electric and electronic circuits. These tools are in the form of computer programs, which provide accurate synthesis and analysis of circuits. Computer programs can also be very expensive. However, tools such as SPICE, Matlab, and Tcl/Tk have public domain versions, which will be or already are available on the internet. Also, commercial versions of Maple and SPW are very powerful with regards to computational and circuit analysis. Matlab and SPICE have actually been integrated into one large program called TOTAL, which will be released as public domain. In order for this to happen, changes needed to be made in the code to enhance and debug the program. The enhancement regarded the "EXEC" command and how it was changed to facilitate the user. The debugging concerned the "QUIT" and "EXIT" commands as well as the "SAVE" and "LOAD" commands. Also, Tcl/Tk has been used to interface programs such as SPICE and Matlab in a windows environment. SPICE can be sourced into the Tcl shell (Tclsh); it will prompt the input and output files and run the program. It can also run in the Tk widget shell (Wish), but the input and output files must be written into the code directly. In addition to using Tcl/Tk, SPICE can be interfaced into Maple. Maple does many matrix manipulations, which is very helpful in solving mesh circuit equations. Maple also puts the results in an easy-to-read format.

## 1. Matlab

Matlab is a program designed to do many mathematical computations. It is especially powerful within the realm of matrices. In addition to simple arithmetic computations, it can manipulate matrices in array operations quickly. It is also very useful in solving mesh circuit equations. For example, the mesh circuit represented in fig. 1.1 has currents which can be solved by matrices in figure 1.2.

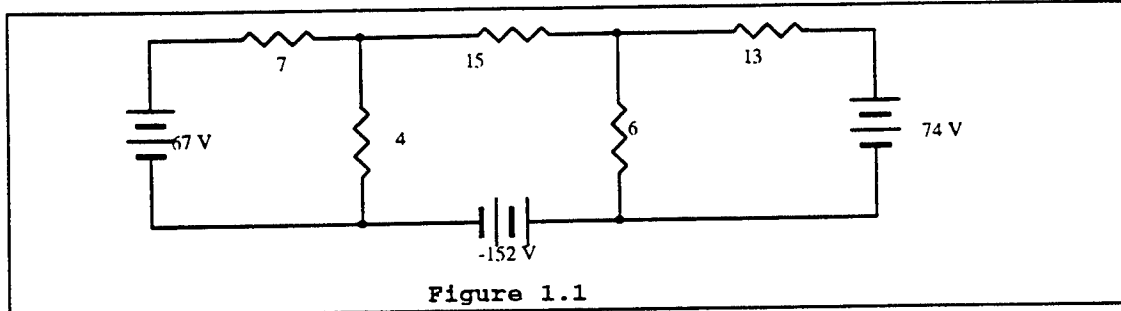


Figure 1.1

```
A=<7 -4 0;-4 15 -6;0 -6 13>;
B=<67;-152;74>;
C=INV(A)*B
```

Figure 1.2

The output of this file in Matlab is shown in figure 1.3.

```
C
=
5
-8
2
```

Figure 1.3

The public domain version of MATLAB is not very friendly, so changes were made in the source code to facilitate the user. First, the execute command (EXEC) was changed so that "EXEC" did not need to precede the file name, rather only the file name was necessary. Matlab executes a file by reading the macro as if it were inputted directly at the prompt. The change was made by looking through the FORTRAN code and rerouting the "undefined variable" error to read a separate macro, which contained the file. Various PRINT statements were also used to track the direction of the program. The following code can be now executed by typing just MAT as opposed to EXEC(MAT). The following example in figure 1.4 is used to find the effective conductivity of a medium with respect to the radius of cylindrical inclusion.

```

//CONDUCTIVITY EXAMPLE
//PARAMETERS
RHO          //RADIUS OF CYLINDRICAL INCLUSION
N            //NUMBER OF TERMS IN SOLUTION
M            //NUMBER OF BOUNDARY POINTS
//INITIALIZE OPERATION COUNTER
FLOP=<0,0>;
//INITIALIZE VARIABLES
M1=ROUND(M/3);      //NUMBER OF POINTS ON EACH
STRAIGHT EDGE
M2=M-M1;           //NUMBER OF POINTS WITH DIRICHLET
CONDITIONS
PI=4*ATAN(1);
//GENERATE POINTS IN CARTESIAN COORDINATES
//RIGHT HAND EDGE
FOR I=1:M1, X(I)=1; Y(I)=(1-RHO)*(I-1)/(M1-1);
//TOP EDGE
FOR I=M2+1:M, X(I)=(1-RHO)*(M-I)/(M-M2-1); Y(I)=1;
//CIRCULAR EDGE
FOR I=M1+1:M2, T=PI/2*(I-M1)/(M2-M1+1); ...
X(I)=1-RHO*SIN(T); Y(I)=1-RHO*COS(T);
//CONVERT TO POLAR COORDINATES
FOR I=1:M-1, TH(I)=ATAN(Y(I)/X(I)); ...
R(I)=SQRT(X(I)**2+Y(I)**2);
TH(M)=PI/2; R(M)=1;
//GENERATE MATRIX
//DIRICHLET CONDITIONS
FOR I=1:M2, FOR J=1:N, K=2*J-1; ...
A(I,J)=R(I)**2*K*COS(K*TH(I));
//NEUMAN CONDITIONS
FOR I=M2+1:M, FOR J=1:N, K=2*J-1; ...
A(I,J)=K*R(I)**(K-1)*SIN((K-1)*TH(I));
//GENERATE RIGHT HAND SIDE
FOR I=1:M2, B(I)=1;
FOR I=M2+1:M, B(I)=0;
//SOLVE FOR COEFFICIENTS
C=A\B
//COMPUTE EFFECTIVE CONDUCTIVITY
C(2:2:N)=-C(2:2:N);
SIGMA=SUM(C)
//OUTPUT TOTAL OPERATION COUNT
OPS=FLOP(2)

```

Figure 1.4

The output is generated as in figure 1.5.

RHO =
0.9000
N =
15.
M =
30.
C =
2.2275

Figure 1.5

```

-2.2724
1.1448
0.1455
-0.1678
-0.0005
-0.3785
0.2299
0.3228
-0.2242
-0.1311
0.0924
0.0310
-0.0154
-0.0038
SIGM =
5.0895
OPS =
17902

```

Figure 1.5(cont'd)

A second change was made regarding the quit and exit commands. It was found that after the first task of changing the execute command, the program went into a loop and it took several attempts to exit the program. In order to remedy this problem, STOP commands were placed after the exit and quit commands to prevent the loop from starting as shown in figure 1.6.

```

PRINT*, ' EXITING < M A T L A B > '
CHAR=EOL
PT=PTZ
CALL COMAND(EEXT(1))
C      RETURN
STOP
PRINT*, ' QUITTING < M A T L A B > '
PRINT*, ' '
PRINT*, ' RETURNING TO TOTAL "WITHOUT" UPDATING MATRIX
VARIABLES'
PRINT*, ' AMAT,BMAT,CMAT,DMAT,FMAT,GMAT,KMAT, AND ZMAT
IN TOTAL'
42   CONTINUE
IF (PT .GT. PTZ) FIN = -16
IF (PT .GT. PTZ) GO TO 98
K = IDINT(STKR(VSIZE-2))
WRITE(WTE,140) K
IF (WIO .NE. 0) WRITE(WIO,140) K
IF ((WIO .NE. 0).AND.(ANSWER)) WRITE(20,140) K
140 FORMAT(/1X,'Total Flops ',I9//,
+1X,'----',
+1X,'RETURNING TO -> T O T A L OPTION>',/)
C      +1X,'-----')
FUN = 99
STOP

```

Figure 1.6

Lastly, the SAVE and LOAD commands did not work properly. The SAVE command is supposed to save all of the current variables under a filename and the LOAD command is supposed to call the variables back from the file. They did not save and load in MATLAB format. It was writing the file in such a way that it could not read the file. The read and write commands in the code were modified so that the program saved and loaded in the same format.

## 2. SPICE

Simulation Program with Integrated Circuit Emphasis (SPICE) is a program with powerful capabilities in the synthesis and analysis of electric or electronic circuits. The source code of the public domain version of SPICE was taken from Wright State University. SPICE can solve differential equations when put in the form of a circuit. Using the transient analysis option (TRAN), the DCTRAN module is invoked. This module can perform dc operating point analysis, initial-condition of transient analysis, dc transfer character analysis, and transient analysis. Consider the following set of partial differential equations in figure 2.1.

$$\begin{aligned}2x + x' + z - z' &= 1 \\x' + y' + y &= 1 \\y + z' + y + 2z &= 0\end{aligned}$$

figure 2.1

In SPICE this can be represented by making the variables currents going through 1-ohm resistors as in figure 2.2.

```
*x=v(1,2), y=v(2,3), z=v(3,4)
R1 1 2 1
R2 3 4 1
R3 5 6 1
L1 2 0 1
L2 4 0 1
L3 6 0 1
G1 0 1 POLY(3) 5 6 2 0 6 0 .5 -.5 -.5 .5
G2 0 3 POLY(2) 2 0 4 0 1 -1 -1
G3 0 5 POLY(3) 3 4 4 0 6 0 0 -.5 -.5 -.5
.TRAN .1 2 0 .1 UIC
.PRINT TRAN V(1,2) V(3,4) V(5,6)
.END
```

Figure 2.2

The output of SPICE is shown in Figure 2.3.

TIME	V(1,2)	V(3,4)	V(5,6)
<b>X</b>			
0.000E+00	4.792E-07	-7.907E-08	-3.195E-07
1.000E-01	5.744E-02	4.034E-02	-3.830E-02
2.000E-01	1.105E-01	8.101E-02	-7.367E-02
3.000E-01	1.597E-01	1.217E-01	-1.065E-01
4.000E-01	2.051E-01	1.621E-01	-1.367E-01
5.000E-01	2.470E-01	2.020E-01	-1.647E-01
6.000E-01	2.857E-01	2.411E-01	-1.905E-01
7.000E-01	3.214E-01	2.794E-01	-2.143E-01
8.000E-01	3.544E-01	3.166E-01	-2.363E-01
9.000E-01	3.848E-01	3.527E-01	-2.565E-01
1.000E+00	4.129E-01	3.876E-01	-2.753E-01
1.100E+00	4.388E-01	4.212E-01	-2.926E-01
1.200E+00	4.628E-01	4.536E-01	-3.085E-01
1.300E+00	4.849E-01	4.846E-01	-3.232E-01
1.400E+00	5.053E-01	5.142E-01	-3.368E-01
1.500E+00	5.241E-01	5.426E-01	-3.494E-01
1.600E+00	5.415E-01	5.696E-01	-3.610E-01
1.700E+00	5.575E-01	5.953E-01	-3.717E-01
1.800E+00	5.723E-01	6.197E-01	-3.815E-01
1.900E+00	5.860E-01	6.429E-01	-3.907E-01
2.000E+00	5.987E-01	6.650E-01	-3.991E-01

Figure 2.3

SPICE was most helpful when solving simple electric circuits. It can compute the voltages, currents, and so on at any given node. In TOTAL, SPICE is enhanced with the capabilities of Matlab and gnuplot, which is a plotting device also integrated within TOTAL.

### 3. Tcl/Tk

Tcl (Tool Command Language) is a language that uses a series of scripts to implement actions. It was expanded to also create windows, buttons, etc. to be known as Tk. The Tk tool kit is used to enhance a program by adding a window interface and making the program more user friendly. We first successfully interfaced Tk with SPICE. Since it is a UNIX based language and I am using a Windows/DOS system, Tcl is a little cumbersome. SPICE was run under Tk by creating the following script in figure 3.1.

```

#!/bin/sh
# the next line restarts using wish \
exec wish "$0" "$@"
frame.mbar -relief raised -bd 2
frame .dummy -width 10c -height 5c
pack .mbar .dummy -side top -fill x
button .b -text Exit -command exito

proc exito {} {exec spice <bench.tex >bench2.out}
pack .b
tk_menuBar .mbar .mbar.file
pack .mbar

```

**Figure 3.1**

The “exec” command is what finds the file and runs it through SPICE. In this case a separate file, bench.tex, was necessary because it contained the input and output files, which could not be entered explicitly in the parent file. In this example, all the processes were run internally, and it was not interactive once the files were entered.

We now can run SPICE through the Tcl shell. This, in contrast with the Tk application, runs interactively and the user is prompted for the input and output files, whereas in the Tk application a predetermined file must be entered in the code. In Tcl the script must be sourced at the Tcl prompt. The following script in figure 3.2 runs SPICE in Tcl.

```

cd ..
cd ..
cd wsuspice
exec spice <bench.tex >bench2.out

```

**Figure 3.2**

The first three commands access the SPICE executable file from its directory. The last line executes the program. The input bench.tex and output bench2.out are apparently not read but are necessary for the user to attain the SPICE prompt. The same format of the script was also used to access MATLAB in figure 3.3.

```

cd ..
cd ..
cd jon3
exec sys3 <aa.tex >cc.out

```

**Figure 3.3**

This runs the first time it is executed but goes into a loop during subsequent attempts. The problem occurred because there needs to be something for Tcl to read and delete. So once it is read and deleted, there is nothing for it to read a second time. The ">" tells the Tcl interpreter that the following name is an output file and should be overwritten (in this case it overwrites it with a blank file). I solved this problem by replacing the ">" with a ">>" this, I discovered, tells the interpreter to append the file rather than overwrite it.

#### **4. Maple**

Maple V for Windows is a powerful program to deal with many levels of math. It solves equations, does many matrix manipulations and all of these are in an easy to read format. Its capabilities can be utilized in SPICE to help solve electric or electronic circuits. During the summer, Maple was only used as a reference tool to help solve equations. Maple is a commercial program that can be very useful for many levels of math. Differential equations and integrals are displayed well symbolically as are matrices. Some of Maple's capabilities are displayed in Appendix A.

#### **5. Conclusion**

The capabilities of these programs have proved to be very useful in the area of circuit design and analysis. Matlab is a standard; its original source code was written in 1980 at UC Berkeley. Matlab can perform simultaneous linear equations, eigenvalue problems, and so on; but its real strength is its matrix capabilities. Matlab is mainly used for its matrix functions because it has so many. It is also interfaced with other programs like SPICE to enhance their capabilities. SPICE has also been a standard in circuit design and analysis. PSPICE and VSPICE are commercial variations of SPICE and have a few different features. SPICE was originally written about twenty years ago also at UC Berkeley. It performs DC, transient, and AC small-signal analyses as well as analysis at different temperatures. SPICE remains one of the oldest programs that is still used frequently today. Tcl/Tk was developed in 1988 by a former UC Berkeley professor. It has risen to be used quite extensively in the area of programming design. Tcl and

Tk were developed as an alternative to a C-program or C-based tool kit. It incorporates windows and buttons into a program to enhance its friendliness and develop the program further. It is also very useful to use it as a front-end to programs that would require a long path to access. Lastly, Maple is a commercial program developed to neatly produce high levels of computational analysis. Maple is a robust program with many strengths. All of the computations are laid out very well symbolically and have numerous capabilities. Maple is used as a computational tool to solve sets of equations, derive expressions, manipulate matrices, and so on. Every computer program has its strengths, so it is necessary to keep up with the best tools to help in circuitry and computer programming.

**Appendix A:**

```

A:=matrix([[5+j*2,j*2,j*2],[j*2,0,-j*2],[j*2,-j*2,5-j*2]]);
A := 
$$\begin{bmatrix} 5+2j & 2j & 2j \\ 2j & 0 & -2j \\ 2j & -2j & 5-2j \end{bmatrix}$$


B:=matrix([[35.5+j*35.5],[35.5+j*35.5],[35.5+j*35.5]]);
B := 
$$\begin{bmatrix} 35.5 + 35.5j \\ 35.5 + 35.5j \\ 35.5 + 35.5j \end{bmatrix}$$


C:=inverse(A);
C := 
$$\begin{bmatrix} \frac{1}{2} \frac{1}{5+2j} & \frac{5}{4} \frac{1}{j(5+2j)} & \frac{1}{2} \frac{1}{5+2j} \\ \frac{5}{4} \frac{1}{j(5+2j)} & \frac{1}{8} \frac{-25+8j^2}{(5+2j)j^2} & -\frac{1}{4} \frac{5+4j}{j(5+2j)} \\ \frac{1}{2} \frac{1}{5+2j} & -\frac{1}{4} \frac{5+4j}{j(5+2j)} & \frac{1}{2} \frac{1}{5+2j} \end{bmatrix}$$


evalm(C&*B);

$$\begin{bmatrix} \frac{79.87500000j + 35.50000000j^2 + 44.37500000}{j(5.+2.j)} \\ \frac{-110.9375000 - 110.9375000j}{j^2(5.+2.j)} \\ \frac{-44.37500000 + 44.37500000j}{j(5.+2.j)} \end{bmatrix}$$


factor(det(A));

$$-8(5+2j)j^2$$


simplify(det(A));

$$-40j^2 - 16j^3$$


adjoint(A);

$$\begin{bmatrix} -4j^2 & -10j & -4j^2 \\ -10j & 25 - 8j^2 & 10j + 8j^2 \\ -4j^2 & 10j + 8j^2 & -4j^2 \end{bmatrix}$$


(adjoint(A))/(det(A));

```

$$\frac{\begin{bmatrix} -4j^2 & -10j & -4j^2 \\ -10j & 25 - 8j^2 & 10j + 8j^2 \\ -4j^2 & 10j + 8j^2 & -4j^2 \end{bmatrix}}{-40j^2 - 16j^3}$$

f1:=2\*X^3+6\*X^2-10\*X;

$$f1 := 2 X^3 + 6 X^2 - 10 X$$

int(f1,X);

$$\frac{1}{2} X^4 + 2 X^3 - 5 X^2$$

int(f(x),x);

$$\int f(x) dx$$

References:

Ousterhout, John K. Tcl and the Tk Toolkit. Addison Wesley Publishing Co.: 1994.

Moler, Cleve. Matlab User's Guide. U of New Mexico: 1981.

Roberts, Gordon and Adel Sedra. SPICE for Microelectronic Circuits. Harcourt Brace Jovanovich pub.: 1992.

Vladimirescu, A. , Kaihe Zhang, A.R. Newton, D.O. Pederson, A. Sangiovanni-Vincentelli. SPICE Version 2G User's Guide. UC Berkeley: 1981.

THE OPTIMIZATION OF AN IMPEDANCE  
MATCHING TRANSFORMER FOR AN EXPLOSIVE  
FLUX GENERATOR AND STATIC LOAD

David R. Mandel

Niceville Senior High School  
800 E John C Sims Pky  
Niceville FL, 32578

Final Report for:  
High School Apprentice Program  
Wright Laboratory

Sponsored by:  
Air Force Office of Scientific Research  
Bolling Air Force Base, DC

and

Wright Laboratory

August 1996

THE OPTIMIZATION OF AN IMPEDANCE  
MATCHING TRANSFORMER FOR AN EXPLOSIVE  
FLUX GENERATOR AND STATIC LOAD

David R. Mandel  
Niceville High School

Abstract

In order to get the best impedance match to ensure the maximum power transfer from the source to the load, the design of the transformer is critical. In order to determine the best transformer for a given source a computer simulation of an electric system was used. The simulation modeled the operation of an explosive flux compressor generator, transformer, and static load. The simulation was run with all combinations of three different variables of interest. These variables were, seed current, primary inductance, and secondary inductance. The peaks of the graphical outcomes were recorded and graphed. Then, three additional simulations were run with no transformers so that these could be compared to the runs in which a transformer was used. This paper describes transformer operation, FCG code, the simulation inputs, the results of those runs, and the conclusions that were made.

## Preface

The code used to run the simulations was written by Dr. Ron Parkison of Science Applications International Corporation (SAIC). The local HSAP program was coordinated by Mr. Don Harrison and Mr. Michael Deiler. Mr. Mark Heyse monitored my progress and helped me through the unfamiliar areas, and Dr. Kieh Jamison and Dr. Brion Cornette assisted me with the project.

## Abbreviations and Acronyms

AC	Alternating Current
DC	Direct Current
FCG	Flux Compressor Generator
FCGS CA	Flux Compressor Generator Scaling
GA/s	Gigaamp per second
GW	Gigawatt
I	Current
kA	Kiloamp
kV	Kilovolt
L	Inductance
MA	Megaamp
MJ	Megajoule
nH	nanohenry
N <sub>p</sub>	Number of Primary Windings
N <sub>s</sub>	Number of Secondary Windings
ODE	Order Differential Equation
PC	Personal Computer
R	Resistance
RK	Runge-Kutta
V <sub>p</sub>	Primary Voltage
V <sub>s</sub>	Secondary Voltage

# THE OPTIMIZATION OF AN IMPEDANCE MATCHING TRANSFORMER FOR AN EXPLOSIVE FLUX GENERATOR AND STATIC LOAD

David R. Mandel

## Introduction

In order to get the best impedance match to ensure the maximum power transfer from the source to the load, the design of the transformer is critical. In order to determine the best transformer for a given source a computer simulation of an electric system was used. The simulation modeled the operation of an explosive flux compressor generator, transformer, and static load. The simulation was run with all combinations of three different variables of interest. These variables were, seed current, primary inductance, and secondary inductance. The peaks of the graphical outcomes were recorded and graphed. Then, three additional simulations were run with no transformers so that these could be compared to the runs in which a transformer was used. This paper describes transformer operation, FCG code, the simulation inputs, the results of those runs, and the conclusions that were made.

## Transformer Operation

For reasons of efficiency, it is desirable to transmit electrical power at high voltages and low current thereby reducing the resistive losses, or ( $I^2R$ ) heating of the circuit and the subsequent loss of power. However, most household items could not run on such high voltage, so the voltage must be brought down to usable levels. The voltage changes can be accomplished with efficiency ease through the use of a transformer.

The transformer is made up of two coils electrically insulated from each other and wound on the same core. An alternating current in one wire produces an alternating magnetic flux in the core, and this alternating flux produces an electric field. The flux is limited by a factor known as reluctance. Just as current is limited by resistance in ohms, flux is limited by reluctance in units of reluctance. This electric field then induces a current in the other winding of wire. The winding to which power is supplied is called the primary; the one in which current is induced is known as the secondary. A transformer is able to have alternating current and voltage pass through it, however, direct current and voltage is unable to pass through a transformer. The circuit symbol for a transformer is shown in Figure 1:

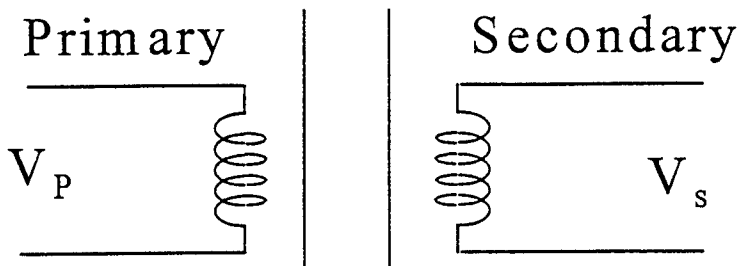


Figure 1. Schematic Diagram of a Transformer

There are three types of transformers. The first is known as a step-up transformer. In this type of transformer the number of turns of the coil in the secondary winding is greater than in the primary, thus, the voltage in the secondary coil is greater than in the primary coil. Second, is a step-down transformer. In this type the primary winding has more coils and thus higher voltage than the secondary. The third and final type is a 1:1 transformer. In this type of transformer the number of turns of wire is the same in both the primary and the secondary windings. Since the coils are the same, the alternating current and voltage do not change, the direct current and voltage, however, cannot pass through the core thus preventing shocks if the circuit were to have a short.

The voltage change a transformer makes is proportional to the number of turns of the wire in the primary and secondary according to the following formula shown in equation 1.

$$\frac{V_S}{V_P} = \frac{N_S}{N_P}$$

Equation 1

This formula states that the ratio of the secondary voltage ( $V_S$ ) to the primary voltage ( $V_P$ ) is equal to the ratio of the number of turns in the secondary winding ( $N_S$ ) to the number of turns in the primary winding ( $N_P$ ).

The power output of a transformer is less than that of the input because of unavoidable losses. These losses consist of  $I^2R$  losses in the primary and secondary windings and eddy current losses in the core. However, by taking certain precautions such as laminating the core to reduce eddy current losses, transformer efficiencies are usually well over 90%, and in large installations may reach 99%.

Pulsed power is a specialized area in which transformers are also used. Pulse power is neither AC nor DC, but in a category by itself. Rather than the constant current of DC or the continuous sinusoidal patterns of AC, pulse power discharges are usually very short pulses of current. The current and voltage waveforms last only briefly, often times only a few micro seconds, before rapidly dying away.

In some cases pulse power involves huge pulses of energy. The currents generated by these pulses are often up to several hundred kilo amps or even Megaamps. The same is true of the voltage, in these cases.

Technically, a pulse transformer is no different than the average transformer in your home. They both have a primary winding, core, and secondary winding. The pulse transformer, however, is constructed specifically to at the high currents, voltages, and short waveform durations associated with pulsed power.

#### The FCG Code

In order to make the comparisons necessary to perform this summer's task, a computer simulation of an explosive FCG circuit was used. Often times when a computer simulation is created for a physical device some compromise must be made between highly detailed "exact" calculations, and faster and more phenomenological treatments. FCGSCA, which stands for Flux Compressor Generator Scaling, was designed to be part of the latter category. It is useful for fast convenient exploratory and scaling studies covering a wide range of device parameters. What makes this model different from other attempted in the past is its user interface. This is due to the programming tools and the speed available in modern PC's, and by its integration of Flux Compressor Generator and static load models. The code's interface is graphically created using Visual Basic; this is linked to a phenomenological core built as a Fortran subroutine. Both the interface and the core model will be discussed.

Visual Basic programming tools make it easy to create an integrated set of graphical windows through which one can set up an exploratory program and view the computational results.

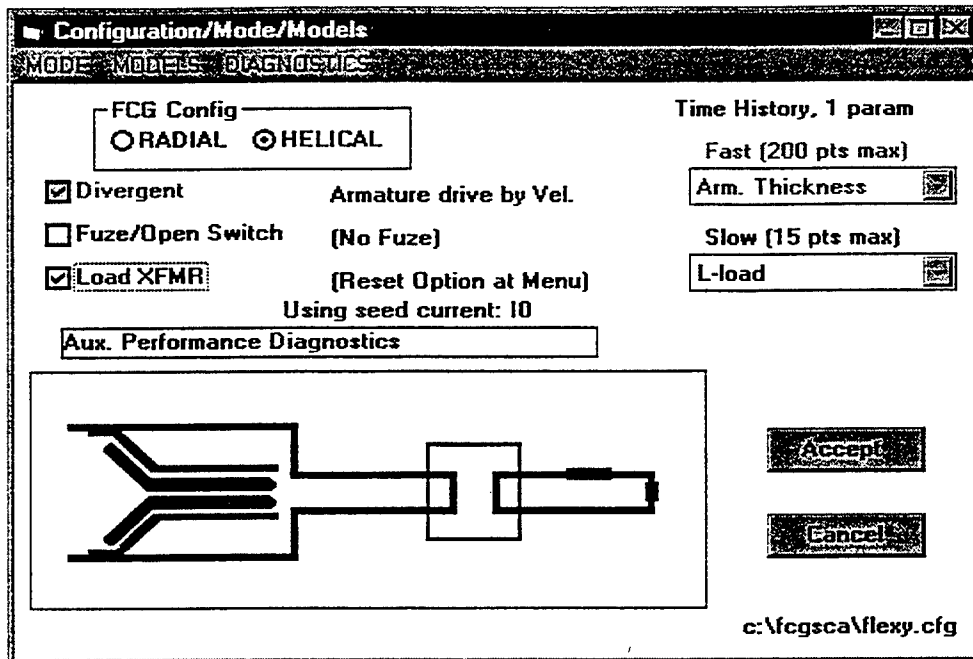


Figure 2. Central Control Window

Figure 2 shows the central control form for general problem definition. Important settings include the FCG, either radial or helical, and other choices in the configuration box. These are choice of L and R elements, the option of and opening switch, and even a matching transformer. Other key choices are the diagnostic output and survey mode on the main tool bar across the top. Available diagnostics include electrical measures (such as stator and load current), energetics (power, mechanical and inductive electrical energy, and ohmic loss), and other performance indices (such as  $dL/dt$  and interval voltage levels). The output is available in two different modes. The first mode is a time history. These can be compared as a single parameter is varied. For example, one could plot voltage versus time for several different load inductances, and by graphing a family of curves, simultaneously compare them. In the second mode, maximal values are accumulated as two parameters are varied. For example, a person can calculate and display peak load current as a continuous function of the load inductance for several values of the generator seed current.

The second window associated with problem definition is the "modify parameters" window.

**Modify Parameters**

ARMATURE		INITIAL	FINAL	# POINTS	
Length (cm)	108.5	10		1	<input type="button" value="Accept edit"/>
Radius (cm)	8.65	2		1	<input type="button" value="Cancel edit"/>
Thickness (cm)	0.9	0.1		1	
Velocity (cm/usec)	0.224	0.2		1	
<b>STATOR</b>					
Radius (cm)	17.8	4		1	
SEED BO / IO	0.413	0.001		1	
HE Mass (g/cm)	50	50		1	
<b>FUZE RS-v (m Ohm)</b>					
Blow Current (mA)	900	300		1	
Blow Time (usec)	20	20		1	
Blow Time (usec)	18	26		5	
<b>XFMR</b>					
k-cplg [1]	0.95	0.95		1	
r-load [1]	0.8	0.8		1	
L-pri (nH)	10	10		1	
L-sec (nH)	100	100		1	
<b>LOAD</b>					
R-load (m Ohm)	1	1		1	
L-load(nH)	60	60		1	
TIME (usec)	0	150	150		c:\fcgsca\markix.cfg

Figure 3. Parameter Input Window

In Figure 3 data can be manipulated such as: the seed current, FCG dimensions, transformer, and the load to within certain specifications. One can adjust the length of time the simulation will run, seed current, primary and secondary transformer inductance, load resistance, and load inductance. One can also vary many other more minor details.

The third and final window that one may vary is the generator window. In this window, one may design the generator in a variety of ways. This is known as the set auxiliaries window and is shown in Figure 4.

**Auxiliary Model Parameters:**

<b>STATOR</b>		<b>ARMATURE</b>		<b>HE DRIVER</b>										
A-S sep lim (cm)		Rho(g/cm <sup>3</sup> )	8.93	U (kJ/gram)	4									
0.05		SpHt(kJ/g K)	0.00039	Rho(g/cm <sup>3</sup> )	1.8									
		Y-shear (Mb)	1.5	f(U-hex)	0.95									
<b>RADIAL STATOR CONFIG</b>														
<input type="checkbox"/> Turns #/#-density Turns/cm 1														
<b>HELICAL STATOR CONFIG</b>														
# of segments		5	Fuze M-factor	300										
# of rings		50	Fuze blow tx (usec)	2										
Flux loss dr (cm)		0.1	Fuze E-burst (kJ)	39										
			Fuzep4	49										
			Fuzep5	59										
			Fuzep6	69										
Seg. #	DZ (cm)	Pitch (cm)	# Cond.	Diam (cm)										
1	21.7	5.425	5	0.93										
					c:\fcgsca\markix.cfg									
<b>Resistivity Table</b> <table border="1"> <thead> <tr> <th>Point 1</th> <th>Point 2</th> <th></th> </tr> </thead> <tbody> <tr> <td>300</td> <td>1000</td> <td>deg K</td> </tr> <tr> <td>0.00172</td> <td>0.009954</td> <td>milliohm cm</td> </tr> </tbody> </table>						Point 1	Point 2		300	1000	deg K	0.00172	0.009954	milliohm cm
Point 1	Point 2													
300	1000	deg K												
0.00172	0.009954	milliohm cm												

Figure 4. Auxiliaries Input Window

As seen in Figure 4, the set auxiliaries window allows one to vary relevant parameters to define the generator in detail. These include stator and armature geometry/dimensions, winding sectors, explosive driver characteristics, and current/field excitation. About 16 parameters are available to adjust in the modes noted above.

To create the simulation code, a Fortran subroutine was written which receives its inputs from a Visual Basic interface. This makes for greater ease in use and a wider variety of options. The FCG core numerically integrates a set of ODE's with a Runge-Kutta (RK) scheme. This consists of a few circuit equations, depending on the circuit configuration, and some equations for the motion of the armature. Other auxiliary quantities, including load voltage and magnetic field energy in the FCG, are developed from the RK variables. Finally, some circuit parameters are calculated as a function of time from the evolving FCG geometry and are graphed for easy outcome analysis.

### Simulation Inputs

For my project three parameters were varied. These were seed current (.2MA, .4MA, and .8MA), primary inductance (50nH, 100nH, and 200nH), and secondary inductance (2000nH, 4000nH, 8000nH, 16000nH, 32000nH, 64000nH, 96000nH, 128000nH). All combinations of these three parameters were run except that the 96000nH and 128000nH secondary were only run with the 200nH primary and not the 50nH or 100nH primary. Also three tests were run without a transformer so that the effects of the transformer could clearly be seen. The three seed currents of .2MA, .4MA, and .8MA were still used. This created a total of 63 runs that were made.

### Results

The results of the 63 computer runs can be seen in Figures 5 through 9.

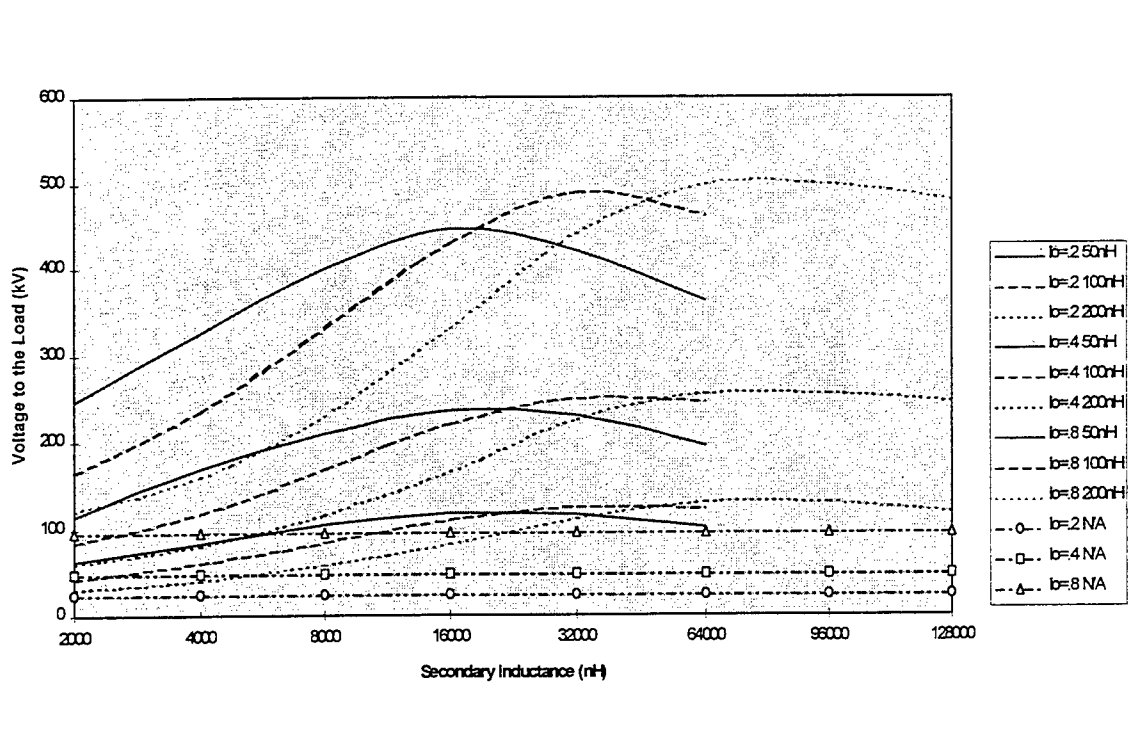


Figure 5. Voltage Versus Secondary Inductance

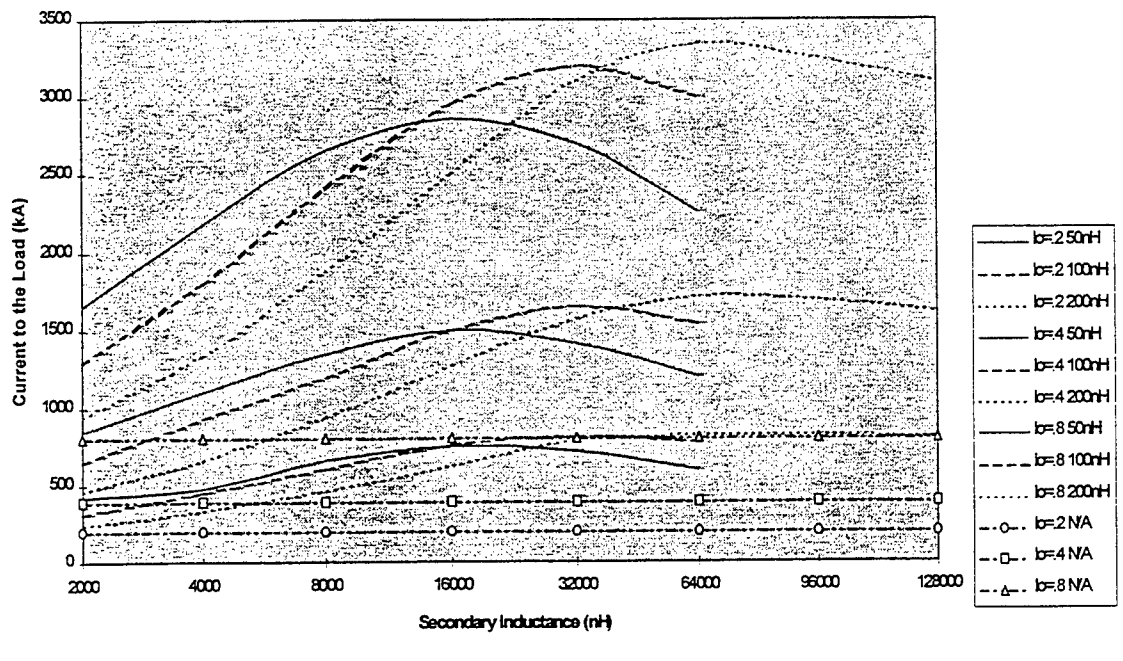


Figure 6. Current Versus Secondary Inductance

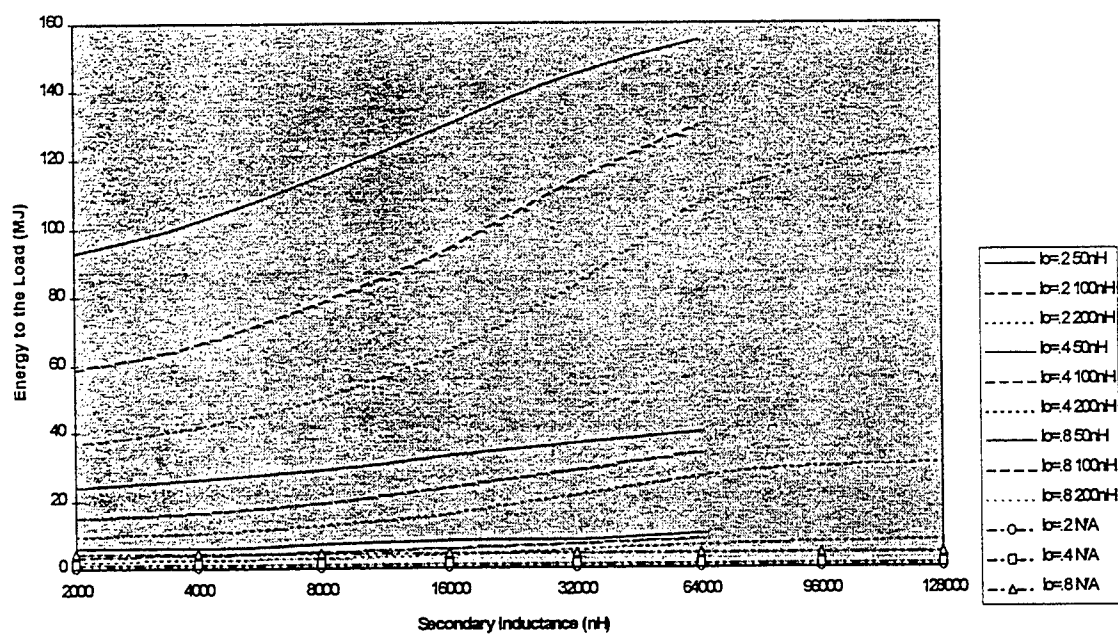


Figure 7. Energy Versus Secondary Inductance

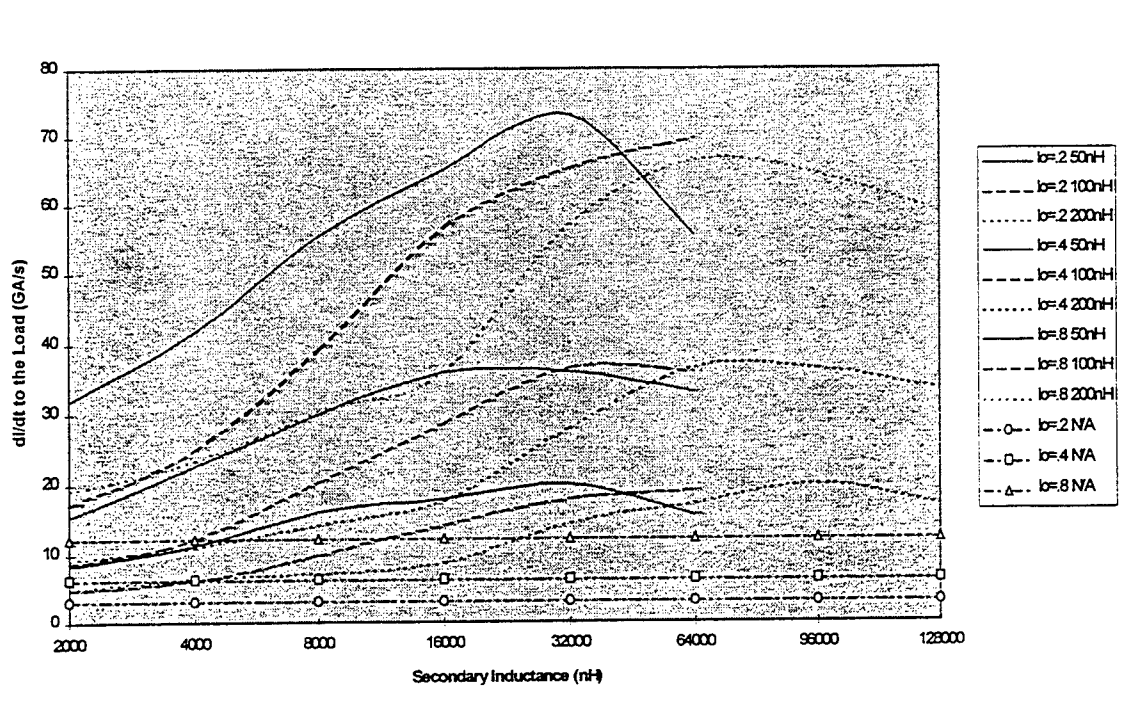


Figure 8.  $di/dt$  Versus Secondary Inductance

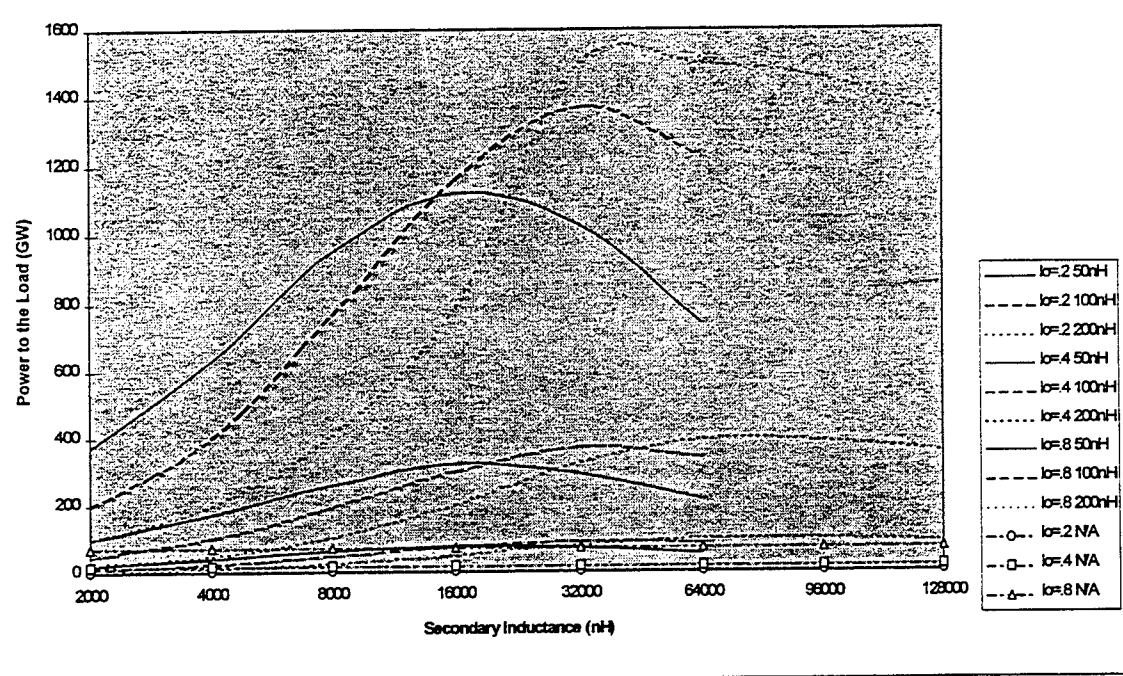


Figure 9. Power Versus Secondary Inductance

Based on maximizing all parameters graphed, the data shows that the seed currents of .8MA had the best results. This holds true for all the parameters being evaluated: voltage, current, energy, di/dt, and power. The primary inductance which produces the best results, however, fluctuates. In the cases of energy and di/dt, the .8MA seed current and 50nH primary produced the highest outputs, whereas in the cases of voltage, current, and power, the .8MA seed current and 200nH primary produced the best results. Also the runs without a transformer fall significantly below the others in which a transformer was used. In all cases, particularly obvious with respect to power and energy, the runs without the transformer are well below the runs in which a transformer was used.

### Conclusions

I conclude that the transformer makes a significant difference in the amount of voltage, energy etc. that gets to the load, thus making it an intricate part of any circuit. Table 1 shows the parameter being measured across the top, and along the side, the primary inductances. The table then shows the secondary inductances at which the primary inductances produce the best output.

	Voltage	Current	Energy	di/dt	Power
50nH	16000nH	16000nH	<i>64000nH</i>	<i>32000nH</i>	16000nH
100nH	<b>32000nH</b>	<b>32000nH</b>	<b>64000nH</b>	<b>32000nH</b>	<b>32000nH</b>
200nH	<i>64000nH</i>	<i>64000nH</i>	64000nH	64000nH	<i>32000nH</i>

All of the following values have a seed current of .8 MA

All of the values in *italics* are the highest outputs.

All of the values in **bold** are the second highest outputs.

Table 1. Configurations that yielded the best performance

A designer, knowing which of the values are most important to his system, could pick the primary and secondary inductances that give him the best results. For example, if a design required the highest energy possible in the load, the designer would look under the energy column to determine that in order to get the maximum energy possible to the load, he should use a .8MA seed current, 50nH primary inductor in the transformer, and a 64000nH secondary inductor. Another example may be that all five of these parameters are of equal importance. In that case, the designer may choose to compromise with a .8MA seed current, 100nH primary inductor, and a secondary inductor of 32000nH. This choice would yield the second highest output for four of the parameters. These are the kinds of decisions that a designer must make upon analyzing the data.

THE REMOVAL OF HAZARDOUS COMPOUNDS USING A NON-THERMAL  
DISCHARGE DEVICE

Michele V. Manuel

Crestview High School  
1304 N Ferdon Blvd.  
Crestview, FL 32536

Final Report for:  
High School Apprentice Program  
Wright Laboratory

Sponsored by:  
Air Force Office of Scientific Research  
Bolling Air Force Base, DC

and

Armstrong Laboratory

August 1996

## THE REMOVAL OF HAZARDOUS COMPOUNDS USING A NON-THERMAL DISCHARGE DEVICE

Michele V. Manuel  
Crestview High School

### Abstract

The use of a Non-Thermal Discharge (NTD) device to reduce hazardous emissions was studied. An exhaust stream which contained an overabundance of nitric oxide was used to see how much of this toxic compound could be removed. The experimental data indicates that there is a direct correlation between efficiency and power, and efficiency and the initial concentration of nitric oxide. Using less power and high initial concentrations of nitric oxide with the addition of ethanol has brought the final nitric oxide concentrations to only trace amounts. This data provides sufficient information to conclude that this is a mature and promising technology.

#### ACRONYM LIST

eV/molecule	Electron Volts Per Molecule
F	Volumetric Flow Rate
FTIR	Fourier Transform Infrared Spectrometer
HNO <sub>2</sub>	Nitrous Acid
HNO <sub>3</sub>	Nitric Acid
Hz	Hertz
L/min	Liters Per Minute
NO	Nitric Oxide
NO <sub>2</sub>	Nitrogen Dioxide
NO <sub>x</sub>	Oxides of Nitrogen
ns	Nanoseconds
NTD	Non-Thermal Discharge
P	Power Drawn In By The NTD Tube In Watts
ppmv	Parts Per Million By Volume
X <sub>initial</sub>	Steady-State Initial NO Concentration (with no tube power)
X <sub>final</sub>	Steady-State Final NO Concentration (with tube power applied)

# THE REMOVAL OF HAZARDOUS COMPOUNDS USING A NON-THERMAL DISCHARGE DEVICE

Michele V. Manuel  
Crestview High School

## Introduction

As industry, transportation, and the need for more energy increases, so does pollution. The industrial revolution has been one of the main causes of pollution [2]. When people crank up their cars, they become oblivious to the fact that they are releasing poisonous gases into the atmosphere. Gases that will eventually harm human health and animal life [1]. The government and various industries have become concerned about this global problem [7]. Acts such as the Clean Air Act Amendment of 1990 have been adopted to push industries to reduce their hazardous emissions. These firm regulations have caused a superfluous of technology to develop which will effectively remove hazardous emissions but at the same time be economical.

One of the main threats to the environment are the oxides of nitrogen ( $\text{NO}_x$ ) [4]. When released, they are usually in the form of nitric oxide. The main source of nitric oxide (NO) comes from the combustion of fossil fuels [3]. The high temperatures inside a gasoline or diesel engine allow nitrogen ( $\text{N}_2$ ) and oxygen ( $\text{O}_2$ ) to react to form nitric oxide which is then emitted into the atmosphere by the way of exhaust gases [8]. With the addition of ultraviolet radiation and oxygen, the nitric oxide will eventually become photochemical smog which is not only extremely harmful to plants and animals, but it can damage materials like paint, rubber, and plastic [2]. Furthermore, if  $\text{NO}_x$  reacts with water vapor in the atmosphere, it can produce  $\text{HNO}_2$  or  $\text{HNO}_3$ , also known as acid rain [8].

There are many ways to rid the environment of its gaseous toxins. One of the most promising and cost-effective is the Non-Thermal Discharge (NTD) device. Theoretically, any compound that can be oxidized by oxygen atoms can be removed with this process, and miscellaneous pollutants can possibly be removed at the same time [5].

Of the many types of NTD devices, the one discussed in this paper is the double dielectric-barrier discharge reactor. This means that the electrodes in this device contain a dielectric barrier on both sides [5]. The electrodes, which are supplied with a high voltage, produce an electric field. As the toxic gases pass between the electrodes, the electric field causes the gas to breakdown and produce a partially ionized plasma. At atmospheric pressures, this breakdown causes microdischarges (current filaments). The presence of the dielectric barrier causes the microdischarges to be shortened to around 100 ns. Due to the short lifetime of the microdischarges, the electrons do not thermally equilibrate so that the temperature of the bulk gas (heavy particles) stays relatively the same, hence, the name non-thermal. The electrons collide with the molecules in the gas to produce free radicals (an atom with at least one unpaired electron) like atomic oxygen. These free radicals drive the necessary chemical reactions to remove the hazardous compounds [4,5,6,7].

#### Methodology

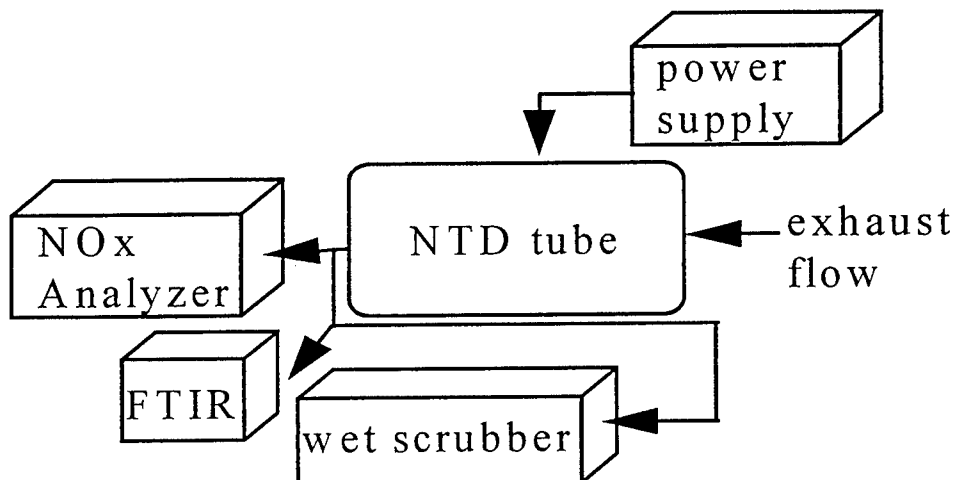


Figure 1. Schematic of the NTD process

In Figure 1, the toxic gas will flow in to the NTD tube were it will decompose or oxidize. The energy required for the tube is provided by the Elgar model 1001C (figure 2) and the output frequency used was 400Hz. This energy came through a 1:100 step-up transformer and then into the NTD tube. The current and voltage probes measured utility power and the total energy consumed [4].

## Power Supply

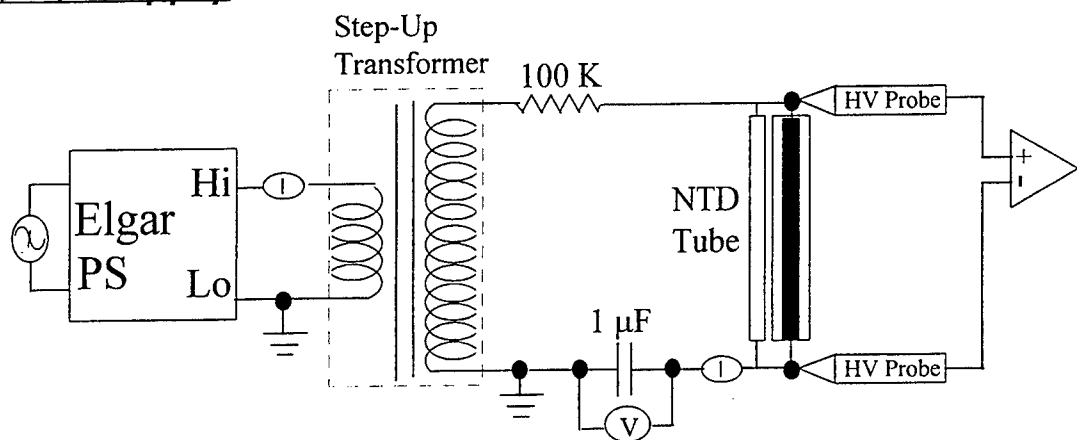


Figure 2. Schematic of NTD Electrical and Diagnostic Systems

The NTD tube consists of several electrodes covered with a dielectric material. The dielectric material not only creates an electric field, but it also prevents the gas stream from coming in contact with the electrodes. Since a dielectric material is being used, the discharge is quiet compared to a direct discharge between the electrodes themselves. As a result, this type of NTD device is also referred to as a Silent Electric Discharge [7].

After the NTD tube, the gas will then flow into two different instruments. The NO<sub>x</sub> Analyzer is a chemiluminescence device which measures and computes every 10 seconds the amount of NO and NO<sub>2</sub> in the gas

stream. The FTIR (which is an acronym for Fourier Transform Infrared Spectrometer) verifies the measurements of the NO<sub>x</sub> Analyzer and determines if there are any other compounds in the gas stream. The percent of NO removed is calculated using this equation:

$$\text{Percentage of NO Removed} = \frac{X_{initial} - X_{final}}{X_{initial}} \cdot 100 \quad (\text{E1})$$

$X_{initial}$  is the initial NO concentration with no power coming into the tube and  $X_{final}$  is the final NO concentration with power being applied to the tube.

When the gas stream is flowing through the NTD tube, various compounds can be injected into the stream to make the NTD process more efficient. A parameter was made to evaluate how much energy was consumed per NO molecule, or how much energy it took to change one NO molecule into one NO<sub>2</sub> molecule. This parameter is referred to as molecular energy consumption. The equation for this parameter is:

$$\text{molecular energy consumption} = \frac{(1.5 \times 10^4)P}{F(X_{initial} - X_{final})} \quad (\text{E2})$$

where  $X_{initial}$  and  $X_{final}$  are the same NO concentrations as defined in equation (E1) and expressed in ppmv. F represents the volumetric flow rate in L/min and P is the power in watts that is drawn by the NTD tube. The number  $1.5 \times 10^4$  is a temperature dependent conversion factor that allows the molecular energy consumption to be represented in units of electron volts per molecule (eV/molecule). Using both equations (E1 and E2), a chart was made to see which compound was the most practical and efficient (figure 3 and figure 4).

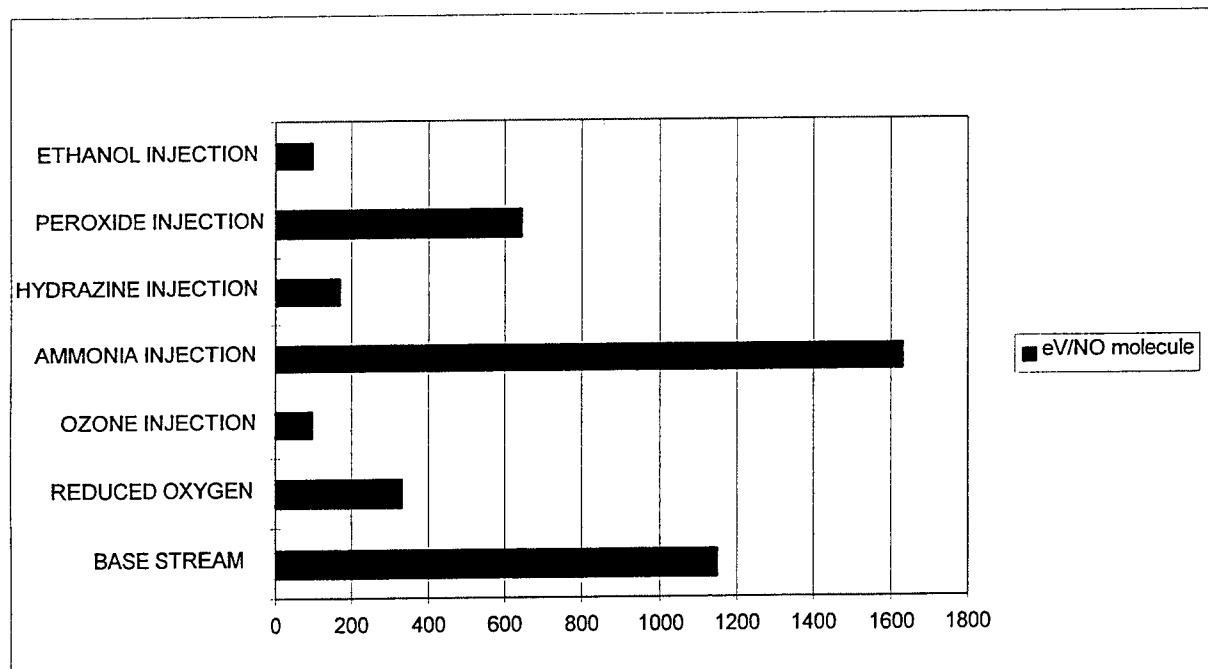


Figure 3. Molecular Energy Consumption at Maximum Removal

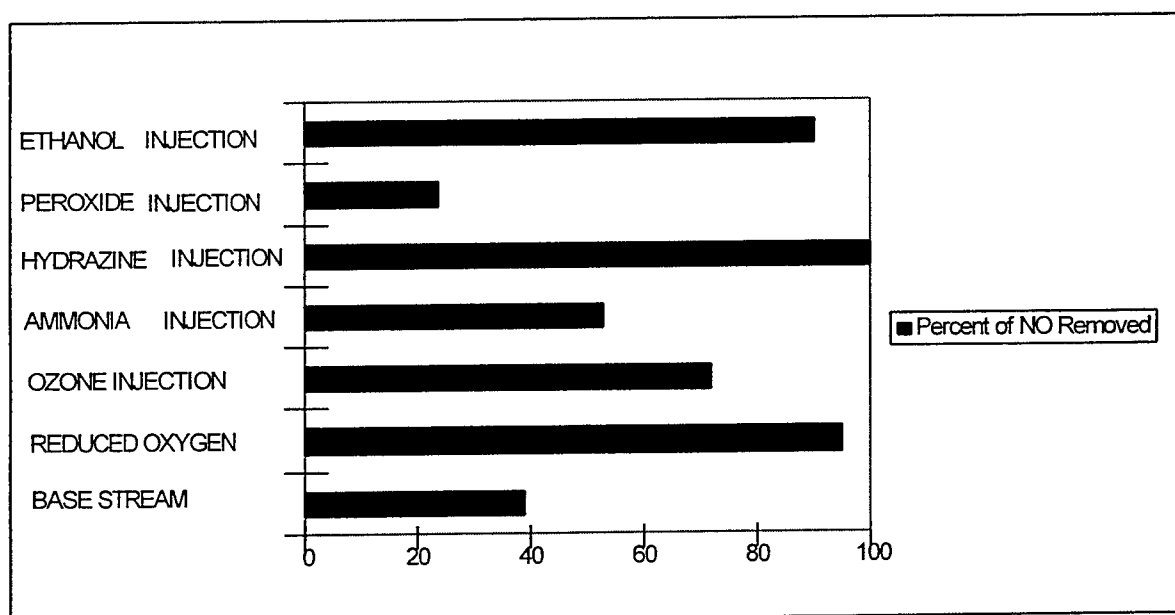


Figure 4. A Comparison of All Types of NO Removal

From both of these charts (figure 3 and figure 4), it is clear to see that injecting compounds into the gas stream performs better than non-injection methods. Of the six compounds shown, ethanol and hydrazine show the most promise. Although the hydrazine is very practical for removing NO from a gas stream, it has a high reactivity which makes it dangerous to work around when using high temperature gas exhaust streams. On the other hand, ethanol's high vapor pressure and widespread availability makes it the most pragmatic and easiest to use. The products formed inside the NTD tube and any excess ethanol can easily be removed by a wet scrubber.

Reverting back to figure 1; the gas stream, now comprised of  $\text{NO}_2$  instead of NO, will go into the wet scrubber. The wet scrubber uses jets to spray water on the gas stream as it passes through the scrubber. Because  $\text{NO}_2$  is highly soluble, it will combine with the water ( $\text{H}_2\text{O}$ ) and make nitric acid ( $\text{HNO}_3$ ), therefore, extracting the  $\text{NO}_2$  from the system [4].

### Results

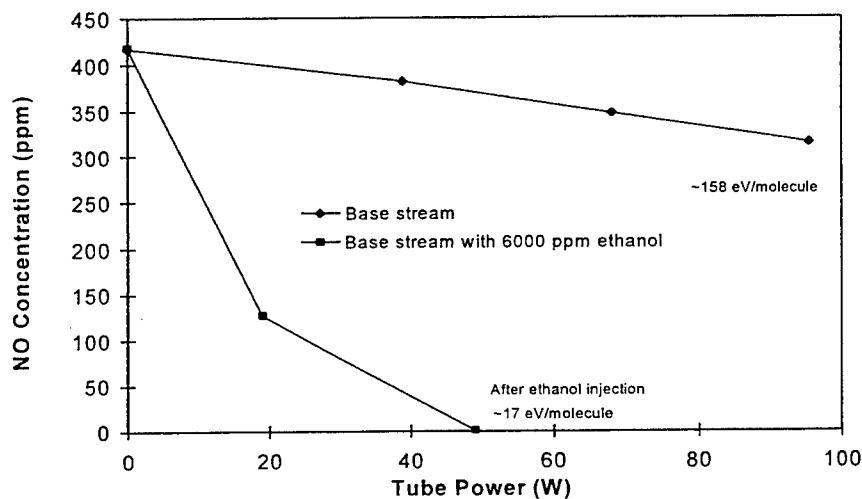


Figure 5. A Comparison Between the Base Stream and the Base Stream After Being Injected With Ethanol

Figure 5 demonstrates the drastic difference between the base stream (exhaust gas without the addition

of other compounds) and the base stream which has been treated with the ethanol. The eV/molecule easily shows that the base stream uses too much energy when trying to convert NO into  $\text{NO}_2$ . The graph reveals that the NO concentration has almost diminished with approximately 50 Watts of power.

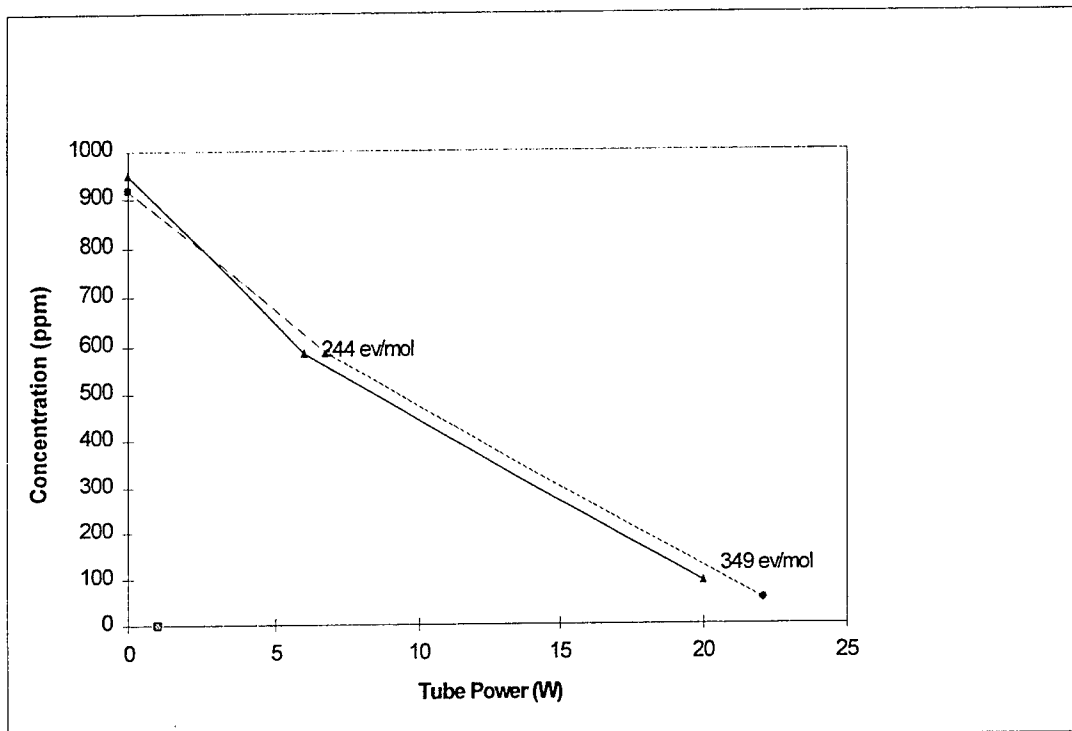


Figure 6. NO Concentration vs. Power

Figure 6 has two different runs using different amounts of power. The run using 349 eV/molecule is always at a higher concentration, however, the run using 244 eV/molecule is always at a lower concentration. This leads one to hypothesize that as more power is being used by the NTD system, the less efficient the process becomes.

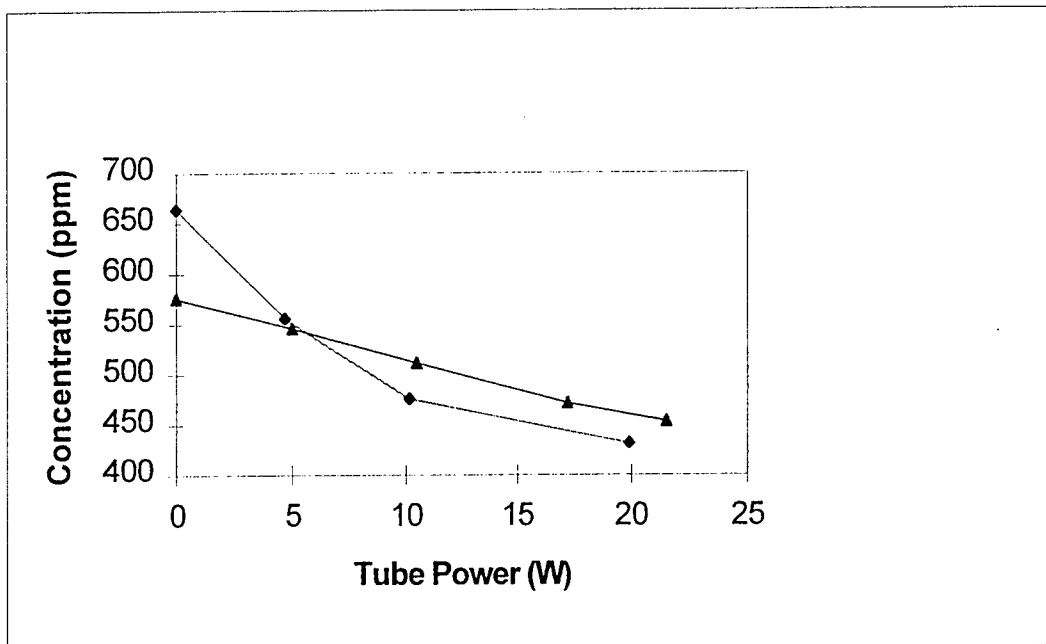


Figure 7. Comparison Using Different Initial Concentrations

It was observed that when two different initial concentrations were compared together, the higher of the two lowered the NO concentration the most, therefore, using a higher concentration makes the NTD process more efficient.

#### Conclusions

In conclusion, the data has been shown that prompts one to believe that efficiency increases with initial concentration and the injection of certain compounds, but decreases with increasing power. Overwhelming evidence has shown that the NTD process does work with high efficiency and at a low cost, the NTD device seems to be the most promising technology for the removal of hazardous compounds to date.

Acknowledgments

Mr. Don D. Harrison and Michael K. Deiler

Mentor: Dr. James B. Cornette

Mr. Mark Heyse

Mr. David Mandel

Mrs. Janice Vacchiani

Mr. Matt Matyac

Dr. Keith Jamison

NTD Team: Mr. Larry Crow, Mr. Steven P. Federle, Dr. Mark Hoffman, Mr. Donald M. Littrell, Mr. Alan Nejezchleb, Dr. John Rogers, Dr. Glen Rolader, and Mr. Ron Toole

And all of the other apprentices

### References

- [1] "Air Pollution." [ht://science.coe.uwf.edu/SI/curr/air.pollution/air.htm](http://science.coe.uwf.edu/SI/curr/air.pollution/air.htm), Online, World Wide Web, 1996.
- [2] "Air Pollution." <http://plq091.okanagan.bc.ca/geodept/G210~7~7~3.html>, Online, World Wide Web, 1996.
- [3] "The Chemistry of Atmospheric Pollutants." <http://www.aeat.co.uk/products/cen/airqual/kinetics/chem.html>, Online, World Wide Web, 1996.
- [4] Federle, P. Steven, et al. The Removal of Nitric Oxide using a Non-Thermal Discharge Device. Eglin Air Force Base: Wright Laboratory, 1996.
- [5] Penetrante, M Bernie, and Shirley E. Schultheis. Non-Thermal Techniques for Pollution Control. vol. G34(A), 1993.
- [6] Rogers, W. John. "Non-Thermal Discharges." <http://www.gnt.net/~rogersjw/research.html>, Online, World Wide Web, 1996.
- [7] Rolader, E. Glenn. "Commercialization of Dual Use Technologies." SAIC Proposal #01-0512-71-0950-201, 1994.
- [8] Zumdahl, S. Steven. Chemistry. Lexington: D.C. Heath and Company, 1986.

COMPUTER APPLICATIONS FOR  
SPEED AND EFFICIENCY

Bud A. Miyahara

Carroll High School  
4524 Linden Avenue  
Dayton, OH 45432

Final Report for:  
High School Apprentice Program  
Wright Laboratory

Sponsored by:  
Air Force Office of Scientific Research  
Bolling Air Force Base, Washington DC

and

Wright Laboratory

August 1996

COMPUTER APPLICATIONS FOR  
SPEED AND EFFICIENCY

Bud A. Miyahara  
Carroll High School

Abstract

At Wright Labs, things must be done quickly and efficiently. This also applies when it comes to the use of the computers, at Wright Labs. Problems come up like shortage of disk space, slow calculating speeds and an ever present "crash" tendency. The files and programs must be manipulated in order to have the best performance out of the program. Another problem that arises is, which system, Macintosh or PC, will it perform on best? These are all problems that have to be taken care of by smart computer management.

## COMPUTER APPLICATIONS FOR SPEED AND EFFICIENCY

Bud A. Miyahara

### Introduction

A workbook was created in *Microsoft Excel 7.0* that calculated a table of data into usable computations which could then be graphed. The workbook performed the calculations and created graphs of those calculations in one step. The user only has to enter the data in once and it calculates several pages of data and graphs. Also a database was created to store the inventory of the lab. This database was created by another person earlier using *FileMaker Pro 2.0*, which was converted to *FileMaker Pro 3.0v3*. The previous database was modified to reduce the size and increase its performance. Also the database includes a full set of color illustrations to help reference the items.

### Calculation Workbook

A spreadsheet was needed to calculate three different functions for a given set of data. First *KaleidaGraph 3.0.4*, Macintosh, was used for this task. The special feature of *KaleidaGraph* was the Macro calculator. It is an internal, programmable calculator that uses Reverse Polish Notation to create macros. The calculator was tedious to program and difficult to use. Then the project was changed to use *Microsoft Excel 7.0* on the PC. It was easier to create, but when it was first created all three calculations were in separate applications. This was difficult to use and had a tendency to “crash” when it was in Macintosh form. The main problem was when you wanted to enter in a new set of data. The data had to be placed in three different sectors of the package. This was very time consuming and not very effective. Finally the program was changed into a new form called a workbook. A workbook is a set of spreadsheets that are all interlinked and are dependent on each other to perform the tasks. The set up of the workbook is as follows:

Sheet 1: Data- the one area designated to hold the set of data for the entire workbook. This page also calculates the average value of each test set.

Sheet 2: Average Relative Error- calculates the relative error point by point and the average relative error for the complete set, comparing every set to one another. Uses the Data page as reference.

$$\frac{|X - Y|}{X} \cdot 100$$

$$\frac{\frac{|X - Y|}{X} \cdot 100}{N}$$

Relative Error

Average Relative Error

Sheet 3: ARE Graphs- displays 4 graphs that show the relationship between four different test sets. Uses Average Relative Error page as reference.

Sheet 4: Mean Square Error- calculates the square error point by point and the mean square error for the complete set, comparing every set to one another. Uses the Data page as reference.

$$(X - Y)^2$$

$$\frac{\sum_{p=1}^N (X - Y)^2}{N}$$

Square Error

Mean Square Error

Sheet 5: MSE Graphs- displays 4 graphs that show the relationship between four different test sets. Uses Mean Square Error page as reference.

Sheet 6: Correlation- calculates the correlation of the test sets. The calculation is so complicated that it needs a calculations page for intermediate figures. Uses the Data and [Correlation] pages for reference.

$$\frac{\sum_{p=1}^N (X - \bar{X})(Y - \bar{Y})}{\sqrt{\sum_{p=1}^N (X - \bar{X})^2} \cdot \sqrt{\sum_{p=1}^N (Y - \bar{Y})^2}}$$

Correlation

Page 7: [Correlation]- acts as a calculations page for Page 6. Does not contain useful calculations. Uses Data and Correlation pages for reference.

Page 8: Final report- lists the Average Relative Error, Mean Square Error, and the Correlation for each test set. Uses Average Relative Error, Mean Square Error, and Correlation pages for reference.

### Inventory Database

The department wanted a database to aid them in recording the periodic equipment inventory. The database was to include a color picture of every item. The pictures were taken with an Apple *QuickTake 100* camera. A Macintosh computer was needed because the *QuickTake 100* camera is not compatible with a PC. It was decided to use the program *FileMaker Pro* as the base of our database. *FileMaker Pro* is extremely "user friendly" and easy to learn. However, problems did arise when the hard drive on the computer, used to store the database, was full. The computer started to "crash" frequently and every time it "crashed" it corrupted the file. When the file became corrupted it had to be ran through a "recovery" program to bring it back. It took a great deal of time to recover a one hundred megabyte file. A *Zip* drive was brought in at no avail, because the database soon out grew that also. Finally, as a last resort, the database was put on the *Novell* network server. The problems ceased because now there was plenty of room for the database to grow while pictures were added. The database was growing extremely large once the pictures were included. The database included close to four hundred and fifty items and a picture for each of them takes up a lot of room.

Another problem that arose was that the program was running slower than expected. This large program was on an older model *Power Macintosh* with a maxed out hard drive. Because of this, the inventory database was in close to two hundred and fifty fragments all over the hard drive. The speed was less than optimal and this was resolved by placing the file on the server so that the file was all together and the computer had more room to work with.

### Conclusion

It was found to be that the Macintosh seemed to be more "user friendly," however, there was better performance out of the PC. The PC's speed was much quicker than the Macintosh and it handled files much more smoothly with less problems. This conclusion is heavily weighted by the age of the two computers. The PC is much newer than the Macintosh, therefore, having a huge advantage. Also the user must use what they are comfortable with and design programs to suit their needs and desires.

## Directions for AAD Inventory v.BUD

### Guide to Loading Pictures into Computer

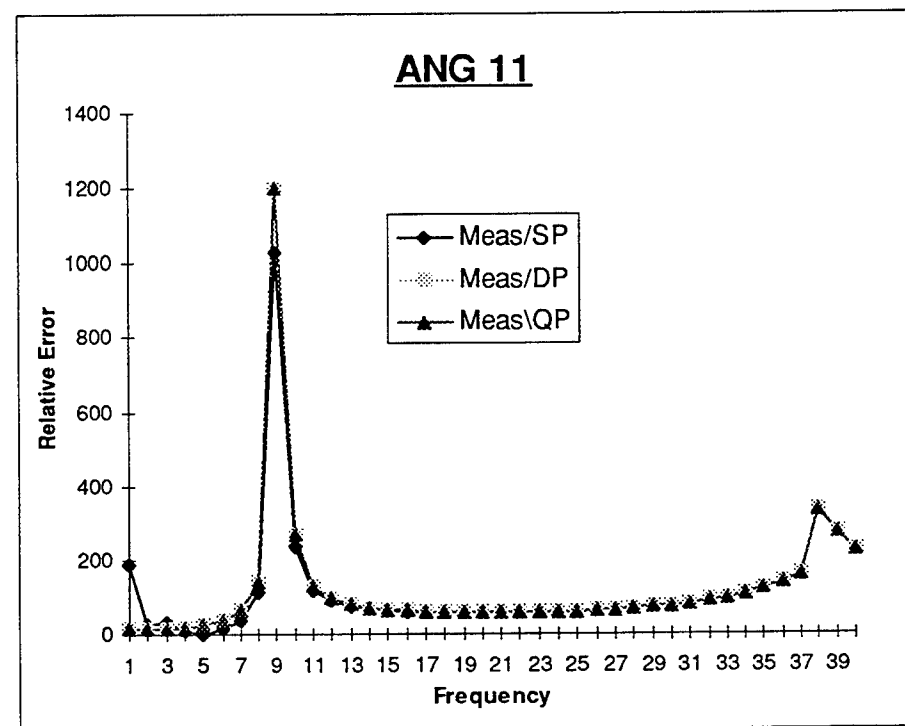
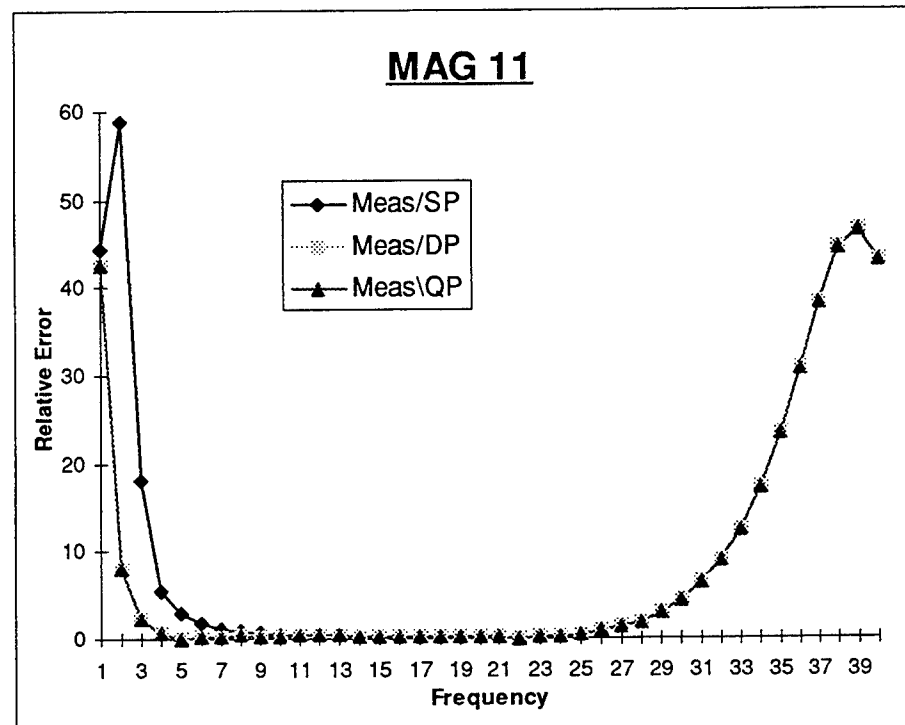
- 1) Turn on *QuickTake* (PM6100\QuickTake\QuickTake executable)
- 2) Go to Camera and select “Move Photos to Disk”
- 3) Select directory to enter photos into
- 4) Click save
- 5) Click on name and change to the desired file name

### Loading Pictures into Inventory

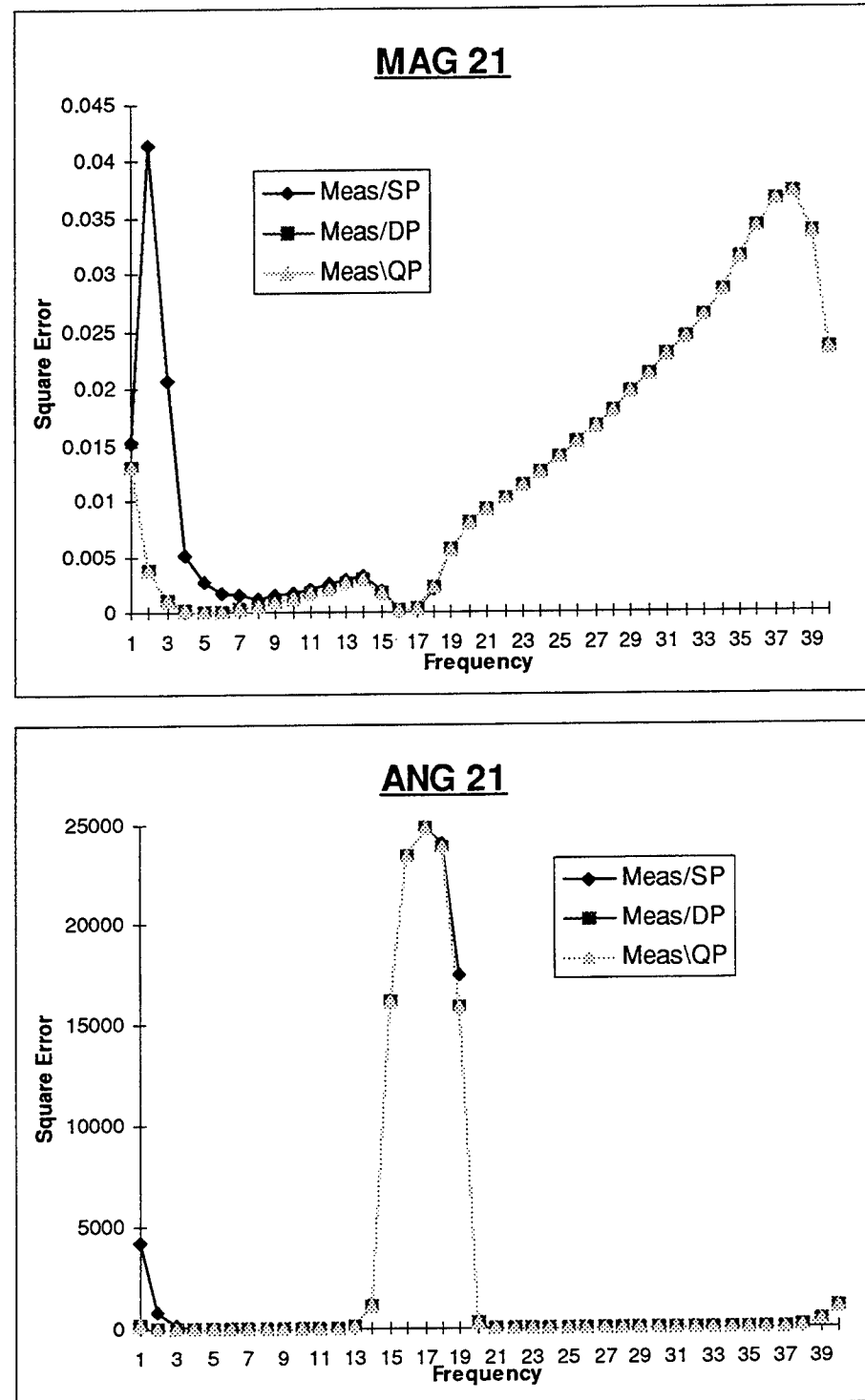
- 1) Open the picture using *JPEG View* (Drag icon onto View executable)
- 2) Select the window size you want by dragging cursor and making a box
- 3) Hit “Open Apple” and “C” simultaneously to copy picture into the clipboard
- 4) Check picture quality by opening the “View clipboard” under the “Edit” bar
- 5) If split screen: repeat steps 1-4 using different size windows
- 6) Once you have a good picture open the Inventory file in *FileMaker Pro 3.0v3*
- 7) Page through and find the correct page
- 8) Scroll down and select the picture window
- 9) Hit “Open Apple” and “V” to paste the picture in the box

Graphs from Calculations Workbook

**ARE Graphs**



### MSE Graphs

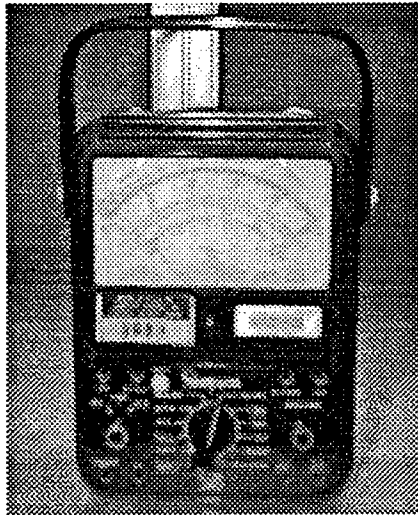


Example Inventory Page

**AAD INVENTORY WORKSHEET**

Account _____	JON _____	Date <u>28 Jun 96</u>
EMAS# (or accountability code) <u>A068792</u>	Item <u>MUTLIMETER</u>	
Manufacturer and address _____	Part Number <u>SIMPSON 260</u>	Serial Number <u>3933</u>
	Cost <u>\$ 129.62</u>	Date Purchased _____
Location (Bldg/Room) <u>B620 RM S2 L48</u>	Point of Contact _____	
Size (lxwxh) _____	Weight (lb) _____	Stock# <u>6625009853951</u>
PME# _____	PMI# _____	Status <input type="checkbox"/> CAL <input type="checkbox"/> NPCR <input type="checkbox"/> PMI <input type="checkbox"/> NP
ADPE ? <input type="radio"/> Yes <input checked="" type="radio"/> No	Is it a system ? <input type="radio"/> Yes <input checked="" type="radio"/> No	Turn in item ? <input type="radio"/> Yes <input checked="" type="radio"/> No
Comments _____	Purchased by: _____	TSSI PO# _____

EMAS# A068792 Item MUTLIMETER



THE STUDY OF THE NEOTAM  
COMPUTATIONAL MODEL

Disha Jayantilal Patel

Kettering Fairmont High School  
3301 Shroyer Road  
Kettering, Ohio 45429-4253

Final Report for:  
High School Apprenticeship Program

Sponsoring Laboratory:  
Wright Laboratory-WL/AACT

Sponsored by:  
Air Force Office of Scientific Research  
Bolling Air Force Base, Washington DC

and

Wright Laboratory

and

Wright Patterson Air Force Base, OH

02 August 1996

THE STUDY OF THE NEOTAM  
COMPUTATIONAL MODEL

Disha Jayantilal Patel  
Kettering Fairmont High School

Abstract

Research was done on the NEOTAM computational model. This model is being developed by a NATO research study group to enable both expert and inexpert users to efficiently conduct R&D on electro-optical aerial targeting. The primary purpose of the research was to give feedback on how to improve the Cantata GUI (Graphical User Interface) for the NEOTAM model, so new users would be able to use the model with ease. The feedback was also being used to inform the NEOTAM phenomenologists about what needed to be done in order to improve the NEOTAM model. However, before commenting on NEOTAM could begin, the concepts of electro-optical aerial targeting had to be understood. Several weeks were spent on studying these concepts. After these concepts were understood, commenting and collecting results began. Experimental results indicated that the NEOTAM model needed improvements, so users could easily execute the model. Experimental results also indicated how Cantata was poorly installed. One example was the main library (FORTRAN 77 library) could not be found on the SUN system and had to be installed. Also, major files that were needed were not found. However, even though errors hindered the research, progress was made in some areas such as, changing the color palette and producing some data from running the sub-models SOBOAT and REP. Overall, the comments that were made will help NEOTAM model builders make NEOTAM more sufficient in the future. The comments will also help the research and development of the USAF Wright Laboratory's AEM\*AT (Advanced Electromagnetic Model for Aerial Targeting), which uses much of the same technology.

## TABLE OF CONTENTS

TITLE PAGE.....	1
ABSTRACT.....	2
INTRODUCTION.....	4-7
PURPOSE.....	7
PROBLEM.....	7
METHODOLOGY.....	8
DATA/RESULTS.....	8-12
CONCLUSION.....	12-14
REFERENCES.....	14
POSSIBLE REP GUI GLYPHS (FIGURE A AND FIGURE B).....	15
POSSIBLE REP GUI GLYPHS (FIGURE C, FIGURE D, FIGURE E).....	16
END-TO-END PHENOMENOLOGY TRIAD DIAGRAM.....	17
SIGNATURE FACTORS TABLE.....	18

## THE STUDY OF THE NEOTAM COMPUTATIONAL MODEL

Disha Jayantilal Patel

### Introduction

Research was done on the utility of the NEOTAM code to support electromagnetic spectrum targeting analysis. NEOTAM stands for NATO Electro-Optical Targeting Analysis Model. NEOTAM is also representative of the technology used in the USAF Wright Lab AEM\*AT (Advanced Electromagnetic Model for Aerial Targeting). The research focused mainly on aerial targeting. Targeting means to find an object of interest and then shoot at it. The electromagnetic spectrum is used to predict the location of aircraft, ground sites (buildings), ships, etc.

Electromagnetic spectrum targeting is a fairly recent, technological advancement in the research and development field. Electromagnetic spectrum targeting started in the 1950's with the evolution and development of the SIDEWINDER "heat-seeking" missile. Since then, the development of technology in electromagnetic spectrum targeting has grown rapidly. Decision-makers have demanded that the performance of new system ideas be forecast with better fidelity before they agree to invest. Computational models like NEOTAM are the response to that demand.

The electromagnetic spectrum is defined as an arrangement of various electromagnetic radiations by wavelength and/or frequency. The electromagnetic spectrum consists of gamma rays, x-rays, ultraviolet, visible, infrared, and radio frequency. The parts of the spectrum mainly focused on during research were visible (0.4 $\mu\text{m}$  to 0.7 $\mu\text{m}$ ) and infrared (IR) (3.0 to 5.0 $\mu\text{m}$ /8.0 to 12.0 $\mu\text{m}$ ). ( $\mu\text{m}$  stands for micrometers.)

Visible radiation is the wavelength band of 0.4 to 0.7 micrometers. It is the area of normal human vision. Visible radiation can be seen with the human eye.

On the other hand, infrared cannot be seen with the human eye. Infrared must be "seen" with instruments. Infrared is part of the invisible spectrum that is contiguous to the red end of the visible spectrum. The range of infrared can be between 0.7 $\mu\text{m}$  to 24.0 $\mu\text{m}$ . The infrared range is divided into smaller divisions. These divisions are near, mid-wave, long-wave, and millimeter-wave. In targeting, any of the infrared ranges can be used.

Most infrared systems used in targeting, operate "passively". "Passive" means that it does not send out any emissions, but it only receives them. Radar, for example, is "active" rather than passive. Radar sends out a signal in order to get a signal back. Your eye, on the other hand, also operates passively. It makes use of electromagnetic energy reflected from objects.

Instead of reflected electromagnetic energy, most infrared targeting systems detect the emission of electromagnetic energy corresponding to heat. Infrared systems detect the differences in heat emissions from the warmer and cooler parts of the target (aircraft). Thus, the heat emissions spotted by the sensor system help in figuring out if the aircraft is a friend or a foe. The heat emission from an aircraft is one of the signatures/characteristics that help in making sure no mistakes are made in targeting. And because the systems permit targeting decisions to be made quickly and beyond visual ranges, IR systems are used to detect the target in an

efficient way.

In order to understand the concept of electromagnetic spectrum targeting, one must understand signatures and variables that affect targeting, like environmental conditions. Signatures are unique characteristics of someone or something. People have fingerprints as one kind of signature. Likewise, airplanes have their own electromagnetic signature. By using the electromagnetic spectrum, a targeting system can tell the difference between aircraft: for example, the country they are from. By using this system, one can tell if the target (aircraft, vehicle, building, etc.) is an enemy or a friend, and one can also tell the difference between an F-15 and an F-16. In other words, when the electromagnetic spectrum is used in aerial targeting, each plane produces its own definite pattern of shapes and intensities.

The weather/environment also plays a very important role in targeting. Weather has strong effects on the target signature. Weather has strong effects on how the signature is propagated to the sensor through the atmosphere. Weather is a major variable that effects the performance of a sensor system. Rain, haze, fog, and snow degrade the performance of sensors. Clouds, gases (like CO<sub>2</sub>, O<sub>2</sub>, O<sub>3</sub>), and precipitation affect electromagnetic energy while it passes through the atmosphere. The target/background radiant signature attenuates (loses energy as passes through the atmosphere). This energy loss decreases the effectiveness of EO (electro-optics) systems. The background (soil, grass, trees, roads, towns, mountains), atmosphere (clouds, humidity, wind speed, air temperature, smoke, dust), and climate (insolation/incoming radiation/sunlight, latitude of the target, solar zenith and azimuth angles) are all part of the environment. Each of the environmental variables has their own effect on electromagnetic targeting. When the variables that affect the targeting are collected, various math algorithms are incorporated in the model to predict the location of the target.

Sensors are used to detect targets, and these sensors use the electromagnetic spectrum. The end-to-end analytical targeting model consists of four major components: a target-background signature model, an atmospheric transmission model, a sensor characteristics model, and a systems performance model. A model is an imitation of some aspect of a real object or process. An equation which predicts the relationship between temperature and voltage in a light bulb is an example of a model. The target-background signature model predicts the background and target signatures, considering all influences. The atmospheric transmission model gives a representation of the atmosphere for the path from sensor to target. The sensor characteristic model describes the transducing of the received signals from the background and target with the sensor components. The systems performance model uses the above models to produce an estimated outcome from the variable data inputted into the computer system.

The way the four components work together are described below. Local weather conditions, regional atmospheric conditions, and battlefield activities are inputted into a computer system. The atmospheric transmission model collects environmental information, processes it, and does various calculations. One of the most important inputs is processed in the target-background signature model. Calculation of energy fluxes are made, and a description of the thermal and physical characteristics of the target and background are needed for calculations in the target-background signature model. Some of the environmental information, required is terrain elevations, weather, soil moisture content, soil and vegetation temperature, vegetation type, zenith and azimuth angles of the sun, latitude of target, and atmospheric concentrations. Weather is the main reason for energy fluctuations. Weather is the most important input into the sensor performance prediction procedure. The weather

must be kept up to date so that no inaccuracy can occur in targeting.

So overall, the phenomenology behind electromagnetic spectrum targeting can be considered as three main topics or a triad: the target and background contrast (signal being sent), the path (noisy propagation medium), and the sensor system (signal being received and processed). The target and background comprises the target itself, the sky background, terrestrial backgrounds (natural and cultural details), and the environmental influences. The path comprises the influences on the signal as it travels from the target to the sensor. These include transmission losses, path radiance, and shimmer (local prismatic properties of atmosphere that cause geometric and intensity fluctuations). All these affect the propagation of the electromagnetic signal to the sensor. They affect the transmission through the path by modulating and degrading the contrast signal being sent by the target. The sensor system includes the optics, detector, electronics, gimbal (a pointing and stabilization mechanism), and display or automated decision making apparatus. As all three parts of the triad function together, outputs are produced. The outputs of the model may be standardized plots, numerical data, and/or radiometric imagery. So the targeting process starts as follows: The sensor system searches for the target by using some portion of the electromagnetic spectrum. The wavelength emitted by the target/background may run into difficulties like a cloud blocking the target from its sensor. Thus, the person or whatever is making sense of the received signal from the sensor must take into account the problems that are faced as the signal traverses the path to the target. Finally, when the signal reaches the sensor, it is transduced, and then calculations and data are inputted and made. An illustration of the phenomenology of electromagnetic spectrum targeting appears on page 17.

Modeling is used as a low-cost, efficient way to predict the utility of various schemes and devices for targeting. It is used to test different variables that may have an effect on targeting by using a computer system rather than buying and flying a multi-million dollar aircraft.

Modeling has progressed so that small computers are usable. Some of the computer systems used in targeting analysis are Suns, Silicon Graphics, Power PC, Hewlett Packard, IBM Unix platforms, and DEC Alpha.

NEOTAM is a computational model for electromagnetic spectrum targeting analysis. This model allows a person to test different variables (environments, target, background) in order to see which ones, when combined, produce an effective sensor system. The research described here concentrated on the NEOTAM GUI (Graphical User Interface). The goals of the GUI are to allow newcomers and novices with very little background on electromagnetic spectrum targeting, to make calculations on aerial targeting situations quickly, efficiently, and correctly, and to raise the productivity of experts. The NEOTAM model uses the Cantata GUI, which is part of Khoros.

NEOTAM consists of sub-models that help in calculating aircraft and missile signatures. They are CET93, NIRATAM, NPLUME, REP, SOBOAT, OSIC, and REP2NIR. CET93 is a NASA code for calculating the engine exhaust species and conditions of a missile motor. NIRATAM calculates the IR radiation emitted from a faceted representation of a target hardbody and the IR radiation from turbine engine plumes. It is a radiation model that is primarily used for the IR and visible bands. NPLUME is the plume model that is used primarily for aircraft plumes and is part of NIRATAM. REP is a rocket plume flow field model. It models only the gaseous constituents of plumes, omitting particles. SOBOAT is from Germany and is a rocket plume flow-field model. OSIC is a UV scattering and atmospheric transmission model. REP2NIR translates the REP output plume flow file to

NIRATAM's input file.

The objective of the research was to exercise the NEOTAM model using different variables. By trying the variables together, one can find the best and the worst ways to accomplish targeting. Since the system that was used was in GUI-style, if one made an error, the system would inform the person that he/she made an error. This would help that person avoid making the same error again. However, trying to run the NEOTAM model successfully was not the main criterion. One of the main criteria was to find the "glitches" in the NEOTAM model (like logic or algorithmic inconsistencies, obscure variable-names or -units, wrong or missing connections, even spelling errors, etc.), and try to correct them. The research products were mainly documented comments on the glitches in the NEOTAM model, in a form which will help NEOTAM developers perfect the program and make the program easier to use.

In order to complete the research, a SUN SPARC2 work station and a Macintosh were set up and used.

Also during this research, a scenario report was written. The report shows how electromagnetic spectrum targeting is used in the scenario of a nuclear bomb.

#### Purpose

There were numerous purposes for this research program. A principal purpose was to learn to use a simplified model of NEOTAM and give feedback to developers on how to make the model user friendly, for those who have a faint background in electromagnetic spectrum targeting. Note that running the NEOTAM model successfully was not the main purpose. The main purpose was to find the "glitches" in the NEOTAM model (like logic or algorithmic in consistencies, obscure variable -names or -units errors, wrong or missing connections, even spelling errors, etc.) and try to correct them if time and skill permitted; otherwise to document them for improvement by the NEOTAM developers. A necessary purpose of this program was to learn how the electromagnetic spectrum is used for targeting and why is it used. Another purpose was to become computer literate with Macintosh and UNIX Platforms. One other purpose was to strengthen my science and math skills. Another purpose was to have experiences which will help me make a choice in what I would like to do in the future. Another purpose was to become familiar with several software programs.

#### Problem

The problem that needed to be solved was how to make the GUI-style NEOTAM simpler so new users, who have had no background in the many sciences and technologies involved in EO aerial targeting, will not have a problem when using the NEOTAM model. But this introduced new obstacles: I had to learn how to use the NEOTAM model successfully and to grasp the basic concepts of electromagnetic spectrum targeting before the eight weeks were up. The expected solution to the problem was to discover the "glitches" in the NEOTAM model and try to give advice in correcting them. One other main problem was to identify where the NEOTAM model needed to offer more help or more explanation, so new users would not have a problem with it. Since one aspect of our task was to try to make the software flow easier so people could use the NEOTAM model successfully on the first try, we have suggested ways to convert the "command-line" input mode of some of the models into the GUI glyphs.

## Methodology

In order to solve the problems, several steps were taken and several materials were needed. The materials needed were a Macintosh computer, a SUN SPARC2 work station, the NEOTAM model, and instructional books on EO targeting/programming/background uses. The very first step was to understand the concept of electromagnetic spectrum targeting. In order to grasp the concept, reading was done, notes were taken, movies were watched, and explanations by the mentor occurred. After grasping the concepts of using the electromagnetic spectrum for targeting, the Macintosh computer was introduced. This was where formatting disks, copying information, and installing software (File Maker Pro, Mac Write Pro, Mac Draw Pro, Mac Project Pro) occurred. Then the SUN SPARC2 station was introduced. The SUN station was where the running of the NEOTAM model occurred. However, in order to use the SUN, UNIX programming was needed. So books on UNIX were read. UNIX commands were also learned. Also, the Khoros Cantata program was learned in order to tinker with the NEOTAM GUI. All this background education took about five weeks, and was only possible by doing some work at home. The rest of the time was spent using the NEOTAM model. Each day was spent with four hours or more working with the NEOTAM model. During the running of the NEOTAM model, notes and comments were taken down. Then the notes and comments compiled were turned into data. The rest of the day remaining was for organizing, learning more about the SUN and UNIX system, and using references, interviews, and the World Wide Web for additional background on the research topics.

## Data/Results

The following data was collected on the first day of actually running the NEOTAM model, using the Khoros Cantata program: Trying to get into Cantata posed a problem. The icon Runneo was selected and then a window asking for a “shell tool” icon appeared. The term “shell tool” was not understood clearly. For a new user, Cantata should have an explanation of what a shell tool is. But that was the only problem getting into Cantata.

When the NEOTAM model started, the first thing executed was trying to make a network that would produce an image. In order to make the image network, input sources, input data file, and the ball image (an exemplary file) were selected. Then the input image was converted to a glyph. (Glyph means a small pictorial icon that is easy to work with.) Then a put\_update glyph was needed. In order to make that glyph, the output, display images, and display with update were selected. The two glyphs had to be connected so the image could be produced. So the arrow in the image glyph was clicked, and the first arrow in the put\_update glyph was clicked. A connection line was made, yet it could not be seen, because the colors had no contrast. There was a black background, black/gray icons, and the connection line itself was black, so the line of connection could not be seen. Thus, the problem of a color palette arose. There should be a color palette control function that can be reached by the user with simple ease so the colors of the screen can be changed. We ignored the changing of the color palette at this time, so we could continue building the image network. The “light switch” on the top right hand corner of the put\_update glyph was turned on. This “switch” told Cantata to begin executing the image network. After a couple of seconds, the image of a 3-D, gray ball appeared. So the image network had executed correctly and the result obtained after running the network was an image of a ball.

Also, other images were made (like a flower, a lizard, a spine, etc.). The only thing that was different for each procedure was, instead of selecting the ball image icon, a flower image (or lizard, spine, etc) icon was selected.

After image networking, it was decided to try some variable networking in order to run the NEOTAM model. We first selected the environment section (click on NEOTAM toolbox to environment) and inputted scenario data. The scenario was entered in as follows:

Climate/Environment  
engagement setup

Site Location:

Latitude: 39.50

Longitude (W): 84.03

Local Start Time:

Month #: 7

Day of month: 10

Hour (24 hr): 1300

Simulation Segment:

Start Time (s): 05

End Time (s): 20

Increment Size (s): 01

Then we attempted to save this scenario. However, when the save button was selected, Cantata did not save it and produced the following message: khorus\_init: Couldn't write to log file "/export/tools/khorus 1.5/log". Every attempt to save the environment resulted in the message above. Different scenarios were tried in order to be sure the failure was not the result of our inputting wrong information. This showed the information was not the problem. The other part of the environment data was entered as follows by clicking on selection boxes with pre-programmed choices:

-Hawaii (Hilo)

-Tropics

-July

-25 km visibility

When we attempted to save this scenario, it was not saved and the same error message came up. Our attempt to figure out why the item could not be saved was still unanswered. NEOTAM should offer feedback which explains why a request is refused.

Also it was frustrating to enter data from the keyboard into the provided spaces. Often after we clicked into the box where we intended to type, it would accept one character and then stop. The cursor had to be in the box at all times in order to enter data. That was frustrating, because the mouse was easy to inadvertently move. The cursor needs to be modified so typing into the blocks becomes easier.

Variables other than environment were run. The CET model variables were run with SOBOAT model

variables at default. However when the two glyphs (CET glyph and SOBOAT glyph) were connected and turned on, the switches automatically turned off and an “unhappy face” was present on the glyphs. At first, it was not known what the unhappy face meant. Later, it was found that it meant an error had occurred. However, the unhappy face did not give a reason for the error. It just said Can’t open file errno 2. The interface should offer an explanation of why the error has occurred and suggest how to prevent it.

The following data was collected on the second day of experimentation: The Cantata workspace was gotten into easily. The first thing attempted was to use the Rocket Motor CET variables. In order to run CET, the workspace was cleared. Then under NEOTAM toolbox Rocket Motor CET was selected. The instructions in the booklet [Schaibly 66] said to glyph CET without any changes in data input, and then switch it on. When we followed these instructions, CET turned on for a few seconds, then the switch turned off with an unhappy face.

We then tried to read the calculated results from CET using the text reader glyph. In order to get this glyph the “Output/Information/ASCII File Viewer” buttons were selected. The output arrow from CET was connected to the input arrow on xvviewer. The switch was turned on. However, a few seconds later, the switch turned off, an error message appeared, and no calculation data appeared. The error message was khorus\_init: Couldn’t write to log file “export/tools/khorus1.5/log” bl.so.1: cet89: fatal:libF77.so.2: can’t open file:errno=2 killed Ice+Frnt ()-failed to launch command: <cet89<cetinput.

Another scenario that was run was with the SOBOAT and REP models. The “run” button was pushed to execute SOBOAT and REP. Some data came up but it made no sense whatsoever. The shell tool must provide an interpretation table for data that comes up, so that new users are not totally confused.

Since the data could not be figured out, a new scenario was tried. The new scenario linked an environment glyph, CET glyph, SOBOAT glyph, REP glyph, NIRATAM PLUME glyph, NIRATAM glyph, and OSIC glyph all together. However, when they were run together, the run failed and several error messages came up.

The following data was collected on the next day: The reason for the error messages for the first two days caused curiosity and frustration. So this day was spent in trying to find out why everything done so far caused errors. The first thing that was looked at were demonstration network runs. The handbook recommendation was to find the demonstration file KHOWOS\_HOME/repos/workspace. However the computer said it could not find the file. The attempt to find the file was repeated several times, but it did not work. We tried to open several demonstration files, but none of them could be opened. There should be a main menu or subform for demonstrations, so new users can see if they are doing anything right or wrong.

However, after some exploring we were able to open the neotam.tif file. In order to open this file, the folder that had to be opened was /-home-dpatel-neotam-neotam-engage. This file came up with a flow connecting chart. It showed that CET was connected to NPLUME, REP, SOBOAT; REP was connected to REP2NIR which was connected to NIRATAM which was connected to Plot/Image. It also showed that SOBOAT was connected to NIRATAM which was connected to Plot/Image. (This latter file was a pictorial diagram showing the difference between running REP and SOBOAT.)

After leaving the NEOTAM folder, the Runneo icon was clicked. However, the command was not found and so the Cantata program was lost. An expert was called in to help fix the problem. It was found that a form file

was missing from inside the engage folder (`engage.form`). In order to restore the `engage.form` file, the original installation tape was needed. This showed that some of the errors were caused from the missing `engage.form` file. Then the expert went into Cantata workspace and tried to run a variable network, but he got an error message. The expert found that the reason for the errors was because of a missing library (FORTRAN 77 library). This library was necessary to run some of the network programs. So some of the errors we had encountered were because of not having the `engage.form` file or the FORTRAN 77 library. The expert tried to install the library, but he could not. However, since the `engage.form` file was installed properly the problem involving the saving of files was now fixed.

We began work to alter the color palette, so networks constructed in the Cantata workspace would be observable and colorful rather than dull. Another expert came in and changed the color palette of the Cantata workspace by altering `xdefaults`. The changing of colors must be made easier. There should be an icon that can be selected by the user in order to change the colors, rather than requiring expert knowledge to program it through `xdefaults`.

The following data was collected on the next day: NEOTAM was turned on with success. This day was spent on trying to optimize the image of the Cantata workspace. The background colors were completely changed. The background was gray with blue 0.5-centimeter grid marks. The connector lines were red now so they could be seen easily. The glyphs were multicolored.

The following data was collected on the next day: Since the FORTRAN 77 library was not yet installed, no work could be performed at the computer. More thinking about experience so far produced this recommendation: there should be an information help system or indicator in the NEOTAM model showing which variable model glyphs are compatible with each other, so the new user does not construct impracticable networks.

The following data was collected on the next day: The expert came in and found that the library was in another directory. (`dpatel` is the name of my folder where items are saved and where network run occur.) So the library was installed to the Cantata workspace directory under the `dpatel` folder. However, the library was not installed properly. The reason for that was `libF77.so.2` should have been in the `/usr/lib` but it was not there. So the library needed to be installed properly, but the tape to install it could not be found. So some of the errors were caused by missing a library in the SUN. Later on, it was found that the FORTRAN 77 library had to be purchased separately: The NEOTAM model at this point could not be used.

The following data was collected on the next day: No operations at the computer could be made until an expert came in to install the FORTRAN 77 library in the late afternoon. The FORTRAN 77 library was successfully installed. Then attempts to run CET model as well as SOBOAT, REP, NPLUME, etc., were made. However, when the network was put together and then executed, it still failed. The reason for the failure was supposedly because of a missing `rep.out` file. However, the `rep.out` file could not be found on any of the disks, hard drives, or the original 4mm tape. So no further operation of the model was possible.

The following data was collected on the next day: The `rep.out` file that could not be found yesterday, could not be found today after two more hours were spent in trying to find the file. The network programming was tried again, but unhappy faces and error messages occurred.

The following data was collected on the next day: E-mail was sent to Dr. Schaibly of California

explaining the problems on the NEOTAM model. In, Dr. Schaibly's late afternoon reply, he felt that the reason why rep.out or other major files could not be opened, was because of directory problems.

The following data was collected on the next day: Another expert in SUNs, came in and was told what Dr. Schaibly said. Later he found that the reason why some files could not be accessed was because not all the files were "given ownership". Instead, the files had a generic owner. So the first thing done was to change the ownership of the files to dpatel.

After getting most of the files into the dpatel folder, the variable network was run again. (CET was hooked to NPLUME, REP, and SOBOAT. In turn, REP was hooked to REP2NIR, which was hooked to NIRATAM, which was hooked to Plot/Image. SOBOAT was hooked to NIRATAM, which was hooked to Plot/Image.) The network was run. CET worked, then NPLUME and REP began to work. However after ten minutes of running the network, unhappy faces and error messages came up. It was found that REP was the problem. The output file rep.out could not be read or written. This was causing the malfunction.

It was found that the REP model was not yet in a GUI-style configuration. Thus the problem of making REP into a GUI glyph arose. An element of this work was to make a GUI-style input screen for REP, so that manual text edit/programming would not be required. A sketch of recommended REP GUI glyphs and GUIs appears as Figures A, B, C, D, E on pages 15 and 16.

Another breakthrough came later in the day. The reason for all the errors when running all the model variables, (CET93, NIRATAM, NPLUME, REP, SOBOAT, OSIC, and REP2NIR) together was because not all of the models were not yet developed to work as glyphs in the Khoros environment. The only two models that were in glyph style were CET and SOBOAT. So the information from glyphing SOBOAT and REP generated errors as well as data, because SOBOAT was the only part outputting data. The only reason why CET works was because the FORTRAN 77 library was installed. The rest of the models, NIRATAM, NPLUME, OSIC, and REP2NIR function like REP. Those all require the technical table edit/programming rather than the user-operable GUIs and glyphs. And since the Cantata workspace works only in GUI style, the technical programming style cannot work. So the rest of my time will be used to try to give system integrators and architects ideas on how to turn the technical table edit/programming inputs of each of the models into GUIs and glyphs like that of SOBOAT and CET. The pictorial diagram on pp.15,16 are sketches of recommended REP GUIs/glyphs.

### Conclusion

After five weeks of learning the fundamentals of electromagnetic spectrum targeting and how to use the SUN system, the NEOTAM computational model was introduced. About three weeks were spent on this model. The research that was done was at times frustrating, confusing, and sometimes exciting. Overall, the research on the NEOTAM computational model was successful in some places and in some places it was not.

Each day posed new problems that could either be solved or could not be solved. All these problems were recorded as data. However, the following are a few helpful comments that will be sent to the NEOTAM and Khoros technologists: A color palette icon is needed so the user can change the background/icon contrast with ease. Programming as a means to enter/read data should be lessened as much as possible so new users can run the model with ease. The Cantata workspace should give the user feedback explaining why items can be saved or why they

cannot, instead of frustrating the user. The cursor function needs to be modified so when typing into a block area, the cursor does not need to remain in the block in order to input data. If the cursor style is changed more efficiency and less frustration will occur. If an error message occurs there should be a laymen-term-type of message so users can understand the mistake that was made. (The error messages right now are only in programming terms.) When any data appears, there must be an interpretation aid in the shell tool so new users do not become totally confused in what the data means. If new users need demonstrations to know what they need to do, there should be a main menu or subform for demonstrations/examples. This will also cut down on confusion and errors and shorten the time for new users to become competent. There should also a "help" indicator saying which model variable glyphs (CET, SOBOAT, NPLUME, etc.) can meaningfully be connected to each other, so error can be cut down.

As mentioned before, there was some research that was hindered because of installation problems. The NEOTAM model was not completely installed and the software was missing information from the installation tape. The engage.form file was not installed properly and caused parts of the workspace to run improperly. The reason for some of the variable network (CET, REP, NIRATAM) errors were because of missing the FORTRAN 77 library. Without the FORTRAN 77 library, the CET model could not be run. If the NEOTAM model was installed properly, more time could have been used to sketch ideas on new glyphs.

However, after installing the library and trying to run the CET model again, another error message came up. This time it said the rep.out file was missing. However, this file was not on the tape and could not be found anywhere. This caused much confusion to researchers and experts. Trying to run the model was hindered because of missing important files. Later (during the seventh week of research), it was found that the reason why variable networking could not occur was because the models REP, NIRATAM, NPLUME, OSIC, and REP2NIR were not in GUI glyph style but were in programming style. Since they were not in GUI/glyph-style, they could not work in the Cantata environment.

The problem of trying to run the NEOTAM model successfully was not the main purpose of this research. The main purpose was to find the glitches and comment on how to fix them. That part of the research was a success, because feedback was given on how to improve the model. The missing of files/libraries and GUI glyphs hindered the progress of successfully running the complete NEOTAM model, but these problems were commented on and were brought to the attention of NEOTAM and Khoros technologists. So even though the total model could not be run successfully, feedback will help NEOTAM and Khoros developers.

Since progress was hindered many times by installation/programming problems, recommendations for GUIs for several of the models could not be done. The design of the REP GUI glyph was made.

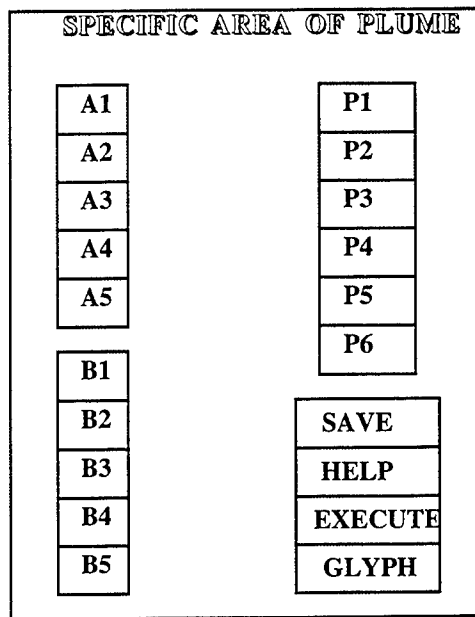
The research that was conducted will help in informing AEM\*AT users on what to watch out for when running the NEOTAM model and what to expect if that person is a new user or novice. Overall, the research that was done brought advancement to the research and development field and in the avionics field. Our method for changing the color palette has already helped a group of NEOTAM users in England. Also, from the knowledge I have gained, I have trained Air Force personnel on how to operate the NEOTAM model.

Not all of the problems were figured out during this summer. Next summer, we hope to continue this work to expand and improve the GUI interface of the NEOTAM model and to keep building on the knowledge and experience we acquired this year.

This research was fun and filled with exciting, mind-boggling experiences. It is great for a high school student to explore this type of hands-on experience.

#### References

1. Capps, W.L., Powlette, D., Tate, S.E., Amick, G.S., Stowell, D., Husted, F. The Aircraft Infrared Measurements Guide. JTCG/AS-81-C-002, March 1983.
2. Electro-Optic Model for Aerial Targeting-Version 2.00-(EMAT 2.00)-User Manual. San Diego: Horizons Technology, Inc., July 1993.
3. Fligor, Patrick D., Zimmerman, Harold P., Hawkins, James E. Electromagnetic Radiation Signatures From 0.2 to 14.0 $\mu$ m for Target and Background Materials and Scene Energy Sources for Naval Night Sensing. Washington DC: Technology Incorporated, July 1970.
4. Hudson, Richard D. Infrared System Engineering. New York: John Wiley and Sons, 1969.
5. Schaibly, John. Dr. NEOTAM\* 0.P.1 (Preliminary) User Guide and Tutorial. San Diego: Horizons Technology, Inc., April 1996.
6. Sorlin-Davis J. Maj., Weather Sensitivities Handbook. Det1 2WS, USAF.
7. Weiss, Richard A., Scoggins, Randy K. Infrared Target Background Analytical Models-Technical Report EI-89-11. Vicksburg: US Army Engineer Waterways Experiment Station, August 1989.
8. Wolfe, William L. Handbook of Military Infrared Technology. Washington DC: US Government Printing Office, 1965.
9. Other references were various unpublished papers concerning aerial targeting in general and the AEM\*AT model (Aerial Targeting Glossary, Engineering and Science Parlance, Introduction to AEM\*AT). Conversations and oral tutorials were given by various people like Roger Beard, Alex Zanfirov, Mary Anne Gaultieri, William Lewis, Dr. John Schaibly, Lt. Tim Parthamore, and William Lanich. Also during my research I discussed topics with my colleague, Angela C. Helm.



**POSSIBLE**  
**REP**  
**GUI**  
**GLYPHS**

**FIGURE A**  
INSTEAD OF USING THE SPECIFIC AREA OF PLUME (ABOVE), A VISUAL TYPE OF SPECIFIC AREA OF PLUME CAN BE USED (BELOW); SO THE SURENESS OF THE AREA THAT NEEDS TO BE TESTED CAN BE SEEN RATHER THAN JUST CLICKING ON A1 AND B5.

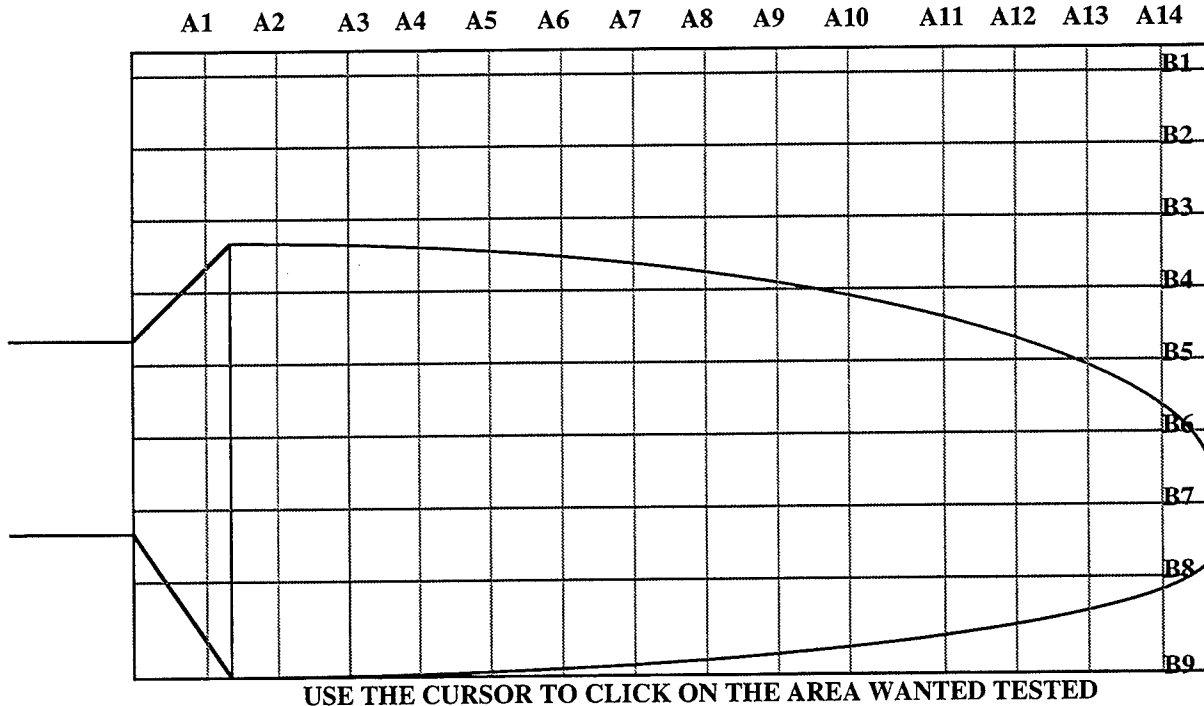


**FIGURE B**

# POSSIBLE REP GUI GLYPHS

INPUT OF COMBUSTION RATES	
N2	OH
H2	O
CO	O <sub>2</sub>
H <sub>2</sub> O	HO <sub>2</sub>
CO <sub>2</sub>	PBO
H	

**SAVE**  
**HELP**  
**EXECUTE**  
**GLYPH**

FIGURE C

ATMOSPHERIC CONDITIONS THAT CAUSE DIFFERENCE IN PLUME

CLOUDS (TYPE OF CLOUDS) \_\_\_\_\_

GASES PRESENT\_\_\_\_\_

ANGLE OF SUNLIGHT AT HITS PLUME\_\_\_\_\_

**SAVE**  
**HELP**  
**EXECUTE**  
**GLYPH**

FIGURE D

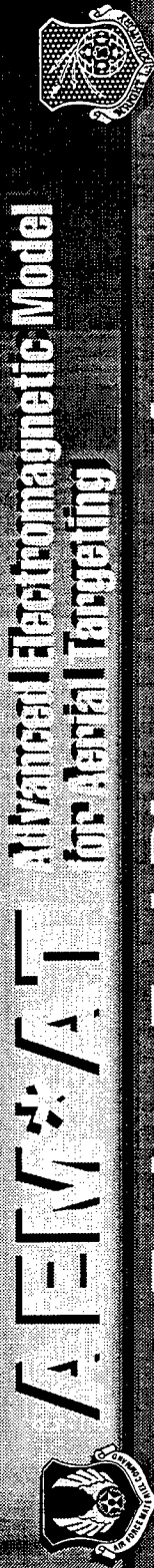
PRESSURE

AIR PRESSURE \_\_\_\_\_

PRESSURE OF PLUME COMBUSTION IN  
A SPECIFIC AREA \_\_\_\_\_

**SAVE**  
**HELP**  
**EXECUTE**  
**GLYPH**

FIGURE E



# $\int_{\Delta} \Gamma = \int_{\Delta} \sqrt{\Gamma} \cdot \sqrt{\Gamma}$ Unified Electromagnetic Model for Target Targeting

## End-to-End Phenomenology

target and background

sensor and processing

path

sky background

environmental influences

transmission losses

target

path radiance

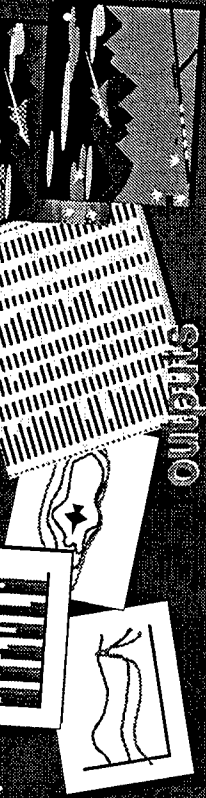
shimmer

turbulence

terrestrial backgrounds

standardized plots

numerical radiometric data



# NEW\*AT

# Signature Factors

FACTOR	TARGET (hardbody emitted / reflected, plume)	PATH	BACKGROUND
not all are independent		signal loss, additive noise, modulation	clutter geometry, spectral content, intensity
<b>Illumination</b>			
• <b>sunshine — current / history</b> bearing, elevation ('ToD), clouds	reflection, glints, heating	path radiance	reflection, heating, clutter: glints (water, cultural detail), shadows
• <b>skyshine — current / history</b> bearing, clouds, surface condition	reflection, heating	path radiance	reflection heating
• <b>cloudshine — current / history</b> type, altitude, coverage	reflection, heating	path radiance	reflection, heating
<b>Meteorology</b>			
• <b>humidity — current / history</b>	skin heating, hot parts temp, plume spectrum	spectral xmsn	transpiration, soil moisture, (cultural detail = target factors)
• <b>air temp — current / history</b>	skin heating, engine temp, plume	spectral xmsn	transpiration, soil moisture (cultural detail = target factors)
• <b>airspeed / wind — current / history</b>	skin heating (total/differential), plume geometry, wake, hot parts contrast reversals	vapor/aerosol sources (cultural detail = target factors) signal loss, contrast loss,	transpiration, soil moisture clutter, rad trap (contrast reduct, hi temps), modulation
• <b>clouds — current / history</b>			cultural detail = target factors
• <b>hardbody construction</b>	skin $\epsilon/\alpha/\rho$ , internal conduction, thermal mass		cultural detail = target factors
• <b>surface coating &amp; condition</b>	aero skin heating, $\epsilon/\alpha/\rho$		cultural detail = target factors
• <b>internal stores (fuel cells, e.g.)</b>	differential skin heating		cultural detail = target factors
• <b>external stores</b>	additive signatures, drag affects flying factors		
• <b>fuel type</b>	plume spectral signature, tgt size (vis/subvis contrasts)	visual/subvisual contrasts (attenuation)	visual/subvisual contrasts (clutter)
<b>) Flying Factors</b>			
• <b>altitude — current / history</b>	skin heating, engine temp, xmsn		sky/horizon/terrain
• <b>speed — current / history</b>	skin heating, engine temp,		sky/horizon/terrain
• <b>altitude wrt flight vector — current / history</b>	differential skin heating		pointing, stabilization
• <b>altitude wrt Los</b>	radiation pattern		water vapor, "cirrus", aerosols
• <b>throttle setting — current / history</b>	plume, hot parts, aero heating		water vapor, "cirrus", aerosols

A STUDY ON DETECTION AND MEASUREMENT OF  
ATMOSPHERIC BACKSCATTER USING  
DIRECT DETECTION BACKSCATTER LIDAR

Neill W. Perry

Crestview High School  
1304 N. Ferdon Blvd.  
Crestview FL, 32539

Final Report for:  
High School Apprenticeship Program  
Wright Laboratory

Sponsored by:  
Air Force Office of Scientific Research  
Bolling Air Force Base, DC

and

Wright Laboratory

August 1996

A STUDY ON DETECTION AND MEASUREMENT OF  
ATMOSPHERIC BACKSCATTER USING  
DIRECT DETECTION BACKSCATTER LIDAR

Neill W. Perry  
Crestview High School

Abstract

A Light Detection And Ranging (LIDAR) system sensitive to atmospheric backscatter was developed and tested. A protective, aluminum casing was also designed to shield the system from electromagnetic interference, dust, and light. The system was tested by measuring atmospheric backscatter off a nitrogen fog was measured with the system in a controlled environment.

# A STUDY ON DETECTION AND MEASUREMENT OF ATMOSPHERIC BACKSCATTER USING DIRECT DETECTION BACKSCATTER LIDAR

Neill W. Perry

## Introduction

Laser/Radar (LADAR) imaging systems are used for the purpose of guidance, target recognition, and surveillance. LADAR systems are adversely affected by poor weather conditions (ex: rain, fog). Degradation occurs in part to increased atmospheric backscatter, or the deflection of laser photons by dust particles, aerosols, and water vapor in the laser's path. Atmospheric backscatter can not only decrease target return, but also can provide false returns. A deeper understanding of atmospheric backscatter and its effects on LADAR systems are required to improve LADAR technology. To accomplish this a LIDAR system that detects and measures atmospheric backscatter will be developed.

## Methodology

The objectives of this project were to: a) develop a LIDAR system that can detect and measure atmospheric backscatter, and b) encase such a system in a protective carrying case to shield the components from electromagnetic interference, dust, and light. The system layout (See Figure 1) designed for this project was as follows: A Nd:YVO<sub>4</sub> laser emitted a pulsed beam. The beam traversed a 3:1 beam expander that utilized a plano-concave and a plano-convex lens, with 25mm and 75.6mm focal lengths respectively. A stationary target, 18.8 meters from the system, in the optical pathway scattered laser beam, of which only a small fraction of photons were reflected back toward the monostatic LIDAR system.(See Figure 2) The reflected photons, or target return, were directed toward the detector assembly via an apertured mirror. An EG&G C30902E Silicon Avalanche Photodiode detector was connected to the input of a Tektronix TDS 744a Digital Oscilloscope and a EG&G 914P Multichannel Scaler. Thus enabling the detection, interpretation, and display of the return signal.

## Components

For the LIDAR system to accurately register a laser return a highly sensitive detector, acting as a photon counter, was required. The detector's response was characterized as a function of bias voltage to allow the diode's

sensitivity to be raised safely with minimal risk of burnout. Characterization was accomplished by maintaining constant optical input, increasing the applied voltage (V), and recording the gain (mV). The data identified regions of linear and nonlinear gain (See Figure 3) and a safe operational bias voltage of at least 225V. Characterization tested only as high as design specifications suggested. Further tests will be required to determine the maximum applied voltage.

Another device of the LIDAR system is the EG&G 914P Multichannel Scaler (MCS). A brief explanation is provided with the MCS User's Manual:

"A multichannel scaler records the counting rate of events as a function of time. When a scan is started, the MCS begins counting input events in the time. When a scan is started, the MCS begins counting input events in the first channel of its digital memory. At the end of the preselected dwell time the MCS advances to the next channel of memory to count events. This dwell and advance process is repeated until the MCS has scanned through all the channels in its memory. A display of the contents of the memory shows the counting rate of the input events versus time. In repetitive measurements, where the start of the scan can be synchronized with the start of the events, multiple scans can be summed to diminish the statistical scatter in the recorded pattern."

Signal capture and display were also accomplished using the digital oscilloscope. The digital oscilloscope was used, instead of the MCS, in this phase of testing because of its superiority in data processing. The oscilloscope has the capability to capture multiple waveforms of a low signal (<1mV), average them, and display the mean. However, discussion of the MCS is included in this report because it is foreseen that it will be used in later tests of this project.

#### Tests

Tests of the LIDAR system were conducted within an indoor testing range. The LIDAR system was mounted 18.8m from the target. Two tests were conducted, a control test and an experimental test with nitrogen fog. In the control test the LIDAR system fired pulses at the stationary target (garage door), and returning laser photons were measured using the photodiode detector and the digital oscilloscope. The multiple waveforms were averaged, and the mean waveform of the test run was displayed and recorded.

For the experimental test, fog was added to increase atmospheric backscatter. The fog was created by positioning liquid nitrogen below the path of the laser. The room temperature of the laboratory ( $20^{\circ}\text{ C}$ ) caused the nitrogen to boil, producing nitrogen vapor in the laser beam path. The laser return was recorded and calculated as previously described.

### Analysis

Two regions of interest can be found on the recorded data (See Figures 4 and 5). Region 1 is produced by reflection from off the beam expander within the LIDAR system. Region 2 is the direct target return. Although the two waveforms look remarkably similar at first glance, closer analysis reveals subtle deviations. These differences become more apparent when the two graphs are subtracted (experimental - control). Region 3 (See Figure 6) indicates a signal increase which correlates in time to the distance of the fog. Region 4 displays a decrease in target return. If laser light is scattered by the fog, then less light is available to reflect off the target back to the LIDAR system. Thus the data shows that the LIDAR device can indeed detect atmospheric backscatter.

### Protective Casing

The second objective of this research project was to construct a protective casing for the LIDAR system. This casing is needed to protect the sensitive equipment from dust, light, and electromagnetic interference. The accuracy and sensitivity of the system will be greatly improved when the system is mounted within this case. With less electrical and optical noise in the LIDAR system the photodiode will more accurately detect the backscatter and its sensitivity can be increased. Furthermore, the box will allow for a portable LIDAR device to conduct field measurements. The case (See Figure 7) consists of six Aluminum plates, each 1/4" wide. When assembled they form three separate compartments which protect and shield their respective components.

### Conclusion

The data collected indicates that the developed LIDAR system can detect atmospheric backscatter. However, the other objectives of this research project remain to be completed. Construction of the protective case cannot begin until the necessary components have been fabricated. Furthermore, without the protection of the case the detector's sensitivity cannot be increased to an adequate level. Thus, this LIDAR system cannot accurately measure atmospheric backscatter outside of laboratory conditions. Calibration techniques also need to be developed. Hopefully, when the needed components arrive this research project can be completed.

### Acknowledgments

The author would like to thank the following people for their support:

My mentor and friend, Captain Ken Dinndorf.

Norman Champigny for his humor and technical support.

My colleagues at the Laser/Radar Research Facility ( Major Jeff Grantham, Jerry Manthey, Mike Tripp,  
Rob Hopkins, and Eddie Meidunas).  
Don Harrison, Mike Deiler, Jeannette Williams and the HSAP directors and managers at RDL.

Trey Reyher and the other high school apprentices at Wright Laboratories.

Mi familia (Pa, Ma, Kyle, Regina, Hugh, and Abby Perry) and to all my really cool friends!!

#### References

Jelalian, , Albert V. Laser Radar System Artech House, Boston. 1992.

Model 914P Multichannel Scaler User's Manual, Software Version 1.0, EG&G Princeton Applied Research

Tektronix Programmer Manual: TDS Family Digitizing Oscilloscopes. Wilsonville, OR. Seventh ed. Nov 1994.

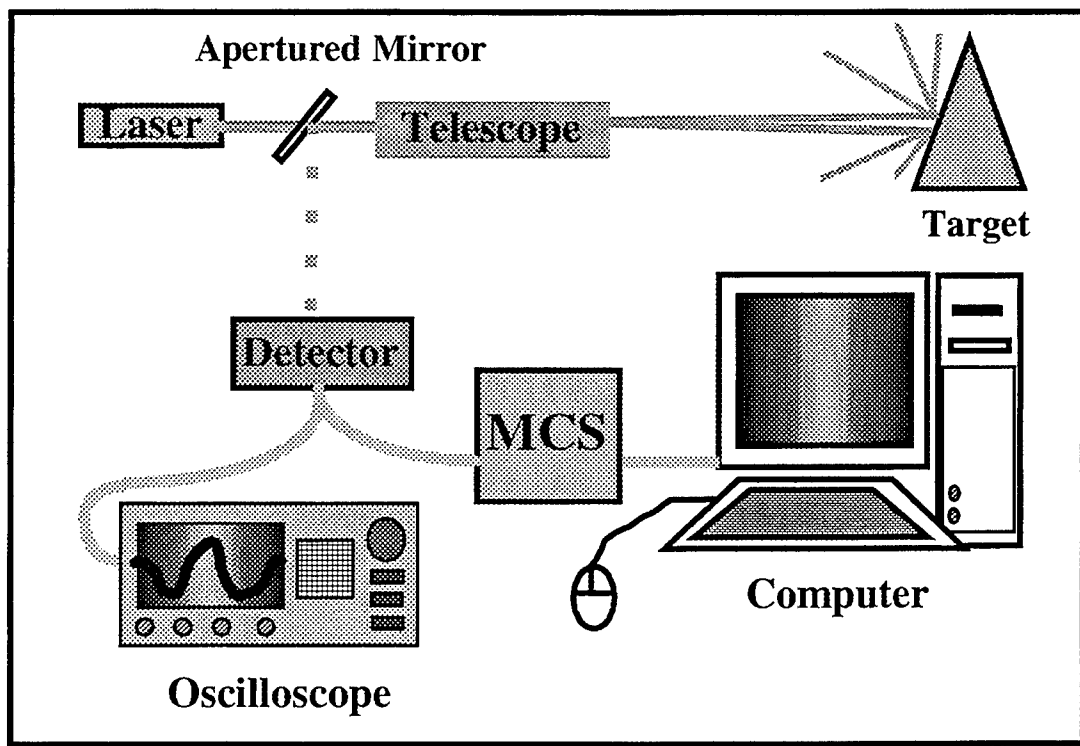


Figure 1: An overview of the LIDAR system designed and tested in this research project

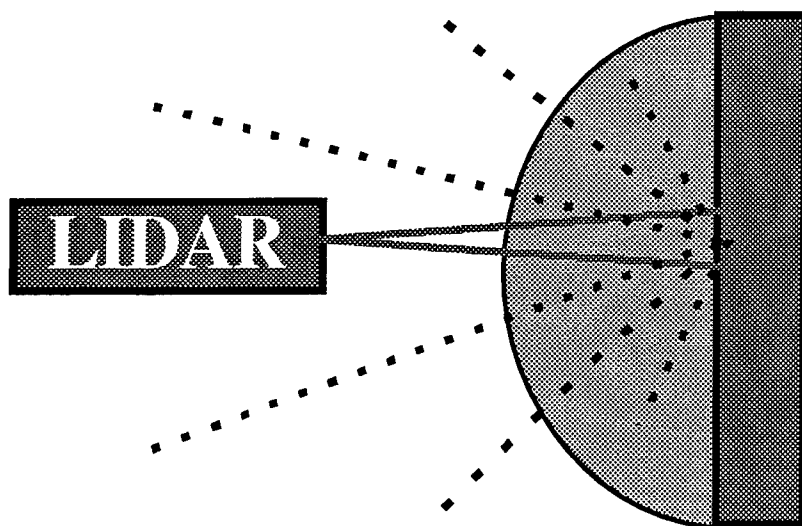


Figure 2: Hemisphere of scatter of the laser off the stationary

The fraction of the laser light that returns to the LIDAR can be calculated. After the beam exits the telescope it travels down range to the target. Laser photons are then scattered in all directions, forming a hemisphere of deflection. Thus, target return can be stated (assuming 100% reflection by the target) as a function of:

$$\frac{\text{Area of telescope window}}{\text{Surface area of scatter hemisphere}} = \frac{\pi r^2}{2\pi R^2} = \frac{r^2}{2R^2}$$

Where:  $r$  = radius of telescope lens,  
 $R$  = distance from target to telescope

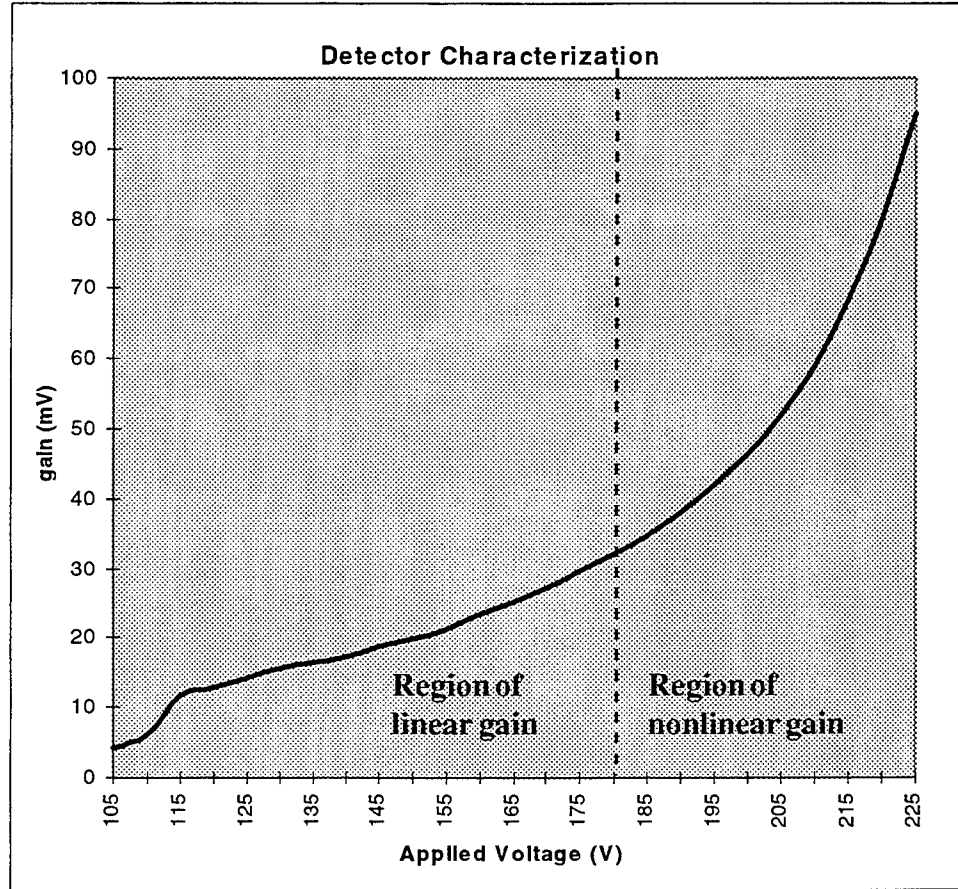


Figure 3 : Characterization of the Silicon Avalanche Photodiode with a 2.0mV laser. Graph displays the exponential rise of gain as the applied voltage is increased

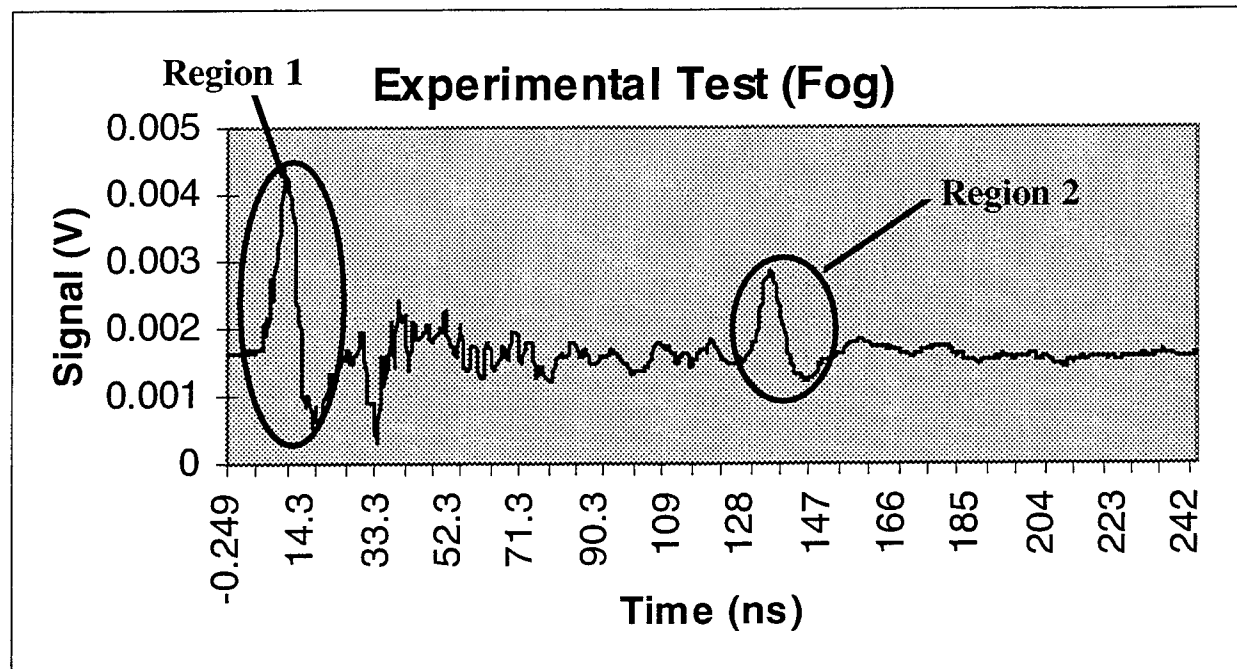


Figure 4: Average waveform of 100 signals captured in the experimental test.

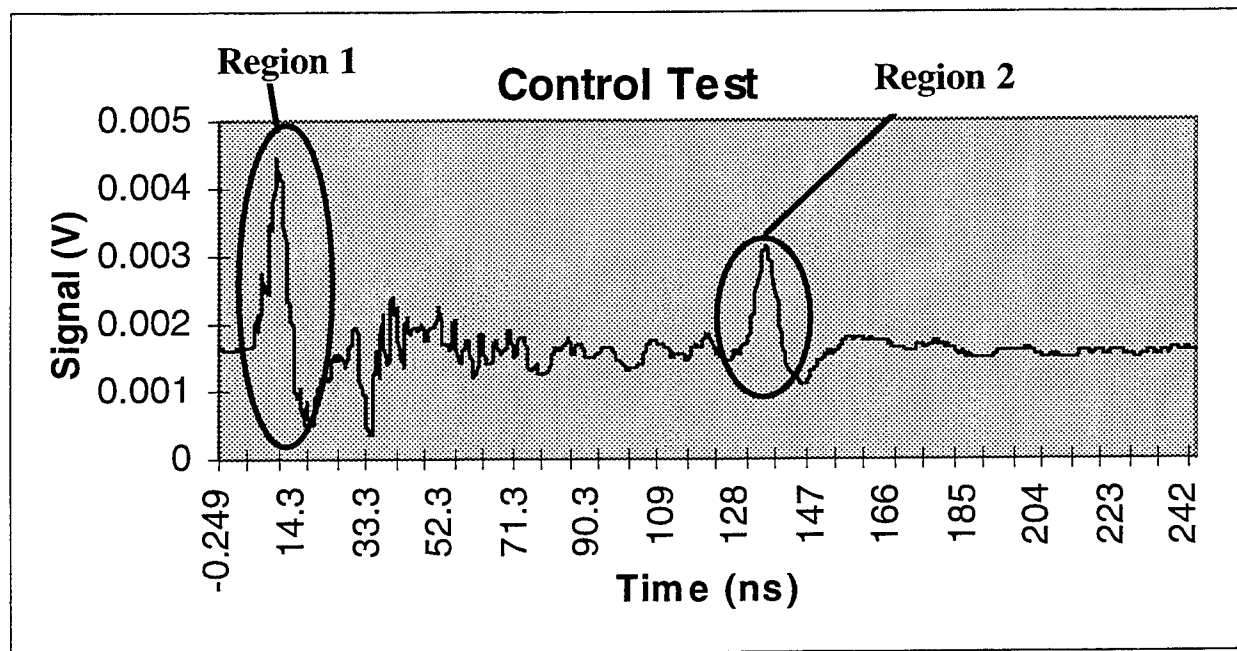


Figure 5: Average waveform of 100 signals captured in the control test

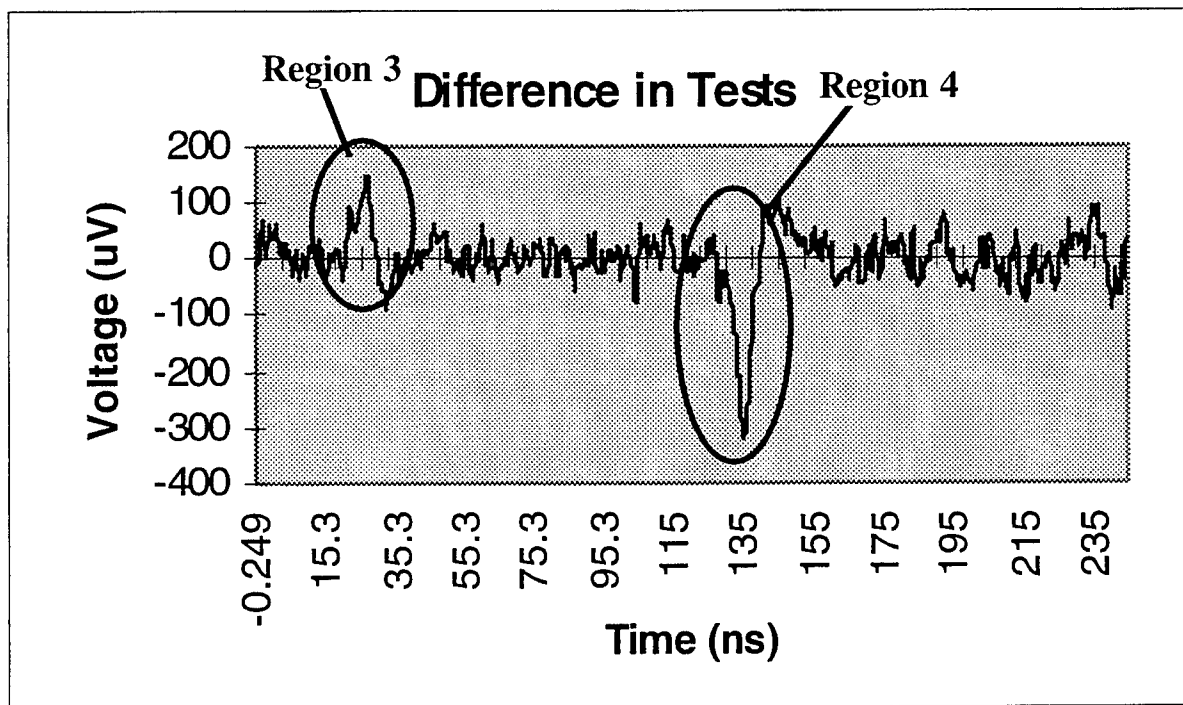
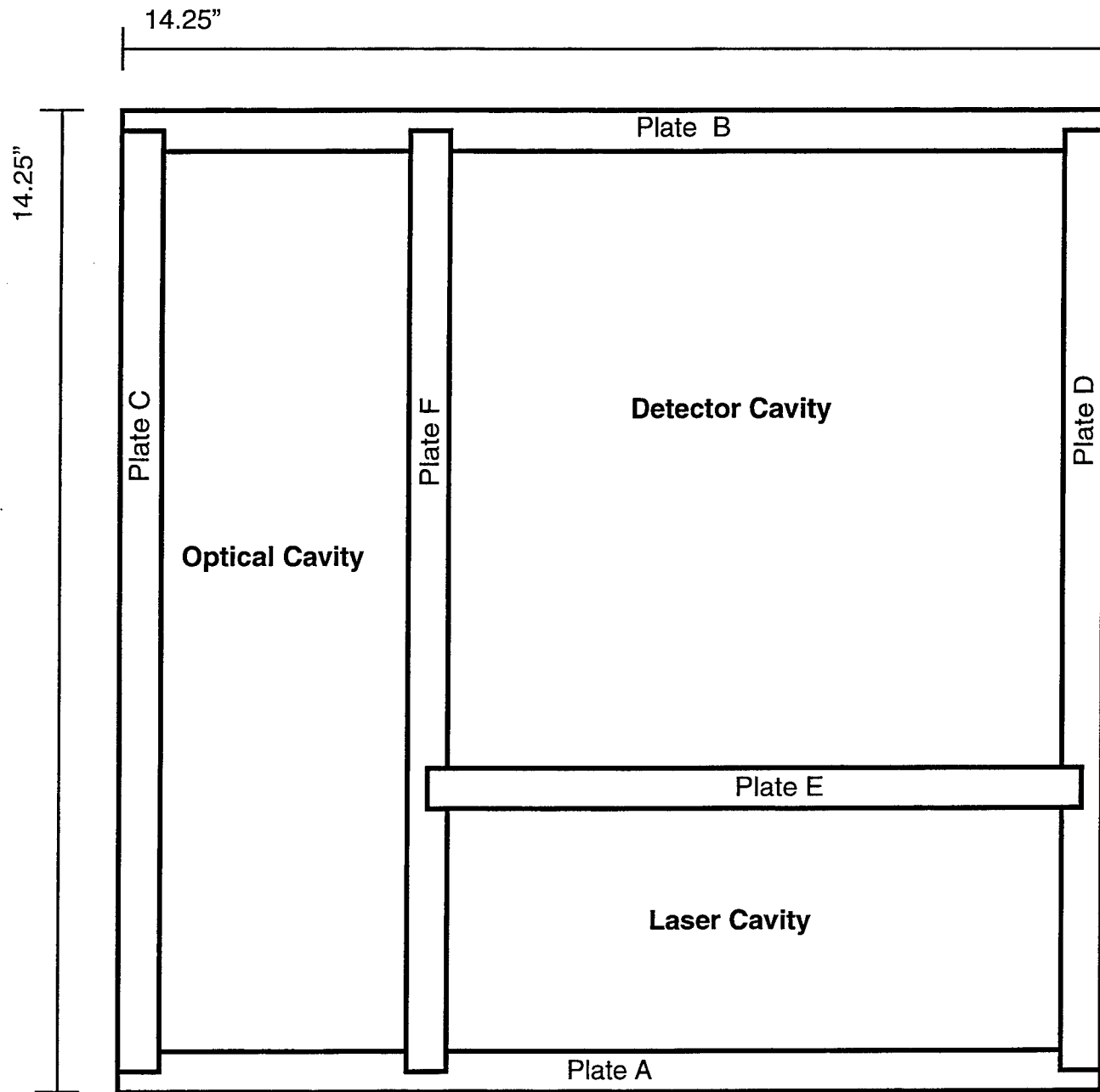


Figure 6: Graph of the difference (experimental - control) between the two tests.



**Figure 7: Design of the Aluminum Protection Case**

- Not drawn to scale
- Box consists of 6 Al plates each 0.25" thick
- Dimensions of completed box are: 14.25" x 14.25" x 6.6"
- Three compartments of box: laser, optical, and detector
- Various holes and windows in the box to allow electrical and optical exchange among the equipment.

DIGITAL SIGNAL PROCESSING OF MAXIMAL LENGTH SEQUENCES

Michael D. Powell

Beavercreek High School  
2660 Dayton-Xenia Road  
Beavercreek, OH 45434

Final Report for:  
High School Apprentice Program  
Wright Laboratory

Sponsored by:  
Air Force Office of Scientific Research  
Bolling Air Force Base, DC

and

Wright Laboratory

July 1996

## DIGITAL SIGNAL PROCESSING OF MAXIMAL LENGTH SEQUENCES

Michael D. Powell  
Beavercreek High School

### Abstract

Pseudorandom sequences and digital signal processing were studied. The Berlekamp-Massey algorithm was used for determining the generating polynomial from a maximal length sequence. This algorithm and the necessary input and output routines were programmed for a digital signal processing board. The program was successfully tested and its operating ranges determined. A circuit for regenerating the maximal sequence from the program's output was also designed.

# DIGITAL SIGNAL PROCESSING OF MAXIMAL LENGTH SEQUENCES

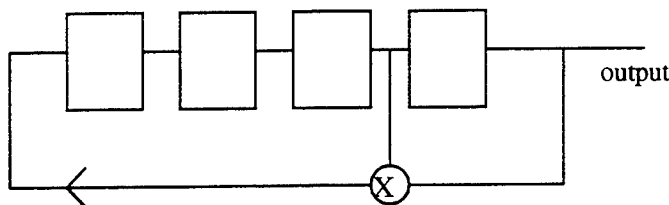
Michael D. Powell

## Introduction

Pseudorandom sequences of binary bits are very useful in communications applications. One such type of sequence is the maximal sequence, which is the longest sequence that can be generated with a given shift register. Though these sequences exhibit the properties of white noise, they can be duplicated with another shift register if the generating polynomial is known. One important element in the duplication process is to compute the generating polynomial from the bits of the pseudorandom sequence. This may be accomplished using the Berlekamp-Massey algorithm.

Maximal length sequences may be generated using a shift register that is the length of the degree of the generating polynomial. A maximal length sequence is one whose length is  $2^n - 1$ , where n is the degree of the polynomial. A maximal length sequence will only be generated by an irreducible polynomial; all others will be shorter or indeterminate. Polynomials are normally represented in octal. For example the third degree polynomial  $x^3 + x + 1$  is represented in binary as 1011 and in octal as 13.

To generate the sequence, the shift register is "tapped" at the points indicated by a binary value of 1 in the polynomial. The output of the shift register is XOR'd with the appropriate tap outputs and then input back into the shift register. The register to generate the sequence from the degree 4 polynomial  $31_8$  would be



1      0      0      1      1

(binary representation of taps)

least significant bit

If the initial fill of the shift register contains a least one 1, this system will continuously repeat the sequence 111100010011010.

As the degree of the generating polynomial increases, the length of the sequence increases exponentially. As the sequences lengthen, they come closer to meeting the definition for white noise. However, they are actually pseudonoise, and the generating polynomial may be computed from the bits of the sequence.

The Berlekamp-Massey algorithm is one method that has been developed for computing the generating polynomial from the bits of the sequence. The function of the algorithm can be summarized as making an initial assumption that there are no taps, looping through the bits of the sequence and XORing them to the presumed taps, and adjusting the taps when the results disagree. Using this algorithm, the taps of a sequence can be solved with no more than  $2n + 1$  bits of the sequence, where n is the degree of the generating polynomial. This means that the taps of a sequence that repeats every 1,048,575 bits ( $2^{20} - 1$ ) can be solved with only 41 consecutive bits of the sequence.

The algorithm was to be ported to an Analog Devices ADSP-21020 processor that in this case is connected to an EZ-Lab 21k evaluation board. In addition to the 32 bit 21020 digital signal processor (DSP), the evaluation board contains two analog to digital converters (ADCs), two digital to analog converters (DACs), 32K X 32 bits of program memory, 32K X 40 bits of data memory, an AD1849 Soundport for stereo audio I/O, and a 16-bit ADSP-2111 as a controller. The 2.5 microsecond sample time for the ADC turned out to be the limiting factor in the acceptable frequency range for input. Programs are written on a PC, assembled, linked, and transferred to the DSP via an RS-232 serial cable. For this project, the program was written in assembly language to allow the most direct access to the I/O features of the processor.

### Methodology

Porting the Berlekamp-Massey algorithm to the DSP board required a significant amount of programming overhead for the input and output routines. The incoming data stream was sampled at 400 KHz, the maximum rate for the analog to digital converter. Over 28,000 8-bit samples are written to RAM, sampling just over 0.07 seconds of the input stream. The program then loops through all of the samples to determine the magnitude and difference between high and low signals. Failure to discern two distinct signals results in an error code and termination of the program. Tolerance for noise and inconsistent signals may be adjusted in the source code. After establishing a reference for high and low signals, the program determines the data input frequency (bits per unit time). Searching for the shortest duration of a high signal, it loops through all of the data samples. The program then assumes this value to be the length of a single bit of data.

The next step is to convert the raw data into binary bits that can be used by the Berlekamp-Massey algorithm. The program finds the first distinct edge within the data samples and then moves the pointer to the middle of that bit. Then thirty-two bits of samples are read and shifted into a thirty-two bit data register. If the bit rate was 500 Hz, this would require looping through 25,600 of the samples; at higher rates it requires fewer. During this conversion process, a check is made at each bit to ensure that the pointer is not approaching an edge in the samples. If it is, the pointer position is adjusted, preventing errors if the frequency computed earlier does not exactly represent the duration of one bit. This condition is most likely if the data frequency does not evenly divide into the sample rate.

The Berlekamp-Massey algorithm is executed using the thirty-two bits from the data register as input. Accordingly, it can reliably solve for the taps of any sequence up to degree fifteen. (However, it successfully solved for all degree sixteen sequences tested.) This implementation of the Berlekamp-Massey algorithm is modeled after a version written for Matlab by Dale Wilson at Wright Laboratory in 1994. Though the same basic approach was followed, some elements were changed to reflect the capabilities of the assembly language. For example, the Matlab code carried out a multiple input XOR

through matrix multiplication, while it was easier to perform a direct XOR in assembler. Overall, the one page Matlab algorithm roughly translated to four pages of assembly code.

Data is output through two different methods. On the DSP board, the FLAG2 LED is flashed once for every bit of output while the FLAG1 LED is on if that bit is high and off if that bit is low. This output format is very slow and requires eight seconds to output sixteen bits. For a more convenient way of viewing the information, the data is output through one of the DSP board's external ports. An external shift register with 16 LED outputs was built to receive this data (See Schematic I.). The data is clocked in at 10 KHz, with the clock signal generated from the DSP board. This transfer is instantaneous to the user, and it occurs before the slower flashing LED output begins.

### Results and Conclusion

The program was tested with input from a New Wave Systems spread spectrum generator, and it functions well over a range of bit input frequencies. Based on the sample rate and I/O methods used, the theoretical range is from 500 Hz to 100 KHz. Though it does work throughout that range, it is most reliable between 1 KHz and 50 KHz. Use of a faster ADC would greatly increase the frequency range. Though the ADC used could only sample up to 400 KHz, the 21020 processor was clocked at 25 MHz.

The program's execution speed is not completely dependent on the degree of the sequence input, because it processes all thirty two bits of data in all cases. Execution of the Berlekamp-Massey portion of the program, without the I/O routines, typically takes between 15,000 and 20,000 clock cycles. Note that the execution time for a particular sequence is dependent on what section of the sequence is input.

Various Sequences and Their Execution Time

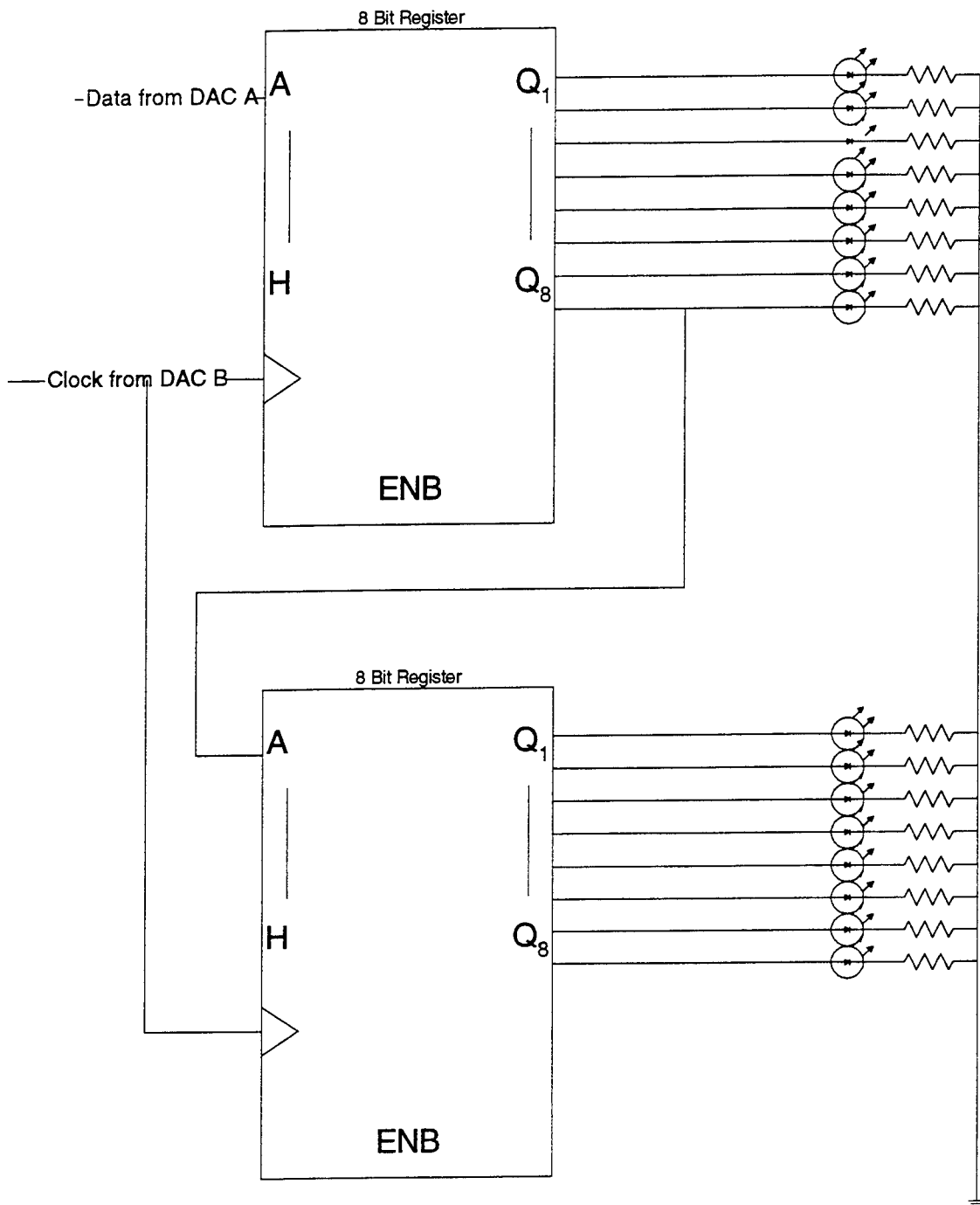
Degree	Polynomial	Bits of Sequence Input	Clock Cycles
5	45 <sub>8</sub>	011110011010010001010111011000	15152
10	3025 <sub>9</sub>	11110111110010001011000100101101	17653
15	100003 <sub>8</sub>	001100000000000010000000000000	17329
15	100003 <sub>8</sub>	0000111000000000000101111111111	16897
15	130745 <sub>8</sub>	001101011111000100100011110100	18460
15	130745 <sub>8</sub>	10000000111001011110011111000011	19548

At a processor clock speed of 25 MHz, a 20,000 clock cycle operation takes 0.8 milliseconds. However, this program was optimized for ease of reading and debugging, not speed. A significant increase in speed could be easily obtained.

The next logical extension to this system is to use the output from the DSP to control the taps of a shift register and regenerate the sequence. This circuit was designed as an addition to the original output shift register (See Schematic II.). In addition to controlling the taps, this circuit also counts the number of bits input to determine the degree of the sequence. AND gate enablers control the taps and the degree in the generating circuit. To use this circuit, the program must be modified to clock an initial high value into the output shift register. This additional bit represents the constant in the generating polynomial, which is not produced by the Berlekamp-Massey algorithm. Though this circuit can regenerate the input sequence, it is not capable of synchronizing its output to the original input. That capability would require a significant increase in hardware and complexity.

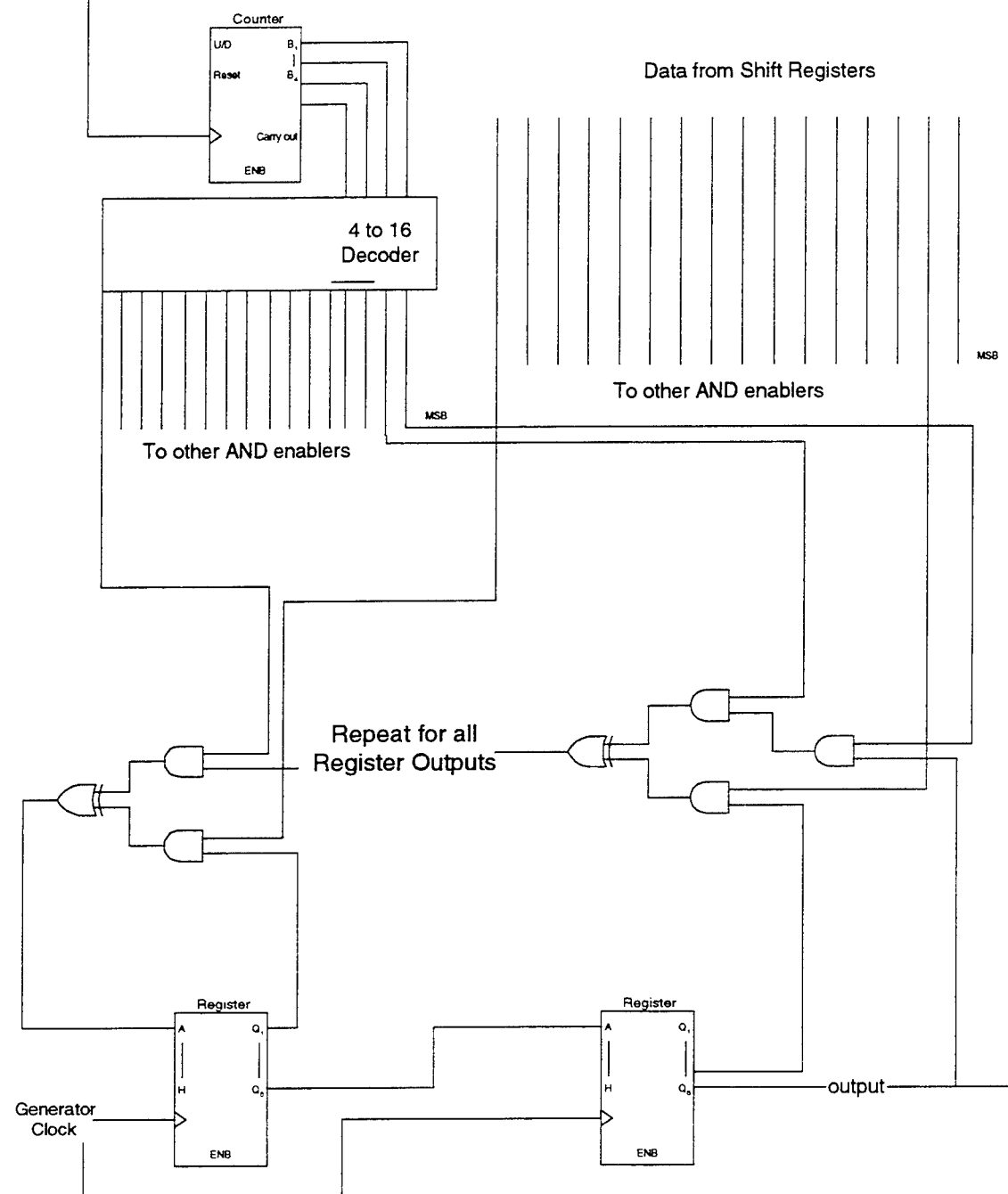
The Berlekamp-Massey program provides an effective visual or digital output of the taps for a maximal sequence. It works over a range of frequencies that could be increased by increasing the sample rate of the ADC. Output may be obtained from the internal LEDs, the external serial data from VoutA, or by directly reading data memory from the 21020 processor. Applications such as this are an important part of modern communications and signal processing.

### Schematic I -- Output Shift Register



Clock from Input Registers

## Schematic II -- Sequence Generator



## Appendix 1 --ADSP 21020 EZ-Lab Evaluation Board Reference Information

By Michael Powell, July 1996

**Author's Note:** This document contains summary information, reference, and recommendations based on the author's experience with the EZ-Lab 21k Evaluation Board. It is not intended to replace the extensive documentation that comes with the EZ-Lab21k, the ADSP-21020 processor, and all related software. The documentation and sample programs contain many useful descriptions and examples.

### I. Programs and Compiling

Programs may be written in C or assembly. C programs must be compiled to assembly using the G21K compiler. Assembly programs may be written as plain text files but should be saved with a .asm extension. The ADSP-21020 User's Manual contains detailed information on the assembly language and system registers. The EZ-Lab21k manual contains specific information about the board's architecture.

Assembler programs (.asm files) must be assembled, linked, and split before they can be run. Each step in the process produces a new file with the same name as the original but with a different extension. Note that for a file named "myprogram.asm", only "myprogram" needs to be included in all of the following filename parameters. The file ezlab21k.ach, a processor architecture file, must be present in the current directory during this process. Other architecture files would be used for systems other than the EZ-Lab21k board. The assembling, linking, and splitting programs are contained on the EZ-Lab disk and can be copied directly to a hard drive.

Programs are assembled through the asm21k program; the command line is "asm21k filename". Linking is performed with the command line "ld21k filename -a ezlab21k". Splitting is performed with the command "spl21k -a ezlab21k -ram -pm -dm -f B filename". The options control the architecture, the use of random access program and data memory, and the type of instructions produced. All of these options must be used to produce executable EZ-Lab21k programs.

Programs are uploaded to the EZ-Lab21k board via the serial port using the lab21k program. The file uploaded is a .stk file with the same base name as the original assembly program. After uploading, choose "Reset and Run" to execute the program.

### II. Input and Output (I/O)

The EZ-Lab21k board contains multiple I/O methods each separately described below.

The three LEDs and pushbuttons can be configured within programs for interactive I/O. The reset button activates the chip's reset vector and transfers execution to the rst\_svc routine. The IRQ2 button activates interrupt 2 and transfers execution to the irq2\_svc routine. The FLAG0 button may be used for input by reading its status in the arithmetic status register (astat). The LEDs (FLAG 1, 2, and 3) are also controlled by single bits within the astat register. Note that before using any IRQ for input or FLAG for input or output, it must be initialized. Interrupts must also be globally enabled by setting the IRPTEN bit in the model register.

The microphone, speaker, and line I/O ports are all designed for audio signals. Their maximum sample rate is 33.075 KHz . They are controlled through the AD1849 Soundport Chip. If IRQ3 is enabled, it is asserted at each sample cycle of the AD1849 To use these I/O ports, they must be initialized as ports in the hip\_regs segment. See the talkthru.asm sample program for an example.

The analog to digital converters and digital to analog converters are accessed through the Vin and Vout connectors. They each must be initialized in their own segment, as demonstrated in the talkthru.asm program. Because one sampling takes 2.5 microseconds, the maximum sample rate on these ports is 400 KHz. A value must be written to the analog to digital converter's memory address after each input to prepare it to collect the next sample. It is not possible to simultaneously read or send data through both channels at once. There must be sufficient delay between accesses to the converter to allow the sample to complete. Attempts to read or write from both ports without sufficient delay will result in the least recently accessed port being ignored.

The EZ-Lab21k board also contains two expansion connectors which can be used to directly access program and data memory.

### **III. Program Debugging**

Data may be downloaded from the EZ-Lab21k to the host computer via the lab21k program. Follow the prompts after choosing upload from memory. Hexadecimal data will be written to a file in text format.

Analog Devices has also included an ADSP-21020 Simulator which is useful for debugging programs. This is a Windows based program which allows tracing and monitoring program flow. To use the Simulator, a program must first be assembled and linked. Load the ezlab21k.ach file into the Simulator, and then load the .exe file with the name of the program. (The .exe file is created by the linker and is NOT a standard DOS executable. Attempts to run it from the DOS prompt may crash the computer.) After loading the .exe file, choose the elements to be monitored. Options include program memory, data memory, registers, counters, and more. Values may be modified by right-clicking on them, and breakpoints can be set by double-clicking on lines of the program.

### **IV. Miscellaneous**

Remarks in assembly programs may NOT contain apostrophes. This will result in "unterminated string constant" errors.

The AD1849 Soundport setup routine contained in many of the sample programs is activated by holding down the FLAG0 button as you press reset, pressing and releasing the IRQ2 button, and then releasing the FLAG0 button. The original documentation is somewhat misleading on this point, but the FLAG0 button must be down AT RESET in order to enter the setup routine.

The lab21k software for interfacing with the EZ-Lab21k board defaults to COM1. Use of any other COM port requires placing -c # on the lab21k command line, where # represents the port number.

Use of the programmable built in timer on the 21020 requires setting the variables tperiod and tcount, unmasking one of the two timer interrupts, enabling interrupts, and enabling the timer. See the documentation and sample programs.

In order to change an LED's status during an interrupt service routine, the status stack must be popped before the change and pushed after the change. Example: pop sts; bit tgl astat FLG1; push sts;. See the documentation.

Appendix 2 --Additional Documentation for Berlekamp-Massey Program for EZ-Lab21k  
Michael Powell, July 1996

Author's Note: For a description of this program see "Digital Signal Processing of Maximal Length Sequences" by Michael Powell

**I. Operating ranges**

Signal Frequency Range:

Theoretical: 500 Hz to 100 KHz

Actual Reliable: 1 KHz to 50 KHz

Sequence Degree: up to 15

**II. Error Codes**

Possible error codes are listed in the order they occur within the program. The first two error codes will not occur unless the source code is modified. Any error immediately terminates program operation.

FLAG1 on, FLAG2 off, FLAG3 off: Program is loaded and executed, but crashed before input.

FLAG1 on, FLAG2 off, FLAG3 flashing: Input routine failed to read data.

FLAG1 on, FLAG2 on, FLAG3 flashing: Unable to find any distinct input signal (high or low). Input may not be a square wave or may be noisy.

FLAG1 off, FLAG2 on, FLAG3 flashing: Unable to find more than 1 distinct input signal (high or low). There may be no input, or input may be a flat signal.

FLAG1 off, FLAG2 off, FLAG3 flashing: Unrecognized bit in input data stream. Data may be noisy or have hiccuped. Try pressing reset and running again.

FLAG1 off, FLAG2 off, FLAG3 off: Unable to complete processing of data. Try processing again.

In the case of any unexpected error, try pressing reset and running the program again. Noise or bad bits in the signal may interfere with processing. If this fails, the data frequency may be out of the reliable range of the analog to digital converter.

**III. Important program variables and data memory locations**

tperiod at beginning of main: controls delay before input (default: .25 seconds/6.25 million clock cycles)

tperiod in main: after {Input data from adc\_a}: controls sample rate (default: 396.825 KHz)

r0 in calibrate routine after toler: controls noise tolerance within signals (default: 0x9)

tperiod in display: after r10=0x0: clock rate for output to shift registers (default 10 KHz)

tperiod in display: before Do outloop until LCE: one third of delay pause time and pause between LED output bits (default .5 Hz)

dm(0x1000) through dm(0x7ff): raw input data

dm(0x0), dm(0x1), dm(0x2): output of Berlekamp-Massey, register length, and data rate (in samples)

### Appendix 3 --Source Code from Berlekamp Massey Program

```
{
Program designed for Ezlab21k evaluation board.
Written by Michael Powell, July 1996
```

This program will read a maximal length digital sequence from analog port a, compute the generating polynomial, and output it through the FLAG1 and FLAG2 LEDs. Output will also be passed through the EZlab analog ports (see output routine). ``ff

Operation:

To assemble this program from scratch use the following commands:

```
asm21k [filename]
ld21k -a ezlab21k [filename]
spl21k -a ezlab21k -ram -dm -pm -f B [filename]
```

The ezlab21k.ach file MUST be accessible for successful linking and splitting.

---



---

```
{ ADSP-21020 System Register bit definitions }
#include "def21020.h"
```

```
.SEGMENT/DM dac_a;
.PORT    dac_a;
.ENDSEG;

.SEGMENT/DM dac_b;
.PORT    dac_b;
.ENDSEG;

.SEGMENT/DM adc_a;
.PORT    adc_a;
.ENDSEG;

.SEGMENT/PM rst_svc;           { Reset Vector }
    call init_21k;   {Chip initialization}
    jump main;
.ENDSEG;

.SEGMENT/PM irq2_svc;         {IRQ2 service routine; does nothing}
    nop;
    rti;
.ENDSEG;

.SEGMENT/PM tmzh_svc; {timer service routine}

    call timer;
    rti;
.ENDSEG;

.SEGMENT/PM pm_sram;          {Main program.
Going to main program memory}
main:
    bit set mode1 IRPTEN; {Enable interrupts}
    bit clr mode1 NESTM; {Disable interrupt nesting}
```

```
bit set astat FLG1; {Turn on FLG1 as lifesign}

{wait one fourth of a second to let data stabilize from reset}
tperiod = 0x5fe10;
tcount = tperiod;
bit set mode2 TIMEN;
idle;
bit clr mode2 TIMEN;

{Input data from adc_a}
dm(adc_a) = r1; {init. trigger for adc}
r12 = 1; {mode register, set as input}
m1 = 1;
i0 = 0x1000;
tperiod = 0x03e; {set timer as near 400 KHz possible}
tcount = tperiod; {set initial timer count}
bit set mode2 TIMEN; {enable timer};

{loop for 28671 cycles}
inputting:
idle;
ustat2 = i0;
bit tst ustat2 0x7fff;
if not tf jump inputting;
nop;
nop;
r0 = dm(adc_a); {account for very last bit}
dm(0x7fff) = r0;

{See if input was successful}
r0 = 0x7ff1;
r1 = i0;
comp (r1,r0);
if LT jump failure;

{Determine what input ones and zeros look like}
bit set astat FLG2;
bit clr mode2 TIMEN; {do not need timer anymore}
call calibrate;
bit clr astat FLG2;

{Determine frequency, and set appropriate step (r8)}
call freqfind;
dm(2) = r8; {debug check. outputs data rate}

{Read the input and convert it to pure binary}
call conversion;

{implement Berlekamp - Massey Algorithm}
call massey;
{move output into higher registers}
r15 = r9; {output data}
r14 = r5; {absolute length of output data}
dm(0) = r9; {output data to data mem}
dm(1) = r5; {register length to dm}
r0 = 0x7fff;
dm(3) = r0; {output placeholder}

{Display output on LEDs. Also available as hex data in r15}
```

```

do stall until forever;
call display;
stall: idle; {wait for an IRQ2 press before repeating output}

nop;
nop;
nop;
nop;

.ENDSEG;

.SEGMENT/PM pm_sram; {Init. Routine}
{_________________________________ initialize the
chip_________________________________}

init_21k:
pmwait =0x00001c21; { pmwtstates=0,sw.wtstates only}
dmwait =0x70a421; { bank2_dmwtstates=1,sw.wtstates only}
irptl =0; {must clear this for interrupts}
bit set mode2 0x10; nop; read cache 0; bit clr mode2 0x10;{clr
cache} {irq2&3 enable, timer
enable high priority}
bit set imask TMZHIIIRQ2I; {Unmask timer and IRQ2 interrupts}
{irq2&3 edge sens, flag 1&2&3
outputs}
bit set mode2 IRQ2EIIRQ3EFLG10IFLG2OIFLG3O;
bit clr astat FLG1IFLG2IFLG3; { clear flag LEDs }
bit clr mode2 FLG0O; {Make Flag 0 an input}
rts; {Return from subroutine}
nop;
nop;

calibrate: {determine what input ones and zeros look like}

r14 = 10000; {number of tries allowed}
r15 = 0; {set r15 as an event counter}

{find first one, look for three consec. identical bits}
i0 = 0x1000; {set to beginning of data}

r0 = dm(i0,m1);
r1 = dm(i0,m1);

search1:
r15 = r15 + 1; {increment event counter}
r2 = dm(i0,m1);

comp(r0,r1);
if NE jump increment1;
comp (r1,r2);
if NE jump increment1;

{if here, a value has been found}

r11 = r1; {set it as standard high for now}
jump findnext;

increment1:

r0 = r1;
r1 = r2;

{Check event counter to see if this is taking an unreasonable
amount of searching}

comp (r14,r15);
if EQ jump failure;
jump search1;

findnext: {find the other value; continue from this part of memory}
bit clr astat FLG1; {LED to indicate position}

r0 = dm(i0,m1);
r1 = dm(i0,m1);

search2:
r15 = r15 + 1;
r2 = dm(i0,m1);

comp (r2,r11); {compare to other value to not get two of the same}
if EQ jump increment2;
comp(r0,r1);
if NE jump increment2;
comp(r1,r2);
if NE jump increment2;

{If here, second value is found}

r10 = r1;
jump determine;

increment2:
r0 = r1;
r1 = r2;

comp (r14,r15);
if EQ jump failure;

jump search2;

determine: {Figure which signal is really high/low}

r0 = r11;
r1 = r10;
comp (r1,r0);
if LT jump toler; {signals are not switched, return from subroutine}
nop;
nop;

{unswitch signals}
r11 = r1;
r10 = r0;

toler: {set some tolerance levels}
r0 = 0x9; {tolerance level in reading}
r11 = r11 - r0; {high does not have to be quite so high}
r10 = r10 + r0; {low does not have to be quite so low}

rts;
nop;
nop;

{_________________________________}
freqfind: {Will determine input rate of data}

i0 = 0x1000; {set to start of data}

r3 = 0x7cd0; {comparison point}
r5 = 1; {event flag to indicate first pass}

r8 = 0xffff; {init length to a very high value}

```

```

freqloop: {look for the shortest 1}
    {look for a 1}
    onesearch:
    r2 = dm(i0,m1);
    comp(r2,r11); {compare to standard high}
    if LE jump gotofirst;
    nop;
    nop;

    {look for change}
    r0 = 0;
    comp(r0,r0); {make LT false}
    do passbits until LT;
    r0 = r0 +1;
    r2 = dm(i0,m1);
    passbits: comp(r2,r11);

    comp(r0,r8);
    If GE jump notadecrease;
    nop;
    nop;
    r8 = r0;
    notadecrease:

    r0 = 1;
    comp(r0,r5);
    if NE jump notfirstrun; {make sure to invalidate first change}
    nop;
    nop;
    r5 = 0;
    r8 = 0xffff;
    notfirstrun:

    r4 = i0;
    comp (r4,r3);

    if LT jump freqloop;
    nop;
    nop;

    rts;
    nop;
    nop;

{-----}

conversion: {routine to convert raw input data to binary bits}
    r7 = 0; {set a bit counter}
    r9 = 0; {init}

    i0 = 0x1000;
    {step to the first change to get in most reliable position}

    comp(r7,r7); {init LT to false}
    do firstbit until LT; {find first low}
    r0 = dm(i0,m1);
    comp(r0,r10);
    nop;
    firstbit: nop;
    nop;

    gotofirst: {now find the first transition point}

    r0 = dm(i0,m1);
    comp(r0,r11); {compare to standard high}
    if LE jump gotofirst;
    nop;
    nop;
    {move slightly back from edge}
    r0 = i0;
    r1 = 0;
    r1 = (r1 + r8)/2; {put position in center of a bit}
    r0 = r0 + r1;
    i0 = r0;

convertloop: {main loop for conversion}
    {pass through data and determine if adjustment needed because of
    edge}
    {convert appropriate data bit into pure binary in r9}

    r0 = 2;
    r8 = r8 - r0;
    lcntr = r8;
    r8 = r8 + r0;

    do passdata until lce;
    r0 = dm(i0,m1); {Get data}
    passdata: nop;

    lcntr = 3; {look at 3 bits for edge check and data}
    i1 = 0xffff;

    do edgecheck until lce;
    r0 = dm(i0,m1);
    comp(r0,r10); {compare to standard low}
    if GT jump notlow;
    nop;
    nop;
    r1 = 0; {set to low}

    jump puttoddm;

    notlow:
    comp(r0,r11); {compare to standard high}
    if LE jump failure; {does not recognize bit within tolerance}
    nop;
    nop;

    puttoddm:
    dm(i1,m1) = r1;
    nop;
    nop;

    edgecheck: nop;
    {adjust data position for extra looping}
    r0 = 1;
    r1 = i0;
    r1 = r1 - r0;
    i0 = r1;

    {retrieve highs and lows from dm}

```

```

r0 = dm(0xffff0);
r1 = dm(0xffff1); {this is the actual data that will be used}
r2 = dm(0xffff2);

{if there is an edge adjust position by 2}
r3 = 2;
r4 = i0;

comp(r0,r1);
if eq jump nomovefor;
nop;
nop;
r4 = r4 + r3;
jump adjustdone;
nop;
nop;
nomovefor: nop;
comp(r2,r1);
if eq jump adjustdone;
nop;
nop;
r4 = r4 - r3;
adjustdone: nop;

i0 = r4;

shiftit:
{shift data into the register}

r9 = r9 or lshift r1 by r7;

r7 = r7 + 1;

ustat2 = r7;
bit tst ustata2 32; {see if completed 32 passes, if done, rts}

if tf rts;
jump convertloop;
nop;
nop;

massey: {implement Berlekamp-Massey Algorithm}

{move data into higher register}
r15 = r9;

r1 = 0; r2 = 0; r3 = 0;
r5 = 1;

{find the first 1 in the sequence}
r14 = 0; {will find bit position of first 1}
findone:
btst r15 by r14;
if not sz jump onefound;
nop;
nop;
r14 = r14 + 1;
jump findone;

onefound: {r14 contains bit position of first one}

r5 = r14 + 1; {register length absolute}
r6 = r5 - 1;
r7 = r5 + 1; {start = reglen + 1}
r7 = r7 - 1; {but this program starts at bit 0, not 1}

{implement reg = pnseq bits from reglen to 1}
r8 = 0;
r14 = r5 - 1; {account for starting with bit 0}
lctr = r5;
r13 = 0;
Do fillreg until LCE;
btst r15 by r14;
if sz jump noset1;
r8 = bset r8 by r13;
noset1:
r14 = r14 - 1;
r13 = r13 + 1;
fillreg: nop;

r9 = 0;

{Begin main loop of algorithm}
mainloop:

{Generate next bit}
r4 = 0; {init next bit to 0}
r10 = 1; {temp use of this variable as a flag}
r11 = 1; {temp comparison value for r10}
lctr = 32;
r13 = 32; {loop counter shadow}
do bitgen until lce; {loop thorough taps to generate next bit}
r13 = r13 - 1; {loop counter shadow decrement, gives bit position}
r13 = -r13;
r0 = lshift r9 by r13;
r13 = -r13;
btst r0 by 0;
if sz jump notap;
r14 = 0;
r13 = -r13;
r0 = lshift r8 by r13;
r13 = -r13;
btst r0 by 0;
if sz jump novalue;
r14 = 1;
nvalue:
{determine if first tap, if first tap, no xoring to do}
comp (r10,r11); {if these two are equal, it is the first tap}
if NE jump normalxor;
{first tap found}
r4 = r14;
r10 = 0;
jump notap;
normalxor:
nop;
nop;
r4 = r4 xor r14;
notap: nop;
nop;
nop;
bitgen: nop;

{determine if generated next bit was correct}
r14 = 1;

r0 = -r7;
r13 = lshift r15 by r0;

btst r13 by 0;
if not sz jump bitisnotzero;
nop;
nop;
r14 = 0;

```

```

bitisnotzero:
comp (r4,r14);
if EQ jump nochanges;
{begin algorithm to change taps}

r14 = r7 - r6;
r14 = r14 + r2;
r1 = max(r5,r14);

r10 = 0;

{make a_n (r10) bits out to reg_len (r5) equal taps}
r14 = 0;
lctr = r5;
do putinbits until lce;
r14 = -r14;
r0 = lshift r9 by r14;
r14 = -r14;
btst r0 by 0;
if sz jump nohigh;
r10 = bset r9 by r14;
nohigh: nop;
putinbits: r14 = r14 + 1;

r11 = 0;

{next two sections reversed from original to ease assembler}

r14 = 0;
comp (r2,r14);
if EQ jump oldissmall; {if oldreglen > 0}
r14 = r7 - r6;
r14 = r14; {+ 1 ? }
r11 = lshift r3 by r14;

oldissmall:
r14 = r7 - r6;
r14 = r14 - 1;
r11 = bset r11 by r14;

comp(r1,r5); {newreglen vs reglen}
if eq jump newisnotbig;
r6 = r7;
r2 = r5;
r5 = r1;
r3 = r9;

newisnotbig:
r9 = r10 xor r11;

nochanges:
{implement reg = pnseq bits}
r14 = r7;
r12 = r14 + 1;
r12 = r12 - r6;
r12 = r14 - r12;
r12 = r12 + 1;
r12 = r12 + 1; {increase by 1 so difference gives accurate bit count}

r0 = 0;
comp (r0,r12);
if EQ jump fillreg1; {do not need to loop if lctr would be 0}

lctr = r12;
r13 = 0;
r8 = 0;
Do fillreg1 until LCE;
r14 = -r14;
r0 = lshift r15 by r14;
r14 = -r14;
btst r0 by 0;
if sz jump noset2;
r0 = bset r8 by r13;
r8 = r0;
noset2:
r14 = r14 - 1;
r13 = r13 + 1;
fillreg1: nop;

r7 = r7 + 1; {figure if loop over}
r14 = 32;
comp (r7,r14);
if NE jump mainloop; {end of main loop}
rts;
{-----}

display: {output routine}

{output to external shift registers. Vout A is data, B is clock}

r11 = 0xcf000000; {set high and low}
r10 = 0x0;

tperiod = 0x9c4; {set timer at 10 KHz}
tcount = tperiod;
bit set mode2 TIMEN;
r12 = 0; {mode for timer to do nothing and return}

r1 = 0; {set a bit counter}

lctr = 16; {dump data into shift register}
do clocking until lce; {clock occurs on low to high}

r3 = r10;
btst r15 by r1; {check data}

if sz jump outputdatazero;
nop;
nop;
r3 = r11;
outputdatazero: nop;

r1 = r1 + 1; {output data}

dm(dac_a) = r3; {output data}

dm(dac_b) = r10; {clock low}
idle;

dm(dac_b) = r11; {clock high}
idle;

clocking: nop;

{output to LED}

bit clr astat FLG1|FLG2|FLG3;

```

```

lcntr = r14; {set loop counter to number of bits}
r10 = r15; {make copy of the data}

tperiod = 0xbefbc20; {set timer at .5 Hz}
tcount = tperiod;
bit set mode2 TIMEN;
r12 = 0; {set mode bit for timer interrupt to simply return}

idle; {wait for 1.5 seconds}
idle;
idle;

Do outputloop until LCE;

{determine if bit high or low}
bit clr astat FLG1;
btst r10 by 0;
if sz jump outbitnotone;
bit set astat FLG1; {output the bit}
outbitnotone:
bit tgl astat FLG2; {show a bit has been output}
idle;
bit tgl astat FLG2;

r10 = lshift r10 by -1; {shift to next data point}

idle;
idle;
outputloop: idle; {wait for timer interrupt}

bit clr mode2 TIMEN; {disable timer}
bit clr astat FLG1;

rts;

failure: {routine to indicate program failure; flashes Flag3}

tperiod = 0x6e6c20; {set timer at 2 Hz}
tcount = tperiod;
r12 = 0; {set waiting mode}
bit set mode2 TIMEN;

do nothing until FOREVER; {Endless loop to flash LED}
bit tgl astat FLG3;
nothing: idle;

{-----}
timer:

{Determine which timer call this is}
r0 = 0;
comp (r12,r0);
if ne jump inputmode;

{simple waiting mode. Does nothing}
rts;
nop;
nop;

inputmode:
r0 = 1;
comp (r0,r12);
if ne jump outputmode;

```

References

*ADSP-21020 EZ-LAB Evaluation Board Manual.* Norwood, MA: Analog Devices, Inc. 1992.

*ADSP-21010 User's Manual.* Norwood, MA. Analog Devices, Inc. 1991.

Dixon, Robert C., *Spread Spectrum Systems.* New York: John Wiley & Sons, 1984.

Peterson, W. Wesley and E. J. Weldon, Jr., *Error Correcting Codes.* Cambridge Massachusetts:

Massachusetts Institute of Technology, 1972.

Stephens, James P., *Direct Sequence Spread Spectrum System Thesis.* Air Force Institute of Technology,  
1990.

Wilson, Dale G. "Massey.m" (Matlab Implementation of Berlekamp-Massey Algorithm). Wright  
Laboratories, 1994.

Ziemer, Rodger E. and Roger L. Peterson, *Digital Communications and Spread Spectrum Systems.* New  
York: Macmillan Publishing Company, 1985.

## DEVELOPMENT OF WEBPAGES

Shaun G. Power

Heritage Christian School  
325 Ledbetter road  
Xenia, Ohio 45385

Final Report for:  
High School Apprenticeship Program  
Wright Laboratory  
WL/AARA

Sponsored by  
Air Force Office of Scientific Research  
Bolling Air Force Base, Washington DC

and

Wright Laboratory

August 1996

## DEVELOPMENT OF WEBPAGES

Shaun Power  
Heritage Christian School

### Abstract

The World Wide Web is the best way to acquire information in the modern world today. This summer I helped participate in an effort, dedicated to making MSTAR target photos and IR imagery available on the World Wide Web. Using HTML (Hyper Text Markup Language), me, and other high school apprentices, designed and composed the two pages necessary to present the given information. By using frames and tables, we presented the images and photos in a very uniformed way. Also by using frames and tables, the pages were constructed in a way that more information could be added to them at a later date.

## DEVELOPMENT OF WEBPAGES

Shaun Power  
Heritage Christian School

### Introduction

Wright Labs had a series of images and photos that researchers wanted to be placed on the World Wide Web. In order to do this, the images and photos would have to be reformatted to fit web requirements to be placed on the web. The best known format for our purposes was the JPEG format. This format allowed us to place images on the Web without taking up a lot of disk space. Finding this solution, we were ready to move onto the next part of our summer task, the Web page layout.

### Methodology

For our pages, we wanted users to be able to visually see all their options. We wanted them not only to be able to see an image, but how they had come to that image, and other images that related. Using frames and tables in HTML, we were able to accomplish this task.

### The MSTAR page

The MSTAR web page was the first of the two web projects. The MSTAR data base contained 150 target photos. These photos were divided into 14 different categories and 24 different subcategories. These color photographs of several military targets were taken with a digital camera, and placed onto CDs. Before we could place these images on a web page, we needed to make a copy of the images, and convert them into JPEG. We did this using a Silicon Graphics machine. After copies were made and converted, the images were ready for the web page.

As a team, we had many thoughts of how to display the data. The first idea was just to have all the images in a directory type of listing. Plain and simple. As we thought more about this option we had decided that this way was too generic and the user could not visually see where the target came from and other related targets. Our second thought was to have the different images broken down into their separate categories and displayed in frames. This got us on the right path. Experimenting with the frames helped determine what the page layout would look like. When first working with the frames, we thought we could have 4 frames laid out vertically next to each other. In the first frame, on the left, users could choose a type of target. That target would then flash a new page, with a list of new options in the next column. Users could then choose an azimuth angle, that would then flash the next page in the next column. Finally a depression angle could be chosen and in the last frame the image could be viewed.

When we began to plug the images into this format, an obvious problem came up. The last frame was too thin to view the image. Wanting to stick with this type of layout, we decided to cram two frames together and rearrange the frame environment. This second arrangement (see figure 1.1) was better suited to handle our requirements. When we placed the azimuth and the depression angle together, we formed a table which better displayed the targets than before. ( see figure 1.1) In this table, we placed small balls inside the frame cell to represent the image. Now that we had this new format, it was just a matter of placing the images into the frames, according to the different paths we set on the web page.

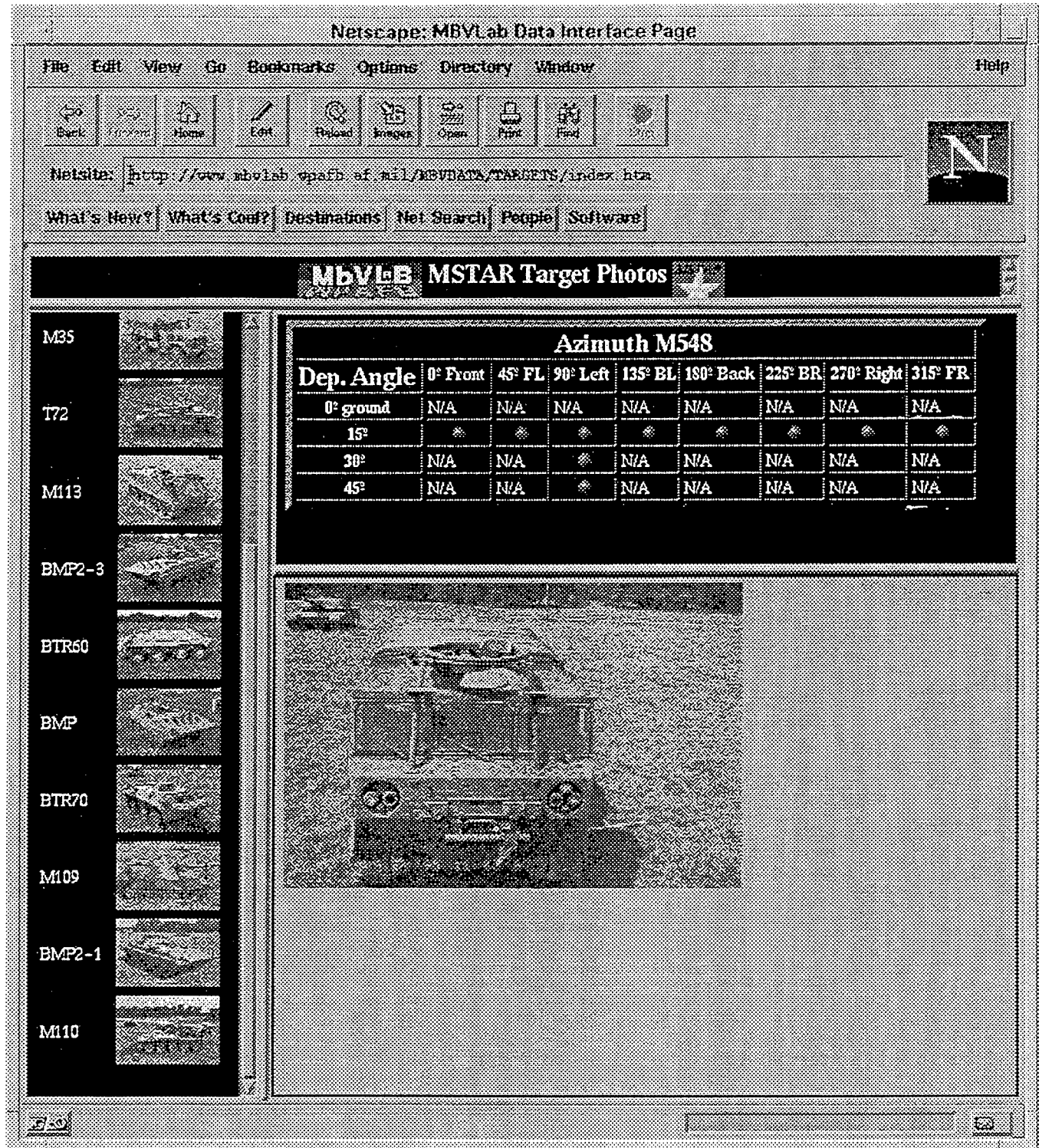


Figure 1.1 - The Azimuth and Depression Angle came together to form an organized table.

#### The IR Data Page

The IR data page was very similar to the MSTAR page. Again, we had a series of images that we needed to present to a user on the Web. The information for the IR page was different than that of the

MSTAR page. The data was infrared images saved in a binary format. To place these images onto a website, we obviously needed to convert them. Using Gif Converter for Macintosh, we converted the images into a JPEG format.

The IR data base was broken down into 2 different months, August '93 and December '94. From each of these months 1 of 5 targets could be chosen. Each of these target data bases, contained 120 categories. Each category contained two IR images, a medium wave image and a long wave image. For the IR page we felt we could pretty much stay with the same type of environment. (see figure2.1) However, the structure of the page layout would have to change to fit the needs of the new data. For this page, we did not add all five sites. In fact, we just posted two sites: site 1 and site 3. Other sites can be added at a later time however persons in charge see fit.

The first frame on the IR page was the month frame. In this frame, a person could decide between August '93 or December '94. Then the new target's frame would pop up. After choosing a target, the table containing the sites and hours of the day would flash up. (figure 2.1) Here viewers could then choose the image they wanted. On the MSTAR page, when users wanted to see an image, they would click on an icon, and that icon would tell the view frame to bring up a specified image. Because the IR data presents two types of pictures for every target, we created a page on which we pasted both images. This way the user can now view both pictures at the same time. This provided us with an opportunity to do something we could not do with the MSTAR page. Because the images were displayed on a page, instead of being called into a frame, we could sequence the pages. By sequencing, the user could view all the images without having to do anything more than hit a button. This was also useful because the sequencing provided the unique opportunity to notice the differences in the images, as they flashed up one at a time. Our first method for accomplishing this was to use the METTA tag in our HTML code. The METTA tag allows a page to load another page or objects, after a given number of seconds. This seemed to be the answer to the sequencing problem, but as we worked with the METTA pages more intensely we discovered that it was not the best method to use. We had assumed that the tag loaded the next page only after both of the images were loaded. What we had discovered was that the METTA tag loads pages at a fixed rate no matter what, if images are done loading or not. Realizing that we could not make the tag work, I personally investigated

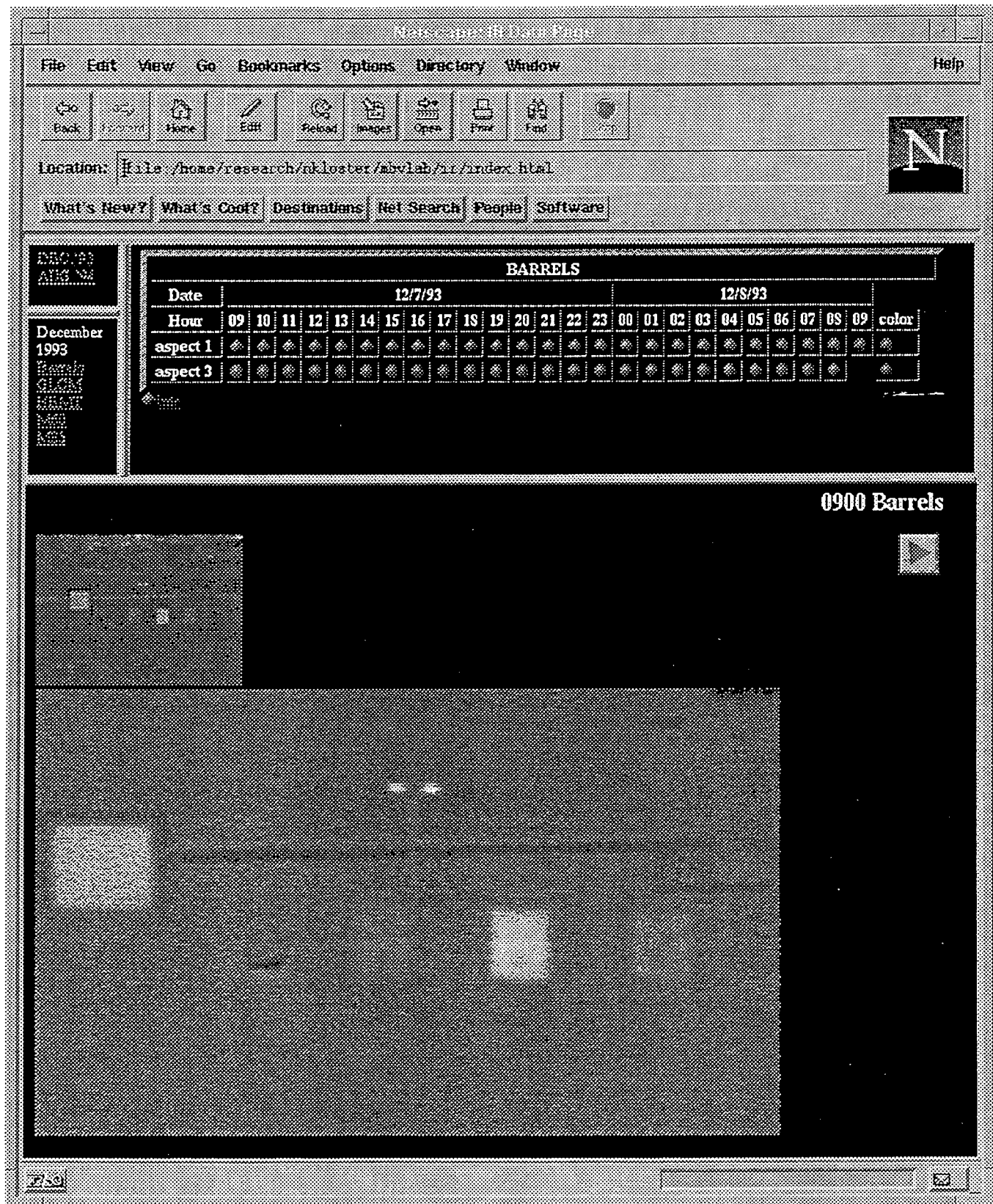


figure 2.1 - Notice the difference between this page and the MSTAR page. Also note, the table, for this page is composed of hours of the day and different aspects.

other options for sequencing. I looked into the possibilities of MPEG and QuickTime movies. When I came across the software, I discovered that the process for making one of these movies was extremely time consuming. Due to the lack of time on this project neither the MPEG or the QuickTime movies were an option. Still wanting to give the user a good interface to work with, we decided to make buttons on each of the pages. Buttons which reference the next page and a previous page. This way users can move at their own pace.

#### Future

Both of the pages that I helped to construct have plenty of room for evolution. We designed the pages so that additional information could easily be added. Both of these pages are posted, or will be posted on a server at Wright Patterson, where our mentors can easily update the pages or make changes as they see fit.

There are several different features which could be added to the pages to improve their quality and make them more user friendly. One of the options we talked about was to display a rotating CAD model of each target next to its icon. This would have to be done using VRML (Virtual Reality Modeling Language) and Java. This task in itself could take an entire summer. Another option could be the MPEG or QuickTime movies. Even though we did not have time to work on it, we still feel that this is an accomplishable task. There are many options and possibilities that would be worth looking into. As HTML, VRML, and Java expand their capabilities, the potential for these pages grow and grow.

#### Conclusion

In the development of these web pages, we experimented to see the very best way to present the image data. We discovered that the data was best presented in a visual “trail.” This way users can see and know all of their options. This was accomplished best by using tables and frames. These pages are not yet the “final product”. On the World Wide Web, there is no such thing. I would not be surprised as to the amazing growth these pages can have.

-Shaun Power

Matthew R. Rabe report was not available at the time of publication.

DIMENSIONAL CHANGES AFFECTING HS50 AND HA50HS  
IRON-COBALT ALLOYS DUE TO ANNEALING

Angela C. Rabe

Carroll High School  
4524 Linden Ave.  
Dayton, OH 45432

Final Report for:  
High School Apprentice Program  
Wright Laboratory

Sponsored By:  
Air Force Office of Scientific Research  
Bolling Air Force Base, DC

and

Wright Laboratory

August 1996

DIMENSIONAL CHANGES AFFECTING HS50 AND HA50HS  
IRON-COBALT ALLOYS DUE TO ANNEALING

Angela C. Rabe  
Carroll High School

**ABSTRACT**

Two different types of iron-cobalt alloys are being considered for use in the integrated power unit of the more electric aircraft. The Telcon material is manufactured in England, and the Carpenter material is produced in Pennsylvania. Both materials were studied in this experiment with the intent of determining the effects of heat treating on their dimensions. Unfortunately, the results of this experiment were inconclusive based on the failure of two sets of heaters and four thermocouples. Despite the difficulty in obtaining reliable data, the setup and procedure of the experiment worked well and could be used again if the experiment were to be finished at a later date.

The rack method, used to hold the thin samples upright so that they had a limited number of contact points with other metal, also worked well. The rack was made with a 90 degree angle to hold the samples. They were held in place by stainless steel wires on either side of them about one inch up from the base. Thermocouples were touching 6 of the 8 samples and were reinforced by stainless steel wires on the other side of the samples for support. The procedure would have been fine if the furnace was capable of reaching 800C while maintaining a vacuum. This was thought to be the case in this experiment, but after two heater failures it is now thought otherwise. One possible explanation for the failures is that at no time during the experiment were all four heaters working at once. This experiment should be carried out fully at a later date. Due to the constraints of time and equipment, the results remain as much in question now as they were before this experiment was begun.

DIMENSIONAL CHANGES AFFECTING HS50 AND HA50HS  
IRON-COBALT ALLOYS DUE TO ANNEALING

Angela C. Rabe  
Carroll High School

INTRODUCTION

This experiment was conducted in order to determine the effects of heat treating at elevated temperatures on the dimensions of iron cobalt-vanadium alloys. This material is being considered for use in an integrated power unit, and distortion of precise dimensions due to the required annealing could lead to several problems. An increase in size will affect the prescribed design tolerance of the iron cobalt parts. There also exists an added concern that the material may expand enough to affect the measurement of the material's magnetism. This is extremely important because the iron cobalt material was chosen for its high magnetic behavior.

BACKGROUND

Iron-Cobalt material with a small percentage of Vanadium is currently being investigated for use in an integrated power unit in the more electric aircraft (MEA). The MEA is currently in the design process. The intention is to increase the electric power of aircraft in general in order to increase reliability, maintainability and supportability and to decrease the amount of downtime. Electrical

equipment should withstand the wear and tear of the high stress environment for extended periods of time. The integrated power unit will perform auxiliary power functions, eliminating many of the hydraulic parts currently in use. It will provide instant-on emergency power for all altitude and attitude conditions as well as start-up capabilities at -65 degrees Fahrenheit. In addition, the setup will allow for minimum maintenance and supportability needs. The iron-cobalt material, or something like it, is essential in achieving all of these requirements.

The material is currently being tested for the necessary mechanical and magnetic properties. Tests are being run on the effects of atomic ordering and the optimal degree of ordering. It is necessary to transform the body-centered cubic solid solution into two interpenetrating cubic lattices. This can be achieved through a process of annealing to order the material. This effect can occur to different degrees by varying the quenching temperature. The ductility decreases as the material changes from no order to total order. The elastic constants change slightly due to ordering, but the effect is minimal. In the fully ordered state, initial yielding occurs at a lower stress. The strength of ordered material is lower at room temperature, but it increases sharply with

increasing temperature. At lower temperatures, a lower shelf exists where the material exhibits low fracture toughness and brittle behavior. The upper shelf, occurring with higher temperatures, illustrates the opposite trend with high fracture toughness and ductile behavior. The ordering also increases the strain hardening, causing the material to behave in a brittle manner in tension tests while exhibiting plastic effects in compression tests. The added Vanadium serves to increase the ductility by forming a diffusion produced  $\text{Co}_3\text{V}$  compound.

This experiment will focus on the effects of high temperature annealing on FeCo-V alloys. A similar test was run almost 50 years ago on the thermal expansion properties of iron-cobalt alloys; however, none of the tested alloys contained vanadium. Previous to the 1948 investigation, ordering was always considered to be accompanied by a decrease in cell size. It was shown, however, that near equiatomic iron-cobalt alloys which have been well ordered have larger cell sizes at room temperature than when they are in the disordered state. When the alloy was heated to 850C and then slow cooled to instill ordering, an expansion was noted to be approximately 0.0006 inches per inch. This corresponded closely with the 0.0007 inches per inch growth calculated by using the change in lattice constants from the ordered to the disordered state. Some of the discussion in this investigation states dimensional decreases for this material which appears to be contradictory to other findings in the same investigation. The reasoning for this apparent contradictions that the decreases were found when the allots being

tested went from the ordered state to the disordered state. Thus all the data support the same conclusion, that ordering results in an increase in dimension.

A slightly more recent study was done in 1971 on vanadium permendur (49Fe 49Co 2V). The material was investigated for possible use in aircraft and space applications due to its weight saving advantages, high magnetic saturation and strong retention of magnetic properties at elevated temperatures. The disadvantages of vanadium permendur include high cost and low ductility. Similar results were found as those in the 1948 study: when a specimen went from an ordered state to a disordered state a dimensional decrease was found, and when the alloys went from disordered to ordered, a dimensional growth was found. This 1971 study by McCunn looked at ordering as well as the transition from ferrite to austenite, which occurred around 1000C. He initially conducted experiments to determine the order disorder transition temperature. The specimen in question was a hot rolled rod that was continuously brine quenched during the manufacturing process. The specimen was generally held at the specified temperature for two hours after heating to the load temperature for three hours. After heating the specimen would be cooled at a rate 28C per hour and then at 140C per hour. The difference in cooling rate showed no effects on the specimen. McCunn reported that the cylindrical specimens lengthened 0.00066 cm/cm after annealing at 850C and then cooling to room temperature. He concluded that the lengthening occurred as the

specimen was transitioned from the disordered state to the ordered state at the end of the annealing process. He also reported that the ordering upon heating began around 400C and the disorder to order transition while cooling began at about 700C.

This experiment will test two types of FeCo-V in a temperature range from 1250-1400 degrees Fahrenheit. The two distinct materials differ in their chemical compositions, their place of manufacture and their various properties. The Telcon material is manufactured in England and reportedly has a higher magnetic saturation but a slightly lower strength. The Carpenter material is manufactured in Pennsylvania and boasts a stronger material with slightly less magnetic performance.

### SETUP

Eight samples were tested at a time, 2 HS50 1.5x1.5x.006 inch, 2 HS50 1.5x.15x.014 inch, 2 HA50HS 1.5x1.5x.006 inch samples, 2 2.5x2.5x.006 inch samples. The samples were housed in a rack made from a sheet of perforated 304 stainless steel. The sheet was 9 inches long by 5.5 inches wide, and bent 90 degrees at .75 inches, 2.75 inches (in the opposite direction), and again at 4.75 (the same direction as the first bend). The two outside bends served as "wings"

to allow the rack to hang on the two pronged rod that attached to the cylindrical extension of the heater cover. The setup is shown in figure 1.

The stainless steel wires across the rack fixed the samples into their space to prevent them from falling over. The samples were spaced one inch apart. Thermocouples were touching 6 of the 8 specimens to attain an accurate reading on the temperature of the specimens. The thermocouples came up through the rack by holes drilled at the 90 degree angle where the samples rested. They touched the specimens and, due to reinforcing wire parallel to but on the opposite side of the specimen, everything was held in place.

These thermocouples entered the furnace through tight fitting ceramic pieces which were covered by a bolt to make the chamber airtight. Each of the thermocouples read directly into the fluke data logger and specimen temperature was monitored.

A vacuum was held throughout the chamber to reduce oxidation to a minimal level. The pressure in the chamber was around 20 milliTorr. The other option here would have been annealing in a dry hydrogen environment. This method was not used due to the explosive nature of hydrogen.

Table 1: Makeup of Material

material	%Co	%Fe	%C	%V	%Ta	%Nb	%Si	%Mn
HS50	49.5	49.66		.27	.45		.08	.04
HA50HS	48.75	48.95	.01	1.9		.30	.05	.05

Fig. 2: Outer Setup

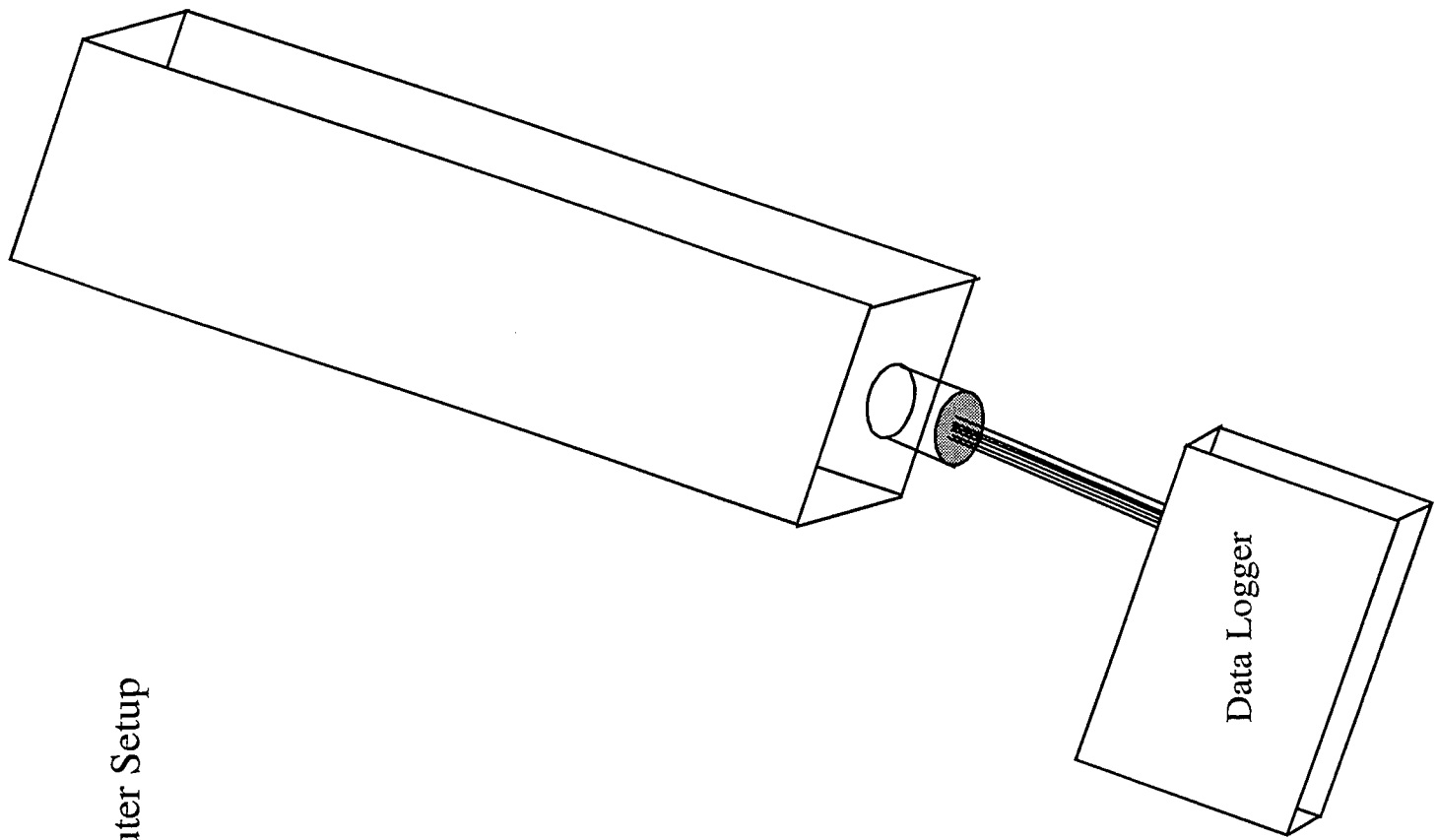
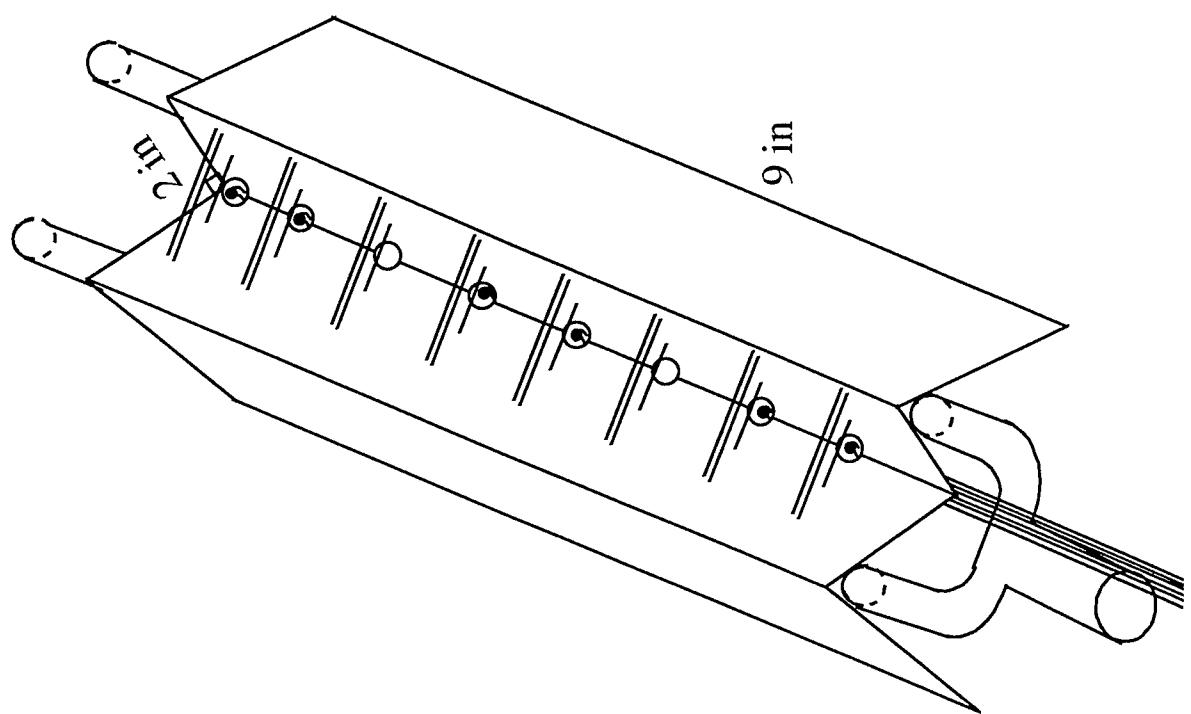


Fig. 1: Inner Setup



The furnace unit housed four heaters with semicircular cutouts that allowed the vacuum chamber to fit perfectly inside. These four heater units were designed to evenly distribute the heat throughout the chamber.

### PROCEDURE

The first two sets of specimens were marked prior to testing by scribing lines about one inch apart on the 1.5x1.5 inch samples and 2 inches apart on the 2.5x2.5 inch samples. This was accomplished using a scribe with a tungsten point and a precision block. The last three tests used a different technique for the 1.5x1.5 inch samples. This technique involved a two pronged punch that left indents about 1 inch apart. This method was more accurate because the lines in the scratch technique were not guaranteed straight or parallel; whereas in the indent procedure the two-pronged punch was more repeatable and guaranteed a consistent measurement.

After they were marked in both the x (determined to be along the rolled lines) and y direction, the specimens were measured using an optical microscope with 5 or 6 significant digits. They were then cleaned in acetone to remove tape (from when they were stored) and grease from being handled. After that they were handled with gloves. The samples were then placed in random positions in the rack. These positions were recorded because in some tests position proved to be a critical factor. The rack was placed in the chamber and the vacuum was sealed. After the appropriate vacuum was

reached, the furnace was activated. The furnace was set at a higher temperature than necessary in order to expedite the process of heating to temperature. The furnace would reach its set temperature in about an hour, but the thermocouples did not reach the intended temperature for another hour or so. The entire process took over two hours to heat the chamber. The temperature was then adjusted manually to reach the desired value.

This temperature was held for one hour in most cases (exact test parameters are shown in table 2). The heater was then turned off as the entire unit began to cool. At any point after reaching 300C the vacuum was released (generally around 200-250C). The samples then cooled rapidly to room temperature.

The specimens were then measured again to determine any dimensional changes. These values are recorded in Table 3.

### ANALYSIS

Test one was a preliminary test to determine any problems with the test cell. At that point it was determined that the thermocouple readings were not reliable and needed to be repaired. Three of the thermocouples had made connections outside the heater and were reading room temperature values. After this problem was solved, test two was begun. The thermocouples were now working, and the kinks in the test cell seemed to have been worked out.

The temperature difference across the nine inch long rack was 100C during the second

Table 2: Test Parameters

	Test 1	Test 2		Test 3		Test 4	
	15 hours	1 hour		1 hour		none	
	607.1-671.8C						
			Position		Position		Position
T1	Telcon	0.006	5	T1	Carpenter	2.5x2.5	2
T2	Carpenter	1.5x1.5	5	T2	Carpenter	2.5x2.5	1
T3	Telcon	0.006	6	T3	Telcon	0.006	9
T4	Telcon	0.014	5	T4	Telcon	0.014	10
T5	Carpenter	1.5x1.5	6	T5	Telcon	0.014	9
T6	Telcon	0.014	6	T6	Carpenter	1.5x1.5	10
			Temperature		Temperature		Temperature
			(C)		(C)		(C)
T1	708.1			T1	763.3		T1
T2	732.1			T2	779.8		T2
T3	770.7			T3	789.9		T3
T4	780.4			T4	792.6		T4
T5	804.7			T5	795.6		T5
T6	808.9			T6	790.5		T6

Table 3: Test Results

test. At the temperature where the specimens were held for an hour, the first thermocouple was reading 708.1C, the second read 732.1, the third 770.7, fourth 780.4, fifth 804.7, and the sixth 808.9C. The cause of the ascending temperatures was later determined to be the positioning of the rack in the heater chamber. The first thermocouple was not far enough from the ends of the chamber which were wrapped with cooling wire. On the other hand, the sixth thermocouple was resting in the center of the heater chamber. The two hours of heater activation were not enough to allow the chamber to attain a uniform temperature. Both sets of samples (from tests one and two) were still measured afterward to detect any dimensional changes, but the results are questionable due not only to the testing difficulty, but also to the measurement technique. The scribing procedure did not yield precise results and was therefore replaced by the indentation technique.

Test three was unique in that when it was heated up to temperature, only two of the thermocouple readings surpassed the critical order-disorder temperature of 700C. This was due to the failure of all four heating elements, some of which were probably already broken. The test was stopped and the heater was repaired. Later, with the new heating elements in place, the samples were held at 200C for 15 hours to determine whether the furnace would function properly since only three of the four heating elements were replaced during repair due to lack of available equipment. Then the specimens were heated to +/-15C of 790C where they remained for one hour. They were then

cooled at a rate of 1-3C per minute to 300C. Then the lid of the furnace was completely opened and the samples cooled at about 5C per minute to 250C when the vacuum was removed. Despite all the difficulties involved in this test, it emerged as the most accurate test temperature-wise.

The fourth test encountered some preliminary thermocouple variation. This was later found to be the direct result of a second heater failure. The failure was almost identical to the first one. This time, however, seven of the eight samples surpassed the order-disorder temperature of 700C, if only briefly.

Due to all the difficulties in testing and the failure of equipment encountered in every test, the results shown can not be relied on. Time constraints along with lack of equipment prohibited further testing. This experiment is useful in displaying the numerous obstacles associated with running tests and the time required to run a relatively simple experiment.

Furthermore it shows good insight for future experiments of this nature. The difficulties in designing the rack and obtaining appropriate measurement techniques were surpassed. With a reliable furnace, capable of reaching and holding 800+C able to withstand a vacuum or the flow of dry hydrogen, this experiment should not present many problems. The main difficulties in this case were the lack of equipment and the time constraints.

At this point, in order to finish the experiment, a new heater must be found that is capable of withstanding the testing parameters. The samples may also be more precisely

measured if they were machine cut to exact dimensions and then measured edge to edge under the optical microscope. This would help to attain a more precise measurement of dimensional change in the intended direction. In the indent technique it was difficult to make the dents exactly parallel and perpendicular to the rolling direction. Since theoretically, if not actually, the samples should change more in the rolled direction, it would be more precise to measure exactly parallel to that direction.

While this test may appear to be a complete failure at first glance, it has set the way for further tests to occur more easily. Through trial and error this experiment can provide insight for others pursuing similar experimentation.

Fingers, Rick, "Fracture Behavior of a Switched Reluctance Starter/Generator Rotor Laminate," *Engineering Science and Mechanics*, Virginia Polytechnic Institute and State University, Blacksburg, VA, 11 May 1994.

McCunn, T.H., "Dimensional Stability of Vanadium Permandur," *Allegheny Ludlum Industries, Inc., Brackenridge, PA, 1971.*

Telcon Limited, "Speciality Alloys and Components," 1993.

#### REFERENCES

Carpenter Technology Corporation, Carpenter Steel Division, Electronic Alloys, CRS Holdings, Inc., 1995.

Dowling, Norman E., Mechanical Behavior of Materials, Prentice Hall, Englewood Cliffs, NJ, 1993.

Ellis, W.C. and Fine, M.E., "Thermal Expansion Properties of Iron-cobalt Alloys," American Institute of Mining and Metallurgical Engineers Technical Publication 2320, Classes C and E, Metals Technology, February 1948.

A STUDY ON THE IMPACT OF VOLTAGE AND FREQUENCY LEVELS ON THE  
CONDUCTIVITIES AND EFFECTS OF POLYMER DISPERSED LIQUID CRYSTAL  
HOLOGRAMS

Rajeev Raghavan

Centerville High School  
500 East Franklin St.  
Centerville, OH 45458

Final Report for:  
High School Apprentice Program  
Wright Laboratory, Materials Directorate

Sponsored by:  
Air Force Office of Scientific Research  
Bolling Air Force Base, DC

and

Wright Laboratory

August 1996

A STUDY ON THE IMPACT OF VOLTAGE AND FREQUENCY LEVELS ON THE  
CONDUCTIVITIES AND EFFECTS OF POLYMER DISPERSED LIQUID CRYSTAL  
HOLOGRAMS

Rajeev Raghavan  
Centerville High School

Abstract

In this investigation, samples of Transmission and Reflection holograms were prepared from Polymer Dispersed Liquid Crystal Syrups. These samples were exposed to varying levels of frequency at constant voltage, current, and temperature. The different voltage levels were analyzed to compare the conductivities and effects of the holographic samples.

A STUDY ON THE IMPACT OF VOLTAGE AND FREQUENCY LEVELS ON THE CONDUCTIVITIES AND EFFECTS OF POLYMER DISPERSED LIQUID CRYSTAL HOLOGRAMS

Rajeev Raghavan  
Centerville High School

Introduction

Today, holograms can be seen in all areas of life, from credit cards to sunglasses to children's toys. These holograms can be created via an immense variety of methods and polymers. Polymers are interesting materials for many applications due to their excellent properties<sup>3</sup>. The foundation of this investigation was to compare different polymer based holograms by measuring and comparing conductivity and effects under an emission of voltage.

The first step of this investigation was to prepare the polymer dispersed liquid crystal syrup which would be used to create the hologram. The syrup which was used is composed of five ingredients: N-Vinylpyrrolidine (NVP), liquid crystal E7, N-Phenylglycine (NPG), Dipentaerythrolhydroxy penta acrylate (DPHDA), and Rose Bengal dye. The NVP solution is primarily used as a chain extender in the syrup. The commercially available liquid crystal mixture E7 is also an ingredient in the syrup<sup>6</sup>. The liquid crystal phase is unique in itself since it is in a fluid phase in that a liquid crystal flows and still will take the shape of its container<sup>1</sup>. It is also unique since its molecules neither occupy a specific average position nor remain oriented in a particular way<sup>1</sup>. NPG is a co-initiator, yet more importantly, it acts in the syrup as an electron donor. This is very important since NPG serves its purpose by producing an initiator for polymerization. DPHDA serves its purpose in the syrup as a crosslinker, which reacts in conjunction to NVP<sup>5</sup>. Finally, the Rose Bengal dye is used as a photoinitiator dye, hence it reacts with light. It is very important to the syrup since it moves to the excited energy state following a jump to the triplet state allowing for NPG to produce a polymerization initiator. The Rose Bengal dye is also particularly attractive for such Polymer Dispersed Liquid Crystal applications as it displays a broad absorption spectrum with a peak molar extinction coefficient of  $\sim 10^4$ ,  $M^{-1} cm^{-1}$  at about 490 nm<sup>4</sup>. A sixth ingredient which is sometimes used in the liquid crystal syrups is a surfactant. Surfactants are used primarily as an agent which works to make the liquid crystal smaller, cleaner, and more efficient. There are five

different types of surfactants: Propylpentanoic Acid, Hexanoic Acid, Heptanoic Acid, Lauric Acid, and Octanoic Acid. However, only the effects of Octanoic Acid were studied in this investigation.

After creating smaller samples from the prepolymer syrups, the second step of this investigation was to set the lasers to convert the samples into holograms. The lasers can be organized in a multitude of ways, depending on the type of hologram. This investigation primarily used two types of holograms: the Reflection and the Transmission hologram. The difference between the two is that a transmission hologram will construct the image on the opposite side of the hologram. Yet on the other hand, when light is passed through a reflection hologram, the image is created on the same side of the hologram.

The third step of this investigation was to design and build an electric circuit for testing the samples. An electric circuit is any combination of a conductor and a source of electricity connected together to permit electrons to travel around in a continuous stream<sup>2</sup>. A basic AC circuit was designed to allow the electrons to move in a complete path directly through the hologram. The components of this particular circuit include an Am-meter, a Volt-meter, a thermocouple, and an AC voltage supplier. The current, voltage, and temperature of the samples were measured while the frequency was kept constant. With these measurements, the impedance can be calculated. Concurrently, with impedance, the conductivity can be determined.

Another type of circuit which was built to test the sample is a Wheatstone bridge. This circuit is more complex than the basic AC circuit above. It includes two known resistors, one variable resistor, one capacitor, an Am-meter, a Volt-meter, a thermocouple, and an AC voltage source.

The focus of this investigation was to use four different holograms and compare their effects and conductivities under a steady emission of voltage though graphs and calculations. The holographic samples used in this investigation were characterized as: a reflection hologram with 0% surfactant, a reflection hologram with 40% surfactant, a transmission hologram with 0% surfactant, and a transmission hologram with 40% surfactant. In addition, another sample with known resistance and capacitance was built and tested as a reference.

### Methodology and Diagrams

The methodology of this investigation involved four separate parts: producing the syrups, manufacturing the samples and holograms, building the circuit and the reference sample, and finally testing the samples in the circuit.

1. Making the Syrup: The ingredients for the syrup are accurately weighed and placed together in a vial. The Rose Bengal dye is a photoinitiator and must be added to the vial in the dark. The five ingredients are then thoroughly mixed in the Ultra-Sonicator. For this investigation, only two syrups were needed--one of which included the surfactant Octonaic Acid.

2. Making the samples and the holograms: First of all, two samples needed to be made from each of the two prepolymer syrups from step one. The sample was made by placing a drop of the prepolymer syrup in-between two glass ITO (Indium-Tin-Oxide) plates. The ITO functions as a transparent conducting film in the sample. Two small pieces of saran wrap, called spacers, are placed on the inside edges of the sandwich, creating a groove for the syrup to settle inside.

**Figure 1** shows an example of how the sample was put together.

#### MODEL OF A SAMPLE

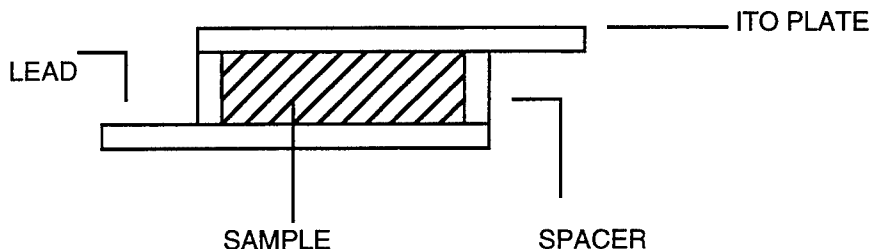


**Figure 1**

Once these four samples were completed, they needed to be converted to holograms, which meant exposing the samples to an intense light beam. Each sample was exposed in the laser for a duration of five minutes. Then the samples were taken out and thin strips of paint, leads, were painted on the outside edges. The leads were painted with CP-40TS-25 Electrically Conductive Thermosetting Paint. The purpose of having leads painted on the holographic sample is to create an improved method of conducting the voltage and attaching Alligator clips.

3. Building the circuit and the reference sample: The basic circuit which was used in this exploration was built according to **Figure 2**.

### MODEL OF A BASIC AC CIRCUIT

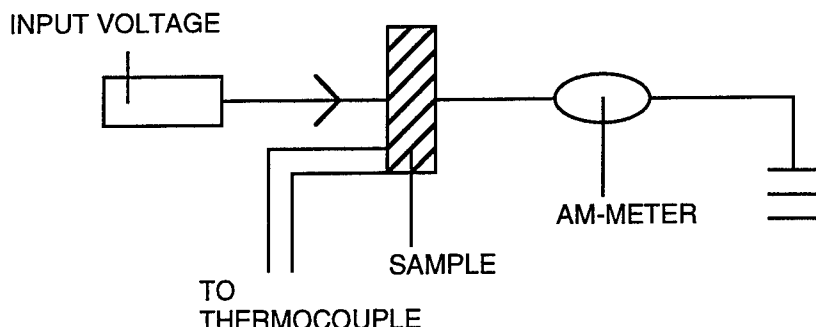


Figure 2

The wires were soldered to the Alligator clips which were used to attach the sample. A Volt-meter, an Am-meter, and a thermocouple were also in series. This basic circuit was attached to a computer to record data. In addition to the four unknown holographic samples, a reference sample was constructed with known values of resistance and capacitance. This sample was built with a ten ohm resistor in series and a mega ohm resistor in parallel with a 190 pF capacitor. The three elements were soldered together in similar fashion to **Figure 3**.

### REFERENCE SAMPLE

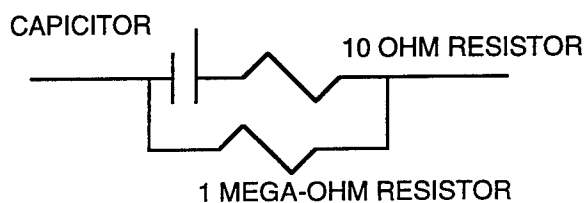
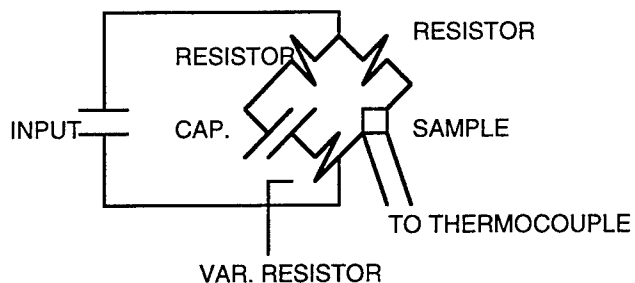


Figure 3

4. Testing the samples in the circuit: The methodology behind the testing was to run five trials at five different frequencies while steadily increasing the voltage throughout the trial. During each trial the voltage, current, and temperature were recorded. The five different frequencies at which each sample was tested at included 500 Hz, 1 kHz, 2.5 kHz, 5 kHz, and 7 kHz. In an AC circuit, the value of the frequency connotes the number of times the current reverses its flow<sup>7</sup>.

A more complex circuit which can also be used to test the samples is the Wheatstone bridge. This circuit is more complex and accurate since it involves two known resistors, one variable resistor, and one capacitor. One method of solving a network such as the Wheatstone bridge is very traditional and based on Kirchoff's Laws<sup>2</sup>. The scheme of a Wheatstone bridge is shown in **Figure 4**. The idea behind such a network is to use the capacitor and the variable resistor to equate the two sides of the bridge and solve for the sample's resistance. A simplified scheme of the Wheatstone bridge is shown in **Figure 5**. **Figure 6** shows the actual Wheatstone bridge built during this investigation.

WHEATSTONE BRIDGE



**Figure 4**

SIMPLIFIED WHEATSTONE BRIDGE

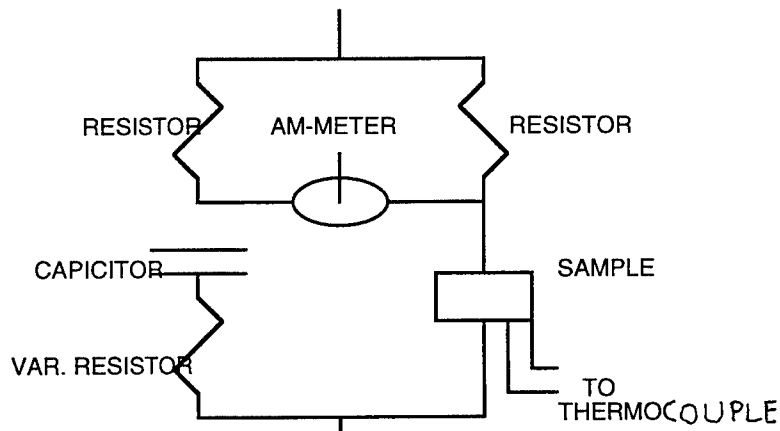


**Figure 5**

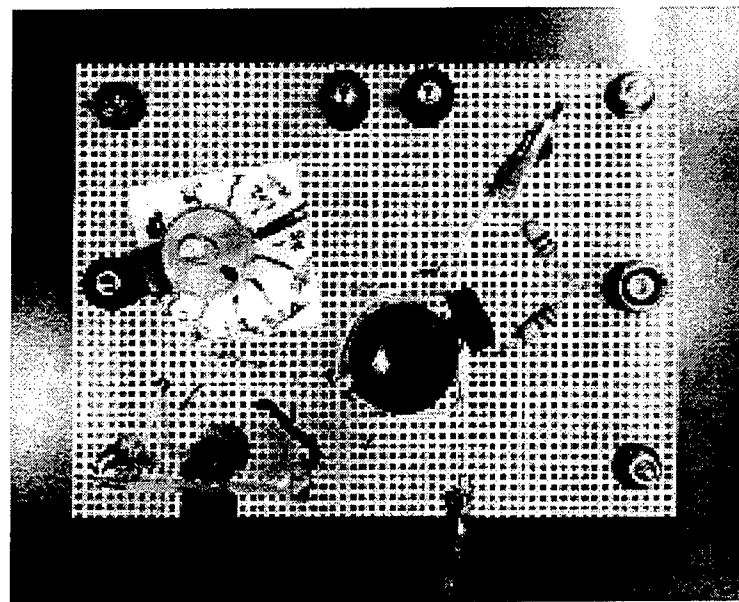


**Figure 6**

### Results and Calculations

The impedance ( $Z$ ) was calculated for every sample at 50, 100, and 150 volts by using the formula  $Z(w) = (R_p^2 + X_c^2)^{1/2} = E_t / I_t$ . Like resistance and reactance, impedance is a V/I ratio expressed in ohms. But unlike  $R$ ,  $X_L$ , and  $X_C$  which do indicate the exact phase angle between  $V$  and  $I$ , the letter symbol  $Z$  gives no such indication<sup>7</sup>. Then with the inverse of impedance ( $1 / Z$ ), conductivity can be calculated. Among the five samples, the highest conductivity was found in the transmission holograms with surfactant. **Figure 7** shows a graph of this hologram at 100 volts.

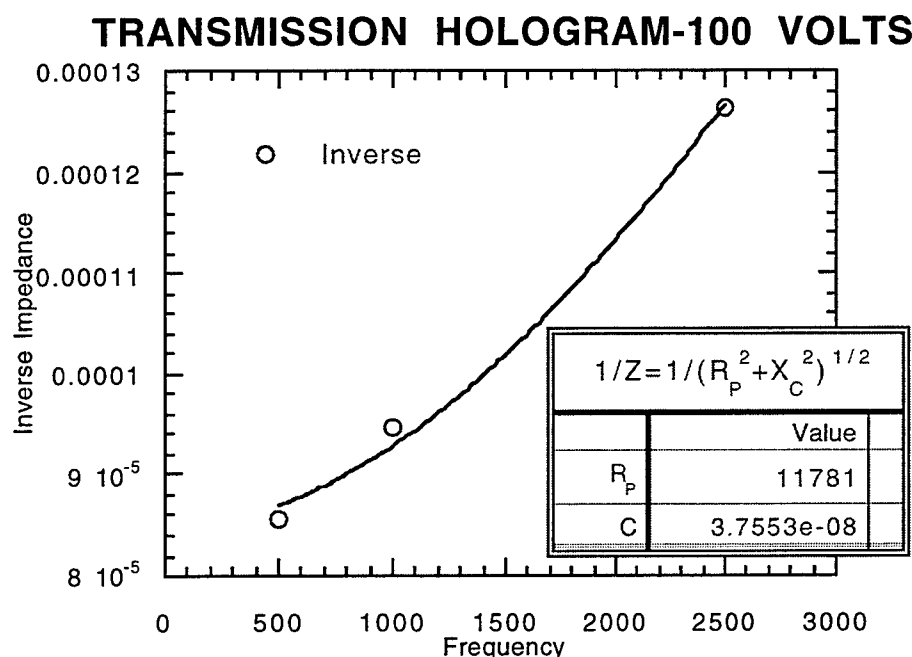


**Figure 7**

Another important discovery is that the three graphs of the reflection hologram without surfactant appear to be fairly linear in the range of study. **Figures 8 and 9** show the plots of this holographic sample at 50 and 150 volts.

## REFLECTION HOLOGRAM-50 VOLTS

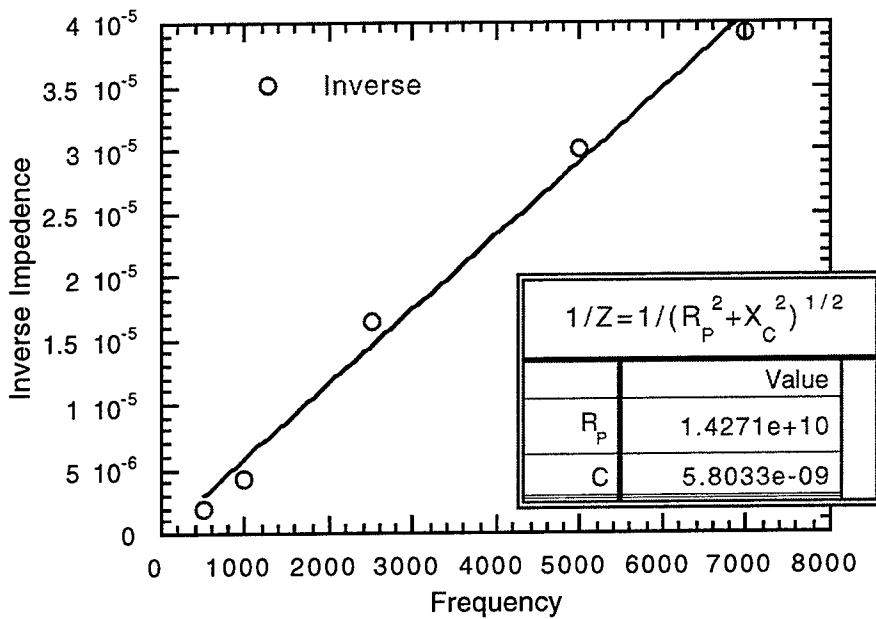


Figure 8

## REFLECTION HOLOGRAM-150 VOLTS

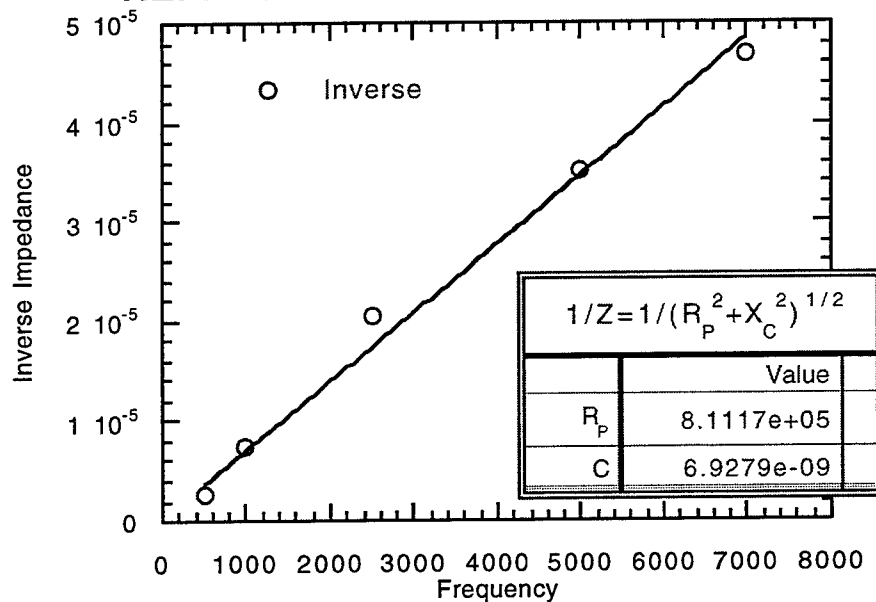
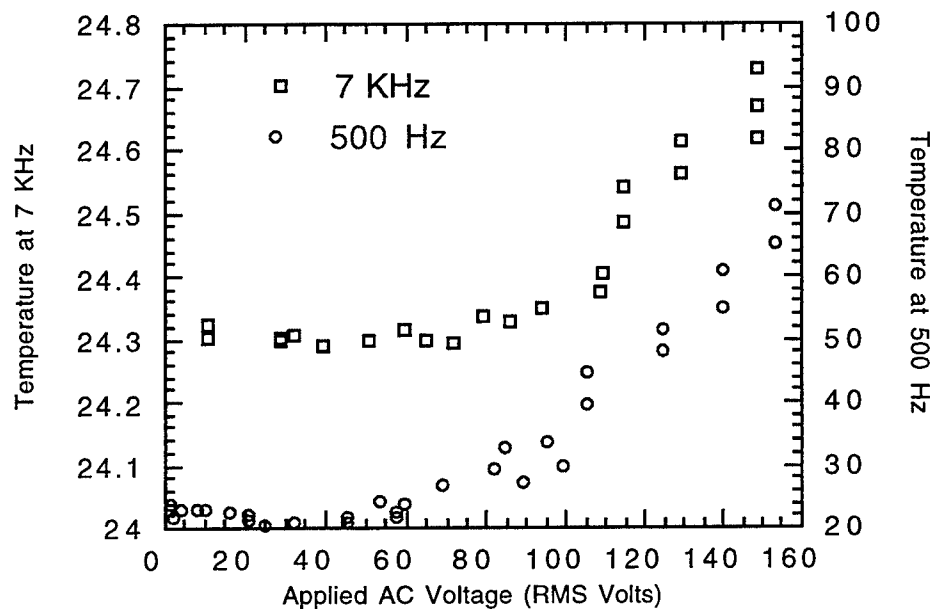


Figure 9

Another interesting discovery is that the frequency of the trial plays a significant role in the heating processes of the samples. **Figure 10** shows a graph plotting the applied AC voltage vs. temperature for the reflection hologram without surfactant at both 500 Hz and 7 kHz.

### REFLECTION HOLOGRAM-500 Hz and 7KHz



**Figure 10**

The built reference sample also exhibited interesting properties. It revealed very low values for conductivity and current. In fact, the *largest* current that the reference sample reached was 1.23 millamps, which was at 150 volts and 7000 Hz. **Figure 11** shows a graph of the reference sample with applied AC voltage vs. current.

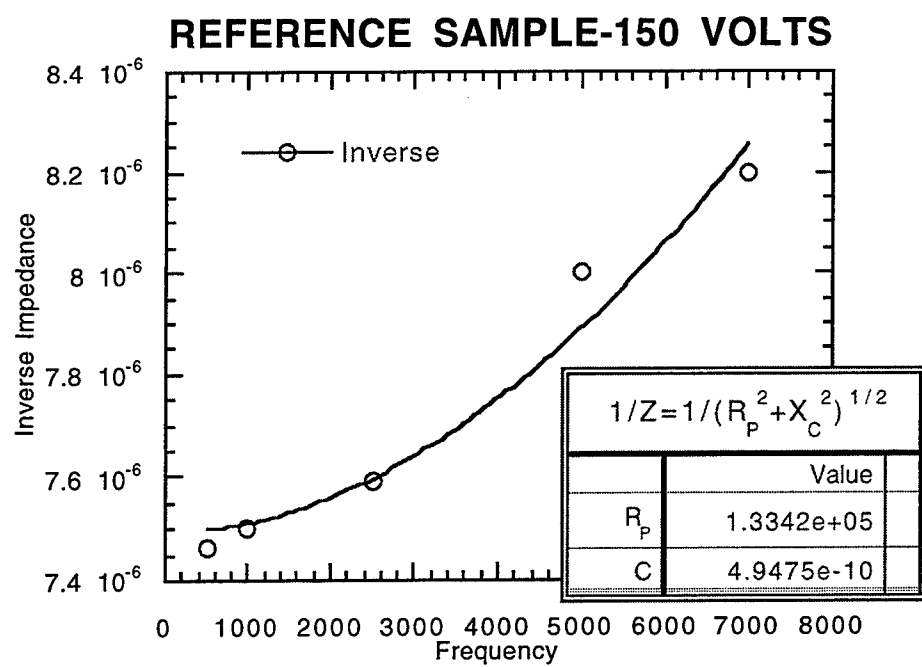


**Figure 11**

### Conclusions

This investigation led to many interesting conclusions all relating surfactants, frequencies, and holograms to higher conductivity. The transmission hologram with surfactant appeared to have the highest inverse impedance value at 100 volts, hence it could be considered the most conductive sample. However, at 500 Hz the reflection hologram without surfactant maintained incredibly low temperatures. This would tend to make it very conductive since it did not heat up as rapidly as the other samples under a large emission of voltage. The conclusion which can be drawn from this is that the most optimal sample would tend to depend greatly on the situation needed.

An additional effect is the linearity of the graphs of the reflection holograms having no surfactant. As the frequency increased, the conductivity increased linearly within the range of study. This is startling because the applied AC voltage vs. temperature graph pointed to a nonlinear curve at higher frequency but a linear curve at the lower frequencies. The conclusion which can be drawn from this is that frequency has a more decisive role in the sample's heating process than it does in its conductivity.

The results of the samples in this investigation displayed more anisotropic than isotropic characteristics. Throughout the testing, the conductivity differed along with frequency and temperature. The impedance values also tended to reveal anisotropic characteristics.

Via this investigation, many important and interesting observations and conclusions have been made relating the conductivities and effects of the holographic samples under an emission of voltage. However, further testing is necessary to determine which holographic sample is in fact most optimal under the constraints of temperature and inverse impedance.

### Acknowledgments

This author thanks the following people for their help, guidance, and support: Dr. Tom Cooper, Dr. L.V. Natarajan, Mr. Vince Tondiglia, and the SOCHE students. He would also like to thank Bolling Air Force Base and Wright Laboratories for funding and assistance.

### References

1. Collins, Peter J. Liquid Crystals: Nature's Delicate Phase of Matter. Princeton University Press: Princeton, 1990.
2. Jackson, Herbert W. Introduction to Electric Circuits. Prentice-Hall, Inc: Englewood Cliffs, 1989.
3. Manivannan, Gurusamy; Lessard, Roger A.; "Trends in Holographic Recording Materials", 1994, 282.
4. Neckers, D.C. "J Photochem. Photobiol.", Chem., 1989, 47, 1.
5. Schulte, Michael D. "Synthesis and Characterization of Chain Extending Monomers for PDLCs." Cincinnati, 1995.
6. Sutherland, R.L.; Natarajan, L.V.; Tondiglia, V.P.; Bunning, T.J.; "Chem. Mater", 1993, 5, 1533.
7. Valkenburgh, Van. Basic Electricity. Hayden Book Company: New Jersey, 1978.

**TUNGSTEN ALLOYS: CORROSION POTENTIAL AND  
DESIRABILITY FOR USE IN MUNITIONS**

Kristan Marie Nicole Raymond

Walton High School  
555 Walton Road  
DeFuniak Springs, FL 32433

Final Report for:  
High School Apprenticeship Program  
Mentor: Elizabeth Vanta  
WL/MNSE  
Wright Laboratory  
Eglin AFB

Sponsored by:  
Air Force Office of Scientific Research  
Bolling AFB, DC

and

Wright Laboratory  
Eglin AFB

August 1996

## TUNGSTEN ALLOYS: CORROSION POTENTIAL AND DESIRABILITY FOR USE IN MUNITIONS

Kristan Raymond  
Walton High School

### Abstract

Tungsten and tantalum alloys are being considered for use in kinetic energy penetrators and other munitions. Their high density and strength make them ideal candidates for these and other purposes. Tungsten alloys are being considered by Wright Laboratory. Therefore, this report concentrates on them rather than tantalum alloys. Currently depleted uranium is widely used in the penetrators, but the relative merits of tungsten alloys are being explored.

Recently, some tungsten alloys were found to readily corrode under humid conditions. Until now, the corrosion of tungsten alloy was not seen as a problem. Several studies have been done on the corrosion potential of tungsten alloys since this discovery. The purpose of my experiment is to gain even more information on the corrosion potential of these alloys and provide a basis for further testing.

I conducted immersion testing on tungsten alloys in solutions with pH's ranging from 2 to 12, stream water, gulf water, and 2.5% and 5% salinity. The solutions were sampled on Day 1 and 32. The alloys showed different amounts of tungsten and nickel. The amount of metal dissolved in solution varied with pH. With the data currently available, there does not seem to be a toxic level of any of the alloyed metals in the solutions.

## TUNGSTEN ALLOYS: CORROSION POTENTIAL AND DESIRABILITY FOR USE IN MUNITIONS

Kristan Raymond

### Introduction:

Tungsten and tantalum alloys are being considered for use in kinetic energy penetrators and other munitions. Their high density and strength make them ideal candidates for these and other purposes. Tungsten alloys are being considered by Wright Laboratory. Therefore, this report concentrates on them rather than tantalum alloys. Currently depleted uranium is widely used in the penetrators, but the relative merits of tungsten alloys are being explored.

Recently, some tungsten alloys were found to readily corrode under humid conditions. Until now, the corrosion of tungsten alloy was not seen as a problem. Several studies have been done on the corrosion potential of tungsten alloys since this discovery. The purpose of my experiment is to gain even more information on the corrosion potential of these alloys and provide a basis for further testing.

### Research:

#### Depleted Uranium Vs. Tungsten Alloys:

Currently depleted uranium is widely used in the penetrators, but the relative merits of tungsten alloys are being explored. Tungsten alloys have several advantages over depleted uranium. Although tungsten alloys have a higher initial material cost than depleted uranium, they have a much lower life cycle cost. This is because of the many costly procedures that are required for the slightly radioactive depleted uranium. Transporting depleted uranium involves special licenses, fees, and transportation procedures. After depleted uranium penetrators are manufactured, the equipment and facilities used must be decontaminated. There are also costly burial methods involved with the disposal of depleted uranium. All these procedures are not needed for the relatively inert tungsten alloys.

#### Environmental Concerns:

The environmental impact of these two materials is also a factor in their consideration. Depleted uranium is toxic and has low-levels of radioactivity. Tungsten alloys do not have obvious environmental impact. However, recently it has been discovered that certain tungsten alloys will readily corrode in humid environments. This questions the alloys' ability to withstand the 10 year storage period in an uncontrolled environment or the 20 year storage period in a controlled environment that is a standard requirement for munitions. Also, this potential

corrosion could affect the environment around the testing ranges. Certain metals that are alloyed with tungsten in the alloys are toxic to humans in certain concentrations. If the alloys' rate of corrosion is too rapid, an environmental hazard may be created as toxic material is released into the environment.

Tungsten alloys can also be considered a hazard during manufacturing. Sintered tungsten alloys are fabricated using powder metallurgy techniques. This process involves a fine powder mix of alloyed metals that is pre-compacted and liquid-phase sintered at about 1500°C. The final alloy systems usually are of two phases: the rounded tungsten grains and the binder phase consisting of tungsten and the other alloyed elements. The fine powders involved in this process pose an inhalation hazard because they have diameters of less than ten microns. Nickel and cobalt, two metals commonly used in heavy metal tungsten alloys, are considered toxic when inhaled. However, current manufacturing personal safety procedures are believed to be sufficient to control this hazard.

Potential inhalation of dusts and aerosols is also a concern during testing of the finished munitions on firing ranges. Some alloy dust may escape the target butt buildings that are designed to contain it. If the personal safety procedures used by industrial workers can be adapted for use on the testing range, soldiers in the field would not be at risk.

### **Toxicity and Corrosion:**

Tungsten alloys considered for use by the Department of Defense contain various heavy metals besides tungsten. Some of these metals are toxic when inhaled or ingested. Figure 1 gives a table of the toxic doses of some of the metals used in tungsten alloys. This is why the corrosion behavior of tungsten alloys is a concern: too much corrosion can release a hazardous amount of certain alloy metals into the environment. Several reports have recently been devoted to examining the corrosion properties of tungsten alloys in hopes of finding out whether their corrosion rates are significant.

#### **Report 1:**

The first such report, "Corrosion Behavior of High Density Tungsten Alloys" by Milton Levy and Frank Chang, investigates their corrosion potential using potentiostatic polarization tests and immersion testing in 5% NaCl solution. Potentiostatic tests were done in aqueous solutions buffered to pH 4, 9, and 12 with and without 0.1 M NaCl. The alloys studied contained various amounts of tungsten, nickel, cobalt, iron and copper.

The potentiostatic polarization tests showed that the corrosion potential of the alloys became more active as the pH of the solution was increased. The chloride ion also produced a slight rise in the corrosion potential. These tests showed that the alloys that contained copper had less corrosion resistance than pure tungsten and alloys without copper. In solutions containing NaCl, the dissolution rate of all alloys was increased and the alloys containing copper were even more susceptible to attack.

Less than a week into the immersion testing, the tungsten alloys that did not contain copper formed a rust colored reaction product in the area of contact between the beaker and the sample. This reaction product gives evidence of crevice type corrosion. Within ten weeks, this product spread over the entire surface of the sample. A yellow reaction product ( $\text{WO}_3$ ) was observed around the alloys containing copper.

Weight loss calculations were made on the alloy samples used in the immersion testing. They found that pure tungsten was the most corrosion resistant, followed by the alloys that did not contain copper. The alloys that did contain copper were found to be the least corrosion resistant. This was attributed to the formation of the more protective  $\text{WO}_2$  on the alloys without copper.

All materials studied in this experiment exhibited acceptable corrosion rates of less than 10 mils per year. However, Scanning Electron Micrographs of the samples showed that the matrix phase corroded more readily than the binder phase. This might cause the loss of tungsten grains, which would result in a loss of strength and ductility. Because the matrix phase is more readily attacked, corrosion in these areas might exceed the calculated corrosion rate. Thus the corrosion might be more serious than previously thought.

#### Report 2:

The second report, "Corrosion of High-Density Sintered Tungsten Alloys Part 1: Immersion Testing" sponsored by the Australian Department of Defense, tested similar alloys. Immersion tests were done in distilled water and a 5% NaCl solution. Plastic O-rings were added to other samples to determine the effects of crevice type corrosion of the alloys.

They found that alloys containing copper had higher corrosion rates than alloys without copper. The alloys that contained copper were attacked by corrosion in both the tungsten grain phase and the binder phase. The other alloys were mainly attacked in the matrix (binder) phase.

The artificial crevices (O-rings) resulted in more corrosion on the sample near the O-ring. There were also different types of corrosion products near the crevices than away from them.

The remainder of the results were similar to that of the report above. However, the authors of this report concluded that the corrosion rates of the alloys were significant, unlike Levy and Chang.

#### Methodology:

Before I began the experiment, I examined several reports (discussed above) that dealt with similar projects. I used some of these procedures as a basis for the preparation of the tungsten alloy samples and other equipment.

#### Beaker Preparation:

To ensure that my results will be accurate, I thoroughly washed the beakers that were to be used in the experiment. They were first washed with soap and rinsed with distilled water. The beakers were then rinsed twice with a 25% solution of hydrochloric acid and again rinsed thoroughly with distilled water.

### **Alloy Sample Preparation:**

Nine samples of each alloy were selected for use in the experiment because of their similar surface structure. This was done to ensure that each sample would undergo similar types of corrosion. I also calculated the surface area of each alloy and found that the HD-17 alloy has a surface area of about  $18.8\text{cm}^2$  and the WL-1 alloy has a surface area of about  $25.8\text{cm}^2$ .

I washed the tungsten alloy disks the day before they went into solution. First they were thoroughly rinsed with distilled water. Then they were allowed to soak in 100 ml of acetone in a 500 ml beaker. After they were removed from the acetone, they were allowed to dry a few minutes before they were placed into 100 ml of ethanol in a 500 ml beaker. Finally, the tungsten alloy samples were placed on a tray in a desiccator to keep them from corroding prematurely. The next day each tungsten alloy sample was weighed individually. This initial mass will be used next year to determine the total amount of mass lost by each sample due to corrosion. Figures 2 and 3 give the type of solution and the mass of the alloy sample in each of the eighteen beakers.

### **Solution Preparation:**

Tall, 1000 ml beakers were used in the experiment. Each beaker contained 800 ml of solution.

Fifty milliliter samples of the following solutions were analyzed on Day 1 for the presence of alloyed metals: pH 4, pH 7, pH 12, stream water, Gulf water, and 5% sea salt solution.

#### **pH Solutions:**

The pH of each solution was as measured as accurately as possible using pH indicator strips. ColorpHast® pH 0-14 indicator strips were used.

A solution of 25% HCl was used to bring the pH of distilled water to a pH of 2 and 4. A 5 M solution of NaOH was used to bring the pH of distilled water to a pH of 9 and 12. Distilled water was used to represent a pH of seven. These solutions were unbuffered.

#### **Gulf and Stream Water:**

Gulf water and stream water were collected from two sites on Eglin AFB Reservation. To hold the water until the tests, several two-liter plastic containers were washed with soap and rinsed with distilled water.

#### **Sea Salt Solutions:**

To prepare the 5% sea salt solution, 82.5 g of sea salt were dissolved in 1650 ml of distilled water. To prepare the 2.5% solution, 41.25 g of sea salt were used for 1650 ml. The remaining 50 ml of both solutions were placed into separate containers; the 5% salt solution was sent off to be analyzed.

**Miscellaneous:**

The Tungsten disks were placed on the bottom of the beakers so that one circular side is in contact with the glass. The level of solution was marked on the side of the beaker. The beakers were covered with Parafilm and placed in a growth chamber to prevent excessive evaporation and contamination. After Day 32, Duraseal was substituted for Parafilm because it prevents evaporation and resists acids and alkalis. The temperature was monitored and remained at 25 °C, except when the air conditioning system of the entire building failed. During this one week period the temperature climbed to 32°C. Corrosion was not accelerated during this time.

Pictures of each beaker were taken on Day 12 and Day 32. Samples of each solution were taken on Day 32. Before sampling, distilled water was used to bring the level of solution up to initial level. The samples were taken with a 10 ml pipette. To obtain a more accurate result, the 50 ml samples were taken at different places within the solution after the solution was stirred. Ten milliliters of solution were taken near the sample on the bottom of the beaker, 10 ml from the bottom of the beaker away from the sample, 20 ml were taken near the middle of the solution, and 10 ml were taken near the surface. The new level of solution was then marked. Sampling will be repeated on Day 90, 180, and 365. Each time the solution will be brought up to the last marked level with distilled water and the new level will be recorded after sampling.

**Observed Corrosion:**

The HD-17 alloy samples, which contained copper, turned a dark gray or black during the experiment. The solution with a pH of 2 turned greenish black. The solution with a 5% salinity turned aqua on the top of the surface. The salt that settled out onto the surface of the sample was also aqua.

The WL-1 alloy samples, which contained iron, exhibited corrosion products similar in color to iron oxide.. The solutions with salt had orange crevice corrosion around the bottom but none on the surface. The rest had the crevice corrosion and their surface was covered with an orange-brown product. These samples (pH 4, pH 7, pH 9, and stream water) also showed evidence of pitting corrosion of their surface. The solution of pH 2 did not corrode visibly and the pH 12 solution turned black.

A more detailed chart of the visible corrosion is given in Figures 5 and 6.

**Solution Analysis:**

Figures 7-12 show the results of the solution analysis. The solutions were analyzed for tungsten, nickel, copper, iron, and chromium. The initial analysis taken on Day 1 was not comparative to the results of the Day 32 analysis.

The amount of most of the metals in solution went up from a few parts per billion to several parts per million. The level of chromium in solution is not significantly large, so it is not graphed.

**Summary:**

In both alloys tested, the solutions with a pH of 2 had the most nickel, copper, and iron in solution. For the HD-17 alloy, pH 2 had the least tungsten in solution. In both alloys, pH 12 had the most tungsten and the least nickel, copper, and iron. The amount of nickel, copper, and iron decreased with pH; the amount of tungsten generally increased with pH. The solutions containing salt exhibited similar amounts of each metal.

The alloy that contained copper dissolved more tungsten into solution (even though the alloy contained a lower percentage of tungsten). The alloy that contained iron dissolved more nickel into solution (it contained a lower percentage of nickel).

**Conclusions:**

These conclusions are based only on initial data. They will be revised if needed after mass loss measurements next year and additional solution sampling throughout the coming year.

**The Effect of pH on Corrosion:**

The wide difference between the amount of tungsten dissolved in the pH 2 and 12 solution may be explained in part by the formation of  $O_3W$ . This oxide of tungsten is insoluble in water. However, it is soluble in caustic alkalis, and very slightly soluble in acids. This might explain why there is more tungsten found in the pH 12 solution than in the lower pH's.

**The Effect of the Chloride Ion:**

The salt solutions in both alloys showed similar results. The chloride ion seems to have a consistent effect. However, the difference between the salt solutions and the moderate pH's and stream water was not as great a difference as there was in previous reports.

**The Effect of Copper:**

Previous studies have shown that alloys containing copper dissolve more of the main tungsten grain phase. This seems to be supported by the data from this experiment.

**Corrosion Products:**

The visible corrosion was the color of iron oxide, suggesting that the corrosion products were iron. However, the solutions that showed the most corrosion products on the tungsten alloy sample had less iron and other metals in solution. This suggests that the corrosion products are tying up the metals in an insoluble form that will not harm the environment.

**Toxicity Appears Minor:**

The solution with the most tungsten in solution has 90.5 mg/L. (HD-17 pH12) A 50 kg person would have to drink 276 L of this solution for a lethal dose.

The solution with the most nickel has 34.3mg/L (WL-1 pH2) A 50 kg person would have to drink about a liter per day over a long period of time to get a lethal dose.

The solution with the most copper has 6.6 mg/L (HD-17 pH2) A 50 kg would have to drink a liter for a lethal dose. The other elements did not have significant amounts in solution. The above listed values are extremes. The more moderate solutions did not have as high an amount of toxic metals.

## **References:**

Batten, J., Mc Donald, I., Moore, B., Silva, V. "Corrosion of High-Density Sintered Tungsten Alloys Part 1: Immersion Testing." Sponsored by the Australian Department of Defense. October 1988.

Gold, K. and Los, Michael. "Environmental Analysis of Tungsten Alloy Penetrators: Manufacturing and Testing Phases of the Life Cycle." Sponsored by US Army Armament Research. May 1996.

Levy, M., Chang, F., "Corrosion Behavior of High Density Tungsten Alloys." Sponsored by US Army Materials Technology Laboratory. August 1987.

Meijer, A. "Environmental Effects of Tungsten and Tantalum Alloys." Sponsored by the Department of the Air Force. June 1996.

Figure 1

Alloyed Metal	Threshold Limit Values	Ingestion Limits
Tungsten	insoluble compounds: 5mg/m <sup>3</sup> soluble compounds: 1mg/m <sup>3</sup>	Oral lethal dose to human: 0.5-5g/kg of body weight
Nickel	insoluble and soluble: 0.05mg/m <sup>3</sup>	Long term exposure safe at .02 mg/kg of body weight per day
Cobalt	insoluble and soluble: 0.1 mg/m <sup>3</sup>	Dose for human not available
Iron	NA	NA
Copper	insoluble and soluble: 1 mg/m <sup>3</sup>	Oral lethal dose to human: 0.12 mg/kg of body weight
Chromium	insoluble and soluble: 1mg/m <sup>3</sup>	Oral lethal dose to human: 71mg/kg of body weight

Figure 2

Allloyed Metals - % of Mass

HD- 17 Alloy	WL-1 Alloy
Tungsten - 89.75 %	Tungsten - 87.63
Nickel - 5.95 %	Nickel - 6.64
Copper - 4.24 %	Iron - 4.25
Chromium - Trace	Manganese - 1.48

Figure 3

Alloy HD-17

Beaker Number	Solution Type	Mass of sample
1	pH 2	84.19185
2	pH 4	83.76235
3	pH 7	84.24500
4	pH12	83.89015
5	pH 9	83.11350
6	Stream Water	79.45565
7	Gulf Water	80.98605
8	2.5% salt	79.26440
9	5% salt	84.34050

Figure 4

Alloy WL-1

Beaker Number	Solution Type	Mass of sample
10	pH 2	113.76605
11	pH 4	112.47555
12	pH 7	115.00020
13	pH12	111.19715
14	pH 9	113.57390
15	Stream Water	114.41185
16	Gulf Water	113.65990
17	2.5% salt	112.01415
18	5% salt	112.10725

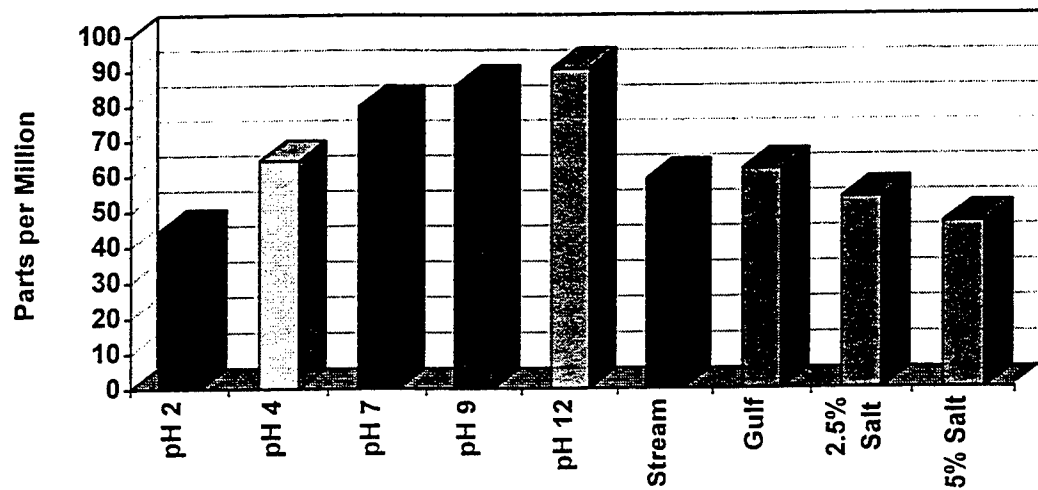
Figures 5 and 6

<u>Solution Type - HD-17 Alloy</u>	<u>Surface Corrosion</u>	<u>Crevice Corrosion</u>
pH 2	Greenish black. Yellow powder visible on bottom on beaker.	None.
pH 4	Blackened.	None.
pH 7	Blackened.	None.
pH 9	Blackened.	None.
pH 12	Blackened- not as much.	None.
Stream Water	Blackened.	None.
Gulf Water	Blackened.	Faint yellowish ring visible.
2.5% Salinity	Blackened.	None.
5% Salinity	Blackened. Top of surface and salt settled onto the surface is aqua.	None.

<u>Solution Type - WL-1 Alloy</u>	<u>Surface Corrosion</u>	<u>Crevice Corrosion</u>
pH 2	None visible.	None visible.
pH 4	Dark orange general corrosion. Brighter orange pitting in the center of the top.	Orange ring.
pH 7	Same as above.	Same as above.
pH 9	Same as above.	Same as above.
pH 12	Blackened.	None.
Stream Water	Same as pH 4.	Same as pH 4.
Gulf Water	None.	Dark orange ring. Yellow film on bottom of beaker.
2.5% Salinity	None.	Yellow film on bottom of beaker.
5% Salinity	None.	Dark orange ring. Yellow film on bottom of beaker.

## HD-17 Alloy

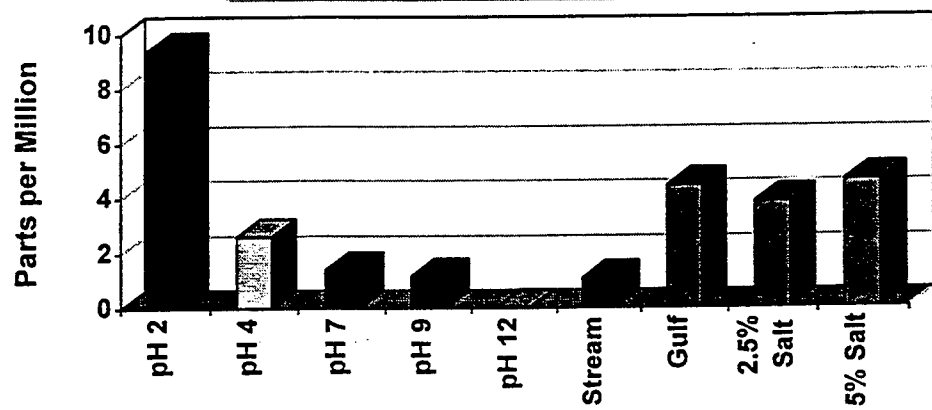
### Tungsten in Solution



Figures 7 and 8

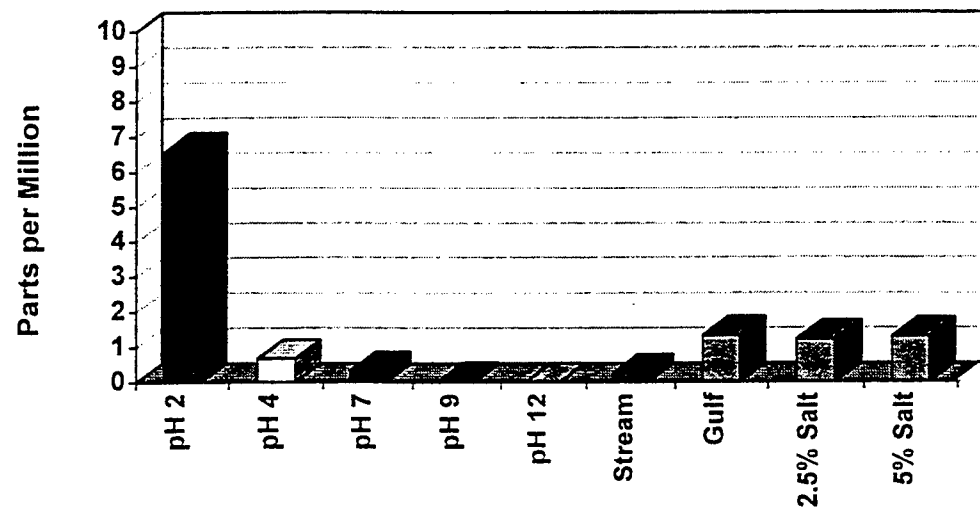
## HD - 17 Alloy

### Nickel in Solution

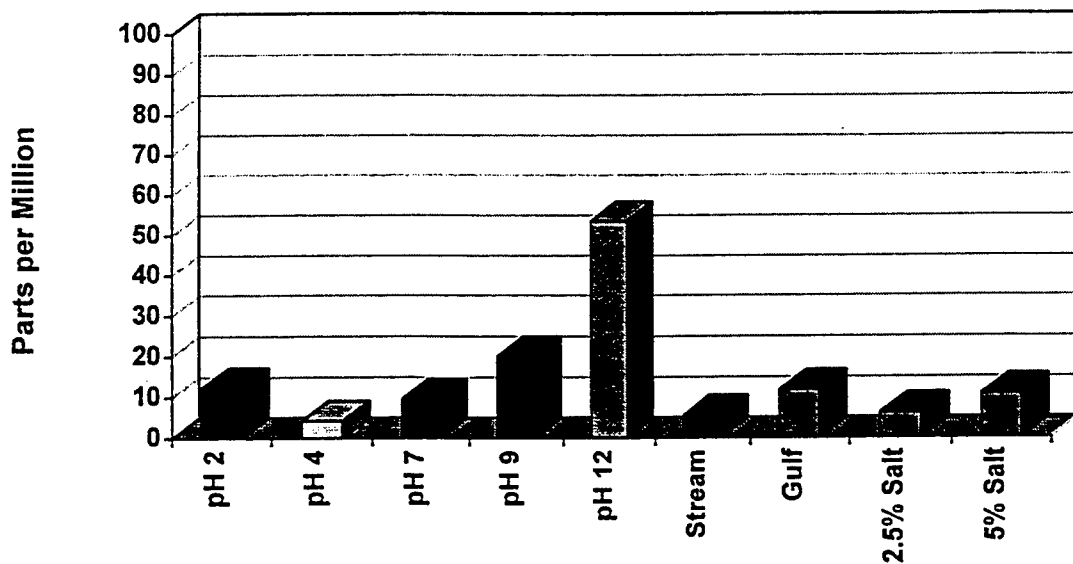


Figures 9 and 10

HD - 17 Alloy  
Copper in Solution

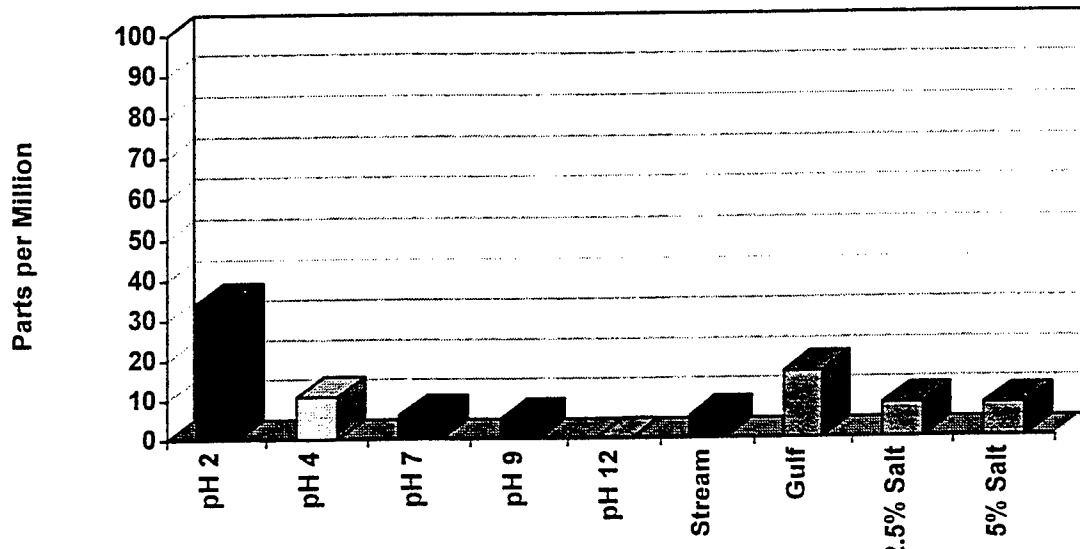


WL-1 Alloy:  
Tungsten in Solution

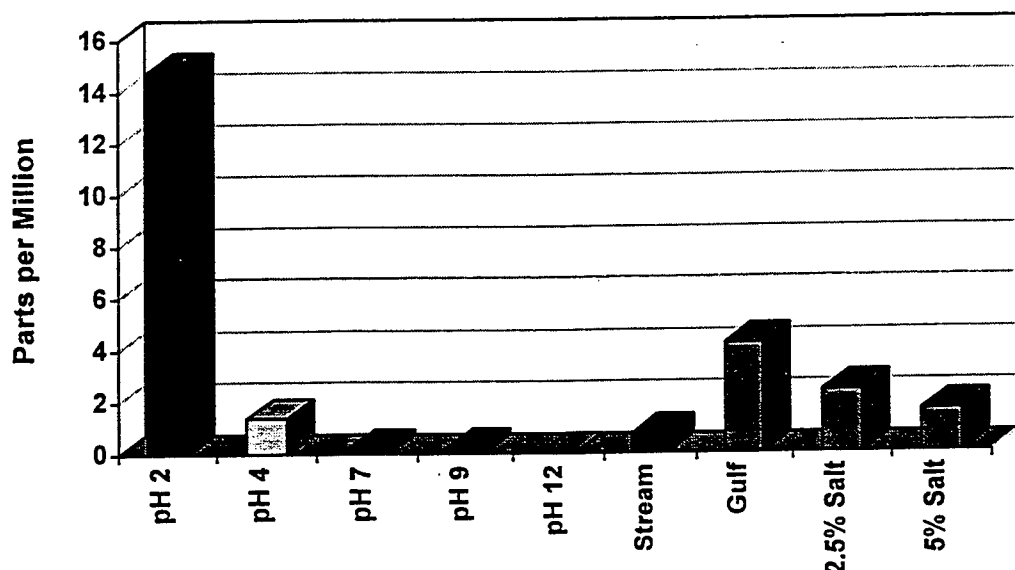


Figures 11 and 12

**WL-1 Alloy:**  
**Nickel in Solution**



**WL-1 Alloy**  
**Iron in Solution**



Improvement of Automatic Data Processing Equipment  
(ADPE) Accountability System

Adam Z. Reed

Tipp City High School

555 N. Hyatt Ave.

Tipp City, OH 45371

High School Apprenticeship Program

Sponsored by:

Air Force Office of Scientific Research

Bolling Air Force Base, Washington DC

and

Wright Laboratory

August 1996

Improvement of Automatic Data Processing Equipment  
(ADPE) Accountability System

Adam Z. Reed  
Tipp City High School

Abstract

Our goal was to create an accountable automatic data processing equipment (ADPE) system. This involved updating and comparing databases, doing physical inventories, and reporting the results to the appropriate people.

Improvement of Automatic Data Processing Equipment  
(ADPE) Accountability System

Adam Z. Reed

Introduction

The 88th Communications Squadron (88th) is responsible for tracking all the ADPE on this base. There are individuals called Equipment Custodians (ECs) who must answer to the 88th for all the ADPE in a certain branch. The 88th's inventory for this branch consisted of 172 items about four years ago. This equipment was divided into two accounts, the responsibility split between two people. Since then, this branch has acquired many new items, and has disposed of many older items. It was thought that this equipment would be easier to track if the equipment was on one account and that a good time to do this would be after I (with the occasional help of Dan Binkis, another HSAP participant) take a current branch inventory.

Methodology

The first step in this process was to take inventory of all ADPE currently in the branch. All items on the current branch inventory were to be considered either "new" or "found" based on whether the item in question was found on the 88th's inventory or not. All items not on the 88th's inventory but on the current branch were considered new. All items on the 88th's inventory but not on the current inventory were to be considered "turned in", "transferred", or "not found". This was based on whether the item in question was turned in during an ADPE turn in drive or transferred to another location. If there was nothing to indicate what happened to the item in question, then the item was considered "not found".

The next crucial step in creating the database was to remove errors from the database. This included searching for and removing any duplicate entrees and adding any items missing

from the database. It was determined that a secondary inventory would be necessary since the previous measures did not remove all the errors.

At this point most of the items had been entered into the database and all major errors had been removed. The last step in setting up this database was to complete a final inventory. This time the equipment custodians (ECs) participated in the inventory. The purpose of this inventory was to correct any minor errors (obvious misspellings in names, serial numbers, ...) and to add any items that had been overlooked in the previous inventories.

In summary, this project has come a long way since I started here. The branch chief sent a memo to describe what I did and to express his appreciation. However, there are still some things that will have to be done after my departure. The ECs will have to handle paperwork regarding the missing items, the 88th will receive a copy of the current branch inventory, and the inventory will have to be constantly updated for incoming and outgoing items.

DEVELOPMENT AND TESTING OF AN OPTICAL SCAN CHARACTERIZER

Franklin K. Reyher III  
WL/MNGS

Niceville Senior High School  
800 E. John Sims Parkway  
Niceville, FL 32578

Final Report for:  
High School Apprenticeship Program  
Wright Laboratories

Sponsored by:  
Air Force Office of Scientific Research  
Bolling Air Force Base, DC

and

Wright Laboratories  
Eglin Air Force Base, FL

August 1996

## DEVELOPMENT AND TESTING OF AN OPTICAL SCAN CHARACTERIZER

Franklin K. Reyher III  
WL/MNGS  
Wright Laboratories  
Eglin Air Force Base, FL

### Abstract

Scanner-driven LAser Detection And Ranging (LADAR) systems may return inaccurate data when their scanners are driven at extremely high speeds. It is desirable to determine which portions of a LADAR scan are nonlinear and may return inaccurate data. An optical scan characterizer was produced using an HP54510A Digitizing Oscilloscope, a Photodiode Detector Array (PDA) designed specifically for this application, and a continuous wavelength Helium Neon laser. These instruments were controlled via LabVIEW on a personal computer through GPIB and parallel interfaces. The scan characterizer was tested in the laboratory environment and determined the areas of the scan where non-uniform spacing of pixels exceeds tolerable limits.

# DEVELOPMENT AND TESTING OF AN OPTICAL SCAN CHARACTERIZER

Franklin K. Reyher III

## Table of Contents

1. Introduction
2. Methodology
  - 2.1. The Scanner
  - 2.2. The Photodiode Detector Array
  - 2.3. Testing the System with LabVIEW
3. Results
4. Conclusions
5. Acknowledgments
6. Figures

## DEVELOPMENT AND TESTING OF AN OPTICAL SCAN CHARACTERIZER

Franklin K. Reyher III

### Introduction

Laser detection and ranging systems, more commonly known as laser RADAR or LADAR systems, are being explored for modern military applications like guidance, surveillance, and target recognition. Imaging versions of these systems employ lasers whose beams are scanned over the selected area in particular patterns - typical scan configurations are circular scans and raster scans. The particular type of scan depends on the application as well as the performance characteristics of the scanner. In a range-imaging LADAR system, the laser produces pulses as the scanner scans; these pulses of light return to a photodiode detector after scattering off the target and surrounding environment. The amount of time taken for the laser pulse to return to the detector is considered the data, and a false-color image is produced based on this time lapse. Additionally, the intensity of the return is occasionally recorded and used as complementary data. This data acquisition must occur rapidly (generally before atmospheric changes occur or before updates are necessary).

These requirements place restrictions upon the scan patterns used by LADAR systems. Slower scan patterns produce accurate data because there is less distortion in the placement of image pixels as the laser accelerates to its constant scanning velocity. On the other hand, acceleration and deceleration are more pronounced in faster scans, which can produce delay and overshoot in pixel position, and, ultimately, an image which appears compressed or stretched in the areas where the angular scan rate is changing. But, since slower scans are undesirable for many LADAR operations, faster scans must be used. To determine the areas where a LADAR system obtains data with uniform pixel separation, a scan characterizer was developed using pre-existing instruments and a custom-designed component.

### Methodology

Five components comprise the optical scan characterizer experiment: a laser, scanner (not a part of the characterizer, but a "control" device used as a representative scanner), detector array, digitizing

oscilloscope (a Hewlett-Packard 54510A), and personal computer (an Austin 486DX2/66). The laser used in laboratory experimentation was a continuous wave (CW) 15 mW Helium Neon (HeNe) laser operating at a fixed wavelength of 632.8 nm. The other components, however, have many adjustable parameters and therefore will be discussed in detail.

- The Scanner

The scanner used in laboratory experimentation was a Two-dimensional Galvanometer-Driven Mirror from General Scanning, Inc. (GSI). The scanner consists of two mirrors; one of these provides X-axis scan capability, the other provides Y-axis scan capability. The scanner was operated by a Digital Electronics (DE2000) controller, also manufactured by GSI. This controller was controlled through the PC's serial port by the program QD.EXE, which translates numerical text files into a scan pattern. The scan used for experimental purposes was a simple box, with the scanner beginning at its home point (32767, 32767) at the upper right corner of the scanned box. The laser beam was then scanned in a small clockwise rectangle. This particular scan pattern was chosen so that the beam could be swept across the entire length of the detector array and so that the detectors could be activated either as the beam passed from right to left (lower edge of the scanning rectangle) or from left to right (upper edge). Since much of the operation of the experiment was dependent upon the layout and operation of the detector array, it is necessary to discuss that component next.

- The Photodiode Detector Array

The Photodiode Detector Array (PDA) was the only component custom-built for the optical scan characterizer, since no pre-existing detector assemblies fully met the requirements of this specific experiment. It was conceptualized and created by Norman Champigny, and was constructed so that its electrical outputs were appropriate for a digitizing oscilloscope. The prototype design consisted of two EG&G C30807 silicon photodiodes, or PINs, spaced 5 inches apart, fed by a 9V and 45V battery. This test component was created to determine whether the conceived final design of the PDA was feasible. Since the laser did not pass over both photodiodes simultaneously, two individual "pulses" of voltage were created in one scanning cycle. These voltage pulses were summed in an operational amplifier (op-amp), and because of the linear distance between photodiodes, two distinct voltage peaks are created, rather than

one summed pulse. In the process of testing, the op-amp was accidentally electrically short-circuited, and diodes were added to the circuitry in order to avoid future accidental shorts. After this adjustment was made, the prototype was connected to the digitizing oscilloscope and the scanner scanned the aforementioned box pattern. By adjusting the timebase of the oscilloscope, the two individual pulses could be seen at all times (provided the laser was passing across the detector region of the PINs) regardless of the scan speed. The design was judged to be adequate and the fabrication of the actual PDA began.

Ten Thorlabs FDS100 silicon PINs were used as the main data-collecting detectors in the PDA. These photodiodes were placed next to each other, with no spacing between them, in a row on the printed circuit board of the PDA. The spacing between the center of each photodiode was 0.406", the diameter of the photodiode. Small spacing was used to make the PDA as compact as possible. The spacing also allowed for a 10° angular area on a standard optical table; the area covered could be altered by changing the distance between scanner and PDA. The PINs were mounted on Thorlabs T05 CANs soldered onto the PC Board; this type of mounting allowed the photodiodes to be replaced or removed from the detector array if necessary. The PDA was powered by two batteries, a 9V and 45V, as well as a 5V power supply, which was added to power the op-amps. The photodiodes used in the prototype design (EG&G C30807 silicon PINs) were used as synchronizers, or syncs, to establish the timing (create a frame of reference) for the voltage pulses created by the ten data-collecting photodiodes. This allows the oscilloscope to display the pulses at a constant position on the screen. The benefit of adding a sync on either side of the main detectors was that data could be read bidirectionally - data could be taken if the PDA was placed in the path of either the upper or lower edge of the rectangle scan. The outputs of the op-amps were connected to two BNC-style connectors, and coaxial cables connected these outputs to the digitizing oscilloscope input channels. The summing circuitry was relatively similar to that used in the prototype; the voltages from all ten photodiodes were summed on one channel and the sync voltages on another. In our experiment, voltage pulses from the data-collecting PINs were passed from the PDA to the digitizing oscilloscope via Channel 1 and the sync pulses were passed to Channel 2. Thus, during experimentation, the researcher could view the frame pulses by viewing the second channel or could view the data pulses by switching to the first channel. After the construction of the PDA was complete, it was connected to the digitizing

oscilloscope, placed in the lower edge of the rectangular scan pattern, and hooked up to its power supplies. The syncs performed as expected, framing the pulses and operating much the same way they had when they were operational in the prototype model of the PDA. Because the C30807s had active areas of 1 square millimeter, compared to the 13.7 square millimeter area of the FDS100s, the pulses produced by the main detectors were much wider than initially anticipated. The capacitive coupling, initially placed in the PDA's circuitry to eliminate DC errors, caused large electronic signal decay because the larger active area detectors added more charge to the capacitors, thus causing a longer decay time when the capacitors discharged, and the last data pulses were indiscernible from the background noise of laboratory lights. To minimize this problem, a metal plate was drilled with holes .032" in diameter directly above the active areas of the photodiodes. This plate was then bolted in front of the PDA, and the final design was complete. The oscilloscope could then read ten distinct pulses from Channel 1. To fully understand these scans, it is necessary to analyze the output of the digitizing oscilloscope and manipulate the data. This was accomplished by using the graphical programming language, LabVIEW, running on the same PC which controlled the scanner.

- Testing the System with LabVIEW

LabVIEW is a powerful tool not only for instrumentation control, but also for data acquisition and analysis. The front panel of the LabVIEW VI, Detector Read Waveform with Offset Adjust.vi, is shown in Figure 1. This shows a sample data run as well as various parameters used for control of the digitizing oscilloscope and for data manipulation. "GPIB Address" is merely the digital "location" of the oscilloscope in the GPIB interface, and can be set on the oscilloscope. The parameters "digitize (ch1:0)" and "read source (ch1:0)" tell the VI which digital channel to read. These are set to Channel 1 for our experiment.

The VI reads 8000 consecutive data points from the digitizing oscilloscope (the 50-300 range shown is a magnification of the entire data return region) and then saves these 8000 points in a spreadsheet file in addition to displaying the data in the VI's graphical display. The data corresponding to the values of the voltage peaks and their position in the data scan can also be saved. "Threshold level" determines the minimum value for data to register in order to be counted as a "pulse." With the threshold level shown,

.10V, it is apparent from Figure 1 that not all the pulses would be saved. Finally, the last two box panels of the VI are data indicators, rather than controls. The "t(0)" panel shows the time of the initial pulse. This value registers at 1.56 microseconds because the data acquisition begins with the first sync pulse, rather than with the first data pulse. Finally, the "dt" panel is the time differential between each data point on the graphical display. In this way, the exact time between the peaks of pulses can be determined. For instance, since the first pulse peaks at data point 62 and the second peaks at point 84, and the time differential between data points is 4 microseconds, it takes the laser 88 microseconds to pass from photodiode to photodiode. For this particular experiment, this translates into an angular velocity of 25.63 rad/sec. With the system operative and each instrument and component working as expected, the experimental optical scan characterizer was tested. The PDA was placed on an adjustable tripod so that it could be moved easily to take data on different regions of the scan.

### Results

Two sample figures are shown to demonstrate the effectiveness of the optical scan characterizer. The first, Figure 2, is similar to the data shown in the graphical display of the previous figure, the LabVIEW VI. There are again ten peaks for the times the laser passes over the active regions of the photodiodes. This data was collected in the center of the rectangular box scan at low speed. These peaks occur at data points 24, 64, 102, 144, 187, 228, 269, 312, 358, and 404. The peaks are separated by a mean of 42.22 data points. The "dt" value is different than that shown in the LabVIEW VI's front panel - rather than 4 microseconds, there is a time difference of 100.33 microseconds between each data point. Thus the first two peaks are 4.0132 ms apart, and the final two are 4.61518 ms apart. The optical scan characterizer is therefore sensitive enough to discern slight deceleration within the scan; the difference between 38 data points (the smallest distance from peak to peak) and 46 (the largest) is barely noticeable to the naked eye, whether it be observing voltage pulses or an actual LADAR image. Angular velocity ( $d\Theta/dt$ ) could also be determined, as long as the distance between scanner and PDA ( $d$  - 180" in our experiment), the distance between two photodiodes ( $s$  - 0.406" between each photodiode in our experiment), and the time required to

sweep between two photodiodes ( $\Delta t$ ) were known, according to the formula  $d\Theta/dt = s / d \Delta t$ . The angular velocity was calculated to be 0.52 rad/sec. Angular acceleration ( $d^2\Theta/dt^2$ ) was also determined by using two  $\Delta t$  variables for two pairs of photodiodes ( $\Delta t_1$  and  $\Delta t_2$ ) and time required for the laser beam to sweep from the first diode in the first pair to the second diode in the second pair ( $\Delta T$ ), according to the formula  $d^2\Theta/dt^2 = [s (1/\Delta t_1 - 1/\Delta t_2)] / (d \Delta T)$ . The acceleration between the first and last diode was calculated to be 1.92 rad<sup>2</sup>/sec<sup>2</sup>.

In contrast, there is a noticeable difference in peak timing in Figure 3. This data was taken not at the center of the scanning rectangle; rather, it was taken at the lower right edge of the scan, when the mirrors were speeding up to the scanner's maximum speed; the "dt" value in this experiment was 97.18 ns, approximately three orders of magnitude faster than that discussed earlier. The dwell time on each detector is very short at higher scan rates, therefore the magnitude of the signal is reduced. This accounts for the seeming angularity of the pulses - many do not approach 10 mV, whereas most are above 10 mV in Figure 2. The peaks occur at data points 8, 39, 65, 87, 109, 128, 145, 162, 178, and 194. The spacing between the first two peaks (31 data points) is almost twice that of the last two (16 data points); therefore, the amount of time between the first two pulses (3.01258  $\mu$ s) is approximately twice the amount of time between the last two pulses (1.55488  $\mu$ s). This uneven spacing clearly shows the acceleration at the beginning of the scan. Angular velocity at the beginning of the scan was calculated to be 748.7 rad/sec and at the end of the scan was found to be 1450.63 rad/sec. Angular acceleration was found to be 38.83 Mrad<sup>2</sup>/sec<sup>2</sup>.

### Conclusions

The data obtained during this research indicates that there are definite regions over which the pixel spacing in a LADAR scan becomes non-uniform. With a detector array such as the experiment's PDA, the entire scan could be characterized and these regions could be identified. Data from the non-uniformly spaced regions of the scan could be discarded, leaving only accurate, uniformly spaced data. It may be possible that an algorithm can be built to account for the acceleration of the scanner during the

initial stages of a scan. However, several aspects of the research have yet to be completed. It was originally intended that different scanners would be tested with the optical scan characterizer, but time only allowed for construction of the system; the 2-D galvo mirror scanner was used as a representative scanner in debugging the system. Other unforeseen problems occurred with the PDA's design; these included the accidental shorting of the op-amp in the prototype design and an electrical short in the final product (which occurred for reasons not yet discovered) which disabled the PDA's left sync photodiode. This limited the operation of the scan characterizer to only a single direction. For the greater part, however, the experiment was a success and the characterizer functioned sufficiently well for laboratory testing.

#### Acknowledgments

The author wishes to express his gratitude to the following people for their support and assistance:

- My mentor, friend, and advisor, Capt Ken Dinndorf
- The Eglin HSAP directors: Mr. Don Harrison, Mr. Mike Deiler, and Mrs. Jeanette Williams
- Neill Perry, my companion at Site C-3, as well as all the other apprentices
- My colleagues at C-3: Maj Jeff Grantham, Jerry Manthey, Mike Tripp, Rob Hopkins, Eddie Meidunas, and last, but surely not least, Norm Champigny, for his technical wisdom, wizardry, and wit

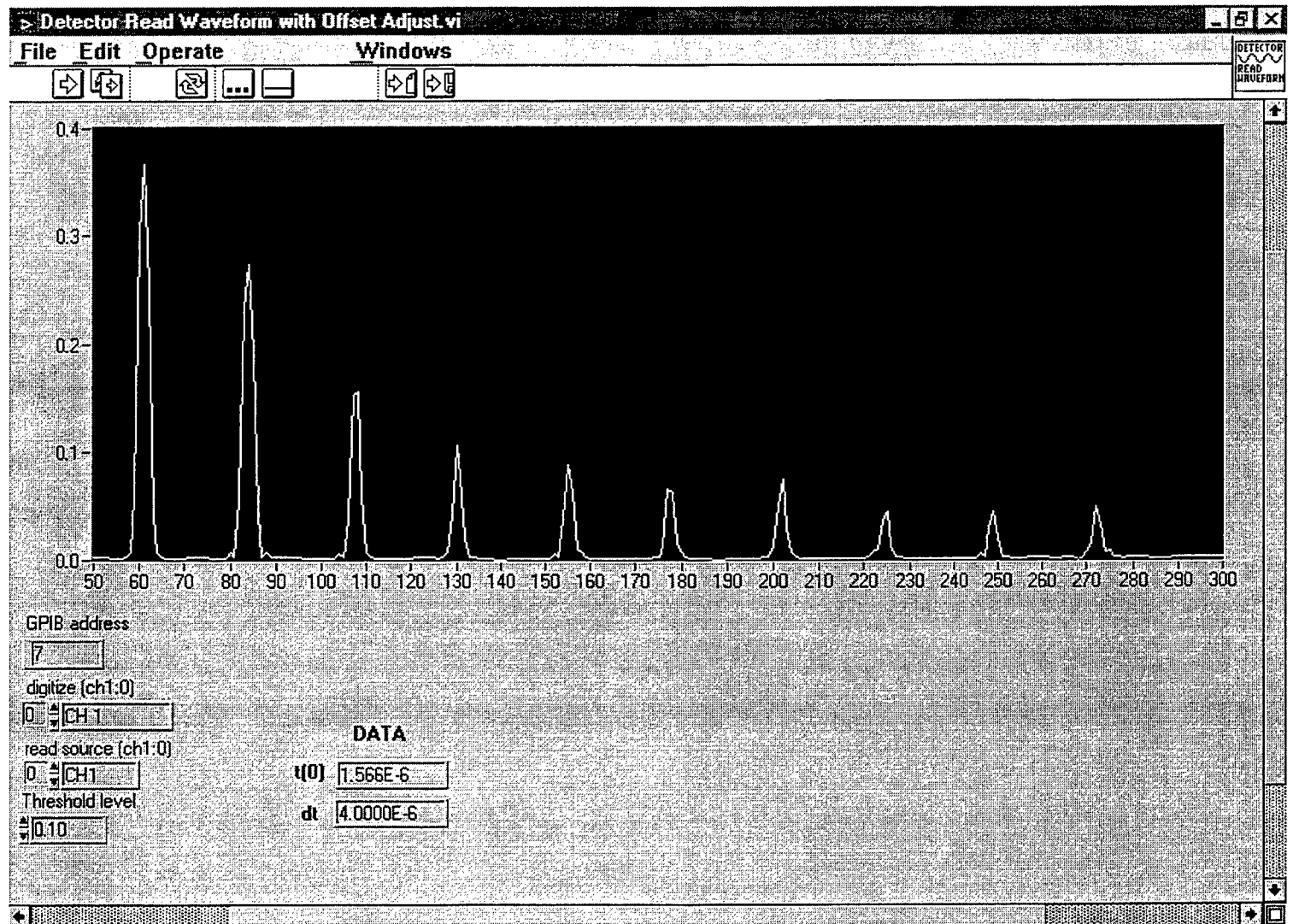
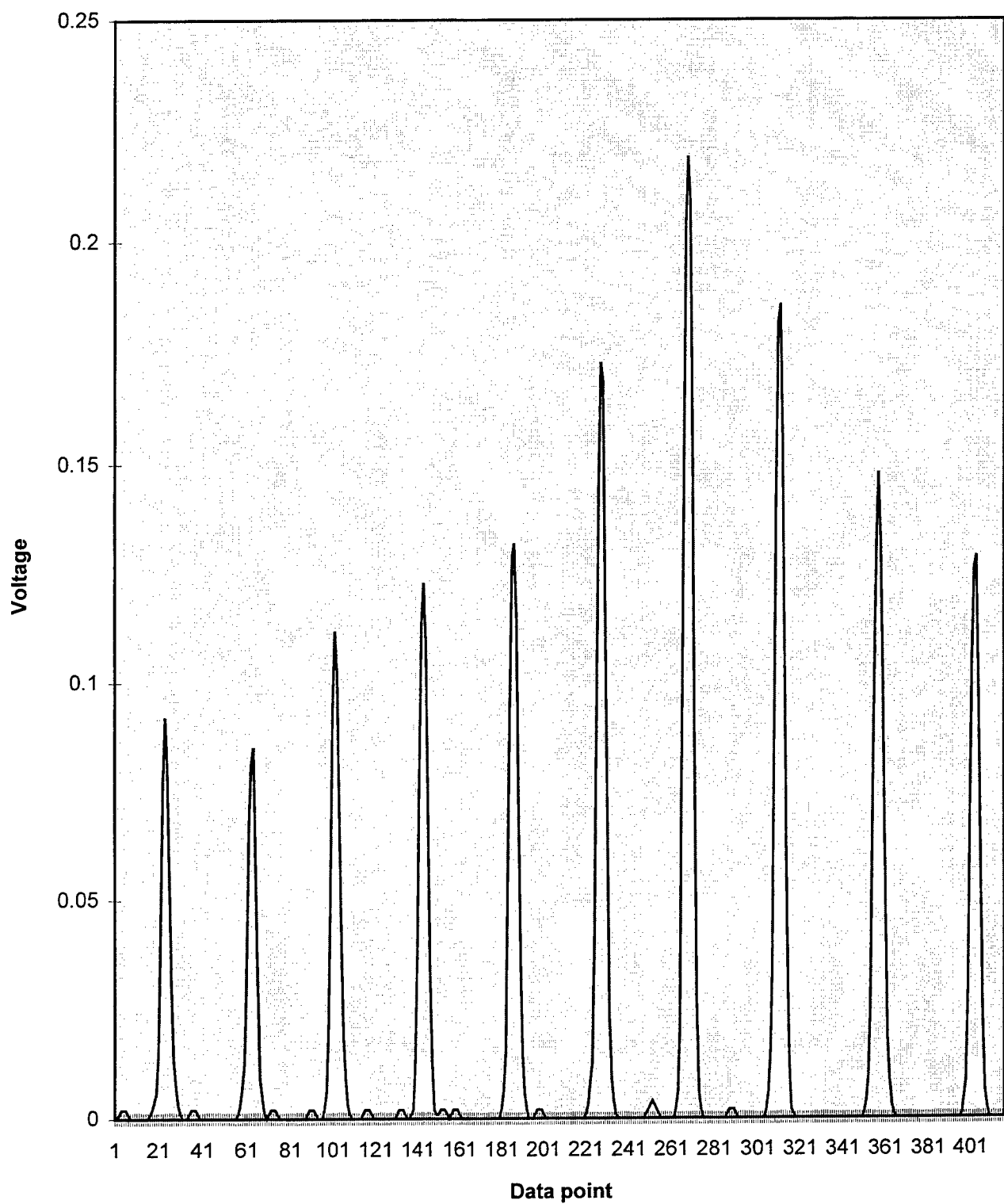
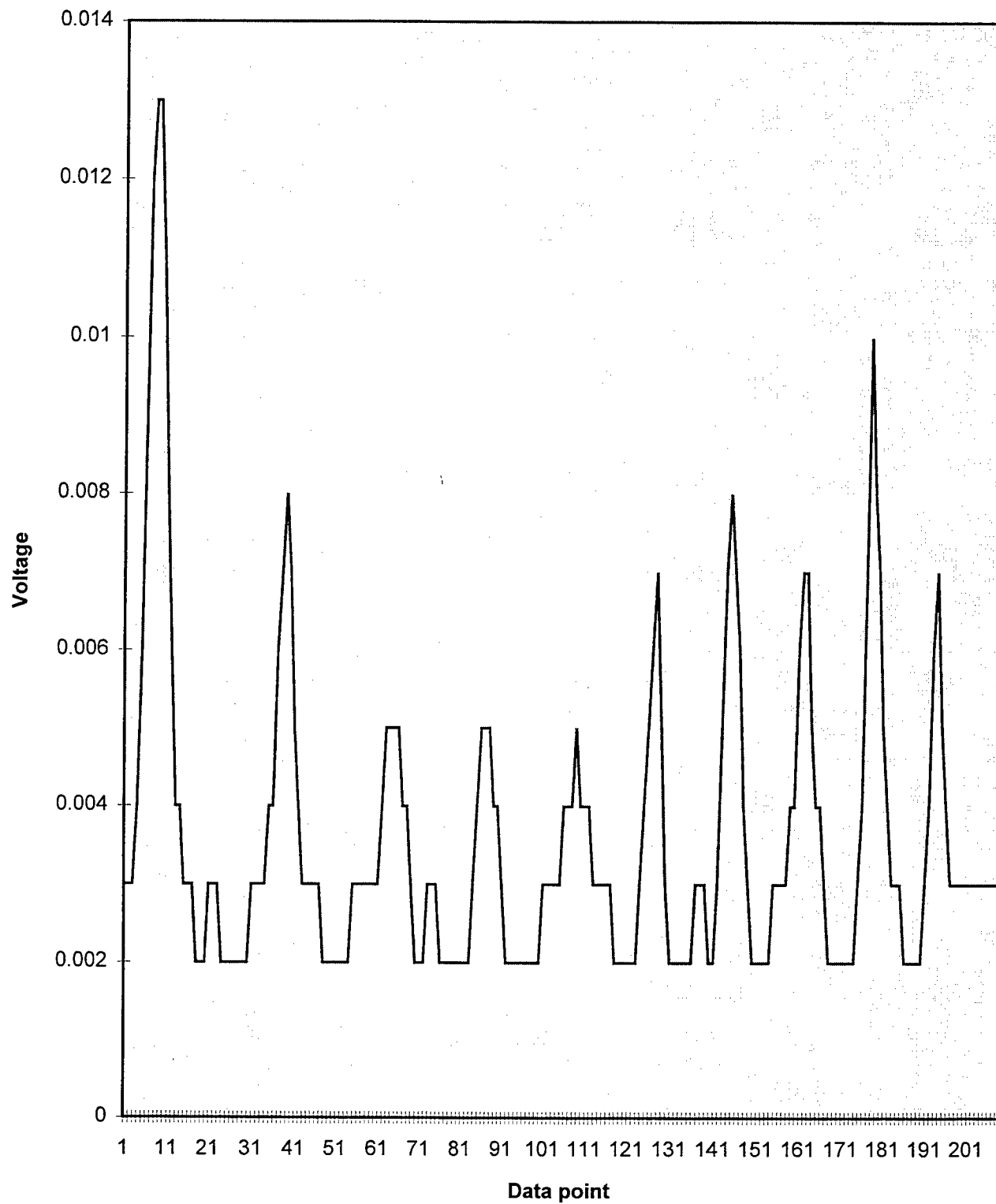


Figure 1: The LabVIEW VI which controls the optical scan characterizer

### Slow-speed Laser Scan at Constant Velocity



**Figure 3: High-speed Laser Scan During Acceleration**



A STUDY OF WEAR  
USING A CAMERON-PLINT TRIBOMETER

Brian Riestenberg

Centerville High School  
500 E. Franklin Street  
Centerville, OH 45459

Final Report for:  
High School Apprentice Program  
Wright Laboratory

Sponsored by:  
Air Force Office of Scientific Research  
Bolling Air Force Base, DC

and

Wright Laboratory

August 1996

A STUDY OF WEAR  
USING A CAMERON-PLINT TRIBOMETER

Brian Riestenberg  
Centerville High School

Abstract

A Cameron-Plint tribometer records data on wear, produced by rubbing a small cylinder across the surface of a disc, in the presence of a lubricating fluid. As the test is running a surface film is produced between the cylinder and the disc. After a test is finished, the cylinder, disc, and fluid are examined. The cylinder and disc show signs of wear that can be measured, and the fluid contains wear debris that can be studied to help determine what kind of film was produced in the process of the experiment.

A STUDY OF WEAR  
USING A CAMERON-PLINT TRIBOMETER

Brian Riestenberg

Introduction

Lubrication is used to reduce friction and wear between solid surfaces having relative motion. Materials used to reduce friction and control wear may be in a gaseous, liquid, or solid state. Liquid lubrication can be done by applying an amount of liquid to the contact point between two surfaces. Additives are very useful in helping a lubricant work better under certain conditions. In today's world nearly all lubricants fall short of being useful at extreme temperatures. Therefore it is essential that we develop new lubricants.

Methodology

To begin a test on the Cameron-Plint Tribometer, it is first necessary to clean the test specimens. The disc and cylinder are immersed in hexane and then methanol, and then put into an ultrasonic cleaner for 15 minutes. After the disc and cylinder are cleaned they are placed in the machine. The disc is placed in a well and secured into place with clamps; the well is then filled with whatever lubricant is going to be tested. The cylinder is clamped in place on the oscillating arm. Next, the environmental control chamber is placed around the test sample. Then, depending on the test situation, the air line must be opened and, if necessary, a humidifier may be turned on to work at a high humidity level. The next step is to turn on the computer and the tribometer. After running the correct program on the computer and correctly programming the tribometer, all that is left is to activate the test sequence.

At the start of the test the load is set at 20 N for 5 minutes. The load is then increased to 250 N for the duration of the test. After completion of the test, the wear scar on the cylinder is measured with an optical microscope. The stressed fluid and the metal surfaces are analyzed by

grazing angle microscope and other techniques. All tests that I was involved with used an M-50 steel disc, polished on one side, and an M-50 steel cylinder. All tests were also done with a load of 250 N, a stroke of 9 mm, and frequency of 6 Hz. The test temperature was varied from 100°C to 150°C and the relative humidity varied from 1% to 95%.

#### Results

Some fluorinated fluids intended for wide temperature applications were studied. Effects of humidity and additives on the wear characteristics of bearing steel were examined. It was observed that at lower humidities (<20%) the wear was high and at higher humidities the wear was low. This indicated that water was reacting with the fluid/metal to form some kind of protective surface film. By adding 1 to 2 percent of various additives in the base fluid, a 50-75% reduction in wear was observed.

# NEURAL NETWORKS AND DIGITAL IMAGE PROCESSING

Douglas M. Ritchie

Niceville High School  
200 E. John Sims Parkway  
Niceville, FL 32578

Final Report for:  
High School Apprenticeship Program  
Wright Laboratory

Sponsored by:  
Air Force Office of Scientific Research  
Bolling Air Force Base, DC

and

Wright Laboratory

August 1996

NEURAL NETWORKS AND DIGITAL IMAGE PROCESSING  
Douglas M. Ritchie

**Abstract**

The focus of investigation was broad, including Sensor modeling software, interpretation and evaluation of IMSS (Infrared Multi-Spectral Sensor), and investigation and evaluation of PCNN (Pulse-Coupled Neural Networks). This was accomplished with the help of Chris Clark, a first-year member of the High School Apprenticeship Program. The summer was divided almost evenly into these three categories and the task concerning each was primarily to gather information. The NeuroSeek Sensor Model, developed initially into Excel, had to be converted to MatLab in order to use multiple processing elements. Next, IMSS data, provided by Pacific Advanced Technology, was examined to determine whether or not the sensor provided enough data to accurately classify a simulated minefield. Finally, code implementing Pulse-Coupled Neural Networks was analyzed and the parameters of the network were tested.

## NEURAL NETWORKS AND DIGITAL IMAGE PROCESSING

### Douglas M. Ritchie

#### Section I - NeuroSeek Sensor Model

The NeuroSeek program concerns the development of an infrared sensor. Without real data off the sensor, however, there can be no attempt at attacking the classification of its output, and so a model must be generated. This model was designed and implemented in Excel and contained all of the necessary blackbody calculations to simulate the sensor. Blackbody refers to a theoretically perfect emitter, and so the calculations from the sensor are under ideal circumstances.

The goal for Chris and myself was to develop a computer model that would simulate the NeuroSeek Sensor. An Excel version of this model had already been created, but was limited in application. This is because the Excel model dealt with calculations from only one element, whereas the sensor would have to deal with calculations from a 128x128 matrix of elements. The effort necessary to do this in Excel is astounding, as one would have to run the Excel Spreadsheet Model 16,384 times in order to get a full matrix of output.

The solution to this problem was deemed to be rewriting the model in MatLab, an environment capable of doing such processing in a matrix as opposed to an iterative approach needed by Excel. In order to implement this solution, several things would first have to be done. The variables and constants of the spreadsheet would have to be coded into a MatLab 'M' file, or MatLab executable file. Then, the formulas used in the cells of Excel would have to be written into MatLab in a loop fashion so as to affect the necessary variables and constants. Finally, the elements must be formed into a matrix using separate calculations for each element so as to accurately model the NeuroSeek sensor.

Converting the constants and variables into MatLab was not a difficult task, but it was a tedious one. Chris and I worked together to do this, each taking half the code from Excel and, after agreeing on a standard method of variable-naming, individually coded the values into MatLab. The process took approximately a day to

## NEURAL NETWORKS AND DIGITAL IMAGE PROCESSING

Douglas M. Ritchie

finish, although the tangible output was negligible, since all the program did was assign variables. The next effort was programming the formulas from Excel into MatLab. This, again, was not difficult, but tedious. The formulas from the individual cells had to be extracted and written into MatLab not only in the correct format, but in the correct order. Excel seems to have the unique ability to call variables from anywhere within the spreadsheet, where MatLab, like many top-down programming languages, can only use variables after they've been assigned in the code. This led to a few changes in the order that the output values were calculated. The MatLab format of the formulas was in most cases similar to the Excel format.

Having done this, it was decided that a Graphical User Interface, or GUI, would be developed to drive the MatLab code. The GUI was written in Visual Basic 4.0 and utilized Dynamic Data Exchange, or DDE, in order to send and receive data through a connection established between Visual Basic and MatLab.

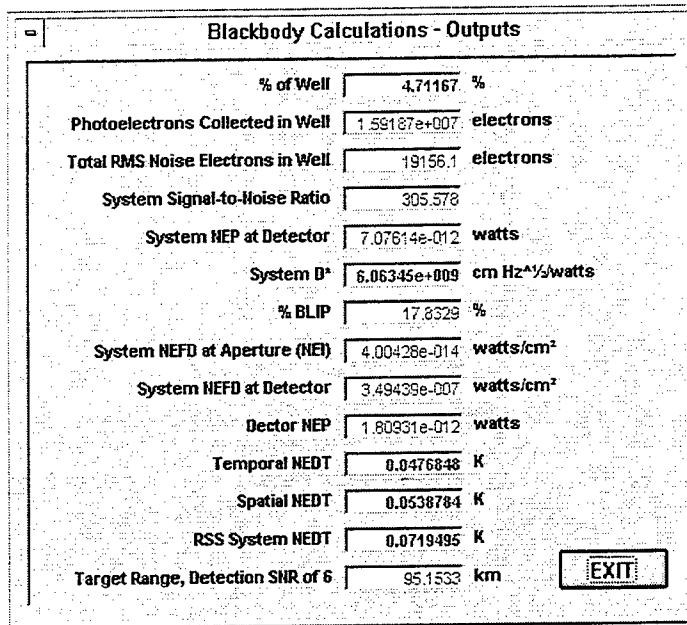


Figure 1: NeuroSeek GUI Output Window

Figure 1 is an example of the GUI's output, containing information that can be used to determine how effective the sensor will be. This output window shows the

## NEURAL NETWORKS AND DIGITAL IMAGE PROCESSING

Douglas M. Ritchie

response of one processing element of the sensor.

The final step of this portion of the summer's work was to construct a 128x128 matrix of these processing elements. This was easily accomplished in MatLab, which caters to such styles of processing. The result of the project was a program package that successfully modeled a 128x128 array NeuroSeek Sensor.

### Section II - Infrared Multi-Spectral Sensor (IMSS)

The Infrared Multi-Spectral Sensor (IMSS) is, as its name suggests, an infrared sensor that obtains data through a multitude of infrared wavelengths, ranging from 3.2 microns to 4.9 microns. The theory is that certain targets respond best at different wavelengths of the infrared spectrum, and if one knew what frequency a target responded to, one could easily filter out all but that frequency and get a clear segmented image of that target.

Pacific Advanced Technology (PAT), based in California, sent mentor Paul McCarley a set of "HyperSpectral Data Cubes" containing data collected from an IMSS. This data was 90 frames of a simulated minefield, each frame at a different wavelength starting at 3.2 microns and moving linearly to 4.9 microns. The minefield was simulated by placing eight pennies, four underground and four above ground, in a rectangular pattern in a field of clutter consisting of grass, soil, and sand. The task given to Chris and me was to determine how effective the sensor was in this range, and attempt to detect and classify the simulated mines using a neural filter.

The first obstacle in this task was to develop a method of observing the hyperspectral datacubes. Four datacubes represented one set of IMSS output of 256x256 resolution divided into four 128x128 segments. The format used by PAT was called "fts," and was incompatible with any standard viewer. The bigger obstacle was, however, that the intensity values in the file were two-byte unsigned characters, a

## NEURAL NETWORKS AND DIGITAL IMAGE PROCESSING

Douglas M. Ritchie

UNIX compatible format. This meant that the file must be byte-swapped to be read on a PC, the machine we were using.

The problem was solved by contacting Mark Massie of Pacific Advanced Technology, the man responsible for sending the data to Wright Laboratories. PAT sent fconvert.exe, a file designed to byte-swap and behead the data files, making them nothing more than 32,768 byte files of 2-byte intensities. After this, the four sets of datacubes had to be combined into one 256x256 image to represent the full output of the sensor. This was done in MatLab by augmenting the image matrices.

Next, a GUI was developed to display the gray-scaled intensity images from frame one to ninety, allowing us to observe the response on each captured frequency. Again, the Visual Basic 4.0 to MatLab connection was established via DDE.

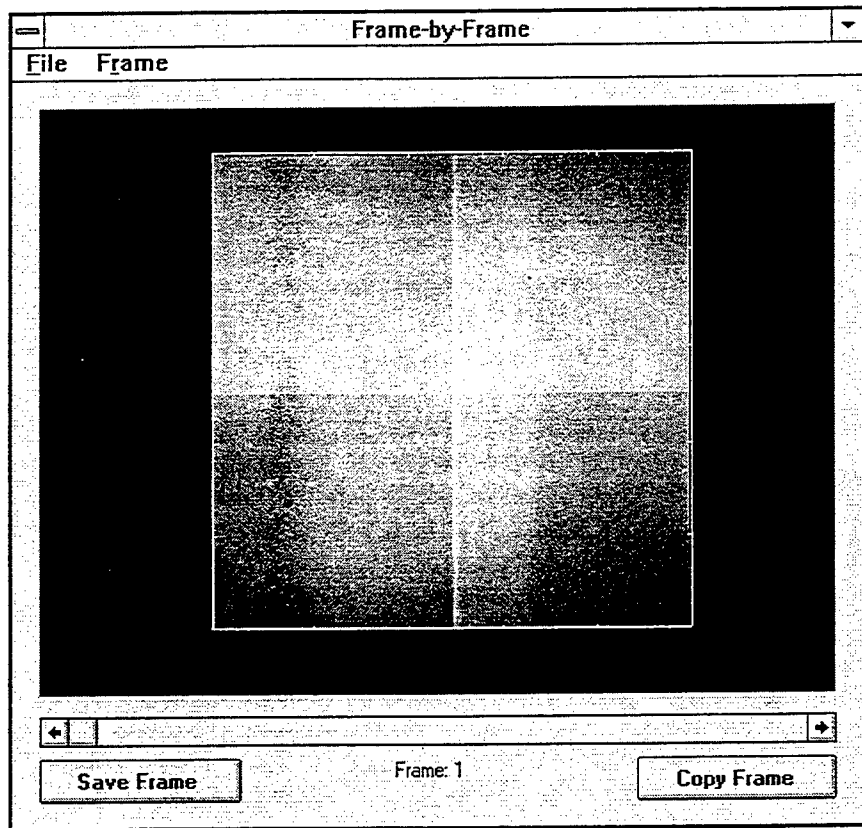


Figure 2: Frame by Frame datacube viewer.

## NEURAL NETWORKS AND DIGITAL IMAGE PROCESSING

Douglas M. Ritchie

Figure 2 shows the interface used with the IMSS sensor output. Using this interface, we moved through the individual frames of the output deck and made manual observations on the segmentation of the camouflage cloth and simulated mines. With these materials in these wavelengths, we determined that segmentation got better as the wavelength increased. Below, figure 3 shows the simulation at 3.2 microns, and figure 4 shows the simulation at 4.9 microns.

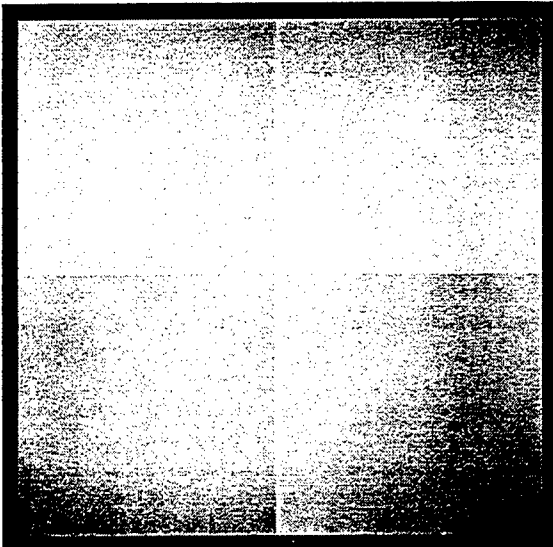


Figure 3

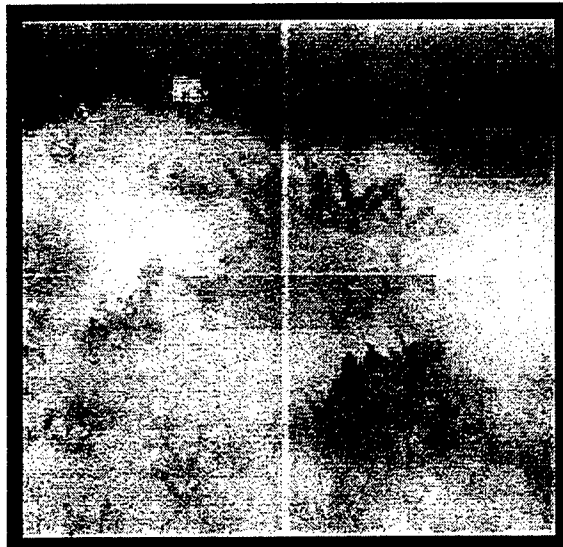


Figure 4

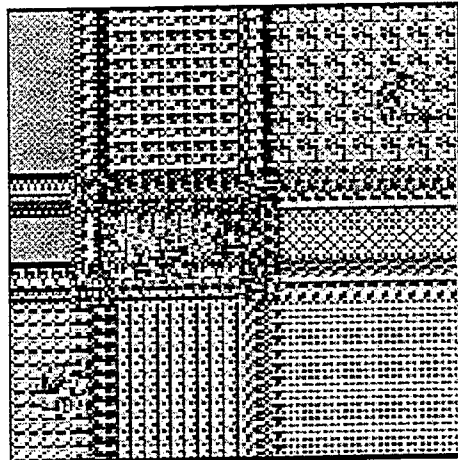
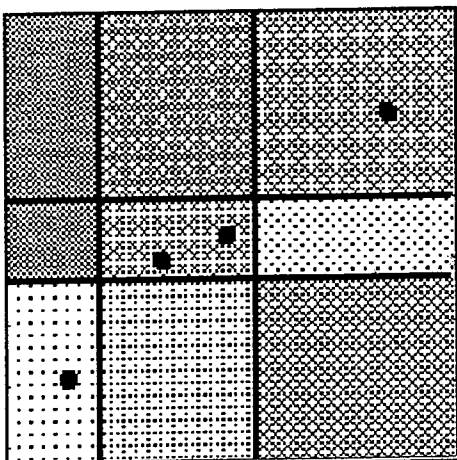
The minefield is located in the lower-left quadrant. It is, as far as our observations go, invisible to the eye and undistinguished in intensity. Our conclusion concerning the IMSS was that it was incapable of significantly segmenting the mines at the wavelengths provided. Nevertheless, the gradual clarity of the image as wavelength increased led us to believe that, given the ability to increase the potential of the sensor to higher wavelengths, the mines could be detected. Pacific Advanced Technology is currently improving the sensor to do just that.

Despite our failure to segment the simulated mines, we attempted to filter the image in an effort to better locate the mines. Equipped with prior knowledge of the location of the mines, we cropped 12x12 targets from the original image and used them

## NEURAL NETWORKS AND DIGITAL IMAGE PROCESSING

Douglas M. Ritchie

to train a neural network. The network consisted of one layer of weights containing 144 values. The values were trained with the target data by backpropagation with a logsig transfer function to output 0.5 for target, and -0.5 for no target. The network trained in 63 iterations, outputting 144 values as weights, which were used in a 12x12 digital image filter. In theory, the logsig of the filter should output close to 0.5 for target, and -0.5 for no target. The synthetic minefield is show below. Beside it is the network filtered output.



The mines, represented by black dots on the synthetic minefield, came close to 0.5 in the filtered image. However, the network determined the spot where black lines in the minefield crossed to be mines as well. This was never corrected, and the filter concept was considered to be a failure. This could be a result of not enough training data, or perhaps the simple design of the network.

### Section III - Pulse-Coupled Neural Networks

Pulse-Coupled Neural Networks, a relatively new concept developed in 1990, are designed to do segmentation and image recognition. The claims made by its designer suggest that it is invariant to any known geometrical alteration, including size, position, rotations, and distortion. Beyond this, it claims to be capable of determining shadows

NEURAL NETWORKS AND DIGITAL IMAGE PROCESSING  
Douglas M. Ritchie

and intensity changes. The theory is that the network examines 'Pulses' of intensity from the image. It develops a time signature based on the sum of the active positions in each pulse. It is said to construct this signature in such a way that the data concerning the relation between pixel positions and relative intensities is preserved, and therefore invariant to alteration. Figure 5 is a diagram showing the algorithm of the network.

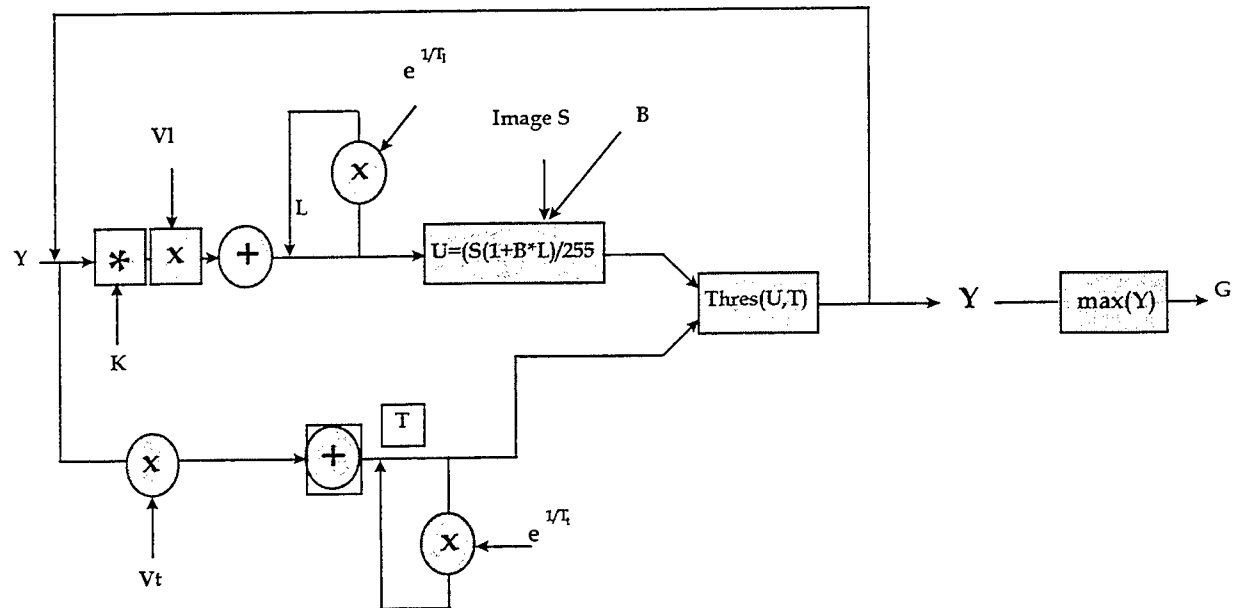


Figure 5

The input image  $S$  is converted into pulses that output a segmented image  $Y$  and a time signature  $G$ . Other parameters include the size of  $K$  (convolution filter),  $V_I$ ,  $V_t$ ,  $T_{aoI}$ ,  $T_{aoT}$ , and beta. All of these parameters help determine the output of the network.

The task for Chris and myself was to determine the validity of the claims of geometrical invariance, and to determine the effects of the parameters of the network. In order to do this, laser radar (LADAR) data of a bridge target was examined. Incidentally, the code implementing the network was found to be inefficient. A change in the thresholding operation of the code made it 1000% more effective in terms of output versus time.

Again, a GUI was developed in order to allow quick setting of parameters for the

NEURAL NETWORKS AND DIGITAL IMAGE PROCESSING  
Douglas M. Ritchie

network. The interface allowed for the input of all network parameters and was linked to MatLab via DDE. To validate the invariance claims, we took two LADAR images of a bridge and compared the time signatures. Then, the first bridge was rotated 90 degrees and compared with the first two time signatures. The time signature output of the bridge from two angles is shown in figures 6 and 7.

Figure 8 represents three curves: The cross-correlation of figure 6 and figure 7, the auto-correlation of figure 6, and the cross-correlation of figure 6 with the time signature of the bridge rotated ninety degrees. This correlation also includes the cross-correlation of figure 6 with the time signature of the rotated bridge, along with the auto-correlation of the first bridge.

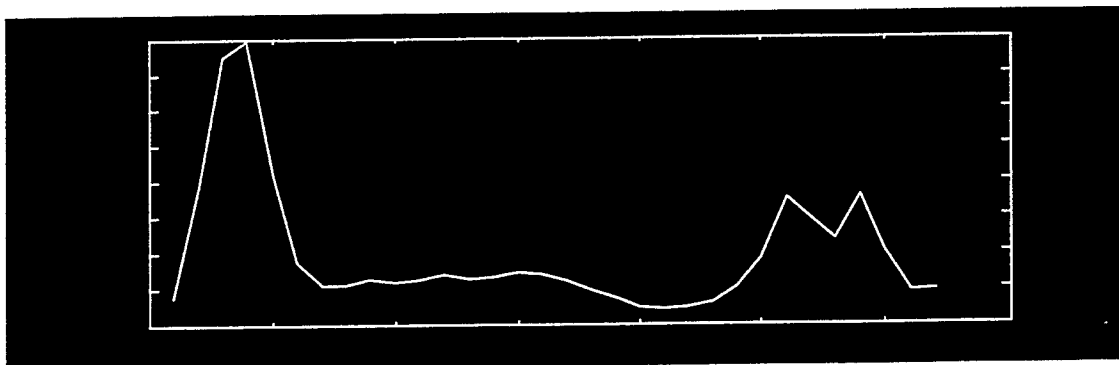


Figure 6

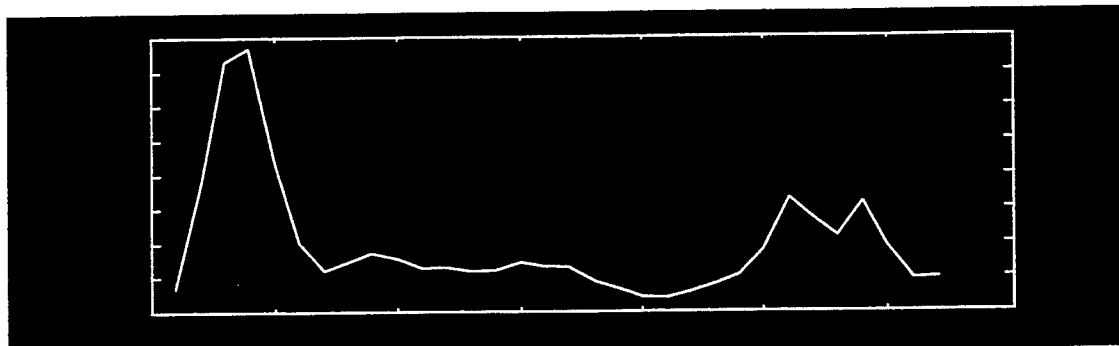


Figure 7

NEURAL NETWORKS AND DIGITAL IMAGE PROCESSING  
Douglas M. Ritchie

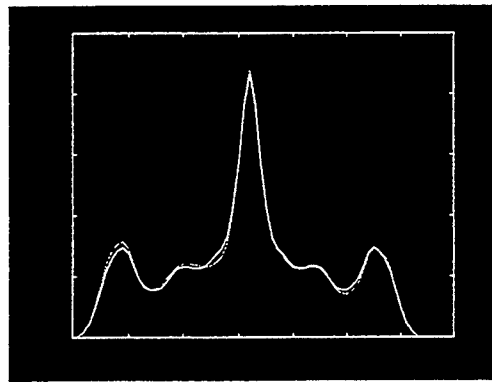


Figure 8

The almost flawless overlap of the signals indicates that the network is invariant to size, rotation, intensity, and position. This confirms the assertion of the networks invariance to these geometrical alterations, making it useful for automatic target recognition applications.

The next task was to determine the effects of the parameters of the network. This was accomplished by using the GUI to change the parameters, first times ten, the one-tenth. The change in segmentation quality and time signature was recorded in observation, and organized into the chart seen in figure 9. The information presented in Figure 9 is based strictly on the observation of Chris and myself.

Parameter	Effect
<i>Radius</i>	<i>Affects Amplitude</i>
<i>Beta</i>	<i>Unknown</i>
<i>Tao<sub>l</sub></i>	<i>Affects Contrast</i>
<i>Tao<sub>t</sub></i>	<i>Affects # Cycles</i>
<i>V<sub>l</sub></i>	<i>Unknown</i>
<i>V<sub>t</sub></i>	<i>Affects Contrast</i>

Figure 9

NEURAL NETWORKS AND DIGITAL IMAGE PROCESSING  
Douglas M. Ritchie

**Conclusion**

The study of these three fields, Neuroseek, IMSS, and PCNN, has yielded tangible results in the form of usable code and information necessary for full evaluation of future options with IMSS and PCNN. The summer's output includes the Neuroseek sensor model, capable of being used to generate processed images to be used in studying filter methods, as well as GUI's for the Neuroseek model, the IMSS data viewer, and the PCNN implementation code. The IMSS data cubes can now be easily viewed and analyzed through the combination of Visual Basic and MatLab. Finally, a data file was created in Excel containing the varied parameters of the Pulse-Coupled Neural Network. The file includes variations of all of the parameters of the network to limited degrees. This information may be useful in the evaluation of PCNN for applications at Wright Laboratories.

A STUDY OF IMPROVING THE COMPUTED  
AIR RELEASE POINT USING NEURAL NETWORKS

Trisha A. Silkauskas and John C. Martin  
WL/FIVMB  
Special Projects Section

Centerville High School  
500 E. Franklin St.  
Centerville, OH 45459

Final Report for:  
High School Apprentice Program  
Wright Laboratory

Sponsored by:  
Air Force Office of Scientific Research  
Wright Patterson Air Force Base, OH

and

Wright Laboratory

August 1996

## **A Study of Improving the Computed Air Release Point using Neural Networks**

Trisha A. Silkauskas  
WL/FIVMB  
Special Projects Section  
Centerville High School

### **Abstract**

The Computed Air Release Point (CARP) using neural networks was studied. When the neural net assumed the expected output would be zero, the output was near zero. Upon closer examination, it was decided that an expected output of zero might not adequately test the neural network. Unfortunately, by virtue of the fact that the expected output of the training data was random in nature, the output of the test data had no predictable expected values to compare it to. This does not mean that the neural network did not work. It means that more airdrop data needs to be collected before the value of a neural network for determining CARP can be accessed.

## A Study of Improving the Computed Air Release Point using Neural Networks

Trisha A. Silkauskas

### Introduction

Airdrop is an effective process of getting personnel and cargo to a specified location via aircraft. Under ideal conditions, using the Computed Air Release Point (CARP) parameters of MACR 55-40, every air load would fall in a ballistic trajectory thus allowing easy calculations {1}. However, under realistic conditions a number of factors have to be considered in every airdrop load. The following elements have to be taken into account: the cargo's weight, height, and shape, the aircraft's type, velocity, height, and stability, the parachute's size, shape, and quality, along with winds and turbulence. At present, the wind is believed to be the largest error source. To reduce the effect of errors in wind data Wright Labs is currently investigating the use of Drop Sondes to accurately measure wind profiles. Budget limitations have restricted the data collection efforts as well as the number of personnel available to work the project. Inspite of these restrictions, CARP improvements are moving in a positive direction.

*Greenlight* is the name given when an airload is released from an aircraft. The airload is in a state of free fall, until the parachutes open and stabilize the load (also known as the *Stability Point*). The real problem in predicting an accurate CARP is not knowing when or where the load will reach its stability point. It's very difficult to predict because it is a non-linear problem. Fortunately, the Neural Network was designed for these problems. In order to use the Yuma Test Data to train and test the neural net, a few things needed to be achieved. Most importantly the Yuma Test Data was conditioned and condensed to a usable format. Then the neural net was "re-built" to fit the given problem.

### Methodology

The basic approach to find CARP is to use the Yuma airdrop test data as input to a neural network whose output is the CARP. To expedite the process "off-the-shelf" neural networks were used.

The Yuma data was processed to find the greenlight point and the stability point. The stability points are the input to the neural network and the greenlight point, (CARP), is the output.

X	Y	Z
-1926.35	-2857.37	-2365.03
4037.741	1402.741	3153.525
-2147.32	-1146.9	1059.422
299.983	176.648	-182.336
-1086.52	596.868	3500772
-3.4379	-19.9168	-0.104
-9.2227	4.6969	3.6952
-3.4427	2.6481	-10.1572
2.1991	-4.6715	-3.7596
-31.4189	-5.106	-22.8531
-7.8156	-16.0042	-15.6741
1.05	1.227	0.817
14.6535	20.0704	14.0636
-23.2353	-49.847	-64.8432

Stability Point Input Data (feet)

Since the neural network used could only accept input values between 0 -1, the input data had to be normalized {2}. The output is also a normalized value, therefore it had to be expanded.

Due to the extremely large data sets received from Yuma, several computer programs were developed to help condition and condense the data into a usable format (see Appendix B). The resulting data was used in the neural network for training and testing..

Out of all the "off-the-shelf" neural networks, backpropagation proved to be the most useful. Neural networks tend to need large amounts of data. The Yuma data was only able to provide 13 usable data sets. Seven data sets were used for training, and the remaining six were used for testing. Each training data set contains the X-Y-Z coordinates of the stability point and the expected output, (greenlight point X-Y-Z coordinates). The stability points used as input were estimated from the Yuma test data. The method of estimating the point required finding the point in time where the forces on the loads parachute, as measured with a strain gage, reached a steady state value. The test data contains the stability point data only. Before any of the data is used as input, it has to be normalized. The following equations were used {3} for this:

$$A = r(V - V_{\min}) + A_{\min}$$

$$\text{where } r = (A_{\max} - A_{\min}) / (V_{\max} - V_{\min})$$

A = normalized value

$A_{\min}$  = minimum practical limit of network

$A_{\max}$  = maximum practical limit of network

V = non-normalized input value

$V_{\min}$  = minimum input value

$V_{\max}$  = maximum input value

Once the data is normalized it can be used to train or test the neural network. Training the neural network is an iterative process. The neural net from Rao and Rao, {2}, would, during the process of training, stop and report that the neurode weights were "Blowing-up". This would require a change in the training constant, beta, and the acceptable error parameter. Therefore the training process required various values before the network would converge and produce acceptable output.

### Results

The first attempt at training the neural net assumed the expected output would be {0,0,0} for the X-Y-Z greenlight point. The network converged using a beta of 0.3 and an acceptable error of 0.05. When the test data was input, the output was near {0,0,0} for all test data. Upon closer examination of the expected output, it was decided that an expected output of {0,0,0} might not adequately test the neural network. A random offset was place in the data and the network trained again. Beta was now 0.2 and the acceptable error was 0.08. Unfortunately, by virtue of the fact that the expected output of the training data was random in nature, the output of the test data has no predictable expected values to compare it to. This does not mean that the neural network did not work. It means that more airdrop data needs to be collected before the value of a neural network for determining CARP can be accessed. Finally, in further examination of the test results, there appears to be an unaccountable trend of values in X, Y, and Z.

X	Y	Z
-4.090	34.356	77.250
-4.345	34.081	77.045
-3.862	34.680	77.451
-4.317	34.067	77.065
-4.572	33.660	76.865
-2.394	36.501	78.685

Output of Test Run with expected output equals 0 for all input vectors.

X	Y	Z
2,162.428	1,448.189	1,335.186
2,135.635	1,406.101	1,395.997
2,132.862	1,406.607	1,383.675
2,073.214	1,449.858	1,320.847
2,062.071	1,457.870	1,307.994
2,083.725	1,436.739	1,318.573

Output of Test Run with expected output does not equal 0 for all input vectors.

### Conclusion

The use of neural networks for determining CARP, while not proven, looks promising. The pitfalls of being data poor when training and testing a neural network were made clear during this experiment. The network did show promise of being capable of generating the expected output when the output was easily determined, but it is still an unknown when the expected output appears to be more random. Also another limitation of the experiment is that it did not take account winds aloft, aircraft airspeed, the particular load and parachute type, or other possible parameters explicitly into account. Many of the parameters were inherent in the Yuma data and not controllable. Also some data was not accurate or reliable due to instrumentation errors. Once sufficient data can be collected, more sophisticated neural networks can be created and tests run to determine their suitability for determining CARP. In conclusion, neural networks for determining CARP look promising, but require more investigation and data.

## References

- {1} Air Mobility Command Regulation 55-40, United States Air Force, June 1992
- {2} Rao, Valluru B., Rao, Hayagriva V., "C++ Neural Networks and Fuzzy Logic", Management Information Source Inc., 1993.
- {3} Masters, Timothy, "Practical Neural Network Recipes in C++", Academic Press, 1993.

## Appendix A: Yuma Proving Ground Airdrop Data

The data arrived at WL/FIVMB via ftp from Yuma. It was in the form of 3 self extracting compressed files:

6064\_ldr.exe  
6065\_ldr.exe  
6067\_ldr.exe

These files represented airdrop data from 4,5, and 7 March 1996 airdrops. Upon uncompressing them, it was discovered that there were 15 files and each one represented a single airdropped load. The size of the individual files ranged from 3.73MB to 14.3MB. It was clear that this was too large for the plotting software, Microsoft Excel, to read. The next characteristic of the data was the way time was stored in the file. It was in a M:SS.FFFF format where M is minutes, SS is the total number of seconds, and FFFF is the fraction of a second. A sample of an actual data file is pictured below:

Time	Triax			Strain Link
	X Axis	Y Axis	Z Axis	Canopy
-0:00.0000	0.165	0.350	0.000	69.169
0:00.0020	0.331	0.350	0.000	-61.086
0:00.0041	0.000	0.350	0.000	69.169
0:00.0061	0.331	0.467	0.306	69.169
0:00.0081	0.000	0.350	0.000	69.169
0:00.0102	0.165	0.233	0.000	-61.086
0:00.0122	0.000	0.233	0.000	69.169
0:00.0143	0.000	0.117	0.000	-61.086
0:00.0163	0.165	0.233	0.306	69.169
0:00.0184	0.165	0.350	0.306	-61.086
0:00.0204	0.000	0.350	0.000	69.169
0:00.0224	0.331	0.233	0.000	-61.086
0:00.0245	0.000	0.233	0.000	69.169
0:00.0265	0.000	0.117	0.000	-61.086

The triax X-Y-Z values are absolute acceleration in G's while the strain link values are the measurements taken from a strain gage attached to the load's parachute. To get position data the acceleration values would need a double integration performed on them. The files also contained many blank lines which represented the time periods where the instrumentation failed. Finally, it was noted that some of the data was questionable. File 6086\_Idr.dat had the Z-acceleration values sitting at zero the majority of time and then instantaneously rise to extreme values. The data would require processing before it would be usable in neural network experiments.

## Appendix B: Software

The experiment to create a neural network was software intensive. It required 5 software program that took nearly 6 weeks to write. Three of these programs, blank.txt, final.txt, and contime.txt were written in the Perl programming language for the purpose of processing the Yuma Proving Grounds data. The other software, a backpropagation neural net, from Rao and Rao, and Excel by Microsoft are commercially available.

### Blank.txt

Blank.txt removes the blank lines from the data. It requires 2 parameters, the input file and the output filename.

### Final.txt

Final.txt does the bulk of the processing. It can accept an input file name, but if it doesn't get one it will prompt the user for one. The program will take a data file and take a range of data, time range or line number range and save it. It will also take every nth, (i.e. every 100<sup>th</sup> ) point and place that in a separate data file. The nth value function of the program will look for and preserve the minimum and maximum values of the data file. Finally, the program will take data points based on a delta value. If the next value is greater than the last value by the delta amount, it is saved, otherwise it is ignored. The nth function of this program was utilized for the data reduction.

### Contime.txt

Contime.txt simply takes the output of final.txt and changes the time into seconds and fractions of second. This was needed since Excel didn't handle the Yuma time format properly. Contime requires 2 parameters, an input and an output file name.

### Backprop

Backprop is the neural network trainer and tester. It asks the user for training or test mode. If it is training it then asks it for acceptable error, training constant, momentum term, noise term, whether or not to use random initial neurode weight values or a file containing them, and the number of layers and neurodes in each layer. The program proceeds to execute and if all goes well the network is properly trained. If the user chooses to test, the program then asks for the number of layers and neurodes in each layer. Again, if all goes well, the neural network will solve your problem.

### Excel

Excel was simply used to plot the Yuma data. There reason for using Excel was that it is very easy to use and is available on most people desktops.

## Appendix C: Neural Network Equations

The backpropagation neural net developed by Rao and Rao{2} uses the following equations for output, error, weight adjustment, adjustment to threshold value, and use of momentum term of the layers.

$M_1$	=	Hidden layer weight vector
$M_2$	=	Output layer weight vector
$x_i$	=	Output of the $i^{\text{th}}$ neurode of the input layer
$y_i$	=	Output of the $i^{\text{th}}$ neurode of the hidden layer
$z_i$	=	Output of the $i^{\text{th}}$ neurode of the output layer
$P_i$	=	$i^{\text{th}}$ component of the desired output pattern
$\lambda$	=	Learning rate parameter for hidden layer
$\mu$	=	Learning rate parameter for output layer
$\theta_i$	=	Threshold value or bias of the $i^{\text{th}}$ neurode of the hidden layer
$\tau_i$	=	Threshold value or bias of the $i^{\text{th}}$ neurode of the output layer
$i$	=	$i^{\text{th}}$ neurode of the $j^{\text{th}}$ layer
$j$	=	$j^{\text{th}}$ layer

Output of the  $j^{\text{th}}$  hidden layer neuron

$$y_j = f( (\sum_i x_i M_1[i][j]) + \theta_j) \quad (1)$$

Output of the  $j^{\text{th}}$  output layer neuron

$$z_j = f( (\sum_i y_i M_2[i][j]) + \tau_j) \quad (2)$$

Note: The function used in the above output equations is the thresholding function. In this case it is the sigmoid function where

$$f(x) = 1/(1+e^{-x})$$

$i^{\text{th}}$  component of vector of output differences

$$\text{desired value-computed value} = P_i - z_i$$

$i^{\text{th}}$  component of output error at the output layer

$$e_i = z_i (1 - z_i) (P_i - z_i) \quad (3)$$

$i^{\text{th}}$  component of output error at the hidden layer

$$t_i = y_i (1 - y_i) \sum_j M_2[i][j] e_j \quad (4)$$

Adjustment for weight between  $i^{\text{th}}$  neuron in the hidden layer and the  $j^{\text{th}}$  output neuron

$$\Delta M_2[i][j] = \mu y_i e_j \quad (5)$$

Adjustment for weight between  $i^{\text{th}}$  input neuron and the  $j^{\text{th}}$  neuron in the hidden layer

$$\Delta M_1[i][j] = \lambda x_i t_i \quad (6)$$

Adjustment to the threshold value or bias for the  $j^{\text{th}}$  output neuron

$$\Delta \tau_j = \mu e_j \quad (7)$$

Adjustment to the threshold value or bias for the  $j^{\text{th}}$  hidden layer neuron

$$\Delta \theta_j = \lambda e_j \quad (8)$$

When using a momentum parameter  $\gamma$  replace equations 5 and 6 with

$$\Delta M_2[i][j] = \mu y_i e_j + \gamma \Delta M_2[i][j] (t - 1) \quad (9)$$

$$\Delta M_1[i][j] = \lambda x_i t_j + \gamma \Delta M_1[i][j] (t - 1) \quad (10)$$

SUMMER SCIENCE PROJECTS

Michael J. Steiger

Oakwood High School  
1200 Far Hills Ave.  
Dayton, OH 45419

Final Report for:  
High School Apprentice Program  
Wright Laboratory  
Materials lab

Sponsored by:  
Air Force Office of Scientific Research  
Bolling Air Force Base, Washington D.C.

and

Wright Laboratory  
Materials Lab

August 1996

## SUMMER SCIENCE PROJECTS

Michael J. Steiger  
Oakwood High School

### Abstract

Throughout the summer several projects have been completed; including temperature dependent transmission studies of conductive polymers and creating a resource database. The conductive polymer transmittance study as a function of temperature was performed to try and see shifts in the band edge of the spectra. The temperatures ranged from -160° C to 200° C. Shifts in the band edge were not seen although a couple of problems came about in the experiment. The two problems were baking off part of the polymer at the high temperatures and the other was frost building up on the windows of the vacuum container, Specac®. The resource database was created to organize electroluminescent articles and make access to those articles an easier process.

## SUMMER SCIENCE PROJECTS

Michael J. Steiger

The physics group at Wright Laboratories Materials Lab Polymer Branch provides support for determining the physical properties of compounds that the synthetic chemists produce. The physics group support is in the form of electrical and optical measurements of the polymers being studied. The summer's effort were spent on several types of projects have been worked on over the summer including transmittance studies of conductive polymers, processing and analyzing data, and setting up experiments for further use. Some of these projects were setting up a resource database, helping to setup a micromanipulator experiment, and working on temperature dependent transmission study.

The major project was assisting in the study of the transmittance of visible light through a polymer sample as a function of temperature. The methodology used to perform the experiment was to take spectra of a sample, 6F-PBO, at various temperatures, from 23° C to 200° C. The sample is to be measured in a Specac® vacuum container so the first step was to measure the pressure inside the vacuum at the temperatures selected. Knowing whether the vacuum would leak an appreciable amount at the various temperatures determined if the instrument was reliable and provided a possible margin of error. The results showed that the vacuum seal was best at 100° C as compared to 200° C and 23° C. The instrument used for the transmittance experiment was a dual beam Hitachi U-4001 spectrophotometer, which measures transmitted versus incident light intensity. The Hitachi's lid was not high enough from the light source to hold the Specac; so a lid was manufactured of cardboard with an opening for the Specac cut into the top of the lid. The cardboard lid had a loose fit as compared to the tight fit of the regular lid, so to help keep light out of the Hitachi aluminum foil covered the area where the Specac protrudes through the top of the lid. Black plastic was draped over the top of the Specac and Hitachi to keep any stray light from

entering or escaping. The Specac stood on a lab jack to adjust to height causing the setup to be extremely sensitive to movement. The alignment of the Specac was performed by hand; making it difficult to have the same alignment if the Specac moved or was bumped. Even placing the plastic over the Specac and lid after alignment would often push the Specac out of alignment. The sensitivity of the Specac may have caused some differences in alignment, but the experiment setup was undisturbed as much as possible.

The experiment was conducted at 23° C, 100°, 200°, and 37.5° C, taken after the sample had cooled down from 200° C. The results from the experiment did not show the band edge shifting due to the change in temperature as was expected from previous experiments conducted by others on different materials. (Redfield, 138) At 196° C part of the sample evaporated and was deposited on the windows of the Specac. This could be seen by the interference fringes seen in the 37.5° C spectrum and a spectrum taken of the windows out of the Specac. (See graph 1) A yellowish, seven micron film was on the windows of the Specac and was visible to the human eye.

In order to try to see some difference in the band edge as the temperature changes the transmission experiment ran using the setup shown in figure 1. The transmission of light that is seen by the OMA CCD is not a true light transmission. The OMA calculates the transmission by subtracting a background scan from the light transmitted through the sample. In this experiment the temperature range was changed to go from liquid nitrogen, -160° C, to 90° C. The transmission spectra were taken in groups of four or five each five; each separated by integrals of five degrees. After the spectrums for a set the heater would be turned on to raise the temperature around fifty degrees where another set of data would be taken. During the experimental run the polymer did not evaporate at the adjusted temperatures. A problem did happen to occur in the low temperatures when frost formed on the windows of the Specac; distorting our data. To remove the frost a heat gun was used and nitrogen gas was blown onto the outside of the windows so that some of the moisture cold be removed. The frosting of the windows distorted the data enough that the

comparisons of band edge were difficult to make. This distortion made it difficult to see the differences in band edge shift of materials as a function of temperature achieved by others. (Urbach, 1324) Although it gave us a hint of what to be careful of when the experiment is repeated.

The initial temperature study led to designs for a part to hold the Specac in place so that measurements can be made from the same point when similar experiments are performed. The project involved designing a piece to hold to Specac and a second sample so that the samples and the light beams were aligned. Two other influences that had an effect on the designs were ease of making the piece and being able to adjust a second sample by hand. The final designs consisted of two pieces both made of aluminum. The first piece would hold the Specac and has a slot for the second piece. (See figure 2) The second piece was designed to hold a sample in a clamp and was to slide in the slot of the first piece. (See figure 3) The slot allows the second pieces to be adjusted up, down, and side to side perpendicular to the second light beam. The two pieces together will help to give uniform reference places so that data can be compared from the same location.

Some of the projects worked on this summer involved processing data to create resource databases so that resources are convenient for others to use. One of these projects was inputting bibliography information from electroluminescence articles collected over a period of years into a Microsoft database. The project involved updating the database so that others can access the database and look up material to see if a particular article is on file. Another part of the project was printing out the database in spreadsheet form for a secondary means of finding information. The data was acquired through a query where the order of columns was arranged for easier use in Excel. After the data was in Excel the entries needed to be sorted by various columns and made for presentation. The presentation form of the spreadsheet had the grid shown around cell blocks and borders around column headings so that the data was able to be distinguished. (To see complete list of directions for processing data in Excel from a database see Appendix A) After all the

journals had been organized in a spreadsheet the articles needed to be separated by date and filed so that they may be retrieved quickly when needed. This was the final step to organizing the articles from a database to a spreadsheet.

During the summer experiments were setup for future use later in the year; one of these was the micromanipulator. The micromanipulator experiment is used to do temperature dependent photo- and electroluminescent studies. The first step in setting up the micromanipulator is moving the nitrogen gas tanks across the lab room. In order to anchor the tanks, holes needed to be drilled into the cement block wall. Eyelets were then secured into the wall with expandable fasteners so that chains could be hooked to them. After the eyelets were in place and the nitrogen gas tanks were moved and chained to the wall for safety.

Each of the projects that was worked on over the summer has been successful in some way. Some of the experiments may have not given the scientific answers that one hoped for but have been a valuable learning experience. While other projects were able to solve the problems that existed previously. This author would like to acknowledge the efforts of Dr. Barney Taylor, Max Alexander, Dr. S.J. Bai, Dr. Gang Du, and Dr. Robert Spry.

Transmittance of Windows after Heating Study

Graph 1

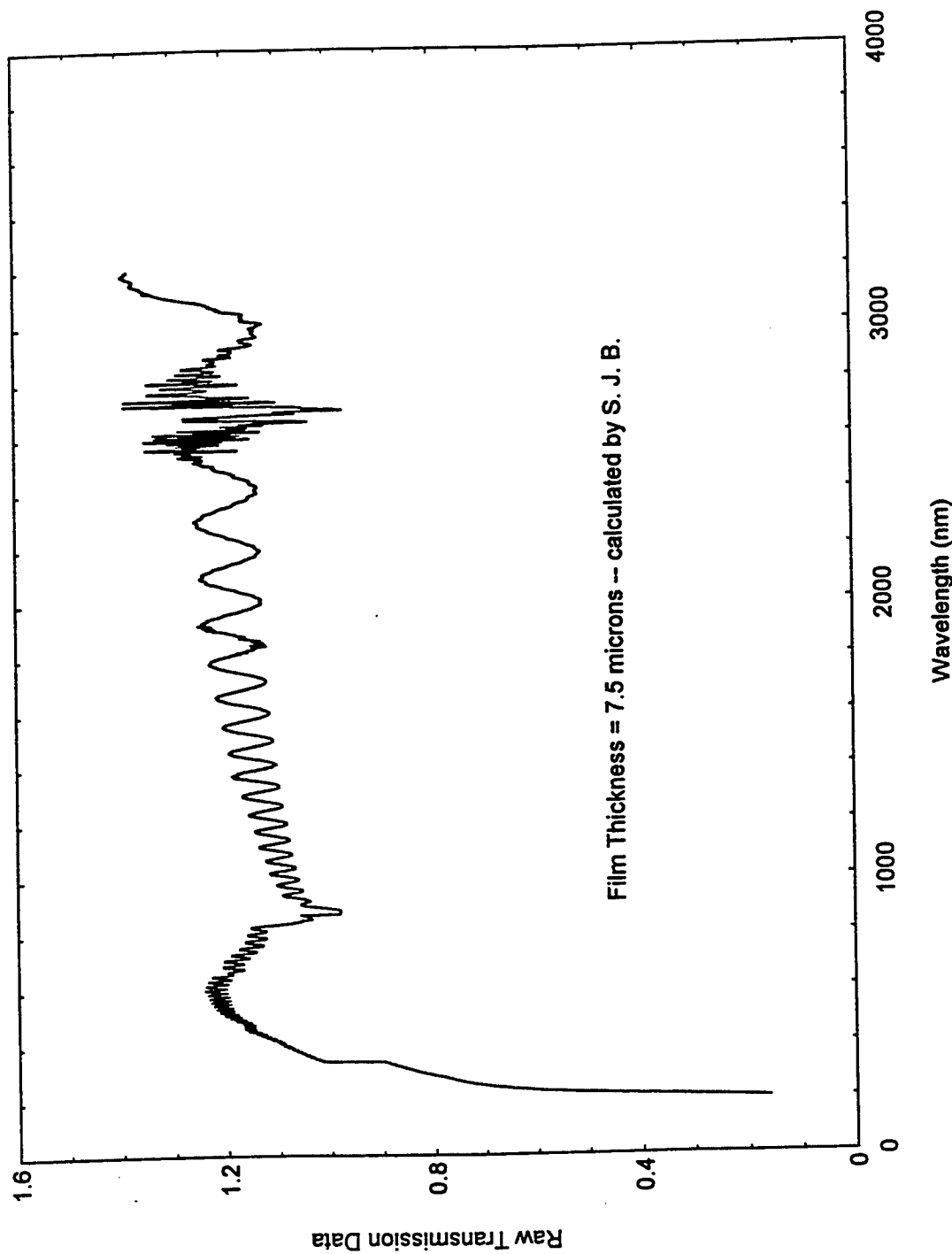


Figure 1

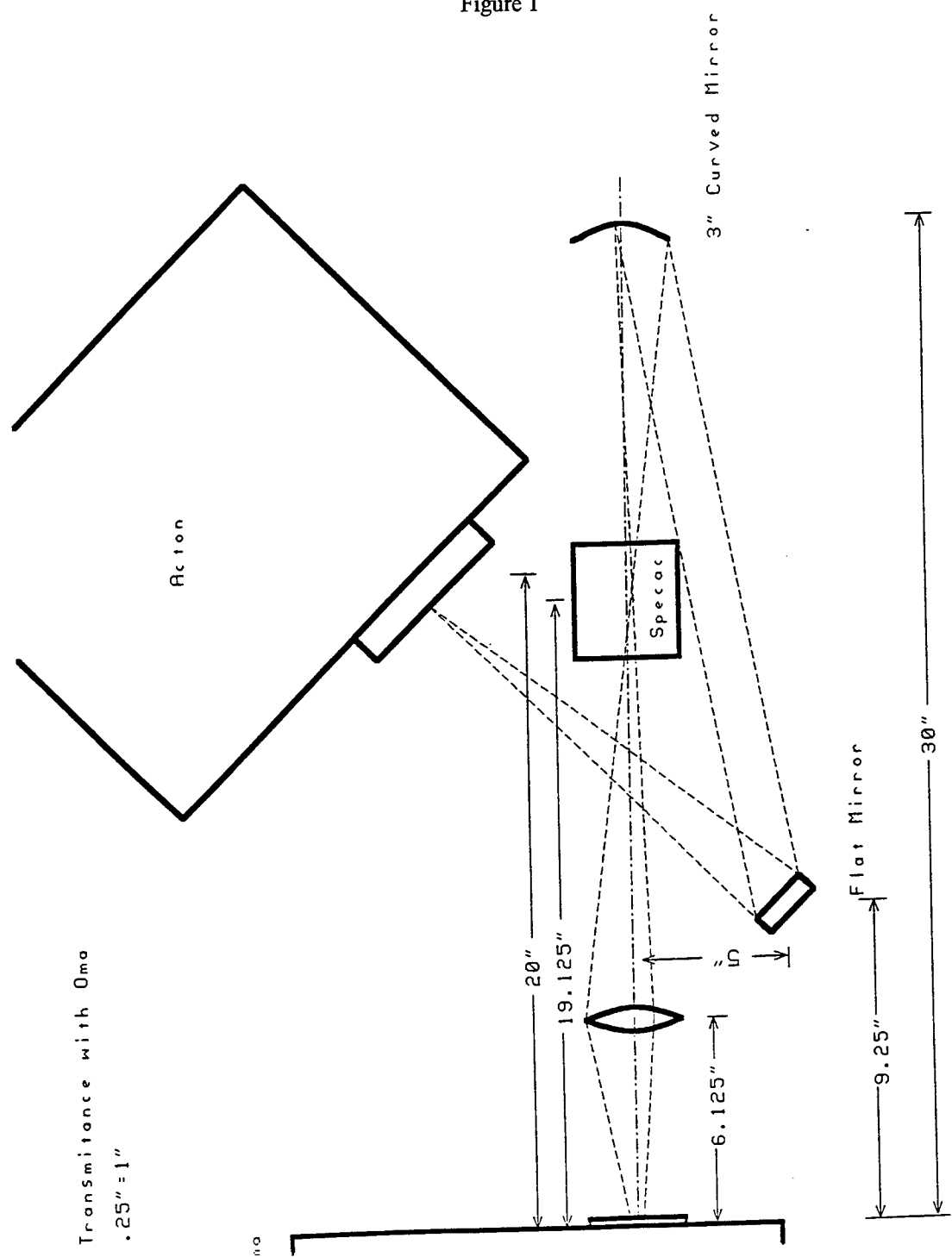


Figure 2

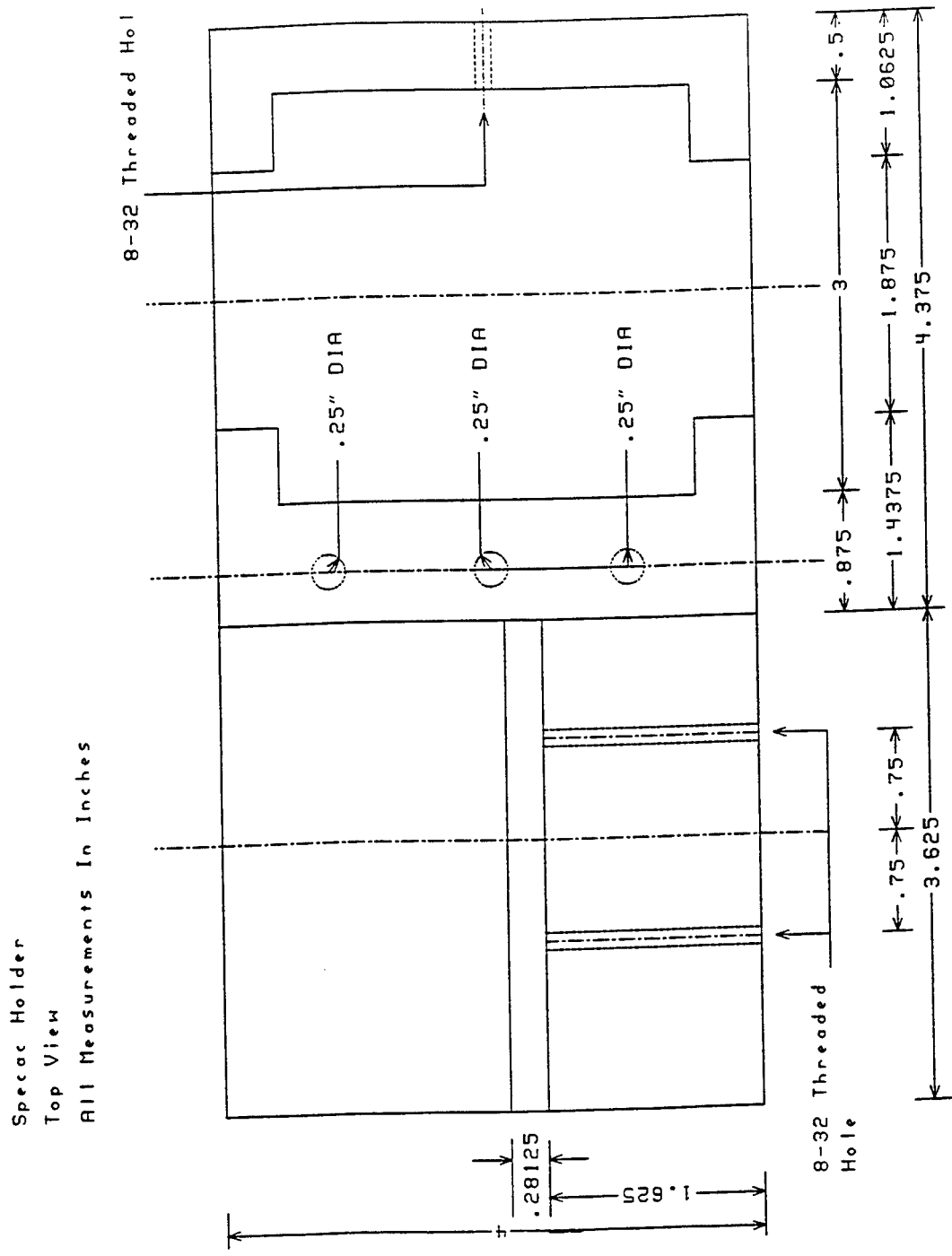
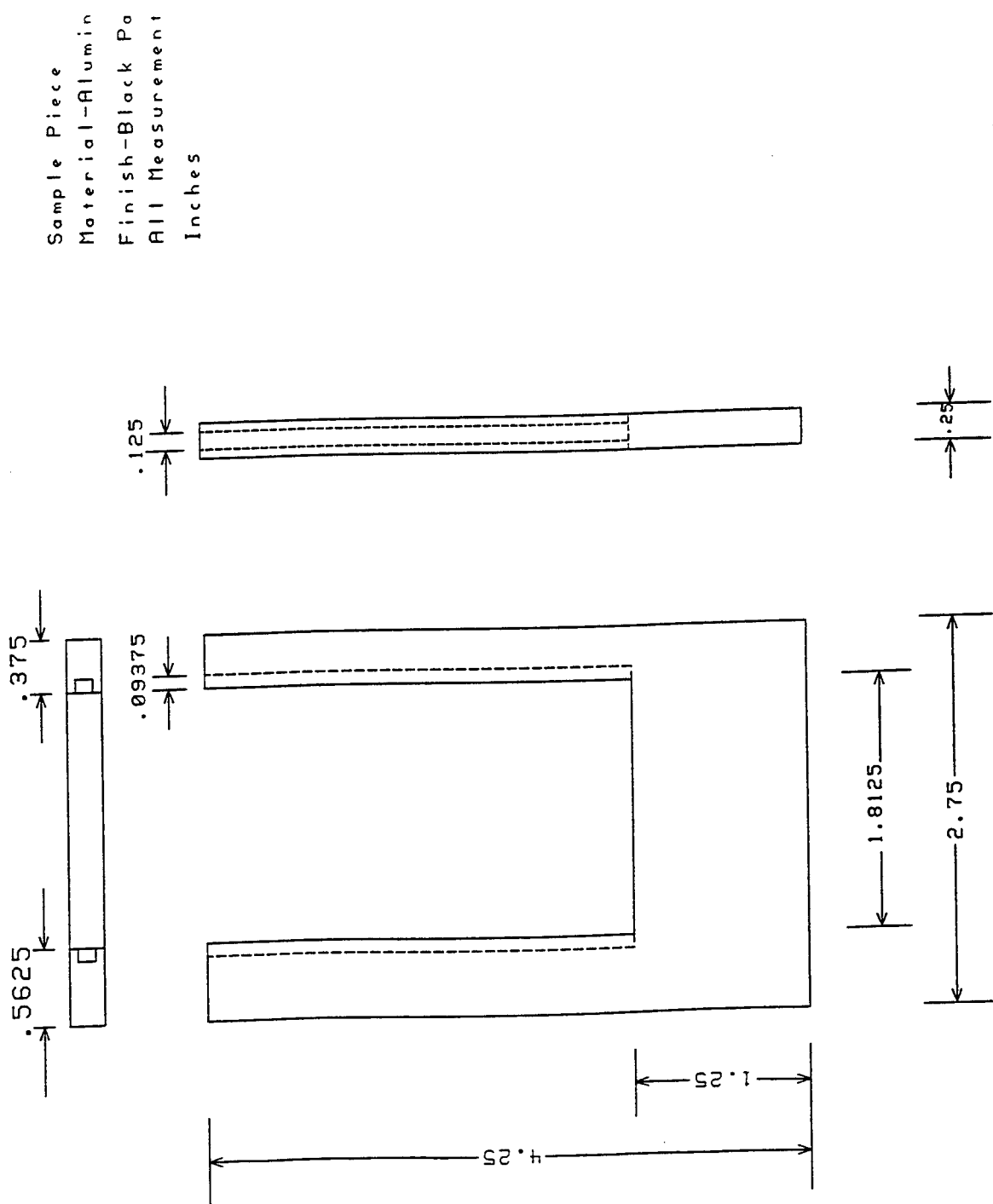


Figure 3



## Appendix A

### Steps for Moving Data from a Database to “Excel”

1. The first step is to go under the Data heading and click on “Get External Data...”
2. A Query will then open; under the “Select Data Source” card choose the “MS Access DB” and then click the “Use” button.
3. The next card that will be shown is a “Select Database” card. Choose the appropriate database and click “Ok.”
4. A “Add Tables” card will come up and the “Loads” option will be chosen, if not choose it, then click the “Add” button.
5. A “Loads” card will now appear in the left corner of the Query screen. First click the “Close” button from the “Add Tables” card. This will leave you with the “Loads” card open. The card will show the headings of the data, click on each heading in the order that it is to appear in the spreadsheet.
6. As the headings are clicked the data will appear at the bottom of the screen to give an image of what the spreadsheet will look like. After all of the headings have been clicked on go under the “File” command and click on the “Return Data to Microsoft Excel” choice.
7. A card will appear in the center of the screen that is titled “Get External Data”; click the “Ok” button and the data will be entered into the spreadsheet.
8. After the data has arrived the columns and rows need to be formatted. The rows should be high enough to allow for four lines of text and the word wrap should be used for the columns. The column width depends on material in the cells and whether the file is to be printed in “Landscape” form.
9. When all of the columns and rows have been formatted to show the data then borders can be selected for desired areas. Generally thick vertical borders in the heading cells with a double line below the headings makes the heading cells noticeable. Other borders can be chosen but with such a large amount of data printing the grid lines can make use of the spreadsheet much easier.

WORKS CITED

Redfield, David and Martin A. Afroumowitz. "The Direct Absorption Edge in Covalent Solids".

Appl. Phys. Lett., 11(15 Aug 1967): p. 138.

Urbach, Franz. "The Long-Wavelength Edge of Photographic Sensitivity and of the Electronic

Absorption of Solids". Phys. Rev. 92(1953): p. 1324.

A STUDY OF THE EFFECTS OF OCTANOIC ACID ON POLYMER DISPERSED LIQUID  
CRYSTAL HOLOGRAPHIC GRATINGS WITH VARYING PERCENTS OF LIQUID  
CRYSTAL

Kari D. Sutherland

Dayton Christian High School  
325 Homewood Avenue  
Dayton, OH 45405

Final Report for:  
High School Apprentice Program  
Wright Laboratories, Materials Directorate

Sponsored by:  
Air Force Office Of Scientific Research  
Bolling Air Force Base, DC

and

Wright Laboratory

August 1996

A STUDY OF THE EFFECTS OF OCTANOIC ACID ON POLYMER DISPERSED LIQUID CRYSTAL HOLOGRAPHIC GRATINGS WITH VARYING PERCENTS OF LIQUID CRYSTAL

Kari D. Sutherland  
Dayton Christian High School

Abstract

The focus of this experiment was to study the effects of the surfactant octanoic acid on polymer dispersed liquid crystal gratings using varying percents of liquid crystal. The different percents of liquid crystal used in the syrups were 30%, 50%, 70% and 79% E7. Samples were constructed of each syrup and exposed for seven minutes to an Argon Ion laser with a wavelength of 514 nm. After exposing, an experiment was set up using a helium neon laser at 633 nm to measure the diffraction efficiency of each sample at s and p polarization. Switching voltage was done to select samples. The best sample from each E7 percent sample was observed under the Polarized Optical Microscope (POM), and pictures were taken. The samples were then peeled and sent to the Scanning Electrical Microscope (SEM) to look further into the samples. The 30% sample showed good improvements in the diffraction efficiency and voltage switching when the octanoic acid was added. The 50% also showed improvement with the surfactant, although more experimentation could be done to improve the results. The 70% and 79% samples showed no real improvement with the surfactant.

A STUDY OF THE EFFECTS OF OCTANOIC ACID ON POLYMER DISPERSED LIQUID  
CRYSTAL HOLOGRAPHIC GRATINGS WITH VARYING PERCENTS OF LIQUID  
CRYSTAL

Kari D. Sutherland

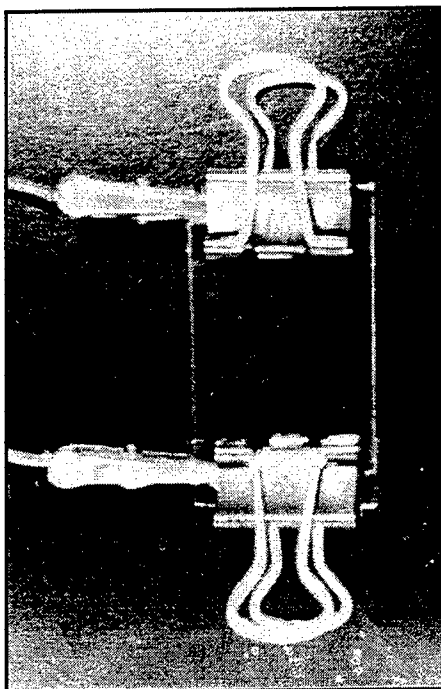
**Introduction**

Previous experiments done by members of SAIC and WL/MLPJ have proven that a surfactant truly does help cure a solution used for making gratings. By using 30% liquid crystal in a photopolymer mixture and adding 4% of octanoic acid, a standard surfactant, small LC droplets formed causing clear gratings. However, the research in this area is now expanding. I chose to focus on the effect of adding octanoic acid, a surfactant, to solutions of Rose Bengal with various percents of liquid crystal compared to the same solutions without octanoic acid. In doing so, I hoped to produce higher diffraction efficiency, lower voltage switching, and better, clearer gratings in the samples with the surfactant.

**Experimental**

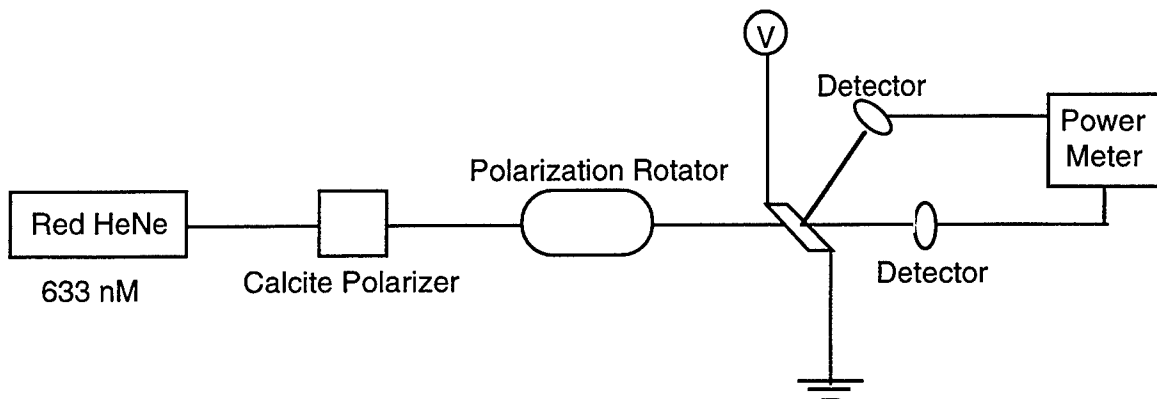
To begin the experiment, syrups were made with varying liquid crystal percents of 30%, 50%, 70%, 79%. The recipe included N-vinylpyrrollidone (NVP), N-phenylglycine (NPG), dipentaerythrol hydroxy penta acrylate (DPHPA), Rose Bengal (RB), and varying percents of liquid crystal (E7). The same syrups were then duplicated, adding the surfactant octanoic acid. After combining the recipe, each syrup was sonicated to mix the ingredients thoroughly. After sonicating, three good samples-one on a glass slide and two on ITO slides-of each percent were constructed. To prepare the samples for recording, the lights were turned off, and the glass and ITO slides were cut in half and spacers were applied to the end of each half. A pipet was used to place drops of the syrup in the middle of each slide. The

slides were squeezed and held together with binder clips. Index matching fluid was applied to each side of the sample to hold the OD filters on. Our



recording setup included the use of an Argon Ion laser with a wavelength of 514 nm and a power of  $7 \text{ mW/cm}^2$  per side. Each sample was positioned one at a time behind a prism that had a square mask to create a square hologram. The beam was split and then crossed when the two beams hit the prism. Each sample was exposed for seven minutes each. When the seven minute exposure time was up, the OD filters were removed and the sample was placed under a postcuring lamp to remove any of the rose bengal dye that might still be remaining.

Following the exposure and recording, each sample was characterized. Our setup included the red HeNe laser (633 nm). The laser was beamed through a Calcite polarizer to a polarization rotator set at p polarization ( $360^\circ$ ), then through a beam concentrator (to reduce scattering) to the sample. Behind the sample the detector was hooked up to a power meter. Before each sample was placed in the holder, a glass slide was inserted to measure



the transmission and that number was used as the calibration factor. Then we would remove the glass slide and place each sample in, measuring the highest diffracted power and then the transmitted power. When each sample had been characterized at p polarization, the polarization was changed to s ( $270^\circ$ ) and the experiment was repeated. After collecting the data, the numbers were calculated to find the diffraction efficiency and transmission of each sample. The diffraction efficiency (DE) was found by dividing the diffracted power ( $P_d$ ) by the calibration factor (C), and the transmission (T) was found by dividing the transmitted power ( $P_t$ ) by the calibration factor as shown below.

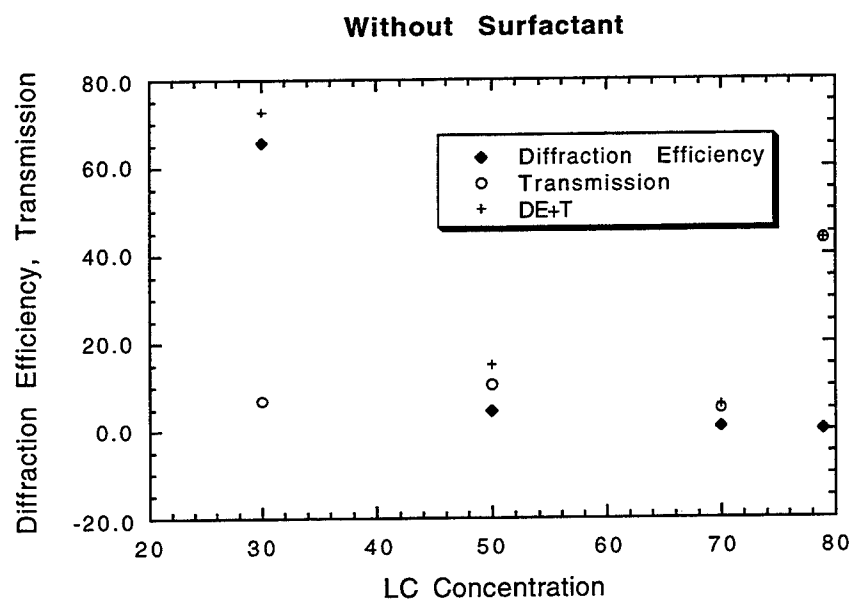
$$\frac{P_d}{C} = DE$$

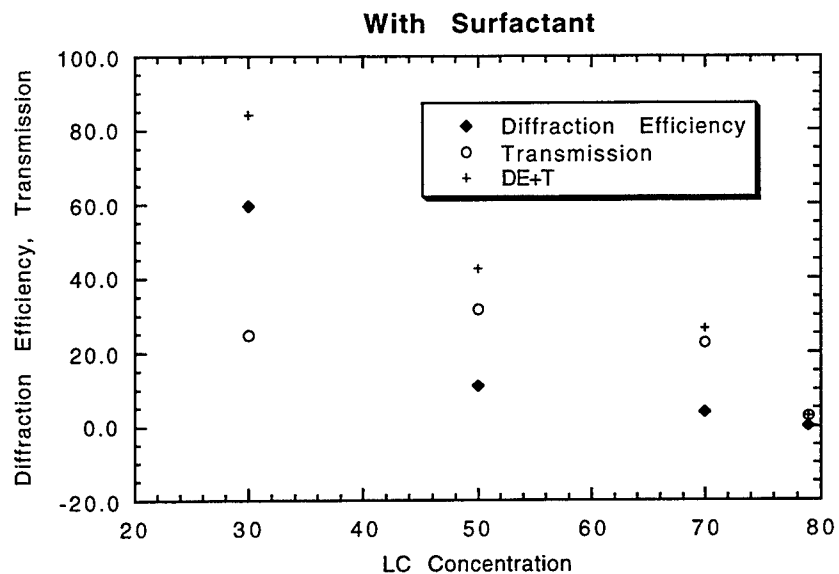
$$\frac{P_t}{C} = T$$

After characterization, voltage switching was done to each sample. The samples were then taken to the Polarizing Optical Microscope (POM) to be observed and to take some pictures. Following the POM, each sample was taken apart and the now polymerized samples were peeled off to take to the Scanning Electron Microscope (SEM) for further observation into what was occurring in each sample.

## Results and Conclusion

After the experimentation, I chose two of the best ITO samples from each varying percent of LC and averaged their diffraction efficiency and transmission. By plotting the data, some interesting results were noticeable. The 30% LC ITO samples showed that there was good diffraction efficiency with and without the addition of the surfactant. With the 50% LC ITO samples, the diffraction efficiency increased slightly when the surfactant was added. The same occurred with the 70% LC ITO samples.



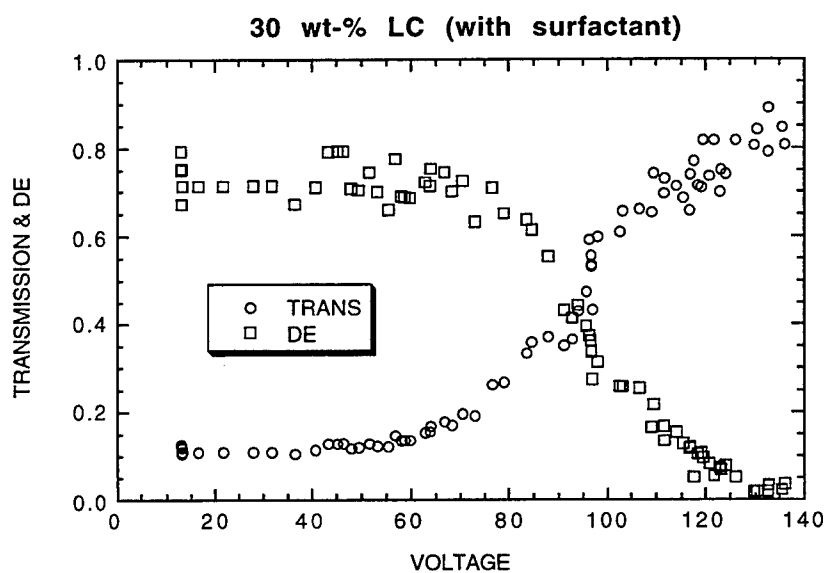
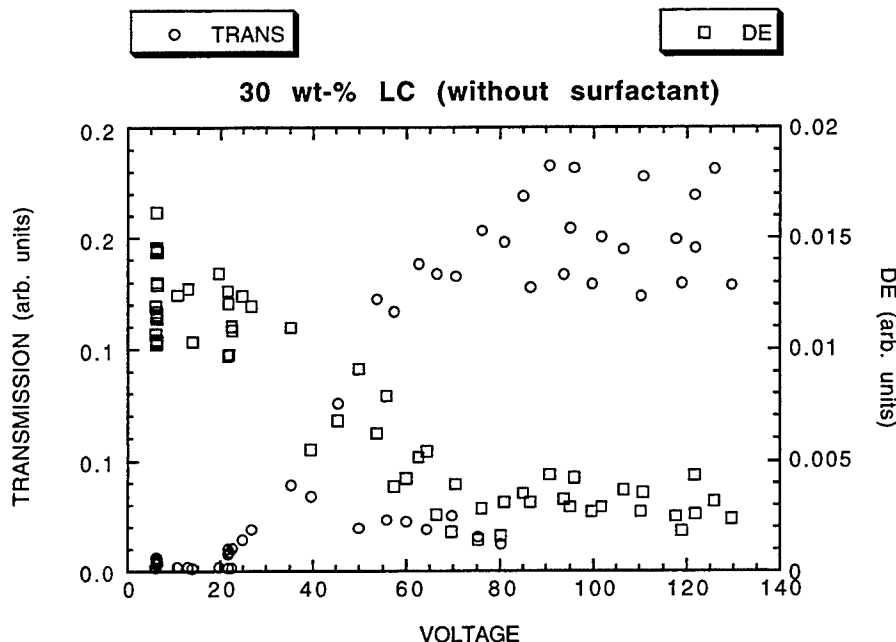


Even though the increase of the diffraction efficiency was not incredibly large, the total light throughput of each sample (79% being the exception) with the surfactant was larger than the throughput of the samples without the surfactant.

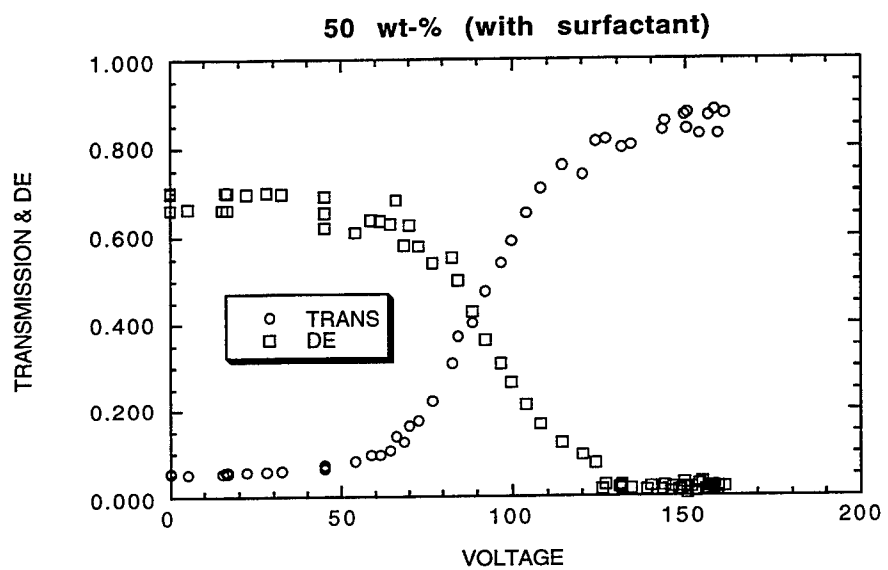
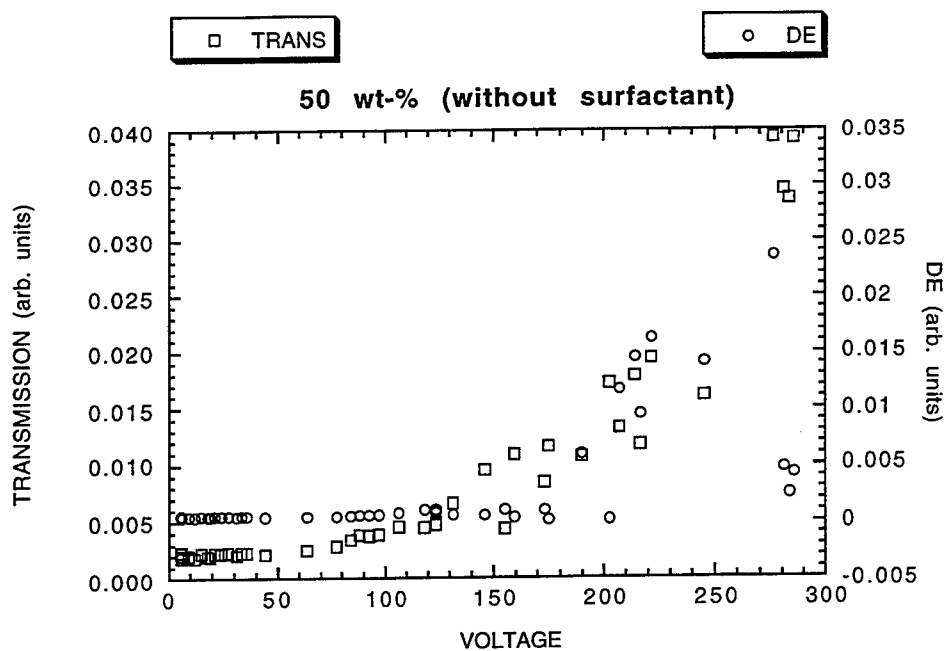
However, with the 79% LC ITO samples, the diffraction efficiency decreased about 30% when the surfactant was added. I believe this was caused by the addition of too much liquid crystal to the syrup. Because of the excess LC, a phase separation occurred (as shown below), and the polymer was not able to hold the LC droplets, leaving the LC to float around freely.



When comparing the results of the voltage switching of the 30% LC samples, the samples without the addition of the surfactant had a very gradual decrease in diffraction efficiency and eventually evened off. However, the results of the 30% LC sample with the surfactant showed that the diffraction efficiency decreased greatly while the transmission increased at about the same rate.



With the 50% LC sample without the addition of the surfactant, the diffraction efficiency remained constant. The 50% LC sample with the surfactant had the same results as the 30% LC with surfactant. This proves that even though the 50% samples were extremely cloudy, the gratings were still very good.



In the 70% and 79% LC samples, with and without the surfactant, no real evident change was taking place in the diffraction efficiency. The only change was the increase on the transmission of the samples with the surfactant.

These results go to prove that the surfactant octanoic acid does work to better cure samples with 30% and 50% liquid crystal. The results from the 30% samples agreed with the

results that others have previously received. No one had experimented with adding the surfactant octanoic acid to a 50% LC syrup. Seeing that the results were positive, more extensive experiments should be done to find how much more surfactant could be added to reduce the cloudiness and make clearer gratings.

The 70% and 79% LC samples had such an excess of the liquid crystal that the gratings could not form. These higher percents may require more octanoic acid or even perhaps a different surfactant to produce clear gratings.

#### Acknowledgments

Special thanks to Dr. L. V. Natarajan, Dr. Richard Sutherland, and Vince Tondiglia for all their encouragement, guidance, and support. I also want to thank Wright Laboratories which made this experience possible.

#### References

Adams, W. W, T. J. Bunning, L. V. Natarajan, R. L. Sutherland, and V. P. Tondiglia.  
“Electrically Switchable Volume Gratings in Polymer-Dispersed Liquid Crystals.” *Applied Physics Letters*, 1993: 1074-1076.

Adams, W. W, T. J. Bunning, L. V. Natarajan, R. L. Sutherland, and V. P. Tondiglia.  
“Volume Holographic Image Storage and Electro-Optical Readout in a Polymer-Dispersed Liquid-Crystal Film.” *Optical Letters*, 1995: 1325-1327.

Adams, W. W, T. J. Bunning, L. V. Natarajan, R. L. Sutherland, VP. Tondiglia, and D. L. Vezie. “The Morphology and Performance of Holographic Transmission Gratings Recorded in Polymer Dispersed Liquid Crystal.” *Polymer*, 1995: 2699-2708.

Bunning, T. J., L. V. Natarajan, R. L. Sutherland, and V. P. Tondiglia. “Bragg Gratings in an Acrylate Polymer Consisting of Periodic Polymer-Dispersed Liquid-Crystal Planes.” *Chemistry of Materials*, 1993: 15331538.

David Halliday, Robert Resnick. Physics for Students of Science and Engineering. John Wiley & Sons, Inc., New York, 1965.



## **FIGP-2 WEB SITE**

Matt Temple

Cahminade-Julienne High School  
505 South Ludlow Street  
Dayton, OH 45402

Final Report for  
High School Apprentice Program  
and  
Wright Laboratory

Sponsored by:  
Air force Office of Scientific Research  
Bolling Air Force Base, DC

and

Wright Laboratory

July 15, 1996

## Objective

This summer I was tasked with creating an HTML-based Web site representing the work of Wright Laboratory's Pilot-Vehicle Interface Technology Integration Section (FIGP-2).

Before I became involved in this project, my supervisor Lt. Heather Myers had written several Web pages, but as the project was not considered critical, she was unable to invest the time needed to produce a viable Web site. During my internship, I was able to develop a general model for the FIGP-2 Web site. I was also able to design several subsites which include reports from Wright Lab studies.

My intent at the outset of this project was to for this site's content to include

- an introductory layer, suitable for those with a casual interest in Pilot-Vehicle Interface Technology, or no previous knowledge.
- an in-depth layer, suitable for researchers who require detailed information.
- e-mail references to the technical leads in each area, so that it would be easy for companies, researchers, or other individuals to contact Wright Lab Engineers for clarification, further digression, or to develop other types of partnerships.

This site would eventually be placed on an Internet server to allow access through the World Wide Web.

## Design

Design of the site was based on the following considerations.

- The purpose of the site is to provide information. The site should be technically and conceptually flexible, enabling individuals to access the site's content according to their needs.
- This project will be extended, not necessarily by the original author, so its structure should support modular extension and improvement.

## Hierarchical Design

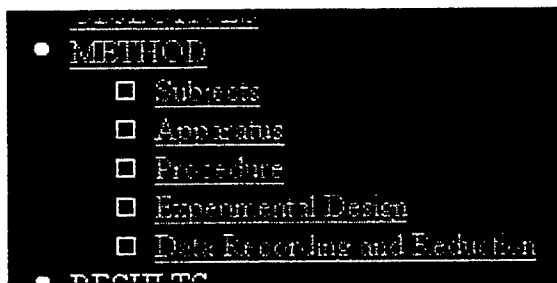
This site follows what I consider to be a class-logical hierarchy. As applied to this site, this implies that larger, more abstract concepts are presented at the topmost or introductory

layer, and that as sub-items are selected, the reader progresses to more concrete layers of information.

This is ideal for allowing individuals to access a site according to their needs. For those who are interested, the detailed information is there; for those who need a brief summary only, the top-most layer is sufficient.

In an attempt to be true to the idea of letting each user access the information of a site in their own way, para-classing was implemented. Applied to web sites, this is the practice of presenting the user with a set of choices which are not all equally weighted. One example of a para-classing is presenting the choices {fruit, apple, orange, vegetable, meat}. These choices are not all of equal weight. If you drew them in an outline, they would look like this:

- fruit
  - apple
  - orange
- vegetable
- meat



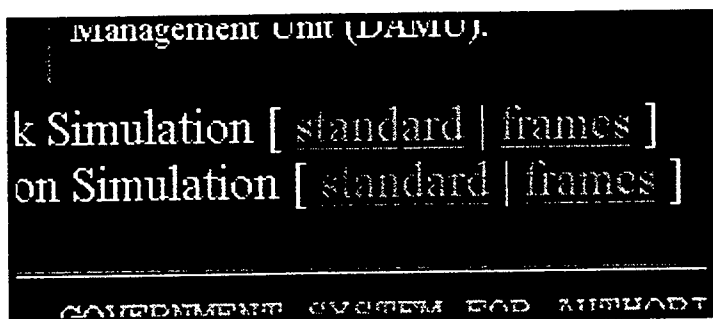
One example of para-classing in this web site is the C-141 table of contents. Subjects, Apparatus, and Procedure are all part of Method, but all four are presented as choices.

Strict hierarchical structure would require the reader to select Method before being presented with the sub-choices Subjects, Apparatus, and Procedure, thus limiting their choices.

Figures and tables were separated from document text to increase flexibility. In this way, users with no graphics or slow graphics can avoid the extra network time associated with loading graphics, and all users can more selectively browse the total document.

iat. These are addressed in sub provided in Figure 3. Most con and the discriminability of the ADI. Comments indicated that

For users with frames support, the table of contents is provided in a frame controlled separately from the document source. This allows the table of contents to remain visible while the reader peruses the rest of the document. It also facilitates reading the document in any desired order, or selectively browsing a part of the document.



For users with no frame support, a [standard] as opposed to [frames] button is provided.

## Page Design

### Frame Organization

In addition to a framed table of contents, some of the web pages offer a glossary. A button toggles between the glossary and the table of contents. This is ideal as it is unlikely the two will be needed at the same time; both are supplements to the main document.

The default size and placement of frames within the browser window are specified in a single file in each directory, usually called "frames.htm". The frames can be reorganized by editing this file, with no adverse effect on the functionality of the document.

### GLOSSARY

	Attitude
ADI	Director Indicator
AFB	Air Force Base
AFCS	Automatic Flight Control System
AFM	Air Force Manual



### Graphical Symbology

The back arrow on each page operates differently than the browser's back function. The browser back function takes you to the last place you visited, while the page back arrow takes you to the next higher layer within the site. A textual title next to the page back arrow corresponds to the title of the next highest page.

## Technical Design

## Hyperlink Structure

Sometimes figures or tables are referred to more than once in the text of a document. Each text that references a graphical resource is hyperlinked to a document containing that resource, and, optionally, a caption. The resource is then linked back to the referring document. To avoid displacement upon return to the referring document, some text references to a particular resource are hyperlinked to different resource pages. The return link of each resource page links to a different place in the referring document. For example, if Figure 8 is called three times, twice in the first paragraph, and once in the fifth paragraph, there will be two different resource pages for Figure 8. Their rendering will be identical; the difference lies in their return link. One will be linked to an anchor located immediately before the first paragraph, the other will be linked to an anchor located immediately before the fifth paragraph. This allows the site to behave in a user-friendly manner, and justifies the required overhead of an additional page which holds identical information.

## Hypertext Format

```
<LI><A HREF  
<FONT SIZE =  
<UL>  
    <LI><A HRE  
    <LI><A HRE  
    <LI><A HRE  
    <LI><A HRE  
    <LI><A HRE  
</UL>  
</FONT>
```

The hypertext source of this site was formatted with readability and modularity as the chief concern. One issue in hypertext transfer protocol is the compromise between improved readability of source code versus the size of the source code. Typically, readability is improved through the padding of hypertext source with spaces, tabs, and carriage returns. These characters allow formatting conventions that serve to visually organize hypertext source code, facilitating quick comprehension and making changes easier to implement through cut-and-paste techniques. Such organization is essential to the hypertext programmer who must edit large quantities of text. Based on the sample in Appendix A, the increase in source code size for this site is 17%.

## Image Format

Image resolution was chosen to embrace advances in display technology. Figures and tables were optimized for a display resolution of 800x600 or 1024x768. Decorative and informational graphics are often not fully visible in their default frame at 800x600 resolution. In a few cases they are not fully visible in any window that can be created at

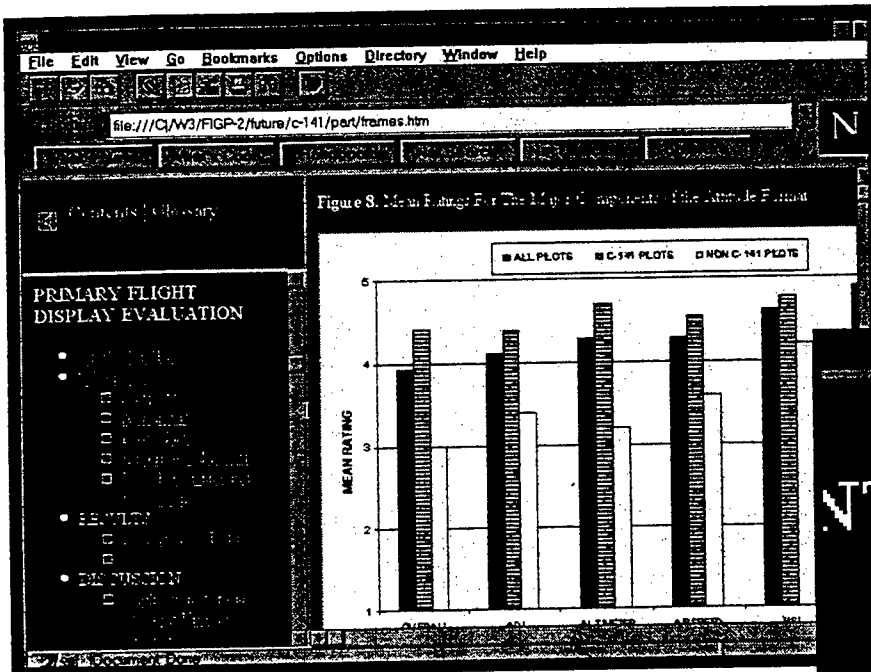


Figure is not completely visible.

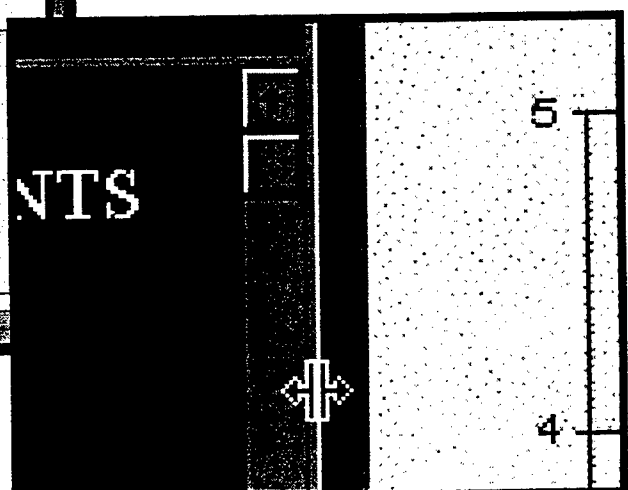
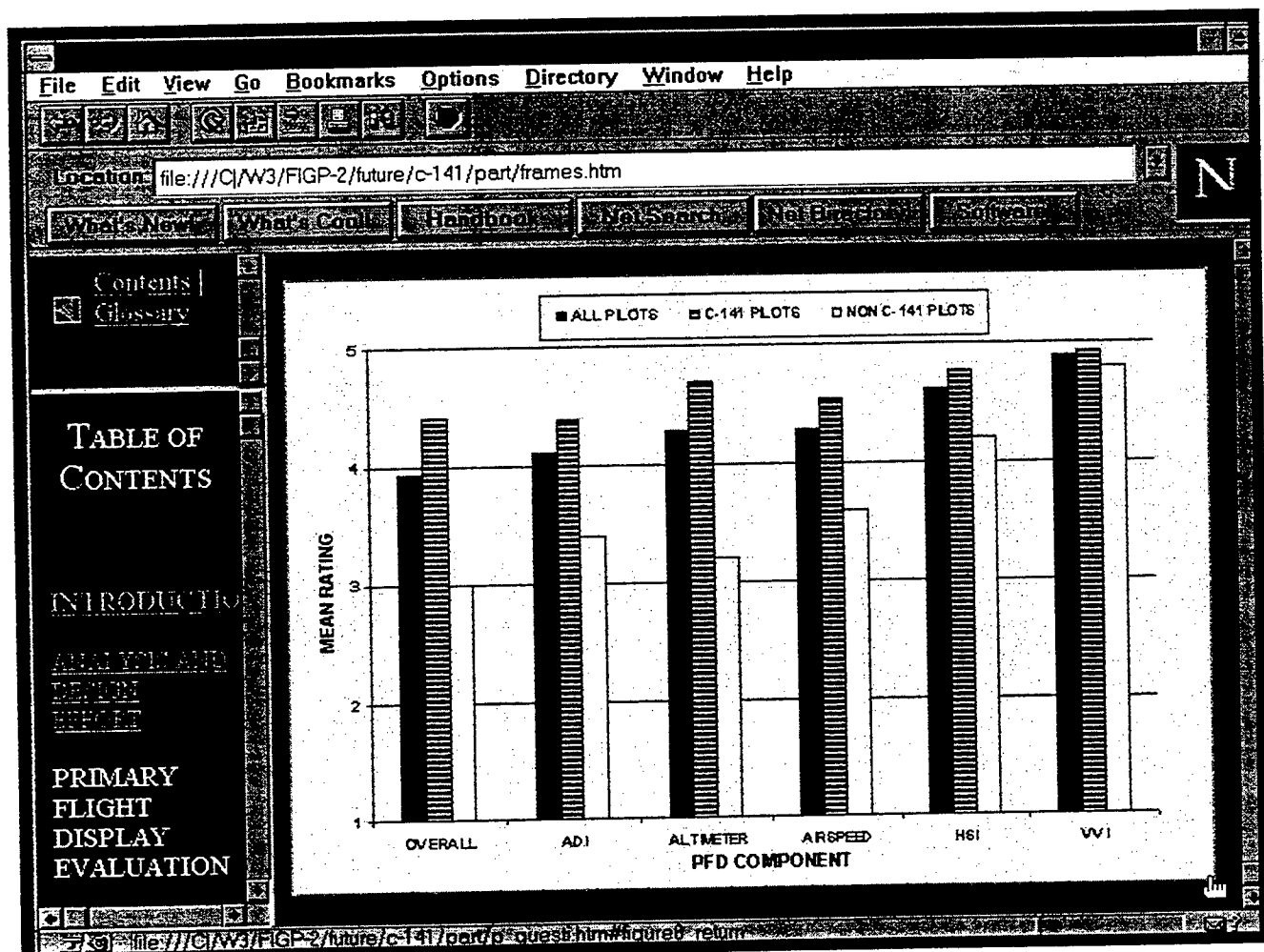


Figure is visible in resized frame.



that resolution. This circumstance is brought about by adhering to the principle that information content and accessibility is more important than aesthetic appearance. It is more important to transmit an image that contains the required information and must be viewed piecemeal through a selective window than it is to make the image look good.

### Directory Structure

The directory structure reflects the hierarchical design of the site. Richer levels of detail are stored in more deeply embedded directories. The back arrow on a page typically links to a page located in the parent directory.

```
/ (FIGP-2)
  art
    current
      display
      design
      assess
      cluster
    future
      c-141
        part
        full
  mrc
```

Global art (art that is used across lines of class) is stored in the /art directory. This includes backgrounds and the back arrow. In this way, it is easy to modify the symbol connected to the definition "up to a higher level". If it is changed it in the /art directory, then all the pages that use that symbol will be modified.

Local art (art that is only used in one class) is stored in the same directory as the referring page. This decision was made on the basis that the art referred by a page is an integral part of that page, and should therefore be stored in the same object as the itself. Multiple art subdirectories for local art were considered, but as they would increase the complexity of the directory structure without providing extra clarity, they were deemed unnecessary. File masks provide the necessary sieve for viewing files of a certain type.

### Aesthetic Design

The most important consideration for aesthetic style was that aesthetic elements of the site should enhance, rather than detract from, the site's accessibility. Colors should

provide adequate contrast between text and background for easy reading. Design schemes could vary from area to area to aid cognitive differentiation between those areas; yet, the site as a whole should maintain an overriding consistency. Currently the entire site shares a similar color scheme, with dark backgrounds and bright contrasting text to aid in readability.

## **Future Improvements**

The original author spent five weeks on this project. In that time, an acceptable first draft was created, but some technical aspects of the site require further improvements. These improvements should be accomplished before making any contextual extensions to the site.

Suggested technical improvements include:

- changing all tables currently stored in graphical format to HTML <TABLE>s
- re-formatting C-141 glossary pages using the HTML definition list tags

```
<DL>
  <DT>term
  <DD>definition
</DL>
```

(The glossary pages are currently formatted with <TABLE>s. It is more correct for a glossary to be formatted with definition tags.)

- add mailto <HREF>s to as many authors' names as feasible
- ASC numbers still have to be added to many images and some reports

## R e s o u r c e s

### A Beginner's Guide to HTML

<http://www.ncsa.uiuc.edu/General/Internet/WWW/HTMLPrimer.html>

### Carlos' FORMS Tutorial

<http://robot0.ge.uiuc.edu/~carlosp/cs317/cft.html>

### Extensions to HTML 2.0

[http://www.netscape.com/assist/net\\_sites/html\\_extensions.html](http://www.netscape.com/assist/net_sites/html_extensions.html)

### HTML 2.0 Specification — T. Berners-Lee MIT/W3C, D. Connolly

<http://www.cis.ohio-state.edu/htbin/rfc/rfc1866.html>

### A Quick Review of HTML 3.0

<http://www.w3.org/pub/WWW/Arena/tour/contents.html>

# Appendix A

## Sample HTML Source

/current/display/design/contents.htm

```
<!
  FIGP-2 Web Site
  Matt Temple
  June 1996
>

<BODY
  BACKGROUND = ".../.../.../art/black.jpg"
  BGCOLOR = "000000"
  TEXT = "#ffffff"
  LINK = "#00ffff"
  VLINK = "#008080">

<BASE
  TARGET = "window_subject">

<A HREF = ".../display.htm" TARGET = "_parent"><IMG SRC =
  ".../.../.../art/triangle.gif"></A>
<FONT SIZE = 4>Advanced Cockpit Display Criteria</FONT>
<HR>

<P>
<CENTER>
  <FONT SIZE = 5>
    T<FONT SIZE = 4>ABLE OF</FONT> C<FONT SIZE = 4>ONTENTS</FONT><BR>
  </FONT>
</CENTER>

<P>
<FONT SIZE = 3>
  <A HREF = "title.htm">Title</A><BR>
</FONT>

<P>
<FONT SIZE = 4>
  <A HREF = "intro.htm">INTRODUCTION</A><BR>
</FONT>

<P>
<FONT SIZE = 4>
  DESIGNING THE TOOL<BR>
</FONT>
<FONT SIZE = 3>
  <UL>
    <LI><A HREF = "background.htm">Background</A><BR>
    <LI><A HREF = "theory.htm">Theory</A><BR>
    <LI><A HREF = "tooldesc.htm">Tool Description</A><BR>
    <LI><A HREF = "dirstruc.htm">Directory Structure</A><BR>
```

```
<LI><A HREF = "modules.htm">FontTool Modules</A><BR>
<UL>
    <LI><A HREF = "symbole.htm">Symbol Editor</A><BR>
    <LI><A HREF = "file.htm">File</A><BR>
    <LI><A HREF = "options.htm">Options</A><BR>
    <LI><A HREF = "analysis.htm">Analysis</A><BR>
    <LI><A HREF = "tools.htm">Tools</A><BR>
    <LI><A HREF = "quit.htm">Quit</A><BR>
</UL>
</UL>
</FONT>

<P>
<FONT SIZE = 4>
    TESTING AND DEVELOPMENT OF FONTTOOL<BR>
</FONT>
<FONT SIZE = 3>
    <UL>
        <LI><A HREF = "object.htm">Objective</A><BR>
        <LI><A HREF = "initdvlp.htm">Initial Tool Development</A><BR>
        <LI><A HREF = "metricsa.htm">Metrics and Methods</A><BR>
        <LI><A HREF = "results.htm">Test Results</A><BR>
    </UL>
</FONT>

<P>
<FONT SIZE = 4>
    <A HREF = "conclude.htm">CONCLUSIONS AND RECOMMENDATIONS</A><BR>
</FONT>

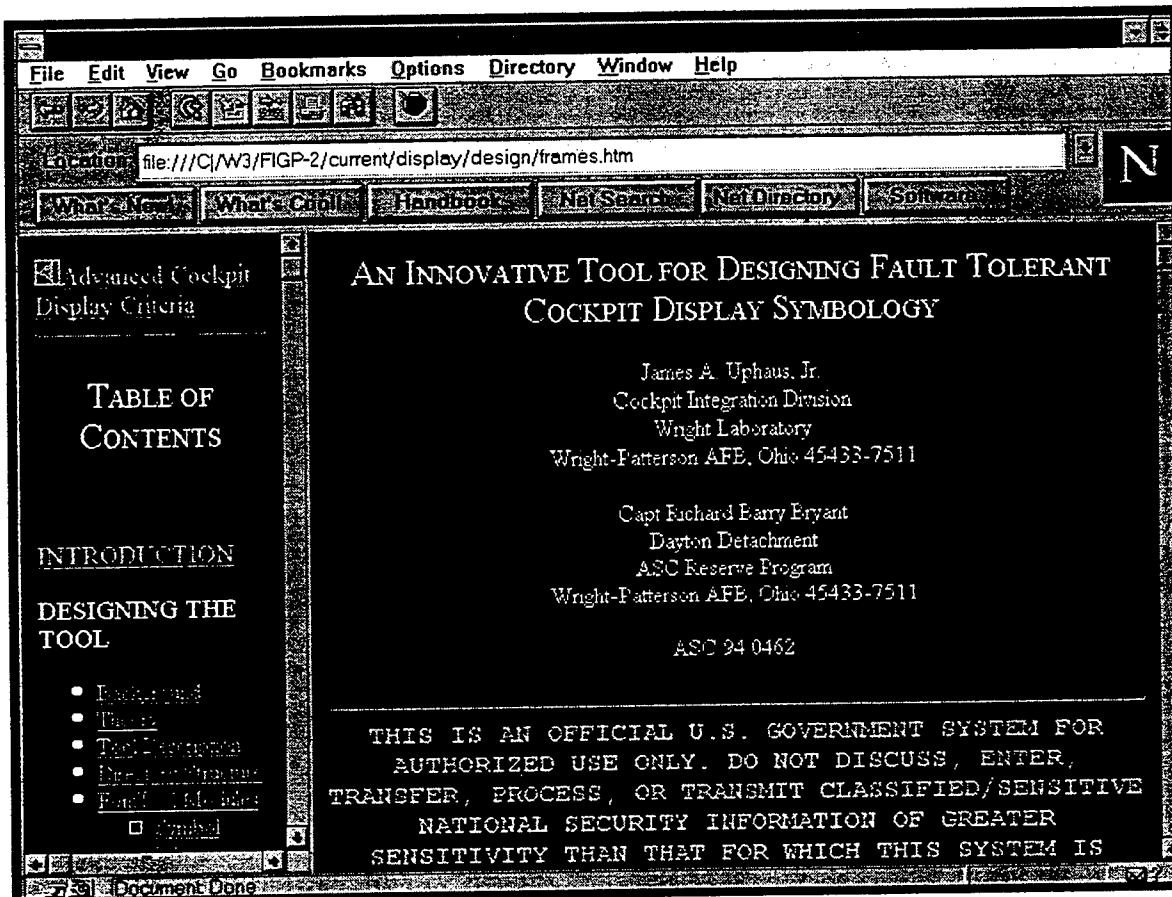
<P>
<FONT SIZE = 4>
    <A HREF = "ref.htm">REFERENCES</A><BR>
</FONT>

<P>
```

# Appendix B

## Sample HTML Rendering

/current/display/design/frames.htm



BANDGAP PROPERTIES OF (100)-GROWN InAs/In<sub>x</sub>Ga<sub>1-x</sub>Sb  
AS A FUNCTION OF GROWTH-INDUCED DISORDER

Jeroen W. Thompson

Beavercreek High School  
2660 Dayton-Xenia Road  
Beavercreek OH 45430

Final Report for:  
High School Apprenticeship Program  
Wright Laboratories

Sponsored by:  
Air Force Office of Scientific Research  
Bolling Air Force Base  
Washington, D.C.

and

Wright Laboratories  
Electromagnetic Material Survivability Laboratory  
Wright-Patterson Air Force Base  
Dayton, OH

August 1996

BAND GAP PROPERTIES OF InAs/In<sub>x</sub>Ga<sub>1-x</sub>Sb  
AS A FUNCTION OF GROWTH-INDUCED DISORDER

Jeroen W. Thompson  
Beavercreek High School

Abstract

InAs/In<sub>x</sub>Ga<sub>1-x</sub>Sb is a useful material for far-IR detectors. While much theoretical work has been done for hypothetical perfect-growth lattices, the growth conditions for InAs/In<sub>x</sub>Ga<sub>1-x</sub>Sb cannot be perfectly controlled. In particular, there is evidence to suggest the bandgap for InAs/In<sub>x</sub>Ga<sub>1-x</sub>Sb undergoes a drastic decrease under random-growth conditions. (100)-grown InAs/In<sub>x</sub>Ga<sub>1-x</sub>Sb is investigated through a Monte Carlo simulation. Our transfer-matrix model calculates a number of possible transitions between the valence and conduction bands of a superlattice with random variations in layer widths, in effect approximating the joint density of states for the superlattice. The joint density is used to propose an effective band gap for disordered InAs/In<sub>x</sub>Ga<sub>1-x</sub>Sb.

## I. Introduction

InAs/In<sub>x</sub>Ga<sub>(1-x)</sub>Sb has been proposed as a useful material in far-IR detectors and has been characterized by several theoretical models. [1] These models, however, rely on the assumption that the superlattice is grown perfectly. Such a lattice is unachievable. This project attempts to clarify the bandgap and cut-off wavelength behavior of InAs/In<sub>x</sub>Ga<sub>(1-x)</sub>Sb under normal growth conditions. A transfer matrix model for InAs/In<sub>x</sub>Ga<sub>(1-x)</sub>Sb is constructed and used in a Monte Carlo simulation of disordered superlattices.

InAs/In<sub>x</sub>Ga<sub>(1-x)</sub>Sb can easily be modeled as a Kronig-Penney potential (using the Envelope Function Approximation as well as the Effective Mass Approximation), with InAs confining electrons and In<sub>x</sub>Ga<sub>(1-x)</sub>Sb confining holes. Allowed eigenstates occur in bands, easily located by solving the Kronig-Penney secular equation:

$$\cos(qd) = \cosh(Kb) \cos(kb) - \frac{\epsilon}{2} \sinh(Kb) \sin(kb)$$

Here  $a$  is the width of the well (InAs in the conduction band and In<sub>x</sub>Ga<sub>1-x</sub>Sb in the valence band,  $b$  is the width of the barrier, and  $d=a+b$ .  $K$  and  $k$  are defined as  $\sqrt{2\mu e/\hbar^2}$  and  $\sqrt{2\mu(U-e)/\hbar^2}$  respectively.  $\epsilon$  is defined as  $K/k-k/K$ . The Brillouin zone ranges between  $q=\pm\pi/d$ .

The Kronig-Penney equation, however, requires a perfectly repeating superlattice. The transfer matrix method can determine the eigenstates for a disordered superlattice. Consider a single barrier opposing an otherwise free electron. The wave equation of the electron on one side of the barrier can be related to the wave equation on the other side, subject to the constraint that the wave equation and its effective mass-weighted derivative be continuous. In matrix form, this can be written as [2]:

$$\begin{pmatrix} A \\ B \end{pmatrix} = \begin{pmatrix} \left( \cosh Kb + \frac{i\epsilon}{2} \sinh Kb \right) e^{ikb} & \frac{i\eta}{2} \sinh Kb \\ -\frac{i\eta}{2} \sinh Kb & \left( \cosh Kb - \frac{i\epsilon}{2} \sinh Kb \right) e^{-ikb} \end{pmatrix} \begin{pmatrix} F \\ G \end{pmatrix}$$

or:

$$\begin{pmatrix} A \\ B \end{pmatrix} = \begin{pmatrix} \alpha + i\beta_1 & i\beta_2 \\ -i\beta_2 & \alpha - i\beta_1 \end{pmatrix} \begin{pmatrix} F \\ G \end{pmatrix}$$

with  $\epsilon \equiv K m_a^*/k m_b^* - k m_b^*/K m_a^*$  and  $\eta \equiv K m_a^*/k m_b^* + k m_b^*/K m_a^*$ . In a superlattice, the coefficients of the wave equation in well  $n$  can be related to the coefficients of the wave equation in well  $n+1$  through barrier  $n$  via transfer matrix

$$P_n \equiv \begin{pmatrix} (\alpha - i\beta_1)e^{ikd} & -i\beta_2 e^{ikd} \\ i\beta_2 e^{-ikd} & (\alpha + i\beta_1)e^{-ikd} \end{pmatrix}.$$

Transfer matrices can relate any two wells:

$$\begin{pmatrix} A_1 \\ B_1 \end{pmatrix} = \prod_{i=1}^n P_i \begin{pmatrix} A_{n+1} \\ B_{n+1} \end{pmatrix}$$

Eigenstates of the superlattice can be determined after imposing the periodic boundary condition:

$$\begin{pmatrix} A_1 \\ B_1 \end{pmatrix} = \begin{pmatrix} A_{n+1} \\ B_{n+1} \end{pmatrix} \text{ and } \begin{pmatrix} A_1 \\ B_1 \end{pmatrix} = M \begin{pmatrix} A_1 \\ B_1 \end{pmatrix} \text{ with } M \equiv \prod_{i=1}^n P_i.$$

This yields non-trivial solutions for  $|M - I| = 0$ .

For numerical reasons, it is desirable to factor the transfer matrices:  $P_i = (\cosh K b_i) p_i$ . Since solutions occur for  $2 = \text{tr } M$ , one can rewrite the determinant equation as

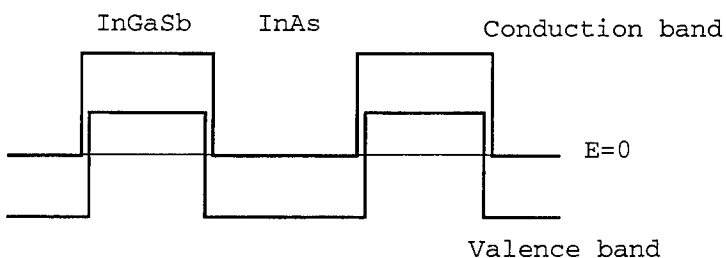
$$\ln 2 = \sum_{i=1}^n \ln(\cosh K b_i) + \ln \left[ \text{tr} \prod_{i=1}^n p_i \right]$$

which, of course, with  $M \equiv \prod_{i=1}^n p_i$  is equivalent to

$$-\sum_{i=1}^n \ln(\cosh K b_i) - \ln(\text{Re } M_{1,1}) = 0,$$

the equation used in this model.

Determining the bandgap for InAs/In<sub>x</sub>Ga<sub>1-x</sub>Sb reduces to solving the Kronig-Penney potential twice. This two band model can be represented schematically through the following type II potential profile. Note that the valence band profile is actually an upside down Kronig-Penney potential for heavy hole states which are confined by the In<sub>x</sub>Ga<sub>1-x</sub>Sb layers.



An electron that absorbs a photon  $\frac{hc}{\lambda}$  will conduct through the

conduction band, leaving behind a heavy hole that conducts through the valence band. Both the electron and the heavy hole, which are governed by similar equations, must have an energy corresponding to an eigenstate in their respective bands.

Strain effects are extremely useful in the optimization of InAs/In<sub>x</sub>Ga<sub>1-x</sub>Sb layer widths and should thus be included in the model. Strain, generated by the indium content in the In<sub>x</sub>Ga<sub>1-x</sub>Sb layers, causes a shifting of band edges and changes in the effective mass of a conduction band electron, which are averaged over the entire lattice for this model. Equations for strain effects and for the effective mass of the coupled light-hole/conduction states are given by [3]. Superlattice constants are given by [1] and interpolated quadratically between GaSb and InSb.

The random layer widths for disordered InAs/In<sub>x</sub>Ga<sub>1-x</sub>Sb were generated using a Gaussian distribution (unless otherwise specified, standard deviation of 3 Å, corresponding to 1 monolayer variation in the growth process) of pseudo-random numbers from a random number generator. The period of the superlattice was held constant. [4]

After determining the eigenstates in the conduction and valence bands, one can determine all possible transitions from the valence band to the conduction band. This is known as the joint density of states (JDOS).

The JDOS will provide the minimum energy needed to cause a transition in the superlattice. This is known as the band gap and corresponds to the cut off wavelength of an infrared detector. However, the band gap energy need not correspond to a large number of non-localized eigenstates. The JDOS plots produced in this project show

virtually no transitions at the band gap, meaning that an infrared detector that conforms to the predicted JDOS will not show appreciable response at the absolute bandgap. A method of determining an effective band gap for disordered superlattices is desired.

## II. Computational Considerations

A number of items are relevant to the computation of the joint density based on the described theoretical model. These include the type and implementation of the random number generator, the ill-conditioning of the transfer matrices, ever-present problems with overflow, and the speed of the computations.

Since this project is a Monte Carlo simulation, a good random number generator (RNG) is necessary to obtain a valid distribution of random numbers. Most, if not virtually all, RNGs that are supplied by system developers display unacceptable properties, so it is necessary to use self-written RNG routines to obtain at least a decent random number distribution. This project utilized the Park-Miller (revised) minimal standard RNG, which yields uniform variates between 0 and 1. The Box-Muller equation  $Z = [\sqrt{-2 \ln(u)}] \sin(2\pi v)$ , given two uniform variates  $u$  and  $v$ , yields Gaussian distributed random numbers, which can be multiplied by the desired standard deviation.

As is well-known, the transfer matrix technique suffers from a large number of numerical difficulties. To begin with, each transfer matrix, and especially the product of the matrices, is ill-conditioned. Ill-conditioning is a term that refers to a matrix whose individual elements are very large but whose determinant is near unity. It is virtually impossible to compute the value of  $|M - I|$  due to the ill-conditioning. However, it is easy to show that determinant of  $M$  is 1, so the previous equation becomes  $2 - \text{tr } M$ , which is easily computable.

Having solved the difficulties with ill-conditioning, it becomes necessary to solve the difficulties of overflow. No analytic method attempted has fully succeeded. A quick glance at the transfer matrices will show two main causes of overflow: the repeated factors of  $\cosh$  and  $\sinh$  and the large values of  $\epsilon$  and  $\eta$  at the top and bottom of the well

(while none of these values may seem particularly large, matrix elements simply on the order of 10 could yield elements on the order of  $10^{40}$  after 40 matrices have been multiplied together). By factoring out a  $\cosh$  from each transfer matrix, the matrix elements are reduced towards unity (applying logarithms on the  $\cosh$  factors ensures their repeated multiplication does not overflow). Factoring  $\varepsilon$  and  $\eta$  is not so simple. However, these will most likely cause overflow only near the top and bottom of the well, areas which can easily be avoided.

Despite the control of overflow, only approximately forty periods can be modeled safely with this transfer matrix technique.

The speed of the computation is extremely slow. Stepping through the energies within the well of the superlattice and checking whether a root has occurred takes far too much time for an extended simulation of multiple lattices to be completed within a few days. However, by recognizing that the eigenstates of a disordered superlattice are related to the eigenstates of a periodic superlattice, one can develop an intelligent guessing routine that will locate a range of energies where eigenstates will be found. For example, assume a superlattice made from alternating well/barrier pairs of widths 40/20 and 45/15 with  $x=.25$ . For the model used, a 40/20 periodic superlattice has a conduction band bounded by 237.7 and 420.9 meV ( $E=0$  at the bottom of the conduction band) and heavy hole band bounded by 105.76 and 105.83 meV. A 45/15 periodic superlattice has a conduction band bounded by 182.1 and 382.9 meV and a heavy hole band bounded by 41.72 and 41.79 meV. Eigenstates for the disordered lattice will therefore lie between 182.1 and 420.9 meV in the conduction band and between 41.72 and 105.83 meV in the heavy hole band. These search regions represent 26% and 10% of their respective band in the averaged 42.5/17.5 case. Thus, search times in this case can be increased by a factor of 4 and 10, respectively. Of course, with more disordered layers and with more disorder within each layer, this increase in speed will not be so great. Even with the speed increases, a simulation of five hundred lattices of forty periods each requires roughly 16 hours to complete on the DECAAlpha used for this project.

With obvious computational difficulties, the possibility of a better theoretical approach becomes more enticing. For instance,

another transfer matrix may allow easier computation. One possibility is provided by [6].

Let  $f(z) \equiv \begin{bmatrix} \Psi(z) \\ \frac{1}{m^*} \Psi'(z) \end{bmatrix}$ . Then  $\frac{df}{dz} = \begin{bmatrix} \Psi'(z) \\ \frac{1}{m^*} \Psi''(z) \end{bmatrix}$ . By the Schrödinger equation,  $\Psi''(z) = k^2 \Psi(z)$  with  $k \equiv \sqrt{\frac{2m^*(V - E)}{\hbar^2}}$ . So,

$$\frac{df}{dz} = \begin{bmatrix} 0 & m^* \\ \frac{k^2}{m^*} & 0 \end{bmatrix} \begin{bmatrix} \Psi(z) \\ \frac{1}{m^*} \Psi'(z) \end{bmatrix} = \Lambda f(z) \quad \text{and} \quad f(z) = e^{\Lambda z} f(0). \quad \text{Thus,}$$

$$f(z) = \begin{bmatrix} \cosh(kz) & \frac{m^*}{k} \sinh(kz) \\ \frac{k}{m^*} \sinh(kz) & \cosh(kz) \end{bmatrix} f(0). \quad \text{Since } z=0 \text{ is arbitrary, this}$$

equation can relate the wave function and its derivatives at one end of a layer (with this equation a layer is either a well or a barrier. In the well, the transfer matrix can be written in terms of cosines and sines.) to the other end of the layer. After applying the periodic boundary condition, a familiar equation emerges:  $2 - \text{tr } M = 0$ .

This transfer matrix suffers from the usual numerical difficulties. However, it does have a significant advantage of the previous transfer matrix in that no complex arithmetic is used in this approach, allowing higher precision numbers in the computation. In fact, this transfer matrix will allow over several hundred periods to be computed at a time without the use of natural logarithms. However, modeling over sixty periods will cause serious problems with root detection in the valence band.

Transfer matrix methods not investigated in this project are also provided by [5].

### III. Results

Sixteen Monte Carlo simulations of five hundred, forty layer disordered superlattices were completed. All possible transitions between the conduction band and the valence band were computed. (Forty transfer matrices will generally yield forty roots in each band, for a

total of 1600 transitions per superlattice.) A stack histogram should give an approximate shape of the JDOS for a real-growth superlattice.

The data were plotted in a consistent manner. First, the stack widths (resolution) are always 1 meV. For clarity the stacks were plotted as points. Stacks of zero height were not included. The total area of all the stacks were normalized to an arbitrary constant, allowing a more direct comparison between graphs. Please note that at higher energies, transitions other than LH1 to C1 will become significant. Thus, the graphs shown are the most accurate at energies near the band gap energy.

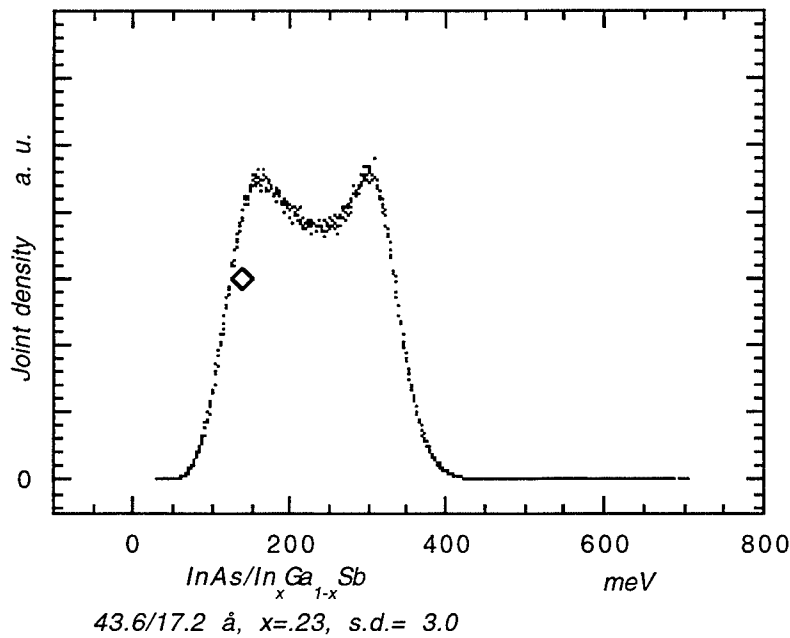


Fig. 1

This graph demonstrates the main characteristics found in all the simulations so far. The Urbach tail at low energies and the double maximum appear in all the simulations (the double maximum is, of course, a remnant of the original JDOS for a perfect-growth superlattice). A  $\diamond$  has been placed on the graph at the band gap energy for a perfect-growth superlattice with the same widths. As is immediately apparent, the band gap for the disordered superlattice (29.5 meV) is nowhere in the vicinity of the band gap for the periodic case (137.3 meV). Such a variation in band gap, and therefore in the cutoff wavelength, is

unacceptable for infrared detectors and shows the need for studies similar to this one. However, it is also apparent that the optical response near the band gap energy is very nearly zero. A detector that conforms to the JDOS shown will not show any appreciable response at wavelengths corresponding to the band gap energy. Thus, an effective band gap is desired.

A few possibilities for defining an effective band gap immediately present themselves. First, a certain percent of the total area underneath the curve may yield the location of an effective band gap. For instance, starting at the zero of energy, 1% of the total area of the graph is reached at 92 meV or  $13 \mu$ . If one desires to detect only wavelengths  $< 13 \mu$ , then longer wavelengths should contribute no more than 1% of the total possible signal. 1% percent is, however, an arbitrary number and some other percentage may more accurately reflect the needs and capabilities of experimentalists and the industry. Secondly, one can fit a straight line to the graph between the Urbach tail at low energies and the first maximum. This line yields two reasonable choices for an effective band gap: first, the energy at which it intersects the x-axis and second, the halfway point between the tail and the maximum. The proposed choices for an effective band gap are summarized in a table on page 13.

For completeness, a few other graphs are shown here.

The graph in Figure 2 is qualitatively very similar to the first graph. Notice how closely the band gap approaches zero meV.

The graph in Figure 3 is qualitatively very similar to the others. This time, however, the absolute band gap is negative. This implies that the disorder creates a conduction band lower in energy than the valence band. The model used in this simulation does not apply to such a case, when charge redistribution becomes important. Nonetheless, only a very few transitions occur below the zero of energy (less than 4E-3 % of the total transitions) so it is hoped that only a few localized eigenstates occur below the valence band energies. Such a case should not significantly affect the validity of this model for the given superlattice.

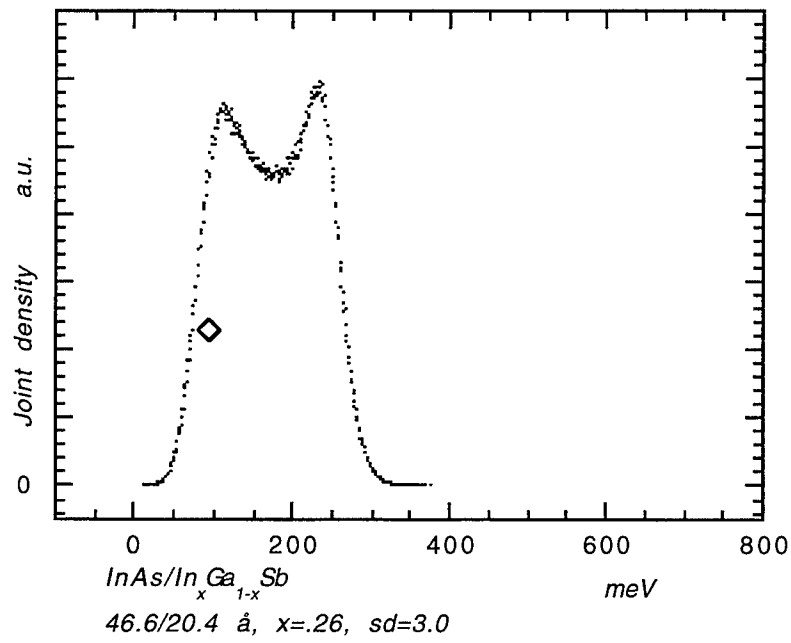


Fig. 2

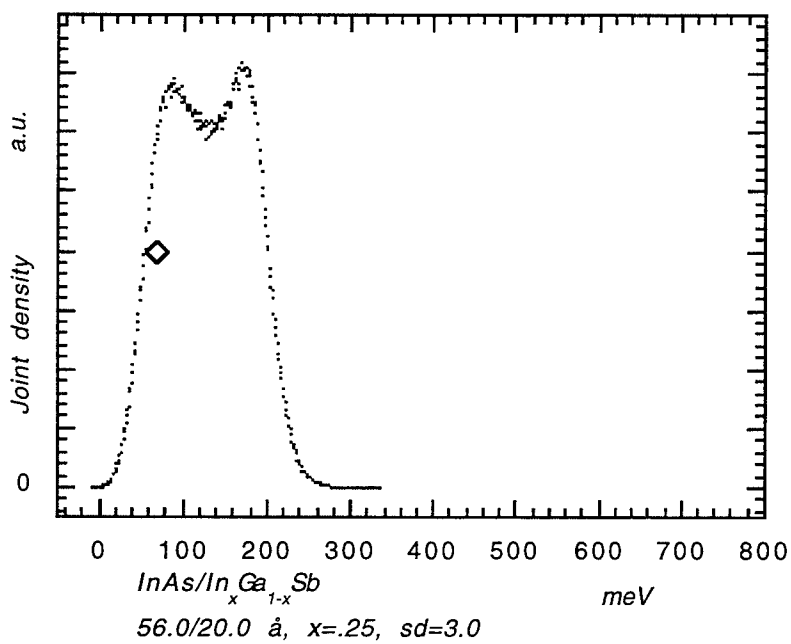


Fig. 3

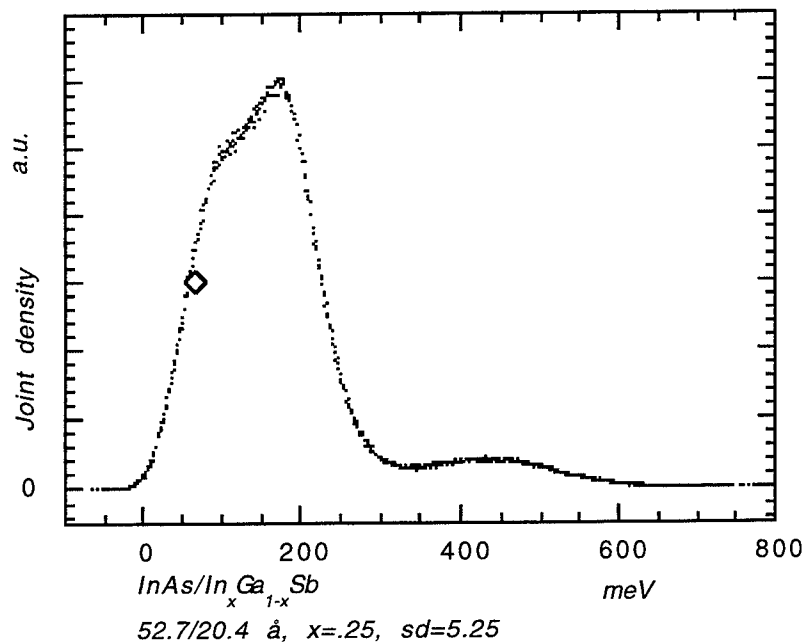


Fig. 4

This simulation used nearly twice the degree of disorder (slightly less than two monolayer standard deviation per layer. This should still be within normal growth conditions) as the other simulations shown. The graph displays a much more significant response in the negative band gap regime, suggesting that this model is inadequate to describe band gap effects at higher disorder.

The following table summarizes the results of the simulations. The column names are interpreted as follows: "Absolute" - the absolute band gap. "Strt. Line" (Straight line) - the intersection with the x-axis of a straight line fit to the first rise. "1%" - the energy at which 1% of the total response has occurred. "Line mdpt" - the midpoint of the straight line fit. "10%" - the energy at which 10% of the total response has occurred. "Perfect" - the expected band gap for this model for a perfect-growth superlattice with the given widths. "1st Max" - the energy corresponding to the first maximum in the JDOS. All units are meV.

InAs/In(x)Ga(1-x)Sb	Absolute	Strt.Line	1%	Line mdpt	10%	Perfect	1st Max
43.6/17.2, x=.23	29.5	76.9	91.5	119	132.5	137.3	161
46.6/20.4, x=.26	12.5	48.3	59.5	80	91.5	95.3	111
56.0/20.0, x=.00	89.5	129.1	137.5	158	165.5	171.0	186
56.0/20.0, x=.05	68.5	106.9	115.5	138	144.5	150.0	169
56.0/20.0, x=.10	55.5	85.5	94.5	115	123.5	129	145
56.0/20.0, x=.15	34.5	64	73.5	94	163.5	108.0	123
56.0/20.0, x=.20	13.5	43.2	52.5	75	82.5	87.5	107
56.0/20.0, x=.25	-7.5	23.3	33.5	55	63.0	67.5	87
52.7/20.4	-----	-----	-----	-----	-----	-----	-----
x=.25, sd=2.0	16.5	46.4	54.5	67	76.5	76.2	87
x=.25, sd=2.5	0.0	39.5	48.0	65	74.5	76.2	90
x=.25, sd=3.0	-17.0	31.1	42.0	62	72	76.2	92
x=.25, sd=3.5	-34.0	23.8	35.5	60	69.0	76.2	97
x=.25, sd=3.75	-42.0	20.5	32.5	62	69.2	76.2	103
x=.25, sd=4.25	-60.0	16.1	27.0	60	68.0	76.2	104
x=.25, sd=4.75	-47.5	10.5	24.0	54	67.1	76.2	98
x=.25, sd=5.25	-66.5	5.7	19.5	52	66.7	76.2	98

With constant well and barrier widths, the mole fraction of indium and the disorder within the superlattice can be seen as independent variables.

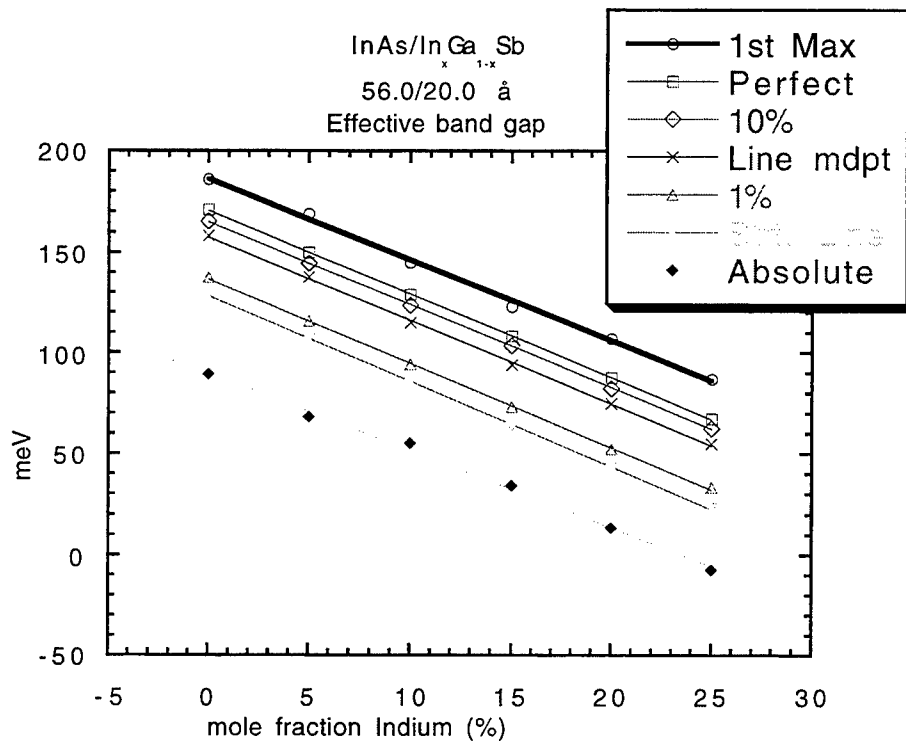


Fig. 5

This graph shows the proposed effective band gaps. A linear fit has been applied. All the lines are very nearly parallel and show the main features of the JDOS decreasing with very nearly the same constant of proportionality. This implies that disorder-induced effects and indium-induced effects are not related.

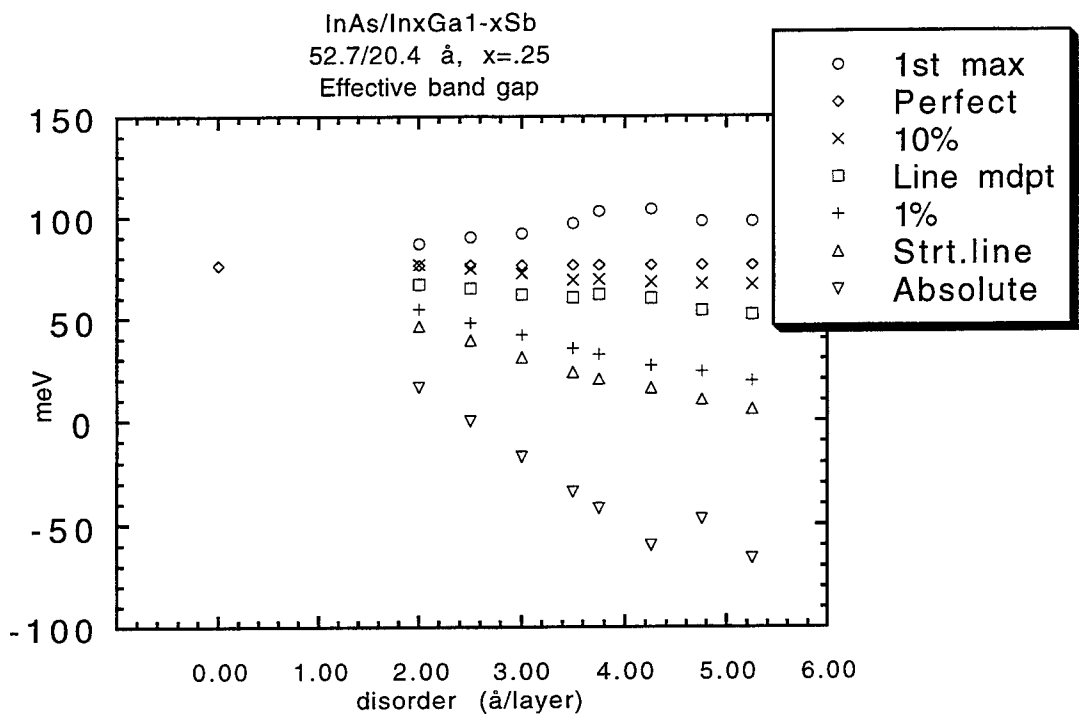
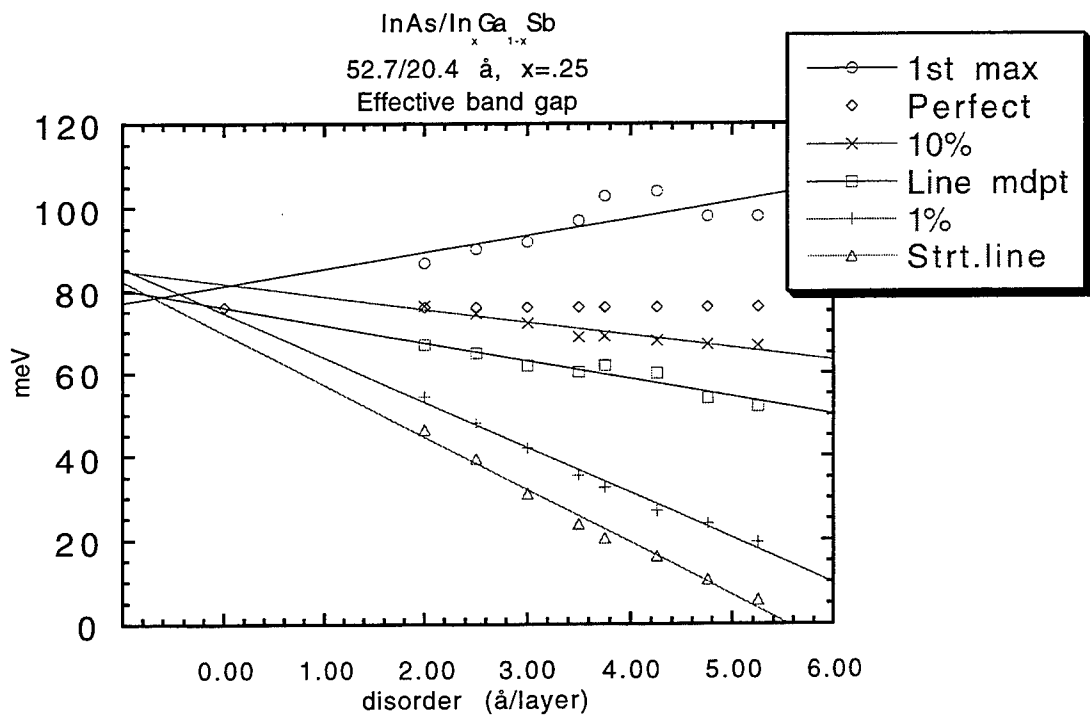


Fig.6

Figure 6 shows the effects of increasing the disorder in a superlattice. The absolute band gap points have been removed to produce Fig. 7, which better shows the features of the other points.



A linear fit has been applied. All the lines, extrapolated to the zero disorder case, show at least reasonable agreement with the theoretical result for a perfect-growth superlattice. However, since only the absolute band gap and the "1st max" lines should pass through the perfect-growth point, it is unclear from this graph alone whether any of the proposed effective band gaps is more realistic than the others.

#### IV. Conclusions and Recomendations for Further Study

Several possibilities for determining an effectived band gap have been proposed. For a (100)-InAs/In<sub>x</sub>Ga<sub>1-x</sub>Sb superlattice with constant disorder, it is seen that increasing the indium content will shift the effective band gap linearly as the band gap shift for the perfect growth superlattice, implying that disorder-induced effects and indium-induced effects are not related. Increasing the amount of disorder in the superlattice yields no conclusive result regarding an effective band gap. A study of the relative absorption of the superlattice at the various eigenstates should give a better indication of the location of the effective band gap. Other theoretical models should improve the accuracy of these results, especially in the negative band gap regime.

#### V. Acknowledgements

The author would like to gratefully acknowledge Dr. Pat Hemenger for sponsoring this project, Dr. Frank Szmulowicz for advice, encouragement, and supervision, as well as AFOSR and Wright Labs for the opportunity to participate in the HSAP program.

#### VI. References

- [1] see, for example, E.R. Heller, K. Fisher, F. Szmulowicz, and F.L. Madarasz, "Superlattice Parameters for Optimum Absorption in InAs/In<sub>x</sub>Ga<sub>1-x</sub>Sb Superlattice Infrared Detectors", J.Appl.Phys. 77, 5739 (1995).

- [2] E. Merzbacher, *Quantum Mechanics* (Wiley, New York, 1970).

[3] F. Szmulowicz, E.R. Heller, K. Fisher, and F.L. Madarasz, "Optimization of Absorption in InAs/In<sub>x</sub>Ga<sub>1-x</sub>Sb Superlattices for Long-Wavelength Infrared Detection", *Superlattices and Microstructures*, Vol. 17, No. 4, 373 (1995).

[4] M. Lakrimi, T.A. Vaughan, R.J. Nicholas, N.J. Mason, & P.J. Walker, "Long Wavelength Photoresponse of Short Period InAs/GaSb Superlattices".

[5] L. Pavesi and F.-K. Reinhart, "Transfer Matrix Method to Compute Energy Levels of Superlattices", *Phys Status Solidi b157*, 615 (1990).

[6] Perng-fei Yuh and K.L. Wang, "Formalism of Kronig-Penney Model for Superlattices of Variable Basis", *Phys.Rev.B* 38, 13307.

INTERIM QUALIFICATION TESTING OF TUNG 5 MOD 6

Jonathan D. Tidwell

Rocky Bayou Christian School  
2101 N. Partin Dr.  
Niceville, FL 32578

Final Report for:  
High School Apprentice Program  
Wright Laboratory

Sponsored by:  
Air Force Office of Scientific Research  
Bolling Air Force Base, DC

and

Wright Laboratory

August 96

## INTERIM QUALIFICATION TESTING OF TUNG 5 MOD 6

Jonathan D. Tidwell  
Rocky Bayou Christian School

### Abstract

Tung 5 Mod 6 was studied; in particular, its sensitivity characteristics were determined using certain standardized tests such as the Henkin time-to-explosion test, the Impact Sensitivity test or Drop Hammer test, the Friction Sensitivity test, the Accelerating Rate Calorimeter (ARC) test, the Large Scale Gap Test (LSGT), and the Electrostatic Discharge (ESD) test. These qualitative tests showed the sensitivity of Tung 5 Mod 6 to heat, friction, impact, electrostatic discharge.

## INTERQUALIFICATION TESTING OF TUNG 5 MOD 6

Jonathan D. Tidwell

### Introduction

Scientists at the High Explosive Research and Development (HERD) facility are developing high explosives approaching the density of steel with the purpose of implementing them into hard target penetrators. An explosive that can penetrate deeply into a hard target without premature ignition is desired. The high density of the explosive would enable the bomb to penetrate into a target deeper than before with a relatively smaller volume. The new explosive, called Tung 5, is a mixture of Tungsten (W), TNT, HMX, and Aluminum. The ingredient which gives the explosive its density is the W. In an effort to decrease sensitivity, modifications were made to Tung 5 including the addition of OD-2 wax. The final formulation, called Tung 5 Mod 6, is composed of 84.25% W, 8.00% TNT, 3.00% class 3 HMX, 3.00% 2 $\mu$  HMX, 1.00% 1401Al, and 0.75% OD 2 wax. Sensitivity testing of Tung 5 Mod 6 is required to give a ranking of sensitivity among other explosives thus enabling the handlers to know the precautions that they need to take when handling the explosive.

### Methodology

The Henkin time-to-explosion Test was the first sensitivity test conducted on Tung 5 Mod 6. The purpose of the Henkin time-to-explosion test is to determine the heat sensitivity of an explosive by showing the maximum temperature at which run-away reactions will not occur; meaning that there will still be reactions occurring, but none will cause a steady-state reaction.

Much time and work is involved in sample preparation. Chunks of HE are ground in a mortar and pestle, then sieved through a number 20 to 50 sieve to give a constant particle size range. Two hundred-fifty-milligram samples of the powder are then transferred into aluminum tubes and capped. Because only 15% of the formulation is explosive, this weight is adjusted. The standard weight used for the test is 40 to 50 mg. The tests require 40 to 50 mg of explosive, as opposed to 40 to 50 mg of material. To obtain the desired explosive weight, the 40 to 50 mg was divided by the percent explosive in Tung 5 Mod 6 resulting in the 250 mg value. Using a Carver press and die, the samples were pressed to 240 psi and crimped at 140 psi to create a seal in the tube.

The Henkin apparatus is an insulated kettle filled with Woods' metal, a low-melting bath composition. A sample is placed into the raised lid of the bath, immersed into the bath, and timed until a reaction occurs or until 2000 seconds has expired. If no run-away reaction, usually indicated by a loud pop, occurs in 2000 seconds, the test is stopped and the run is recorded as a no-go. The times and temperatures of each run-away reaction are recorded in a special notebook.

The next test conducted on Tung 5 Mod 6 was the friction sensitivity test. To run the test, a sample of approximately 100 mg of Tung 5 Mod 6 powder is placed on a ceramic plate. An arm holds a ceramic pestle above the sample. The arm is lowered so that the pestle is resting on the explosive, and a specified weight is

attached to the end of the arm. The ceramic plate then moves to and fro one time, causing the ceramic pestle to run back and forth across the sample, thus creating friction. A reaction occurs if a flash is visible, a pop is heard, a discoloration is seen, or a smell is detected. This test is valuable to handlers because it tells them the necessary precautions to take when handling the explosive.

The Large Scale Gap test (LSGT) was conducted on Tung 5 Mod 6 to determine its sensitivity to shock. The detonator, donors, and HE used were the RP-2 Explosive Bridgewire Detonator (EBW), Pentolite, and Tung 5 Mod 6 housed in an NOL tube, respectively. The donor and detonator are placed on top of the charge with a specific number of PMMA cards (one card equals .01 inch) placed in between. This assembly is then placed on a steel witness plate. The criteria for a "go" is a visible hole in the steel witness plate. The tests are continued by the Bruceton Up-Down method until the PMMA thickness is altered by one or two cards to obtain the opposite result of the previous "go" or "no-go".

The Drop Hammer test or Impact Sensitivity Test was conducted on Tung 5 Mod 6 to determine the sensitivity of Tung 5 Mod 6 to impact. The testing apparatus consists of a 200.5 cm measuring device and a pulley connected to a wire connected to a magnet which adjusts the height of the magnet. The magnet holds a 5-kg drop hammer. The hammer is raised to specified heights and then, by turning the magnetic field off, is dropped onto an anvil resting on top of the sample. The sample rests on a piece of sandpaper and is placed onto a platform in the drop hammer system. Before the test is started, the apparatus must be calibrated by testing five inert salt samples. The amplitude of sound produced by each test is recorded by a sound graph. The average amplitude of the five samples is multiplied by three to determine the "go/no-go" line. If a "no-go" is achieved, the drop hammer height is raised; if a "go" is achieved, the hammer height is lowered, according to the Bruceton Up-Down method.

The Electrostatic Discharge (ESD) test was conducted to determine the electrostatic shock sensitivity of Tung 5 Mod 6. To test the explosive, an electric shock is sent through the sample explosive to see if the material reacts. A reaction, or "go", will produce a visible reaction or detectable odor. If only a small spark is produced, the test is considered a "no-go". To prepare the samples, Tung 5 Mod 6 was ground into a powder in a number 20 to 50 sieve. About twenty-five ESD sample cup holders are filled to three-quarters full (about 30 - 40 mg) with the powder. The samples are then placed onto the platform of the testing apparatus. A needle is adjusted so that the tip of it is just brushing the top of the explosive and then raised four units above the sample. After setting the needle height, the energy level applied to the sample is set by adjusting the capacitance level of the capacitors which are connected to the 5 kilovolt machine.

The Accelerating Rate Calorimeter test or ARC test was run on Tung 5 Mod 6 to determine its thermal stability. In this test, approximately 800 mg of Tung 5 Mod 6 powder is placed into a tiny "bomb" which is then placed into the ARC oven. The sample is subjected to a constant rise in temperature which is measured by thermocouples placed around the inside of the oven and close to the sample. The thermocouples not next to the sample control the thermostat until an exothermic reaction is observed in the sample. At this point, the

thermocouple next to the sample becomes the controller. The heat is then raised gradually until a run-away reaction takes place, and the sample is completely decomposed.

### Results

The results of the Henkin test show that the critical temperature of Tung 5 Mod 6 is  $230 \pm 2^\circ\text{C}$ . These results show that Tung 5 Mod 6 is thermally stable. The testing results are shown in Figure 1.

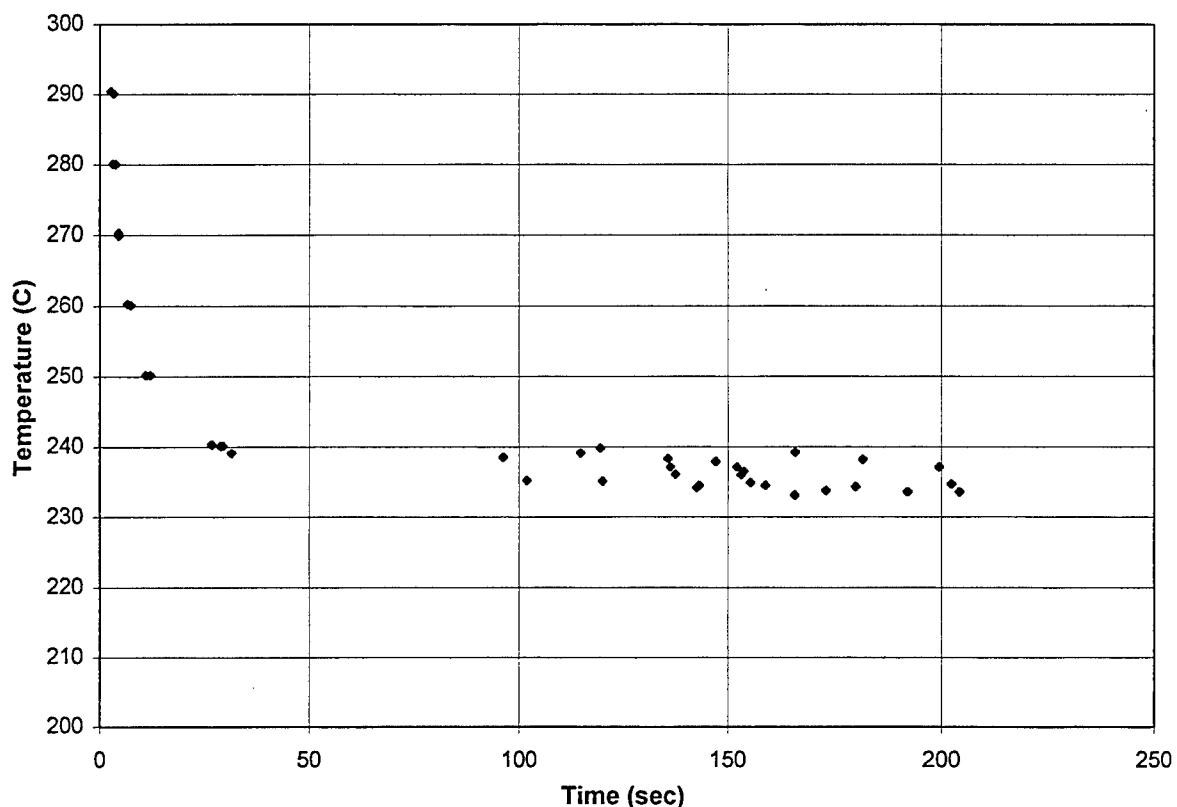


Figure 1: Henkin Results

The Drop Hammer test results show that Tung 5 Mod 6 has an H 50% point of 150.7 cm. The testing results are shown in Table I.

**Table I: Drop Hammer Results**

TRIAL #	HEIGHT (cm)	RESULT	TRIAL #	HEIGHT (cm)	RESULTS
1	161.8	NO GO	14	130.6	NO GO
2	200.5	GO	15	161.8	GO
3	161.8	NO GO	16	130.6	NO GO
4	200.5	GO	17	161.8	GO
5	161.8	GO	18	130.6	GO
6	130.6	NO GO	19	105.4	NO GO
7	161.8	GO	20	130.6	NO GO
8	130.6	NO GO	21	161.8	NO GO
9	161.8	NO GO	22	200.5	GO
10	200.5	GO	23	161.8	GO
11	161.8	GO	24	130.6	GO
12	130.6	NO GO	25	105.4	NO GO
13	161.8	GO			

The results of the Friction Sensitivity test show that Tung 5 Mod 6 is highly insensitive to friction stimuli. Each test produced a definite "no-go". This gives an idea of the relative insensitivity of Tung 5 Mod 6 to friction. These results are shown in Table II.

**Table II: Friction Sensitivity Results**

Shot	Weight(kg)	Optical	Sound	Odor	Color
1	24	N	N	N	N
2	36	N	N	N	N
3	36	N	N	N	N
4	36	N	N	N	N
5	36	N	N	N	N
6	36	N	N	N	N
7	36	N	N	N	N
8	36	N	N	N	N
9	36	N	N	N	N
10	36	N	N	N	N
11	36	N	N	N	N

The results for the ESD test can be seen in Table III below. The electrostatic sensitivity of Tung 5 Mod 6 is greater than .25 Joules. This literally means that Tung 5 Mod 6 has a static discharge sensitivity between 1.25 Joules and .25 Joules, but for convenience, the standard notation is: ESD > 0.25 Joules.

**Table III: Electrostatic Sensitivity Results**

<b>TEST #</b>	<b>ENERGY SETTING</b>	<b>RESULTS</b>
1	12.5 Joules	GO
2	6.25 Joules	NO-GO
3	6.25 Joules	GO
4	1.25 Joules	NO-GO
5	1.25 Joules	NO-GO
6	1.25 Joules	NO-GO
7	1.25 Joules	GO
8	.25 Joules	NO-GO
9	.25 Joules	NO-GO
10	.25 Joules	NO-GO
11	.25 Joules	NO-GO
12	.25 Joules	NO-GO
13	.25 Joules	NO-GO
14	.25 Joules	NO-GO
15	.25 Joules	NO-GO
16	.25 Joules	NO-GO
17	.25 Joules	NO-GO

The results of the LSGT can be seen in Table IV below. The cards denote the number of PMMA cards and the Kbar represents the pressure value derived from the number of PMMA cards. The tests show that the addition of the OD-2 wax in Tung 5 Mod 6 decreased its shock sensitivity when compared to that of Tung 5. Tung 5 Mod 6 had a shock sensitivity of 34.9 Kbar while the value for Tung 5 was 28.8 Kbar.

**Table IV: LSGT Results**

<b>Cards</b>	<b>Kbar</b>	<b>Results</b>	$\rho$	Avg $\rho$	Std Dev ( $\rho$ )
200.00	20.7	No Go	7.07	7.13	0.07
175.00	18.0	No Go	7.24		
162.50	33.1	No Go	7.13		
159.25	34.4	No Go	—		
157.75	34.9	Go	7.09		
156.25	35.8	Go	7.09		
150.00	38.9	Go	7.22		
100.00	57.1	Go	7.09		

The results of the Accelerating Rate Calorimeter test (ARC) show that Tung 5 Mod 6 is thermally stable. The temperature of the maximum self-heating rate was 238.6°Celsius. Results are shown in Figures 2 and 3.

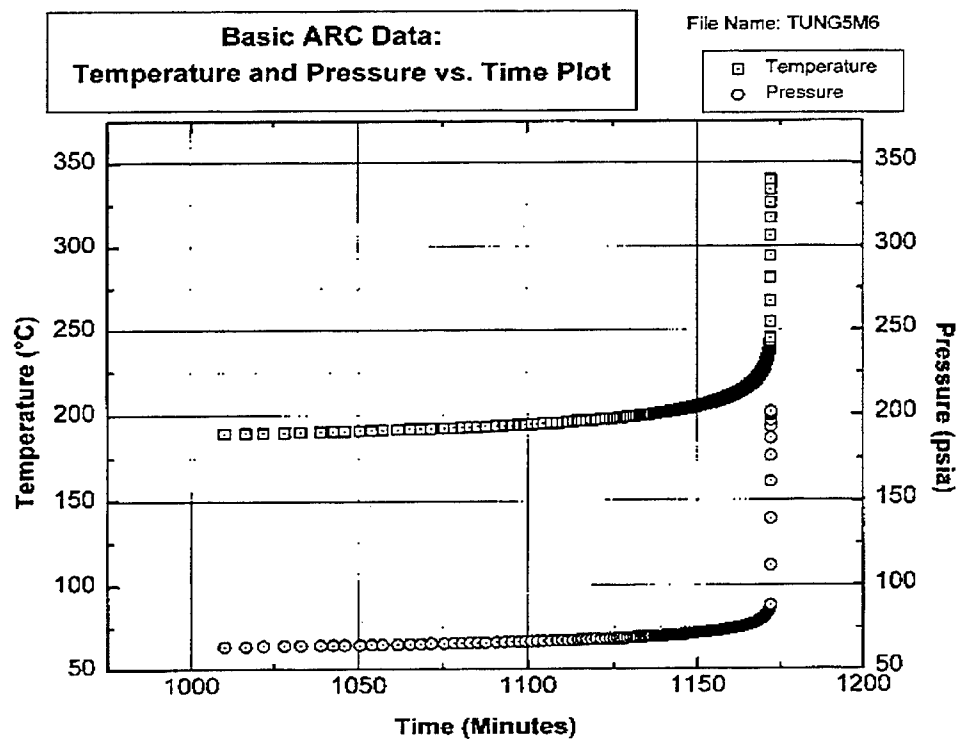


Figure 2: Temperature and Pressure vs. Time

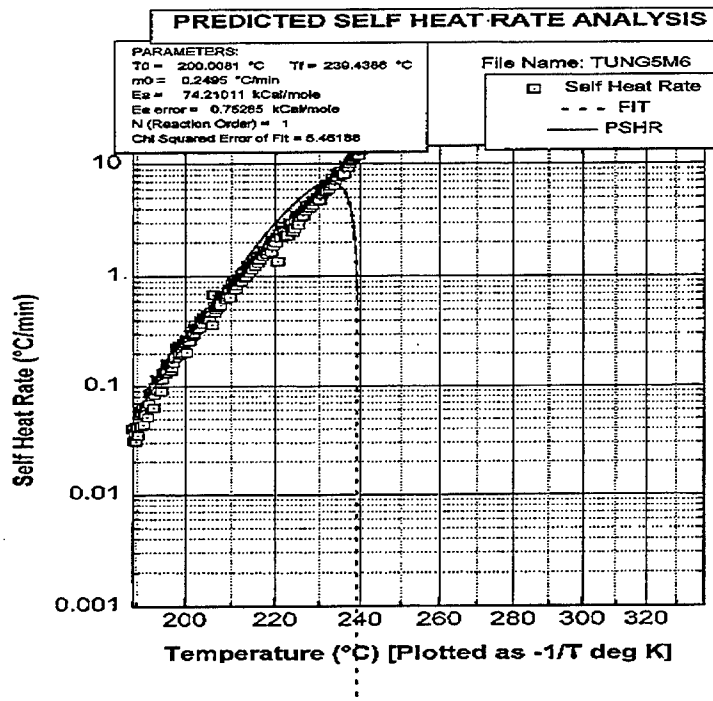


Figure 3: ARC Self-heating Rate

### Conclusion

From the results of the sensitivity characterization tests, it was determined that Tung 5 Mod 6 was very insensitive to the different external stimuli such as friction, heat, and static discharge. The test results also show that the addition of the OD 2 wax into Tung 5 decreased its sensitivity. Further characterization tests are still to be conducted on Tung 5 Mod 6. The results of the sensitivity characterization tests have enabled explosive processors to scale up, meaning that they can process Tung 5 Mod 6 in larger quantities. Tung 5 Mod 6 is safe to handle.

## **Hydrocode Support Development**

**Joshua A. Weaver**

Niceville High School  
800 East John Sims Parkway  
Niceville, FL 32578

Final Report for:  
High School Apprenticeship Program  
Mentor : Mike Nixon  
WL/MNMW  
Wright Armament Laboratory  
Eglin AFB

Sponsored by:  
Air Force Office of Scientific Research  
Bolling AFB  
Washington DC

and

Wright Armament Laboratory  
Eglin AFB

August 1996

## **Hydrocode Support Development**

Joshua A. Weaver  
Niceville High School

### **Abstract**

While projectile design and experimentation are critical to the Air Force's development, limitations require the most economical use of scarce resources. For this reason, much of the actual research and development of modern munitions is conducted through computer simulations, saving the cost of building and physically testing new designs. Unfortunately, many of these tools interact with their users through primitive interfaces, relics from the entirely text-based days of computer operating systems. While these programs are still fully functional and beneficial, a more sophisticated interface would maximize productivity while eliminating many of the common user errors through automation.

Graphical User Interfaces (GUIs) were developed in Visual Basic for two programs in common use in Computational Mechanics section of WL/MNMW. Moments is a simple utility program that calculates standard information for axisymmetric projectiles. The EPIC hydrocode dynamically simulates projectile impact scenarios and is the most heavily used program in Computational Mechanics.

## **Introduction**

While projectile design and experimentation are critical to the Air Force's development, limitations require the most economical use of scarce resources. For this reason, much of the actual research and development of modern munitions is conducted through computer simulations, saving the cost of building and physically testing new designs. Unfortunately, many of these tools interact with their users through primitive interfaces, relics from the entirely text-based days of computer operating systems. While these programs are still fully functional and beneficial, a more sophisticated interface would maximize productivity while eliminating many of the common user errors through automation.

Graphical User Interfaces (GUIs) were developed in Visual Basic for two programs in common use in Computational Mechanics section of WL/MNMW. Moments is a simple utility program that calculates standard information for axisymmetric projectiles. The EPIC hydrocode dynamically simulates projectile impact scenarios and is the most heavily used program in Computational Mechanics.

## **Project 1 - Visual Basic**

Visual Basic was determined to be the optimum language for the development of the GUIs. This selection was based upon the relatively minor level of programming expertise needed to create sophisticated programs. In order to offer support for Windows 95 and NT, the latest version of Visual Basic (Visual Basic version 4.0) was requested and used for all programming tasks.

In addition to the support for Windows 95 and NT, version 4.0 of Visual Basic also provided new programming features and a slightly altered programming environment. The first week of this summer was spent reviewing the language structure and learning the new features. Additionally, time was spent teaching and offering advice to Dann Holmes, a second apprentice working jointly on the GUI design process for EPIC, who had never been exposed to structured programming.

## **Project 2 - Moments**

In the summer of 1982, the utility program MOMENT was written to quickly calculate the weight, center of gravity location and the polar and transverse mass moments of inertia for axisymmetric projectiles. MOMENT would load the projectile's information, stored as text in a separate file, and would output a line drawing of the projectile and its calculations.

Finding that this arrangement complicated the design process, many users asked for an updated version of MOMENT. Three summers ago, my first task at Wright Laboratory was to incorporate the conveniences found in more modern programs into a GUI for MOMENT. Moments, as the GUI was called, combined the text-based input data into the same screen as the graphical output and result calculations, simplifying the revision and modification process. Last summer, Moments was completely rewritten to incorporate a more sophisticated programming style that featured a memory management scheme optimized for low-memory computers.

This summer's revision of Moments focused primarily on generating a version optimized for Windows 95 and Windows NT. The easiest way to accomplish this was by updating the program code to Visual Basic version 4.0, which includes automatic support for 32-bit operating systems (Windows 95 and NT).

Additionally, the documentation for Moments was updated to reflect all of the modifications made. Full-featured installation disks were made to help automate the installation process. Because Visual Basic is an interpreted language, it requires a substantial run-time library of supporting files that must be located in various directories in the Windows hierarchy. The installation program manages the placement of the files into their proper directory.

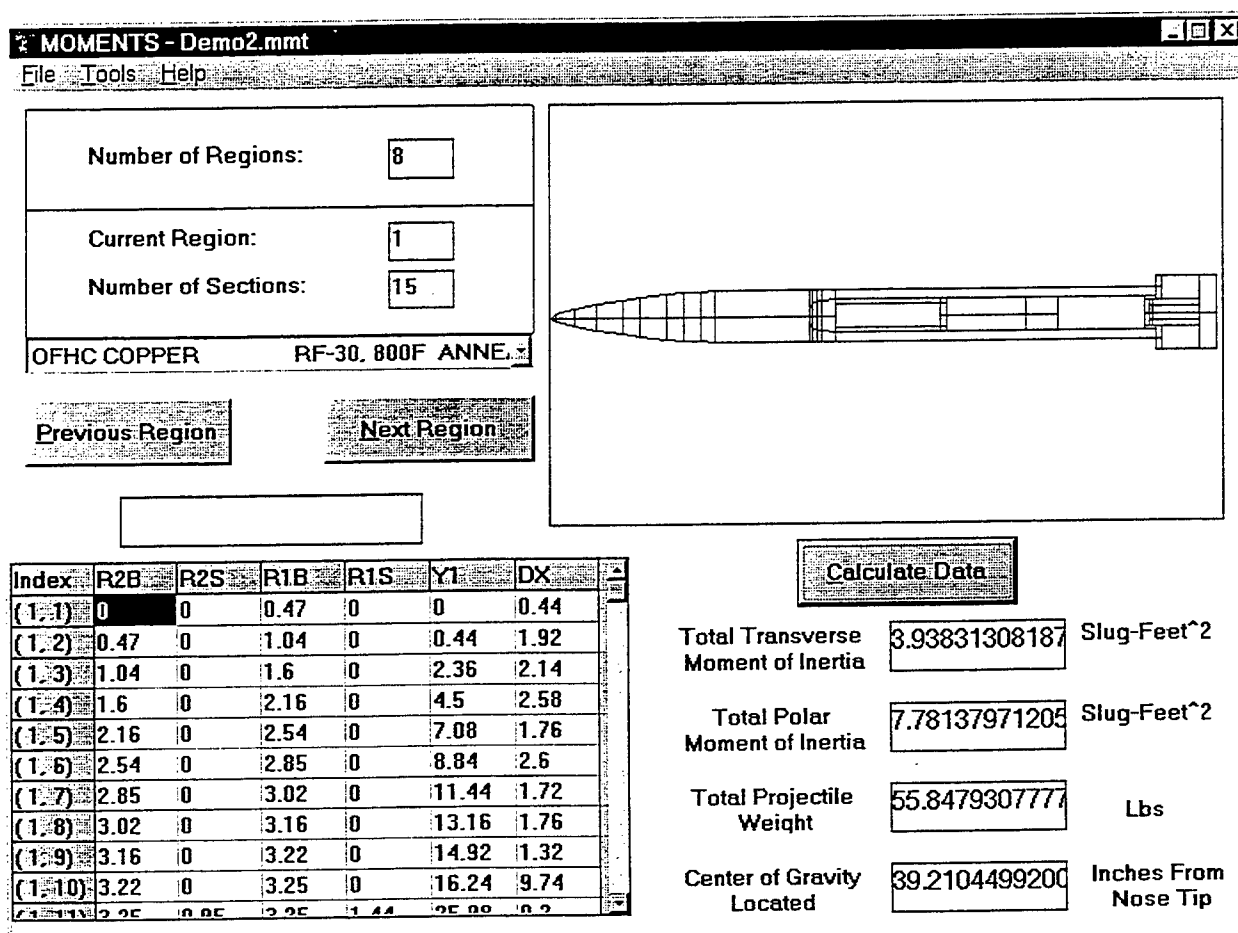


Figure 1. Main window of Moments 96 Graphical User Interface which combines the text-based input, projectile simulation, and result calculation into one easy to use interface.

### **Project 3 - GUI design of EPIC**

EPIC is a FORTRAN program that dynamically simulates the impact, penetration, and blast of a warhead penetration scenario. The computations evaluated in the 130,000 lines of code are derived from Lagrangian finite-element formation where the equation of motion is directly integrated rather than using a traditional stiffness matrix.

EPIC, like many large FORTRAN programs of its era, stores variable configurations in a text-based description file. To create these input files, the user is required to adhere to strict spacing and numbering formats to meet the FORTRAN input syntax. While this format is not difficult to follow, it induces a high user error rate -- an extra character can invalidate an otherwise perfect data-file. Automating the file's creation would eliminate this problem.

In addition, the user needs to have a working understanding of a 300-page manual to design a moderately complex simulation run. For a novice user, designing even a simple simulation takes many hours. Modifying an existing simulation is also time consuming, even for an experienced user. To make this design process more efficient, much of the complexity could be hidden behind a sophisticated, user-friendly interface.

In order to remove these problems, a GUI was designed to automate the EPIC input-file construction for a single-penetrator impact scenario. The construction process was completed in four stages -- General GUI Considerations and Goals, Version 1 (AEPP), Version 2 (FEMP), Version 3 (EPEG).

#### **General GUI Considerations and Goals**

Developing the user interface is naturally the most important aspect of designing a graphical user interface. Creating the visual objects and programming the interface is a completely different aspect of the project than logically sequencing the interaction between the user and the program. For that reason, the goals of the GUI were identified before the actual project began.

The primary goal of the EPIC GUI was to create an environment that would allow a novice user of EPIC to quickly design a complicated projectile impact simulation. In addition, the GUI would also be capable of allowing the user to modify existing EPIC input files through the same user-friendly interface. By automating the input file creation, the GUI would also eliminate the simple typos made by rushing users.

The GUI development was a joint project between myself and the other Computational Mechanics HSAP, Dann Holmes. We shared the development tasks until I left on vacation, at which point Dann took over finalizing the project.

#### **Version 1 (AEPP)**

The first version of the GUI, called AEPP - Another Epic PreProcessor, was designed as a dynamic test of our ability to read and modify the FORTRAN formatted input files. The visual interface was a direct model of the EPIC data structures, mirroring the format of the input file into text boxes on the screen. This version eliminated the need for the user to directly create the input file and thus removed the possibility of creating a typing mistake.

```

$TYPE CASE....DESCRIPTION OF PROBLEM.....  

 2 1  

$GEOM PRNT SAVE NSLD NMAS NRST NRIG NCHK NOCK SCATpcRTZ SPLT DP3 UNIT//// PER  

 6 0 1 2 0 0 0 0 0 0000 0 0 0 0 0  

$MATEL 0 DAM FAIL DFRC EFAL solids from library  

 1 0 1 1 1.0999.0  

14 0 1 1 1.0999.0  

$Blank for end of materials  

$Begin of Projectile data  

$ X/RSCALE YSCALE ZSCALE X/RSHIFT ZSHIFT ROTATE SLANT X/RO ZO  

 1.0 1.0 1.0 0.0 0.0 0.0 0.0 0.0 0.0  

$ ROD NODES  

$ 2 NOR NIR NPLN RAD AX CROS JOIN N1 NTOP ZTOP ZBOT EXPAND  

 2 4 0 5 1 0 1 0 1 0 60.0 55.0 1.0  

$ ROTOP RITOP ROBOT RIBOT  

 6.0 0.0 4.0 0.0  

$ ROD NODES  

$ 2 NOR NIR NPLN RAD AX CROS JOIN N1 NTOP ZTOP ZBOT EXPAND  

 2 4 0 35 1 0 1 1 37 0 55.0 20.0 1.0  

$ ROTOP RITOP ROBOT RIBOT  

 4.0 0.0 4.0 0.0  

$ ROD NODES  

$ 2 NOR NIR NPLN RAD AX CROS JOIN N1 NTOP ZTOP ZBOT EXPAND  

 2 4 0 10 1 0 1 1 343 0 20.0 10.0 1.0  

$ ROTOP RITOP ROBOT RIBOT  

 4.0 0.0 4.0 0.0  

$NOSE NODES  

$ 3 TYPE NOR NIR RAD AX CROS//// N1//// ZTOP ZMIN  

 3 3 4 0 1 0 1 429 10.0 0.0  

$ ROTOP RITOP  

 4.0 0.0  

$Blank for end of Projectile

```

Figure 2. The top of a sample EPIC input file. The formatting is crucial for proper input to be achieved.

The data in EPIC input files (see Figure 2) is stored as numerical text delimited through a specific spacing which must be adhered to for the data to be properly evaluated. In order to manipulate this data, since Visual Basic cannot directly read data in this format, two procedures were created to convert strings of FORTRAN formatted text into Visual Basic variables -- FRead and FWrite.

While this interface does handle the typing errors, it does not make the actual design and construction process any easier for the user to construct the basic parts of a projectile (objects). For that reason, a second version of the interface was designed which features a friendly interface to the object construction.

### Version 2 - (FEMP)

In the second version of the GUI, called FEMP – First Epic Meta-Preprocessor (There were not any other EPIC preprocessors), the focus was on designing a user-friendly interface for creating objects. The same Input/Output routines were used that were found in the first version, but the display interfaces were completely rewritten. Rather than just mirroring the data-file format, the lowest-level interfaces were replaced with a more user-friendly interface. Unfortunately, even though the interface allows the user to design moderately complex objects, representing the connectivity used to bind these objects into the main simulation Region (Penetrator, Target) proved to be impossible.

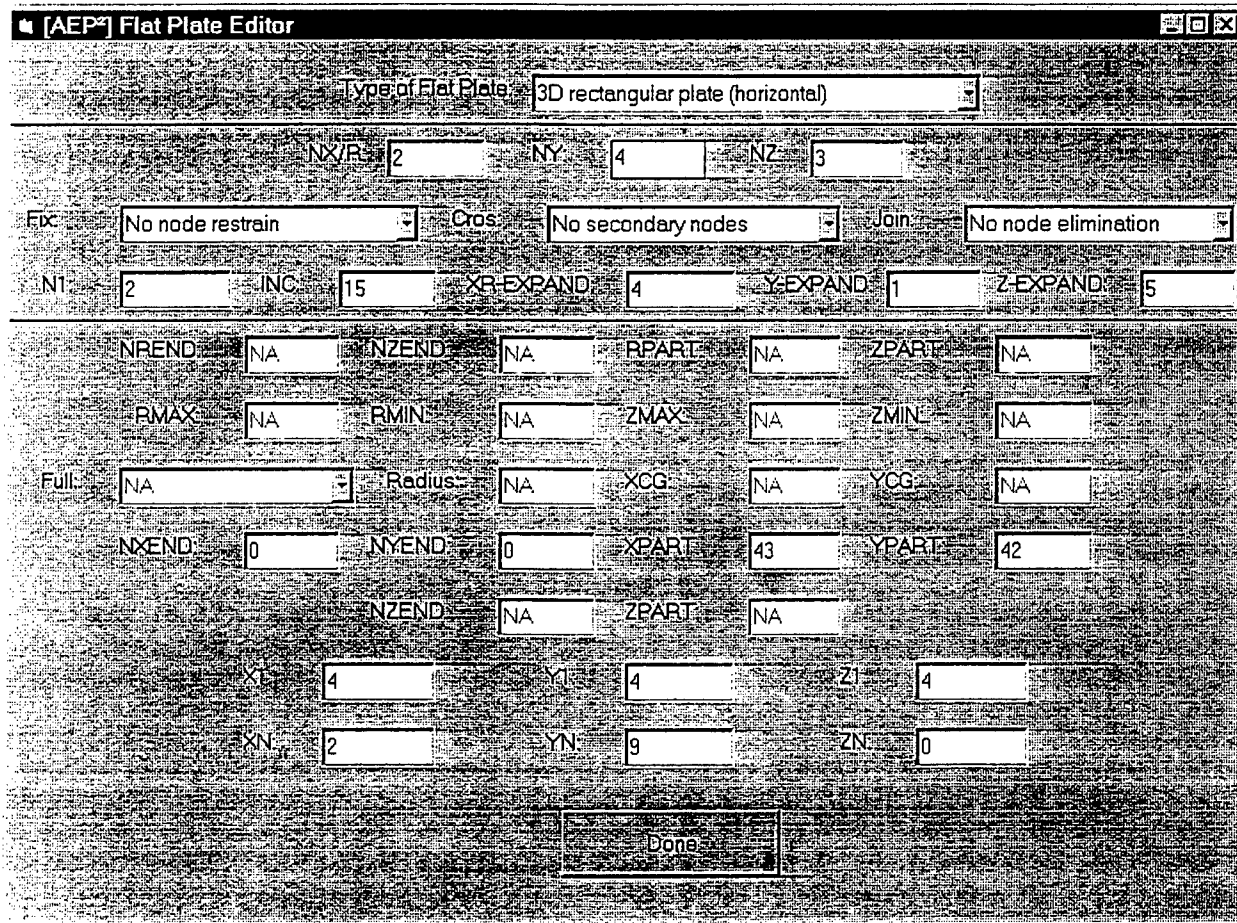


**Figure 3.** Original AEPP interface screen for designing a Flat Plate object. In this version, the interface was a direct model of the format of the input file. Depending on the type of flat plate selected, the proper options would become available for the user to input data into.

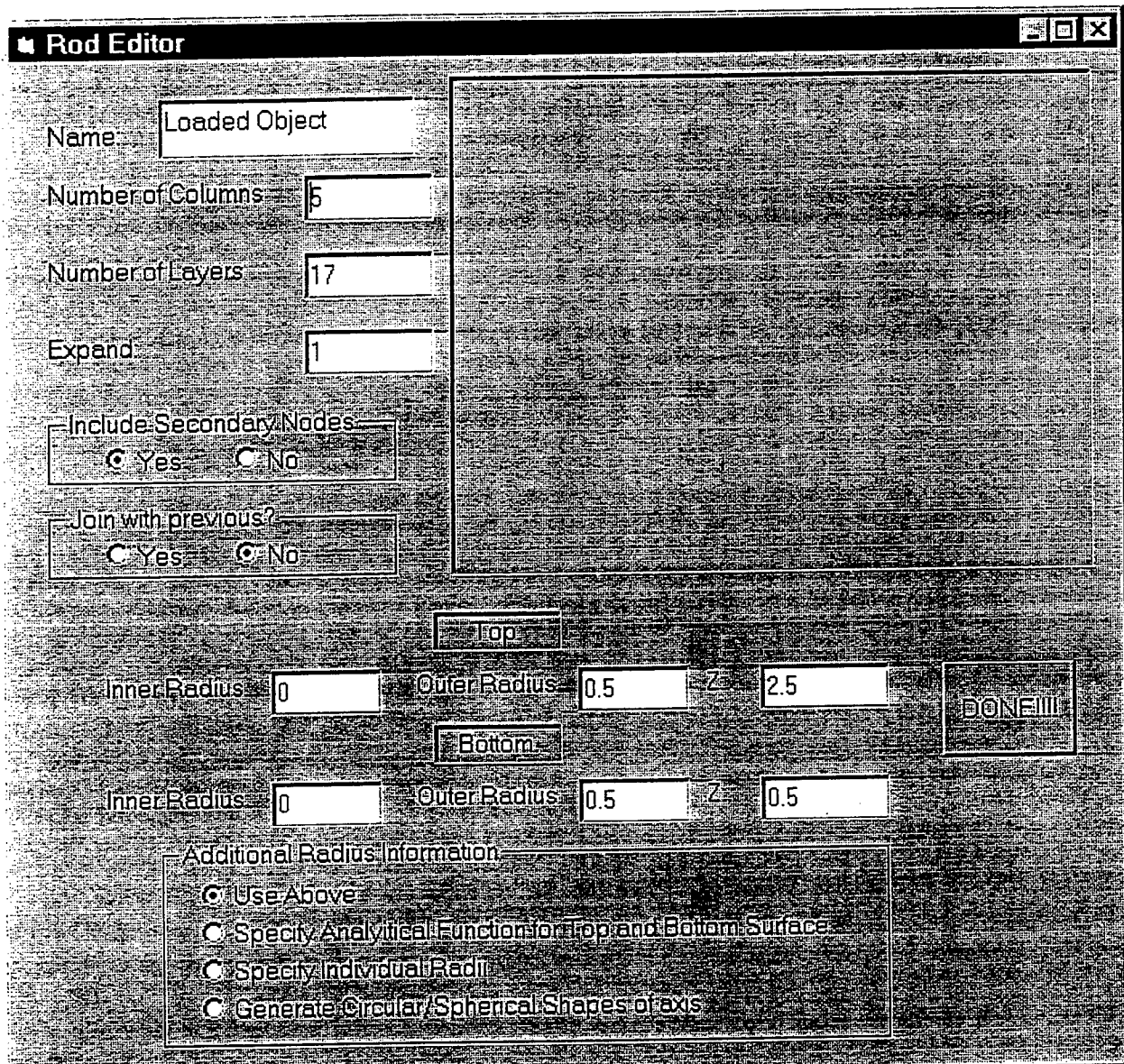


Figure 4. The main interface screen for designing a rod object in FEMP, where the design goal was to create a friendly interface. To accomplish this, the complexity of the data file was hidden behind multiple interface screens which would appear only as needed options were requested.

### **Version 3 - EPEG**

In order to further simplify the design process, Version 3 (EPEG - EPIC Penetration Event Generator) of the interface was written. In this case, the user is limited to a single ‘scenario’ of projectile simulation. While this limits the applicability of the program to a specific instance, it gives the user interface the maximum ability to provide comprehensive help to the user.

During the design phase of version 3, I left on my vacation and Dann Holmes took over development of EPEG. It represents the current state of the program, with future modifications planned for the addition of extra simulation scenarios and the inclusion of multiple minor features.

Aaron B. Wilson's report was not available at the time of publication.

PRE AND POST MICROSTRUCTURE DAMAGE  
ANALYSIS OF TUNG 5 MOD 6

Tuan P. Yang

WL/MNME  
Energetic Materials Branch  
High Explosive Research and Development Facility

Final Report for:  
High School Apprentice Program  
Wright Laboratory

Sponsored by:  
Air Force Office of Scientific Research  
Bolling Air Force Base, DC

and

Wright Laboratory

August 1996

PRE AND POST MICROSTRUCTURE DAMAGE  
ANALYSIS OF TUNG 5 MOD 6

Tuan P. Yang

Abstract

The goal of this investigation was to document explosives of pre and post test procedures using density tests and microstructural analysis. As specified in the title, Tung 5 Mod 6 was the explosive of choice to be studied. However, another explosive, PBXN-109 was also incorporated into the polishing and density tests. These samples were sectioned off and analyzed. Documentations were made in polishing, density measurements and microscope analysis. These procedures contributed to the overall identification of the extent of microstructure damages in each specimen.

The first step taken in this procedure was to section the samples into workable pieces. The sample preparation involved designing a device to hold the explosives while they were being polished and coding the samples to know the exact location from which they were extracted.

Polishing was the next step in the procedure. It was done in the presence of water to minimize frictional heating. The polishing medium used was sandpaper that varied from an initial 320 grit to a final 8000 grit. The latter grit was used for a more polished texture than the smaller grits. The purpose in polishing the explosive was to remove any damages caused during cutting operations.

Pictures were taken of the samples before and after they were polished. Equipment used was a stereomicroscope equipped with a 35mm camera and a scanning electron microscope (SEM). These pictures helped in validating the topography of the explosives before and after polishing.

## PRE AND POST MICROSTRUCTURE DAMAGE

### ANALYSIS OF TUNG 5 MOD 6

Tuan P. Yang

#### Introduction

As a continuation of last summer's project titled "Microstructure Analysis of PBXN - 110 to Determine Void Volume Fraction and Particle Distribution", this project involves the thorough analysis of Tung 5 Mod 6 in one test configuration and of PBXN-109 in another. Tung 5 Mod 6, developed at the High Explosive Research and Development Facility, was the fifth mix of the tungsten based explosive with its sixth modification. These analyses will be carried out prior to and after testing of this to document the type and extent of damage the external strain stimuli has on the explosive component. The test was called the Shear Punch test and damages were caused between the interaction of the explosive and the steel punch. The steel punch would penetrate through the explosive.

Tung 5 Mod 6 was subjected to a 'Shear Punch Test,' which is designed to determine the behavior of an explosive under an unconfined shear loading. PBXN-109, the other explosive studied in this project, was subjected to the 'Bulk Modulus Test.' This test was specifically designed to provide a volume displacement for a given pressure. Samples will be taken from the post test charge mainly for cataloging the change in microstructure due to hydrostatic loading. Pre and post test samples were polished and analyzed with a stereomicroscope equipped with a 35mm camera and a Scanning Electron Microscope. These analyses will be used to catalog the changes in microstructure due to no confinement in one case and hydrostatic loading in the other.

#### Methodology

PBXN-109 is composed of sixty-four percent RDX, twenty percent aluminum, and sixteen percent plastic binder. Two cylindrically-shaped castings were made with this explosive that were six inches long

and four inches in diameter. One cylinder was sent to the OTI test range for the bulk modulus test while the other was used for pretest analytical procedures such as polishing, density tests, and photographic analysis.

The cylinder was cut radially to afford one-half inch thick sections from the top, center and bottom. Two cubes each, one from the center and one from the outside edge, were cut from each section. Each cube was given a special code designated to document its location in the original cylinder.

These cubed samples were then prepared for polishing. A device was designed to hold two of the cubes in place so they would be sanded across a flat surface, as well as result in ninety degree angles. The cubes were placed in the device such that one-fourth of an inch of the explosive could be removed. This will remove any damage imposed on the specimen during cutting operations and also allow one to view the internal matrix and not just the surface.

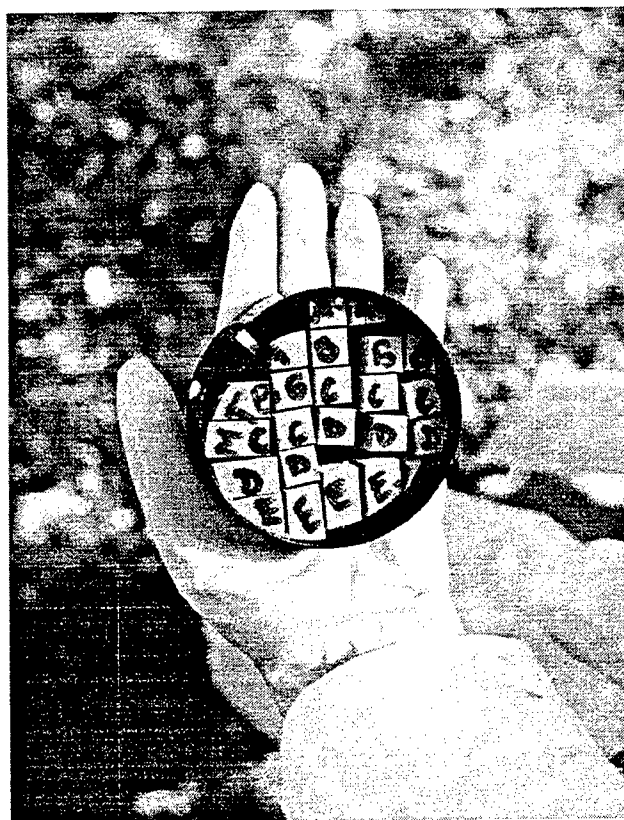


Figure 1 Cubed Samples of PBXN-109

Polishing operations were carried out in the presence of water to minimize frictional heating. The grit of the sandpaper ranged from an initial 320 to a final 8000. The latter was of a finer texture therefore producing a smooth, glass-like, polished surface. The polishing motion involved moving the specimen in the form of a figure eight to ensure that the samples were both polished with the same pressure and at the same time maintaining a perfect edge.

After the samples were polished, they were coated with an anti-static cream, and subjected to several different procedures for determining the densities of the specimen. Theoretical maximum density (TMD) for PBXN-109 was calculated to be 1.65 g/cc. The samples were first measured geometrically : length, width, and height and weighed for its mass. They were measured several times due to the elasticity of the explosive. These values were then averaged and used along with the mass in the calculation of the density by dividing mass by volume.

The Penta-Pycnometer was another density procedure incorporated. The pycnometer utilizes helium gas to penetrate into the porous surface of the material inside the cell. After calibration, the only input data fed is the mass of the cube. The output data are the volume displacement value and the density. Eight experiments were carried out on each sample to determine the precision of the experiment. The readings were then calculated into a standard deviation number with a precision technique.

The Mettler Water Density displacement procedure was also used. In this procedure, the specimen is immersed into a water filled beaker that rests upon a Mettler balance. The sample first rests in a gem holder while its mass is being weighed. The balance is then re-zeroed and the sample is immersed into the beaker. At this time another reading will come up. Along with the temperature readings, they are carried through a series of calculations resulting in the density. All of the density values from the three procedures were then placed into a chart and compared with TMD of PBXN - 109. Since the pycnometer density procedure will afford a density value that excludes the volume of the open porosity and the Mettler procedure does not, it should be possible to subtract the potentially lower Mettler value from the potentially higher pycnometer value and qualitatively account for the open porosity in each cube.

After the density tests, the samples were then photographed using two different cameras. First,

a 35mm camera was used for close-up pictures, then the samples viewed with the stereomicroscope equipped with a microcam that provided pictures up to a magnification of eighty times. Finally, samples were sputter coated and analyzed using a scanning electron microscopy (SEM). Five pictures were taken of each sample, each with increasing magnification. The SEM pictures provided a superior view of the matrices which aided in the analysis.

The other explosive to undergo these same procedures was Tung 5 Mod 6, which is composed of 84.25% Tungsten powder, 8% TNT, 6% HMX crystals, 1% Aluminum powder, and .75% wax. It was subjected to the Shear Punch test which involves firing a steel rod at a statically mounted piece of unconfined explosive. The rod will induce a shear motion into the explosive. Pieces from the shear induced region were recovered and polished. Since the SEM was out of operation for this analysis, other analytical procedures were used. Rough sketches were made of the views obscured with the stereomicroscope. Millimeter rulers were attached to the side of the specimen to aid in estimating the sizes of the crystals and voids. Analysis and conclusions were then formed based on these sketches. The pre-test specimens underwent the same polishing technique and analyses as PBXN-109

## Testing

### **Shear Punch Test Diagram**

## Pure Shear Impact Experiment

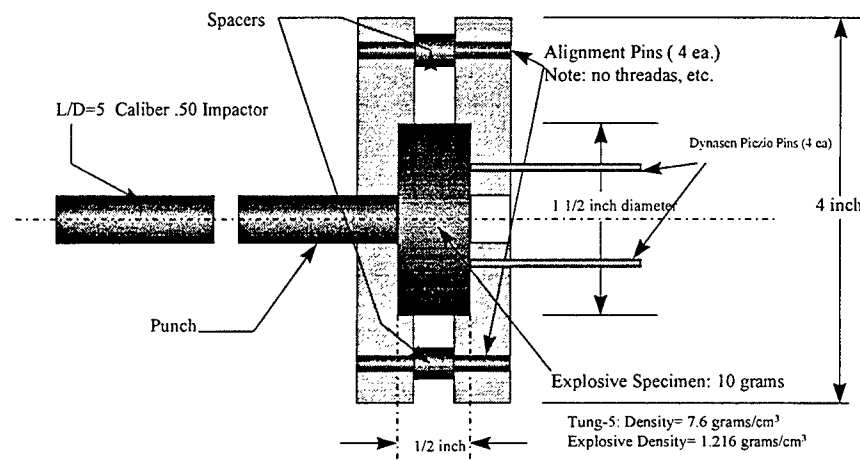


Figure 2 Pure Shear Impact Diagram

Figure 2 is a drawing of the Shear Punch test. It involves firing a steel rod at another steel rod that is in contact with a statically mounted piece of unconfined explosive. Tung 5 Mod 6 underwent this test and the damaged pieces were used in this project.

## Results

After viewing the polished explosives under the stereomicroscope and using parts of the SEM analysis, it was determined that the Tung 5 Mod 6 and PBXN-109 mixtures were homogeneous. There was an even distribution of explosive crystals, with no apparent clumping. The crystals appeared to be well coated with the continuous matrix (binder) resulting in few visible voids around the crystals. In addition there were few voids throughout the entire matrix external to the crystals. The limited SEM data,

the explosive crystals had no apparent damage induced by the mixing or polishing processes.

No post test specimens from the Bulk Modulus test were analyzed due to operational problems with the test.

After the shear punch test however, the matrix of the Tung 5 Mod 6 explosive looked very different. From the mechanical stress induced during the testing, multiple fractured crystals were observed and the majority of the voids were closed. After polishing the post test specimens, the surface of the explosive did not have the same reflective appearance as with the pre test samples.

Results from the density tests performed with PBXN-109 showed that the mix was essentially at TMD as is generally the case with PBX-type mixes. Void volume is presumably nil. The Tung 5 Mod 6 explosive exhibited variable density readings. The results were greater than 95% of TMD with the pycnometer densities higher than those from the Mettler, thus suggesting some of the porosity present is open.

## Density Tests Results

### PBXN-109

p-polished      u-unpolished

Type	TMD	Pycnometer	Mettler	Geometrical
Center C -p	1.65 g/cc	$1.65 \pm 0.01$ g/cc	1.66 g/cc	1.68 g/cc
End C -p	1.65 g/cc	$1.65 \pm 0.01$ g/cc	1.65 g/cc	1.66 g/cc
Center 3 -p	1.65 g/cc	$1.68 \pm 0.02$ g/cc	1.66 g/cc	
End 3 -p	1.65 g/cc	$1.66 \pm 0.01$ g/cc	1.66 g/cc	
Center A -u	1.65 g/cc	$1.66 \pm 0.01$ g/cc	1.66 g/cc	
End A -u	1.65 g/cc	$1.66 \pm 0.02$ g/cc	1.65 g/cc	

Chart 1 PBXN-109 Density Results

Chart 1 shows the results from the different density tests on PBXN-109. As in Figure 1 Center C and End C represents cubes that came from the center and end of the top layer. Center 3 and End 3 mean that they came from the center and end of the middle layer and Center A and End A mean that they came from the bottom layer. The consistency of the densities from the top to bottom and with TMD suggest the mixture is homogeneous.

## Density Tests Results

### Tung 5 Mod 6

p - polished      u-unpolished

Type	TMD	Pycnometer	Mettler
Tung 5 Mod 6	7.43 g/cc	$7.23 \pm 0.03$ g/cc	7.20 g/cc
Center C - p			
Tung 5 Mod 6	7.43 g/cc	$7.35 \pm 0.02$ g/cc	7.24 g/cc
End C - p			

Chart 2 Tung 5 Mod 6 Density Results

Chart 2 shows the results from the density tests on Tung 5 Mod 6 and that they were 97% TMD suggesting 3% open porosity.. The Mettler data, which represents bulk density, shows that the castings, at least from the top section, was approximately 97% of TMD. The pycnometer densities, while varied, suggest that some of the porosity is open.

## Picture Analysis Scanning Electron Microscope PBXN-109

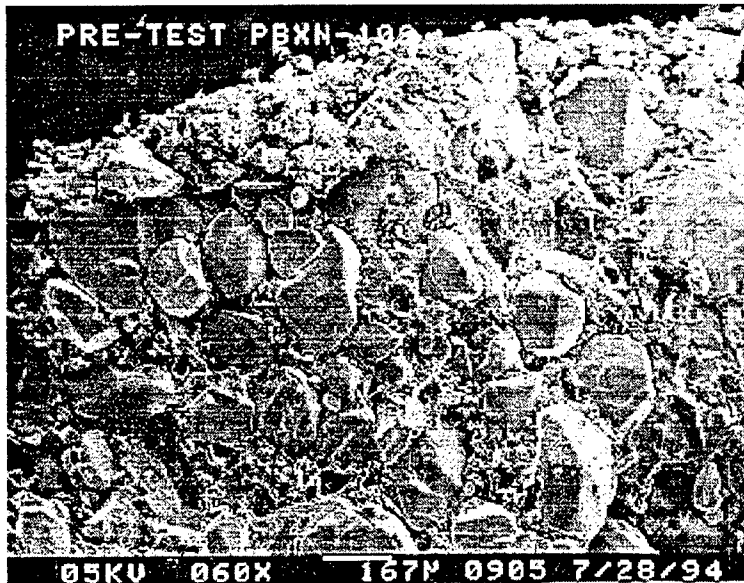


Figure 3 Pre Damaged PBXN 109 Before Polishing

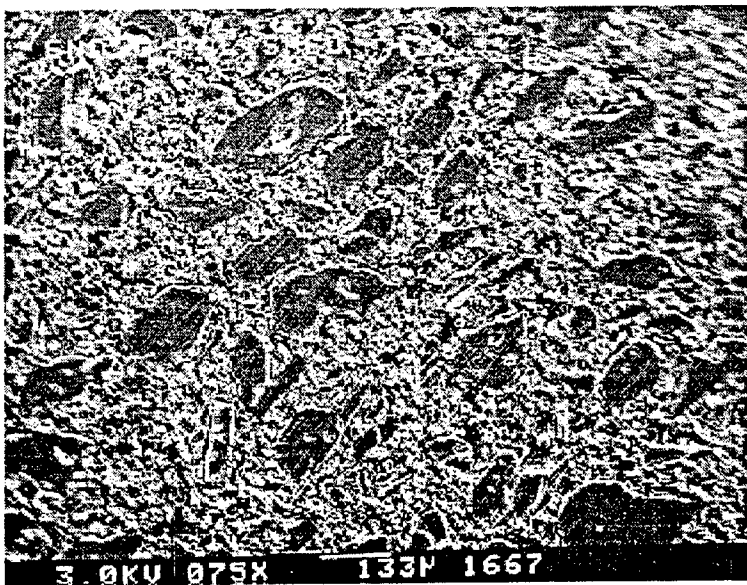


Figure 4 Pre Damaged PBXN-109 After Polishing

### Conclusion

It was determined that the cylinder of PBXN-109 was homogeneous and at TMD.

After examining the post test specimen from the Shear Punch Test, it revealed that the mechanical stress causes the HMX crystals in Tung 5 Mod 6 to fracture. After polishing, the crystals were not as evident as before impact. They blended in with the rest of the matrix and didn't have the same reflective shine as before.

The majority of the voids viewed before impact were evidently crushed out. There were fewer voids and those left, were significantly smaller in size. These conclusions suggest that the external strain stimuli induces a significant amount of change into the matrix of an explosive.